ISSN: 2382-6533 (Print)
ISSN: 2424-810X (Online)
Volume 11 · Issue 2
April 2025

Journal of Clinical and Translational Research

Acoustically-mediated drug delivery and neurodeg eneration

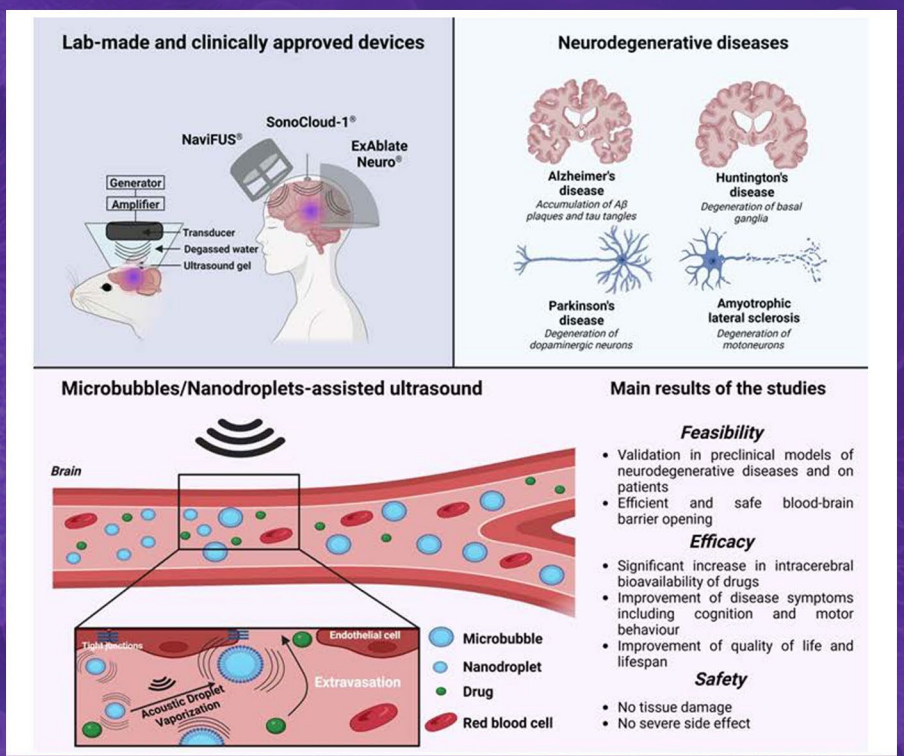

Intracerebral drug delivery using microbubble/nanodroplet-assisted ultrasound to address neurodegenerative diseases

ACCSCIENCE PUBLISHING

ABOUT JCTR

Aims and scope

The Journal of Clinical and Translational Research (JCTR) is an open access, peer-reviewed, multidisciplinary scientific journal that publishes studies with at least an ex vivo, in vivo, or clinical component. The published research is centered on any clearly defined clinical problem, which may comprise a disease or the basis of disease, a form of therapy or intervention, and clinical diagnostics or prognostics. Articles (original research, reviews, technical reports, medical hypotheses, commissioned articles, special issue articles, and editorials) are published continuously online and bimonthly in print. Studies performed in cells only will generally not be accepted unless they contain critical data that are in line with the scope of the journal. Some examples of such studies include molecular pathways that lie at the basis of a disease, novel biotechnological approaches for e.g., the production of drugs, or new techniques that improve clinical diagnostics and prognostics. Articles that combine preclinical and clinical data are given priority. Contributions from academic institutions and industry are welcome.

The research areas that JCTR covers include but are not limited to:

Internal medicine (all branches)
Vascular medicine and phlebology
Oncology
Cardiology
Intensive care medicine
Ophthalmology
Neurology and neurosciences
Anatomy, physiology, and embryology
Pathology
Clinical physics
Epidemiology
Medical devices
Pharmacology
Microbiology
Parasitology
Biomedical spectroscopy and spectrometry
Gastroenterology and hepatology
Surgery and transplantation
Hematology
Nephrology
Dermatology
Endocrinology and metabolism
Anesthesiology
Radiology and nuclear medicine
Clinical chemistry
Genetics and epigenetics
Global health
Nutrition
Immunology
Virology
Biomedical engineering

Key features

- Open access
- Reputable international editorial board
- Easy and fast submissions - no formatting rules (“your paper, your way”)
- No word count or reference restrictions
- Double blind review process to minimize bias
- Rapid online publication of articles upon acceptance
- Outlet for academic institutions and industry

Indexing

The Journal of Clinical and Translational Research is currently indexed by Chemical Abstract Service, Google Scholar, CNKI, and Peking University Library, and is currently working towards being indexed (PubMed, Science Citation Index Expanded, BIOSIS, Scopus, etc.).

Volume 11 • Issue 2 • April 2025
ISSN 2382-6533 (print) ISSN 2424-810X (online)

JOURNAL OF CLINICAL AND TRANSLATIONAL RESEARCH

ACCSCIENCE PUBLISHING

Journal of Clinical and Translational Research

Editorial Board

*Editorial Board Members as of April 29, 2025

ACCSCIENCE PUBLISHING

Volume 11 | Issue 2 | April 2025 | Page 1 – 105 |

Journal of Clinical and Translational Research

https://accscience.com/journal/JCTR

CONTENTS

ACCSCIENCE PUBLISHING

Journal of Clinical and Translational Research

REVIEW ARTICLE

Intracerebral drug delivery using microbubble/nanodroplet-assisted ultrasound to address neurodegenerative diseases

Karen Ea[1], Nicolas Taulier[2], Christiane Contino-Pépin[3], Wladimir Urbach[2,4], Stéphane Desgranges[3], Hélène Blasco[1,5], Yara Al-Ojaimi[1], Philippe Corcia[1,6], Patrick Vourc'h[1,5†*], and Jean-Michel Escoffre[1†*]

[1]Université de Tours, INSERM, Imaging Brain & Neuropsychiatry iBraiN U1253, Tours, France

[2]Laboratoire d'Imagerie Biomédicale, LIB, Sorbonne Université, CNRS, INSERM, Paris, France

[3]Équipe Systèmes Amphiphiles bioactifs et Formulations Eco-compatibles, UPRI, Université d'Avignon, Avignon, France

[4]LPENS CNRS UMR 8023 PSL, Paris, France

[5]Service de Biochimie et Biologie moléculaire, CHRU de Tours, Tours, France

[6]Centre de référence SLA et autres maladies du neurone moteur, CHRU Tours, Tours, France

[†]These authors contributed equally to this work.

***Corresponding authors:**
Patrick Vourc'h
(patrick.vourch@univ-tours.fr)
Jean-Michel Escoffre
(jean-michel.escoffre@inserm.fr)

Citation: Ea K, Taulier N, Contino-Pépin C, *et al*. Intracerebral drug delivery using microbubble/nanodroplet-assisted ultrasound to address neurodegenerative diseases. *J Clin Transl Res*. 2025;11(2):1-27. doi: 10.36922/jctr.24.00061

Received: September 12, 2024

1st revised: November 26, 2024

2nd revised: December 8, 2024

3rd revised: January 8, 2025

4th revised: January 18, 2025

Accepted: February 9, 2025

Published online: February 27, 2025

Abstract

Background: The blood–brain barrier (BBB) is a selective and semi-permeable barrier essential for protecting the brain's parenchyma against pathogens and toxic molecules present in the bloodstream. It consists of a monolayer of brain capillary endothelial cells, pericytes, astrocytic end-feet, and neurons. The tight junctions between endothelial cells prevent paracellular transport, further reinforcing its selectivity. However, this high level of selectivity represents a significant challenge for the delivery of therapeutic molecules to the central nervous system. **Aim:** Microbubble-assisted ultrasound (US) is a promising strategy for transiently permeabilizing the BBB to enable safe, non-invasive, localized, and efficient drug delivery to the brain. This approach enhances drug extravasation and bioavailability. Recently, nanodroplets (NDs) have emerged as good candidates to replace MBs. The aim of this review is to provide an updated overview of the rapidly expanding field of MB/ND-assisted US for the treatment of neurodegenerative diseases. This exciting field bridges research in biology and chemistry (MBs, NDs), US technology and the development of new drugs, small molecules, and biomedicines. The review begins with an update on MBs and NDs and discusses laboratory-manufactured and clinically approved devices such as Sonocloud®, NaviFUS®, and ExAblate Neuro®. It then focuses on the potential use of MB/ND-assisted US in treating neurodegenerative diseases, particularly Alzheimer's disease, Parkinson's disease, amyotrophic lateral sclerosis, and Huntington's disease (HD). **Relevance for patients:** Acoustically mediated BBB opening is an innovative and rapidly advancing strategy that holds great promise for improving the efficacy of existing treatments for neurodegenerative diseases. It also facilitates the discovery of new therapeutic molecules by enhancing their delivery to the brain.

Keywords: Blood–brain barrier opening; Sonoporation; Ultrasound; Microbubbles; Nanodroplets; Neurodegenerative diseases

1. Introduction

The large family of neurodegenerative diseases includes Alzheimer's disease (AD), Parkinson's disease (PD), amyotrophic lateral sclerosis (ALS), and HD. Over 33 million people worldwide are affected by these conditions and, with the rapid aging of the population; they have become a major public health problem and a heavy socio-economic burden.[1] In developed countries, the population over 65 has grown considerably over the past 50 years, coinciding with a rise in the incidence of neurodegenerative diseases. These diseases are now among the leading causes of mortality. Their management is often challenging and complex for caregivers and imposes substantial costs on healthcare systems. These diseases are characterized by a loss of neurons, leading to deficits in memory, cognition, and motor behavior.

At present, most treatments are either palliative or ineffective, offering no curative solutions. They mainly alleviate the clinical symptoms of these diseases but rarely target the underlying pathophysiological mechanisms. Some patients do not respond to pharmacological treatments, while others develop drug resistance. In addition, several of these diseases lack any form of treatment altogether.

In this context, the scientific and medical community has made significant efforts to design and validate pharmacological treatments that target the brain regions affected by these diseases. However, many systemically administered therapeutics show limited or no accumulation in the brain parenchyma and often cause off-target effects due to non-specific accumulation in healthy tissues. One of the main barriers to the delivery of therapeutics from the vascular compartment to the brain parenchyma is the blood–brain barrier (BBB).

The BBB is one of the most selective and semi-permeable endothelial barriers. It consists of a monolayer of brain capillary endothelial cells, surrounded by a basal lamina, astrocytic perivascular end-feet, pericytes, and neurons.[2] The presence of tight junctions (TJs) between adjacent endothelial cells reinforces the selective permeability of the BBB, preventing paracellular diffusion of molecules (Figure 1). The primary function of BBB is to physically and metabolically control the transport of endogenous and exogenous molecules, thereby maintaining brain homeostasis and function while protecting the brain microenvironment from systemic neurotoxic substances and pathogens (e.g., bacteria, viruses, etc.).[3] The transport of molecules at the level of brain and blood vessel cells is governed by two main pathways: One passive and the other active. The passive pathway is the paracellular pathway, which allows water-soluble molecules to pass through TJs. The active pathways are the transcellular pathways, which depend on the physicochemical properties of the transported molecules and include the transcellular lipophilic pathway (e.g., lipid-soluble molecules), transport proteins for specific molecules (e.g., glucose, amino acids, etc.), receptor-mediated transcytosis (e.g., insulin, transferrin, etc.), and adsorptive transcytosis (e.g., albumin and other plasma proteins). These pathways are responsible for transporting the nutrients and gases required to control brain homeostasis and functions.[2]

Because of its vital physiological roles, the BBB poses a significant challenge to treating brain diseases by severely limiting or completely blocking the intracerebral (i.c.) bioavailability of therapeutics. Indeed, this BBB excludes nearly 100% of large neurotherapeutics (*e.g.* monoclonal antibodies, recombinant proteins, nucleic acids) and over 98% of small molecules (<400 Da),[4] largely due to their physicochemical properties. This barrier explains the limited efficacy of many therapies for brain disorders.[5] In addition, the presence of active efflux transporters (e.g., ATP-binding cassette transporters) at the BBB

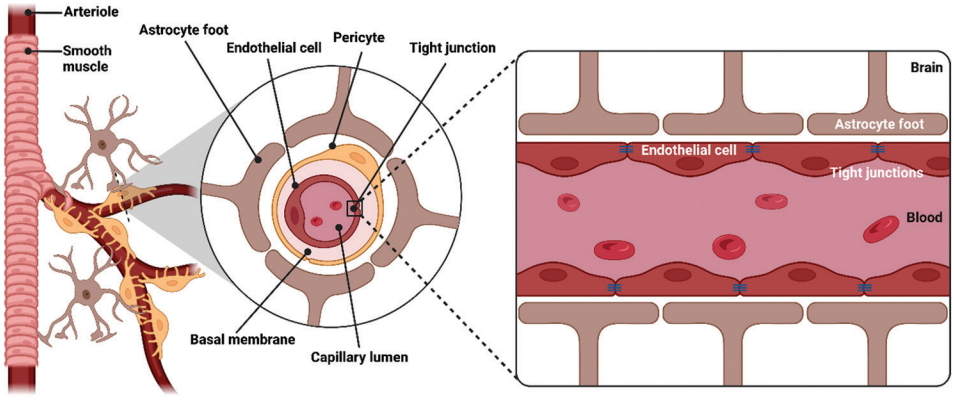

Figure 1. Schematic diagram of the blood–brain barrier and tight junctions. Adapted from "Brain vascular system". Retrieved from https://app.biorender.com/biorender-templates.

further contributes to the exclusion of these therapeutics by transporting them out of the brain tissue and back into the bloodstream.[6]

The integrity and various functions of the BBB are often compromised in many brain diseases, for example, due to neuroinflammation.[7-9] Such BBB disruptions are the consequences of disease progression. The increase in BBB permeability observed in Alzheimer's[10] and PDs[11] is positively correlated with improved i.c. bioavailability of therapeutic molecules, although it still fails to reach an efficient therapeutic dose. The intra-individual and inter-individual heterogeneity of these BBB disruptions might explain this observation.[12] In this context, the design and validation of targeted drug delivery systems are needed to increase the i.c. dose of therapeutic molecules while minimizing off-target effects.

For several decades, the scientific community has been developing safe and efficient methods for i.c. delivery of therapeutic molecules. These methods can be classified into two categories: (1) the invasive methods, which require surgical interventions to insert i.c. implants or microchips or to perform intraventricular and intrathecal infusions; (2) the non-invasive methods, which rely on either biochemical agents (e.g., mannitol, vasoactive agents, etc.) or physical agents (*e.g.*, electric field, magnetic field, etc.) to transiently disrupt the BBB, or on genetic/chemical modifications (e.g., fusion proteins, cell-penetrating peptides, etc.) of therapeutics or the use of biopharmaceutical vectors (e.g., nanoparticles, Trojan horses, viral vectors, etc.) to deliver molecules through the BBB's native transport pathways.[13-16] Among these drug delivery methods, acoustically mediated drug delivery using microbubbles (MBs) or nanodroplets (NDs) is a promising modality for the non-invasive and targeted delivery of therapeutic molecules into brain tissues.[17-21]

In this review, we will first discuss the different approaches using MBs and NDs in combination with ultrasound (US). We will then review pre-clinical and clinical studies employing this strategy for the treatment of neurodegenerative diseases, including its efficacy, safety, limitations, and future prospects.

2. Methods

The electronic databases PubMed® and ClinicalTrials.gov were screened using pre-defined search dates (January 1995 – July 2024) and terms related to i.c. drug delivery using microbubbles/NDs-assisted US for brain diseases. The search terms for the PubMed® database were: (BBB opening [MeSH terms]) AND (drug delivery [MeSH terms]) AND (US [MeSH terms]) AND (microbubbles [MeSH terms] OR NDs [MeSH terms]) AND (neurodegenerative diseases [MeSH terms]) AND ('English'[language]). The search terms for the ClinicalTrials.gov database were: 'blood–brain barrier opening' AND 'drug delivery' AND 'ultrasound' AND 'microbubbles OR nanodroplets' AND 'neurodegenerative diseases'. The inclusion and exclusion criteria are summarized in Table 1. The results of our database analysis are presented in Figure 2.

3. Acoustically mediated drug delivery using microbubbles and NDs

The great interest in acoustically mediated drug delivery using MBs and NDs for the treatment of brain disorders, particularly neurodegenerative diseases, is clearly reflected in the increasing number of publications in this field, as shown in the histogram chart in Figure 3. This US modality induces transient, efficient, and safe permeabilization of the BBB, thereby enhancing the extravasation and the i.c. bioavailability of therapeutics (Figure 4).[22-25]. The resulting increase in the i.c. dose of therapeutics improves their therapeutic efficacy while minimizing their off-target effects on healthy tissues.[25] Hynynen *et al.*[26,27] were the first to report BBB disruption in a rabbit model without causing neuronal damage.

As described below, MBs and NDs can also act as sonoresponsive drug carriers, releasing their payload specifically in the target tissue under US action. Furthermore, these sonoresponsive particles can be functionalized with targeting agents to bind membrane biomarkers that are overexpressed on target cells (e.g., endothelial and cerebral cells, etc.), thereby improving the specificity of therapeutic delivery.[28] This US modality is non-invasive, easy to apply, and cost-effective, making it a viable method for i.c. delivery of a wide range of therapeutics, including chemotherapeutics, monoclonal antibodies, nucleic acids, viral vectors, stem cells, and immune cells. The technique is typically guided by magnetic resonance imaging (MRI) and monitored using passive cavitation detection devices (PCD).[29] Therapeutic delivery can be triggered on demand and precisely controlled spatially and temporally by US focusing and directed propagation. In this section, we will describe MBs and NDs, including their composition,

Table 1. Inclusion and exclusion criteria used to select studies

Inclusion criteria	Exclusion criteria
In vivo	*In silico, In vitro*
Original article	Review papers, comments, and letters
Efficacity, bioavailability, safety	Neuropsychiatric disorders,
BBB opening and drug delivery	Neurooncological diseases
Neurodegenerative diseases	Drug delivery with US only
MB/ND-assisted US	Other languages
English	

Abbreviations: MB: Microbubble; ND: Nanodroplet; US: Ultrasound.

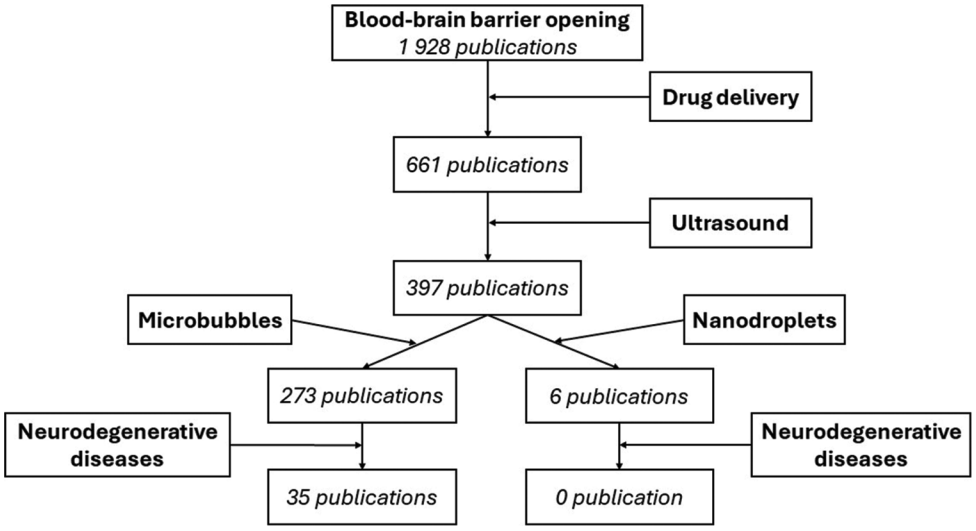

Figure 2. Flow diagram detailing the search and selection process applied during the review

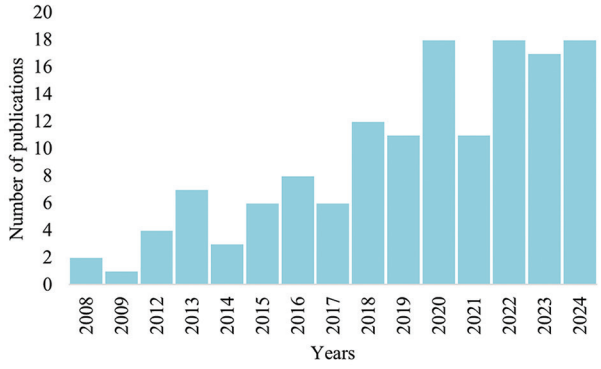

Figure 3. The literature of microbubble/nanodroplet-assisted ultrasound for drug delivery into the brain

applications, advantages, and limitations, as well as the biophysical mechanisms underlying BBB disruption.

3.1. Description of sonoresponsive agents

3.1.1. Microbubbles

Common ultrasound contrast agents consist of an aqueous solution of micrometer-sized bubbles (MBs) filled with a heavy-weight hydrophobic gas (e.g., perfluorocarbon [PFC], sulfur hexafluoride) and encapsulated by a biocompatible shell (e.g., lipids, polymers).[30] These purely vascular agents are administered intravenously to enhance US image contrast, thus improving diagnostic accuracy[31,32] in fields, such as cardiology and radiology. At present, four MB formulations have received clinical approval (Tables 2 and 3).

For over 30 years, the combination of high-frequency US (0.5 – 10 MHz) and MBs – often referred to as MB-assisted US, sonoporation, or sonopermeabilization, which induces pore in the tissue – has emerged as a promising approach to improving the therapeutic efficacy of drugs by increasing local delivery to brain tissue while minimizing side effects on healthy tissues.[33] MBs are typically co-administered or injected sequentially with therapeutics through the intravenous (i.v.) route. These two strategies enable the use of clinically approved MBs and therapeutics, facilitating a rapid clinical translation of this drug delivery method. The doses of MBs[34,35] and therapeutics can be easily adjusted to achieve the desired therapeutic outcomes. However, the main limitations of these strategies lie in the differing spatiotemporal biodistributions of MBs and therapeutics due to their distinct physicochemical properties, their rapid degradation, and the non-specific accumulation of free therapeutics in healthy tissues.

To overcome these limitations, MBs have been designed to function not only as cavitation nuclei but also as carriers for therapeutics. Lipophilic therapeutics can be incorporated into the lipid monolayer shell of MBs or dissolved in an oil cavity situated between the gas core and the MB shell. Hydrophilic therapeutics, on the other hand, are typically loaded into the aqueous lumen of nanoparticles (e.g., liposomes, polyplex) which are then attached to the MB surface. However, identifying the optimal MBs for a specific therapeutic molecule – those with the most suitable physicochemical and pharmacological properties – can sometimes be challenging. These various approaches are shown in Figure 5.[28]

The main limitation of drug-loaded MBs is their low drug-loading capacity. To overcome this, several strategies have been developed to enhance drug loading. In addition, the i.v. administration of higher doses of drug-loaded MBs or the application of consecutive treatment sessions is an alternative solution. Moreover, MBs can be functionalized

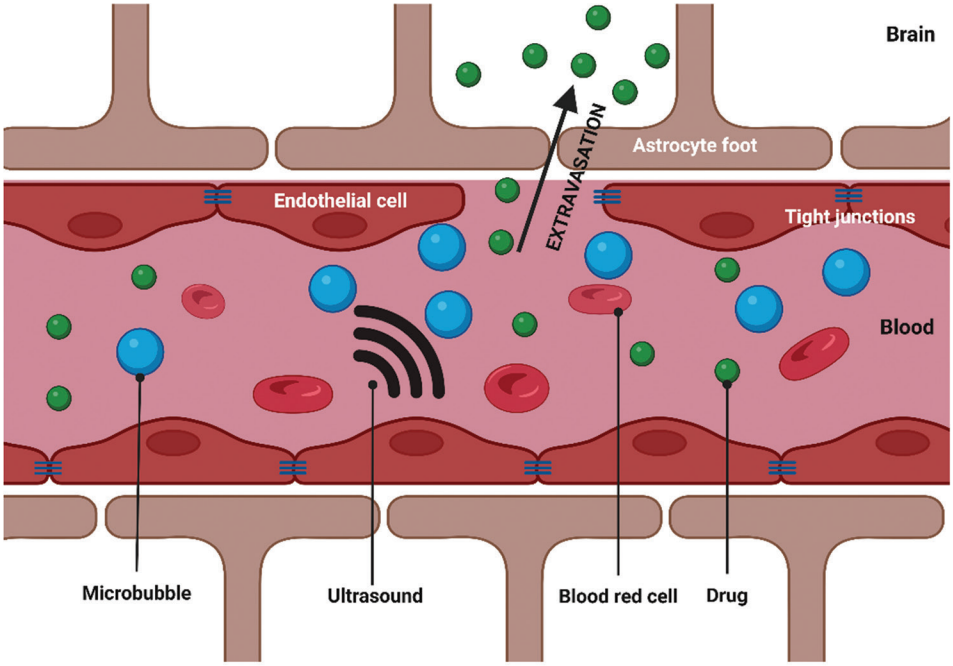

Figure 4. Intracerebral drug delivery using ultrasound contrast agent-assisted ultrasound. Adapted from "Blood–brain barrier (simple longitudinal)". Retrieved from https://app.biorender.com/biorender-templates.

Table 2. Characteristics of different clinically approved MBs

Name	Optison®	Lumason®/SonoVue®	Definity®/Luminity®	Sonazoid®
1st approved for clinical use	1998	2001/2014	2001/2006	2007
Diameter (μm)	3 – 5	2.5	1.5	2.6
Shell's composition	Hydrogenated egg PS	Phospholipid	Phospholipid	Hydrogenated egg PS
Charge	-	-	-	-
Gas	C_3F_8	SF_6	C_3F_8	C_4F_{10}
Provider	GE HealthCare	Bracco	Lantheus	GE HealthCare
Country	Norway	Europe, China, USA	USA	Japan, South Korea

Abbreviation: PS: phosphatidylserine.

Table 3. Comparative table between the composition of MBs and NDs

Particule	Shell composition	Core	Size	Functionality	Load	Administration	Extravasation	Lifespan
MB	Lipids, polymers	SF_6 C_3F_8 C_4F_{10}	1.5 – 5 μm	Intravenous	Yes	Co-administration or sequential	No	Few minutes
ND	Lipids, surfactants, polymers, proteins	PFC	20 – 200 nm	Intravenous	Yes	Co-administration or sequential	Yes	Few hours

Abbreviations: MB: Microbubble; ND: Nanodroplet: PFC: Perfluorocarbon.

with targeting agents to bind specific overexpressed biomarkers on cerebral microvasculature (e.g., transferrin receptor, which is expressed on vascular endothelial cells).[36,37] This targeting strategy can increase the accumulation of MBs in target brain regions, enhance BBB permeabilization, and improve the i.c. bioavailability of therapeutics.

The use of MBs for acoustically mediated i.c. delivery of therapeutics faces two main limitations. First, most clinically approved or custom-made MBs used for this purpose exhibit polydispersity in size. Since the effectiveness of MBs depends on the relationship between the central frequency of US waves and the size of MBs, only a fraction of MBs

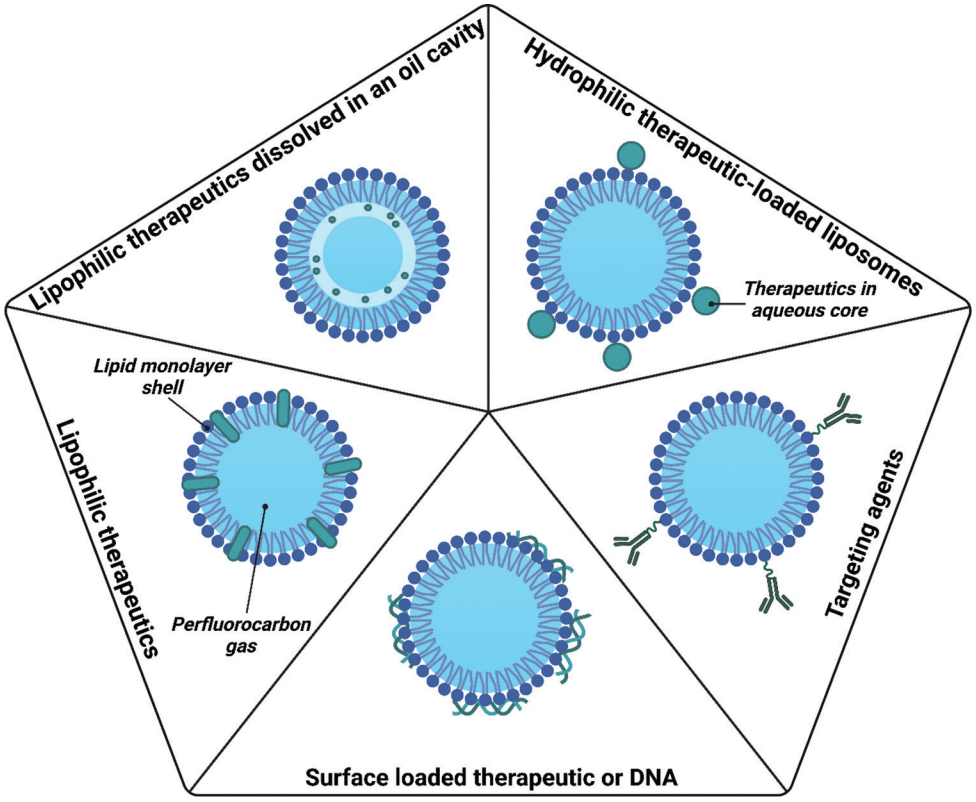

Figure 5. Schematic representation of various drug-delivery vehicle designs. Created with BioRender.com.

responds to a given frequency and contributes to BBB permeabilization. This relationship, as described by Shapk *et al.*[38] using the Rayleigh-Plesset equation, highlights the need for a population of MBs with uniform size, which would be more effective in permeabilizing the BBB.[39] Second, MBs have a limited lifespan in the bloodstream, ranging from 5 to 15 min.[40,41] This relatively short lifespan necessitates either continuous infusion of MBs or repeated bolus injections to achieve efficient permeabilization of the BBB. These requirements increase the complexity of the protocol and the overall cost of the procedure.

3.1.2. NDs

NDs have recently emerged as phase-changing sonoresponsive agents, attracting significant interest in biomedical applications for both imaging and therapeutic purposes. These NDs consist of a liquid core (e.g., PFC) stabilized by a biocompatible shell (e.g., surfactants, lipids, proteins, polymers, etc.) (Table 3).[42] Their size typically ranges from 20 to 200 nm, and they generally exhibit narrower size distribution compared to MBs. In addition, NDs have a prolonged systemic lifespan of up to 4 – 5 h.[43] Similar to MBs, NDs can be co-injected, administered sequentially with therapeutics, or used as drug nanocarriers. Moreover, the liquid core of NDs remains in its liquid state at body temperature but can vaporize into MBs in a controlled, non-invasive, and localized manner under the effect of an acoustic process known as acoustic droplet vaporization (ADV).[44,45] During ADV, the applied US disrupts the vapor pressure equilibrium of the saturated PFC liquid, causing it to vaporize and form MBs, which in turn induces cavitation and opens the BBB (Figure 6).[46]

Under specific US conditions, this process can promote the reversible permeabilization of the BBB as well as the plasma membrane of cerebral cells when NDs are located in the vascular and brain compartments, respectively. Unlike MBs, NDs can easily extravasate and accumulate in target tissues due to their nanometric size and the enhanced penetration and retention effect (EPR effect). Consequently, their acoustic activation not only induces the transient permeabilization of cerebral cells but also facilitates the release of therapeutics loaded into NDs and their intracellular uptake when NDs are used as drug nanocarriers (Figure 7). This strategy holds significant potential for improved tissue targeting, particularly in the treatment of brain tumors.[43] At present, these NDs have not yet received clinical approval, despite offering clinical prospects comparable to, or even exceeding, those of MBs. Nevertheless, further research is needed to clearly establish the efficacy and the safety of acoustically mediated drug delivery using NDs.

3.2. Mechanisms of acoustically mediated drug delivery

The effectiveness of i.c. delivery of therapeutics dependents heavily on: (1) The presence of sufficient amounts of sonoresponsive agents (i.e., MBs and NDs) and therapeutics near the biological targets (i.e., BBB and cerebral cells). This is influenced by their physiochemical properties (e.g., size, composition, etc.) and pharmacological characteristics (i.e., pharmacokinetics, pharmacodynamics, bioavailability), as well as their mode of administration (i.e., i.v. bolus vs. perfusion, co-administration versus sequential administration) and the physiological state of biological targets (e.g., healthy versus pathological cells/tissues, microenvironment, etc.); (2) The US setup, including the type of probe (e.g., mono-element US transducer versus transducer array, focused versus unfocused transducer, etc.), the device used (i.e., laboratory-made device, US imaging scanner, clinically approved therapeutic US device), and the parameters applied (e.g., frequency, acoustic pressure, pulse duration, etc.), which must be optimized to ensure safe and efficient activation of the sonoresponsive agents near the biological targets; (3) The treatment protocol including the time interval between the administration of sonoresponsive agents and therapeutics on one hand and the subsequent US exposure on the other, the number of treatments, and the intervals between sessions.[47]

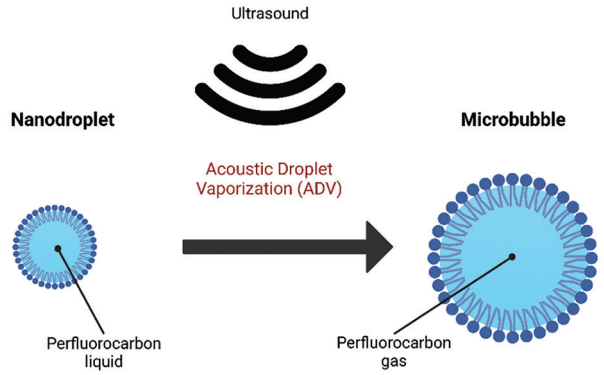

Figure 6. Schematic representation of the acoustic droplet vaporization process. Vaporization of perfluorocarbon droplets following exposure to ultrasonic pulses leads to the formation of gas bubbles. Created with BioRender.com.

3.2.1. Microbubbles

As described above, the properties of US and MBs, along with *in vivo* environmental conditions (e.g., hydrostatic pressure and dissolved gas saturation) influence the response of MBs to US waves. The high compressibility and the low density of the gas core of MBs create a significant impedance mismatch with the surrounding medium, making MBs highly responsive to US waves. During the rarefaction and compression phases of the wave, MBs alternately expand and contract, a phenomenon referred to as MB oscillation.[40] At low acoustic pressures, MBs oscillate in a symmetrical and linear manner, a process known as stable cavitation.[25,30,48] When in close proximity to biological barriers (e.g., cell membrane and BBB), these oscillations can induce "cell massage" (i.e., a pushing and pulling effect)

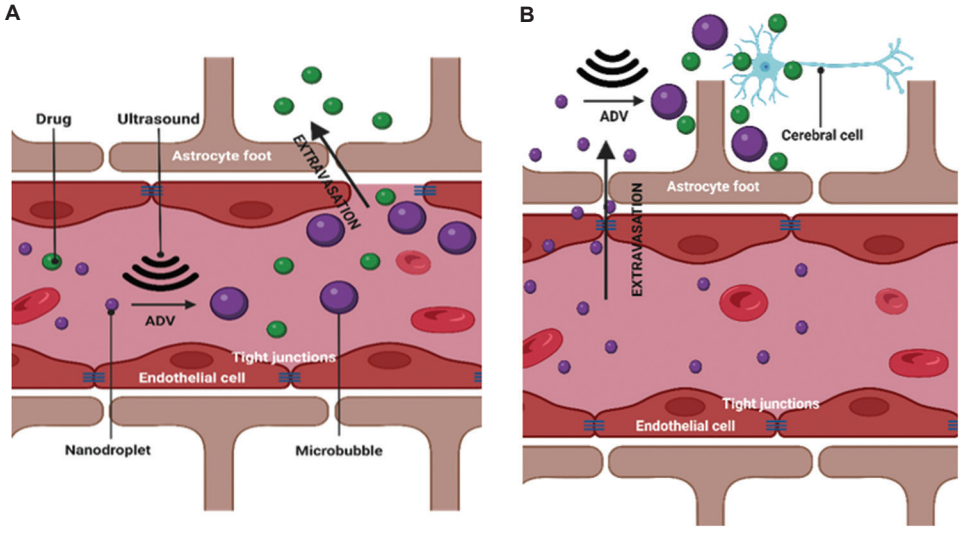

Figure 7. Acoustic activation of NDs. (A) Transient permeabilization of the BBB promoted by ADV under specific US conditions. (B) Upon extravasation of NDs through the EPR effect, ADV facilitates the release of therapeutics loaded into NDs and reversible permeabilization of cerebral cells. Adapted from "Blood–brain barrier (simple longitudinal)". Retrieved from https://app.biorender.com/biorender-templates.
Abbreviations: ADV: Acoustic droplet vaporization; BBB: Blood–brain barrier; EPR: Enhanced penetration and retention; NDs: Nanodroplets; US: Ultrasound.

and generate fluid flows around the MBs, known as acoustic microstreaming. Both of these biophysical processes exert shear stress on biological barriers, enhancing their natural permeability to therapeutics.[35]

At much higher acoustic pressures, MBs exhibit a nonlinear acoustic behavior, characterized by larger expansion amplitude relative to compression. This more violent oscillation often leads to the collapse and destruction of MBs, a phenomenon termed inertial cavitation. This disruption of MBs during inertial cavitation generates shock waves in the surrounding medium, producing greater shear stress on biological barriers and thereby increasing their permeability.[30,48,49] In addition, the asymmetrical collapse of MBs can create high-velocity jets (i.e., microjets) that transiently damage biological barriers, further enhancing the permeability of tracers (e.g. MR contrast agent, fluorescent dyes) and/or therapeutic molecules (e.g. monoclonal antibodies, recombinant proteins, nucleic acids). These biophysical processes promote the permeabilization of the BBB by stimulating paracellular pathways (i.e., disruption of TJs) and/or transcellular pathways (i.e., transcytosis), thereby facilitating the extravasation of therapeutics.[47] They also improve the intracellular uptake of therapeutics by forming membrane pores[50] and/or stimulating endocytosis pathways.[51,52] At present, scientific and medical consensus favors the use of stable cavitation of MBs over inertial cavitation due to the potential tissue damage associated with the latter.

3.2.2. NDs

As previously mentioned, the core of NDs remains in a liquid state at body temperature but vaporizes into MBs through the process of ADV. Vaporization occurs when the vapor pressure of volatile liquids in the liquid state (e.g., PFCs) exceeds the surrounding gas phase pressure.[44,45] This phenomenon is presented in Shpak *et al.*[38] US reduces the pressure around the NDs below the vapor pressure of the volatile liquid in their core, triggering vaporization and the subsequent formation of MBs.[45,53,54] In recent years, PFCs have become the primary volatile candidates for ND cores due to their low solubility in aqueous formulations, low toxicity, and suitability as low-boiling-point liquids.[55]

The ADV process depends on various factors, including ND properties (e.g., the type of volatile liquid and ND size), acoustic parameters (e.g., pressure and frequency), and ambient parameters (e.g., pressure and temperature).[53] Following i.v. administration, the ADV process can occur in the vascular compartment, enabling the release of therapeutics from NDs when used as drug nanocarriers.[56] Subsequently, the stable or inertial cavitation of newly formed MBs can transiently permeabilize the BBB, enhancing the i.c. bioavailability of therapeutics. For instance, Chen *et al.*[57] demonstrated transient BBB permeabilization using ND-assisted US in the rat model, showing more homogeneous dextran delivery to the targeted hippocampus without inducing inertial cavitation or compromising safety. In addition, the ADV process may occur within the cerebral parenchyma due to ND extravasation. In this case, therapeutics are released in close proximity to targeted cerebral cells. The stable cavitation of MBs can then further permeabilize these cells, facilitating the intracellular uptake of therapeutics.

One significant limitation of NDs is that they cannot be imaged before ADV, unlike MBs. To address this, multimodal imaging NDs have been developed by incorporating imaging tracers for various modalities, such as gadolinium for MRI,[58,18]-F for positron emission tomography,[59] or DiR fluorescent dye for fluorescence imaging.[60]

4. US devices

Several pre-clinical and clinical investigations have demonstrated significant progress in the development, optimization, and validation of acoustic sequences to achieve efficient and safe i.c. delivery of therapeutics. Among these studies, two main categories of US devices have been highlighted: lab-made US devices and clinically approved US devices specifically designed for therapeutic delivery.

4.1. Lab-made US devices

The lab-made US devices typically consist of three main components: a generator, an amplifier, and a commercial or custom-built single-element US transducer. The US waves are generated by the US transducer which operates at a fixed center frequency (ranging from 0.250 to 1 MHz). The transducer is driven by an electrical signal produced by an arbitrary waveform generator and subsequently amplified using a power amplifier. To ensure effective coupling with the animal's head and precise targeting of the focal point within the brain region of interest, the transducer can either be placed in direct contact with the animal's head using US gel, or inserted into a dedicated degassed water-filled adaptor, allowing for proper alignment and positioning of the focal point within the targeted brain area (Figure 8).[61]

Spherically focused US (FUS) transducers are commonly used to significantly increase US intensity within a small, targeted brain area. These transducers are typically calibrated in a separate setup using a calibrated hydrophone.[62] Lab-made US devices provide flexibility to control various US parameters (i.e., center frequency, pulse repetition frequency, duty cycle, acoustic pressure, and total exposure time), allowing these parameters to be optimized

for therapeutic delivery. The exposure of brain tissue to FUS is generally guided by MRI or neuronavigation systems, enabling more precise and safe treatments.[63] For several years, lab-made US devices have been paired with PCD devices to monitor and manage acoustic intensity in real-time during FUS exposure, ensuring safe and effective treatment within the brain tissue.[29]

4.2. Clinically approved devices

At present, three clinically approved US devices—SonoCloud®, NaviFUS®, and ExAblate Neuro®—are available for i.c. delivery of therapeutics. Below, their distinct characteristics are described.

4.2.1. SonoCloud®

CarThera© (Lyon, France) has designed innovative therapeutic US-based medical devices known as SonoCloud® for delivering therapeutics into the brain. SonoCloud® is an intracranial US implant that transmits US waves to a target brain region, bypassing the skull and transiently opening the BBB before or after i.v. administration of therapeutics. The device is implanted in a skull window, positioned beneath the skin, and remains invisible externally. After an i.v. injection of MBs, SonoCloud® is activated through a transdermal needle connected to an external control unit. Low-intensity pulsed US exposure to the targeted brain area disrupts the BBB for several hours (typically 4 – 6 h), thereby increasing the effective concentration of therapeutics in this brain area. This acoustically mediated BBB disruption can be repeated with each cycle of pharmacological therapy.

CarThera© has developed and validated two MRI-compatible SonoCloud® devices: SonoCloud-1® and SonoCloud-9®. SonoCloud-1® is an 11.5-mm diameter biocompatible implant containing a 1-MHz planar US transducer,[64,65] while SonoCloud-9® consists of nine 1-MHz planar US transducers arranged on an implantable grid (Figure 9). SonoCloud-9® safely and efficiently disrupts the BBB over a large volume of brain tissue and significantly increases the i.c. bioavailability of therapeutics in the brain compared to SonoCloud-1®. This US protocol is fully compatible with conventional pharmacological treatments and does not require patient anesthesia. In addition, BBB disruption can be monitored using dynamic contrast-enhanced MRI (DCE-MRI) following the i.v. administration of an MRI contrast agent. These SonoCloud® devices are currently being evaluated in clinical trials for treating brain tumors[66-68] and AD.[69]

4.2.2. NaviFUS®

NaviFUS® Corp. (Taipei, Taiwan) has developed a neuronavigation-guided transcranial FUS system known as NaviFUS®. This custom-designed system features a multichannel hemispherical FUS-phased array operating at a frequency of 0.5 MHz. It delivers FUS to brain tissue in a transcranial, non-invasive manner (Figure 9). Before the FUS intervention, a personalized treatment plan is designed for each patient based on cranial bone data obtained from their MRI and/or CT scans. Physicians determine the target brain regions and specify the positioning of the transducers. The intervention is conducted on an outpatient basis, with the patient remaining awake and seated in a chair for the duration of the procedure which typically lasts <30 min. After i.v. administration of MBs, a neuronavigation tracking device guides the FUS to the targeted brain regions, ensuring precise treatment delivery.[70]

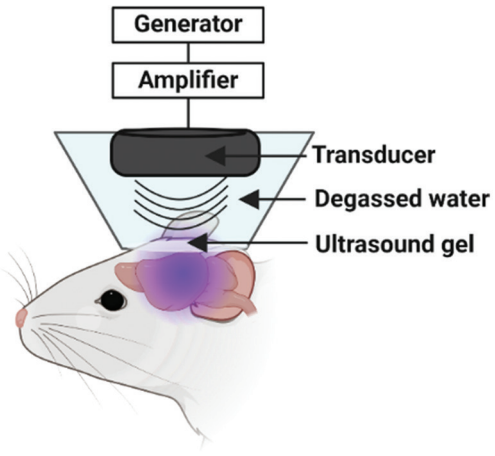

Figure 8. An example of lab-made ultrasound device. Created with BioRender.com.

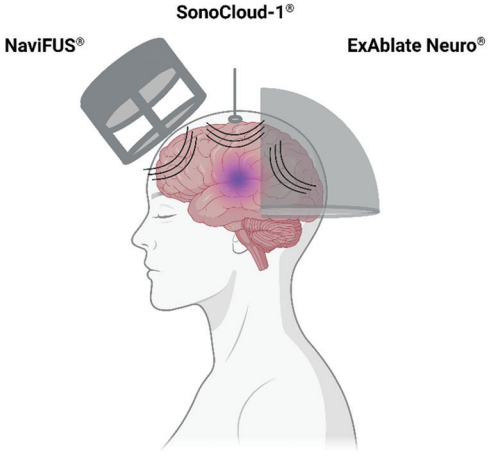

Figure 9. Illustration of the different models of clinically approved US devices—NaviFUS®, SonoCloud-1® and ExAblate Neuro®. Created with BioRender.com.

The NaviFUS® system also integrates a real-time PCD device to manage the acoustic energy in real-time during the procedure. Pre-clinical studies have demonstrated the safety and efficacy of BBB disruption using NaviFUS® in both small and large animal models.[70,71] Notably, the BBB disruption is reversible within 24 h. At present, the NaviFUS® system is under clinical investigation specifically for the treatment of recurrent glioblastoma.[57,71,72]

4.2.3. ExAblate Neuro®

InSightec© Ltd. (Israel) has developed an MRI-guided FUS (MRgFUS) system known as ExAblate Neuro®. Similar to the NavisFUS® system, this extracorporeal MRgFUS device delivers noninvasive acoustic energy into targeted brain tissues through the intact skull. The ExAblate Neuro® Type 1.0 system was originally designed to treat essential tremor and PD by partially ablating the thalamus through acoustically mediated thermal ablation at a center frequency of 0.65 MHz. Later, this system was adapted to enhance the native BBB permeability for therapeutic delivery to targeted brain tissues at a center frequency of 0.220 MHz, now referred to as ExAblate Neuro Model 4000 Type 2.0.

The ExAblate Neuro® system consists of a high-field 3T MRI scanner and a hemispherical 1,024-element phased array US transducer, which is integrated with computer systems. These systems utilize computed tomography (CT) scan data to align, steer, and control the transducer array (Figure 9).[73] Before FUS exposure, the treatment parameters are precisely planned for each patient based on anatomical and functional data of cranial bone and target brain tissues provided by MRI and CT scans. During the intervention, the awake patient lies on an MRI-compatible robotic positioning table, with the patient's head is immobilized in a stereotactic frame to prevent any movement during the procedure, which lasts between 2 and 4 h.[74] The stereotactic frame enables precise target selection and intraoperative MRI confirmation, ensuring electronic steering of the FUS beam with submillimeter accuracy (<1 mm) to one or multiple brain targets, as defined by the planned volume geometry. US sequences are initiated immediately after the i.v. injection of MBs. The MRI scanner precisely guides the US beam to the targeted brain regions during the procedure, and the BBB opening is monitored using DCE-MRI after the i.v. administration of gadolinium-based contrast agents. Notably, the BBB disruption is reversible within 20 h.

Clinical investigations have demonstrated the safety and efficacy of BBB disruption using the ExAblate Neuro® system. At present, this system is undergoing clinical trials for the treatment of brain tumors (e.g., recurrent glioblastoma and brain metastases[75]) and neurodegenerative diseases (*e.g.*, ALS, AD, and PD[74,76]).

After reviewing the state-of-the-art of acoustically mediated therapeutic delivery using MBs or NDs – including the biophysical mechanisms, sonoresponsive agents, and US devices – we will now turn our focus to the application of this US modality for the treatment of neurodegenerative diseases. First, we will provide the definition of these diseases, followed by a detailed discussion of pre-clinical and clinical investigations of these diseases using this US-based approach.

5. Applications in AD

5.1. AD

AD is the most common neurodegenerative disorder, characterized by its progressive and fatal nature.[77] In 2000, AD affected 15.3 million people worldwide, a number projected to rise to 63 million by 2030.[78] It represents a growing global health challenge, with an annual incidence of 1.8 million cases in the USA and Europe.[79] AD progresses as a continuum, with stages that vary in duration for each patient: (1) The pre-clinical or prodromal stage, where no clinical symptoms are apparent, but biomarkers such as amyloid-tau-neurodegeneration can be detected; (2) The mild cognitive impairment stage, during which symptoms, such as memory, language, and thinking difficulties emerge but do not significantly interfere with daily life; and (3) The dementia stage, marked by a loss of autonomy, further categorized into mild, moderate, and severe levels.

The progression from the pre-clinical stage to the onset of dementia can span 15 – 25 years. AD is characterized by the extracellular accumulation of beta-amyloid protein fragments, forming clumps known as beta-amyloid plaques, and the intracellular accumulation of an abnormal form of the tau protein known as tau tangles. Amyloid-β (Aβ) is believed to play roles in synaptic homeostasis, immunity, and lipid processing.[77] However, abnormal cleavage of the amyloid pre-cursor protein by β- and γ-secretases results in the production of Aβ peptides, which form the core of plaques.[80] Tau protein is crucial for microtubule stabilization, axonal transport, and signaling pathway modulation. Abnormal phosphorylation of tau leads to its aggregation, disrupting pre-synaptic and post-synaptic compartments by altering signaling cascades, mitochondrial function, and axonal transport, ultimately causing neurotoxicity.[77] The presence of Aβ plaques and tau tangles is linked to chronic neuroinflammation and progressive synaptic and neuronal loss.

These aggregates remain the main targets for the development of imaging tracers and therapeutic molecules.

Present pharmacological treatments do not address the underlying causes of the disease (curative) but instead alleviate the symptoms (palliative) by acting primarily on acetylcholinesterase and N-methyl-D-aspartate (NMDA) receptors. Numerous experimental molecules, including those targeting Aβ or tau accumulation, are under investigation for AD.[81,82] However, the results of recent clinical trials have been less promising than pre-clinical findings, with many therapeutics failing to reach their brain targets. This is due not only to their physicochemical and pharmacological properties but also to the presence of biological barriers. To overcome these challenges, specialized US protocols have been designed and validated in pre-clinical and clinical studies to facilitate the delivery of therapeutics using MB/ND-assisted US.

5.2. Pre-clinical phase

Several pre-clinical studies have demonstrated the feasibility, safety, and efficacy of MB-assisted US for reversible BBB opening in various transgenic murine models of AD, including APP/PS1dE9,[63,83-86] PDAPP,[83] TgCRND8,[87-89] 5xFAD,[61,90] pR5,[91,92] and K3.[93] For instance, Choi *et al.*[63] investigated BBB opening in three transgenic APP/PS1 mice and three wild-type mice using an acoustically mediated US approach. After an i.v. injection of SonoVue® (25 μL), the left hippocampus was exposed to US waves (1.525 MHz, 20% duty cycle (DC), 20 ms pulse duration, 0.6 MPa) for 1 min using a lab-made MRgFUS device. DCE-MRI revealed that MB-assisted MRgFUS successfully induced reversible BBB opening in the hippocampus of both wild-type and AD mice without causing any tissue damage. Similarly, Burgess *et al.*[87] validated these findings in TgCRND8 transgenic mice. Collectively, these studies underscore that MB-assisted US can safely and reversibly open the BBB in mouse models of AD.

In addition, MB-assisted MRgFUS has facilitated the delivery of various therapeutics in AD mouse models, including full-size antibodies and antibody fragments targeting Aβ,[61,83,85,86,88-90] or tau,[91-93] as well as antioxidant and anti-inflammatory molecules.[84] Regardless of the US protocol or the MBs used, MB-assisted MRgFUS significantly increased the i.c. the concentration of anti-Aβ antibodies (e.g., BAM-10, IVIg, Aducanumab, anti-pGlu3 Aβ, anti-$Aβ_{1-40}$,) in the hippocampus of AD mice compared to antibody treatment alone.[61,83,85,86,88-90] These antibodies bound to Aβ plaques, activated phagocytic microglia, and increased the number of astrocytes associated with Aβ plaques,[61,85,86] leading to a significant reduction in Aβ plaque load in the hippocampus.[61,85,88,89] Furthermore, this therapeutic strategy significantly enhanced hippocampal neurogenesis.[61,85,88,89] As a result, cognitive functions in treated mice were notably improved compared to antibody treatment alone.[61,85]

Preclinical studies have shown the potential of MB-assisted US for delivering therapeutics in AD. For instance, MB-assisted US using a lab-made device (1 MHz, 10 Hz PRF, 0.7 MPa, 10 ms pulse duration, DC 10%, for 6 s) with lab-made lipid-shelled MBs effectively delivered the 2N tau isoform-specific single chain antibody fragment (RN2N) across the forebrain of P301L human tau transgenic pR5 mice.[91,92] This approach improved the i.c. bioavailability of RN2N compared to the RN2N treatment alone, resulting in reduced anxiety-like behavior. Similarly, a novel tau-specific monoclonal antibody (RNF5) was delivered by MB-assisted US to the forebrain of the K369I tau transgenic K3 mouse model.[93] Although i.c. bioavailability was improved with the US, no behavioral improvement was observed in these mice. In addition, Liu *et al.*[84] evaluated the delivery of quercetin, an antioxidant and anti-inflammatory molecule, using MB-assisted US. Quercetin was loaded onto lab-made MBs, which were intravenously injected, followed by exposure of the parietal cortex in APP/PS1 mice to US waves (1 MPa for 5 min) using a lab-made US device. MB-assisted US facilitated BBB opening, quercetin release, and its i.c. accumulation. Quercetin treatment significantly reduced neuronal apoptosis, neuroinflammation, calcium homeostasis variation, and oxidative stress, ultimately enhancing learning and memory capacities in AD mice.

Furthermore, Gouveia *et al.*[62] explored ND-assisted US (lab-made US device; 2 MPa, 10 ms bursts, 1 Hz, for 180 s) to deliver the anesthetic pentobarbital into the amygdala of TgCRND8 transgenic mice to achieve neuromodulation (Table 4). The NDs were composed of Definity® MB shells and loaded with pentobarbital. ND vaporization did not disrupt the BBB, but the released lipophilic pentobarbital crossed the BBB, localizing the therapeutic effect to the target area. Pentobarbital-loaded NDs significantly improved agitation and aggressive behavior in AD mice compared to unloaded NDs. However, only behavioral tests were conducted. Further studies assessing the brain drug bioavailability with or without ND-assisted US are needed.

Collectively, these findings underscore the promise of MB/ND-assisted MRgFUS as an innovative modality for delivering therapeutics to treat AD.

5.3. Clinical phase

Recent clinical investigations have explored the feasibility, safety, and efficacy of acoustically mediated BBB opening and therapeutic delivery in AD patients. Three clinical trials demonstrated the feasibility, reproducibility, safety, and

Table 4. Drug delivery with MB/ND-assisted US for pre-clinical studies in Alzheimer's disease

References	Drug, dye, particle	Animal model	US devices/parameters	Targeted area	MB/ND	Therapy duration
Choi *et al*., 2008[63]	Gadolinium	APP/PS1dE9 mouse	Lab-made MRgFUS device; 1.525 MHz, DC 20%, 20 ms pulse duration, 0.6 MPa, for 1 min	Left hippocampus	SonoVue® MBs (25 μL)	1 sonication
Raymond *et al*., 2008[83]	Anti-Aβ antibodies	APP/PS1dE9 and PDAPP mouse	Lab-made US device; 0.69 MHz, 10 ms burst length, 1 Hz PRF, 0.67 – 0.8 MPa, for 40 – 45 s	Hippocampus	Optison® MBs (30 – 50 μL)	1 sonication
Jordão *et al*., 2010[88]	BAM-10	TgCRND8 mouse	Lab-made US device; 0.3 MPa, 120 s, 10 ms bursts/Hz	Right hemisphere	Definity® MBs (160 mL/kg)	1 sonication
Burgess *et al*., 2014[87]	Gadolinium	TgCRND8 mouse	Lab-made US device; 10-ms bursts, 1 Hz burst repetition frequency, for 120 s	Hippocampus	Definity® MBs (0.02 mL/kg)	1 sonication per week for 3 weeks
Nisbet *et al*., 2017[91]	RN2N	pR5 mouse	Lab-made US device; 1 MHz, 10 Hz PRF, 0.7 MPa, 10 ms pulse duration, DC 10%, for 6s	Whole brain	Lab-made lipid-shelled MBs (30 μL)	1 sonication per week for 4 weeks
Janowicz *et al*., 2019[92]	RN2N	pR5 mouse	Lab-made US device; 1 MHz, 10 Hz PRF, 0.7 MPa, 10 ms pulse duration, DC 10%, for 6 s;	Whole brain	Lab-made lipid-shelled MBs (40 μL)	1 sonication
Dubey *et al*., 2020[89]	IVIg	TgCRND8 mouse	Lab-mad US device; 1 Hz burst repetition frequency, 10 ms bursts, for 120 s	Hippocampus	Definity® MBs (0.02 mL/kg)	1 sonication
Liu *et al*., 2020[84]	Quercetin	APP/PS1dE9 mouse	Lab-mad US device; 1 MPa for 5 min using a	Parietal cortex	Lab-made lipid-shelled MBs	1 sonication per week for 5 weeks
Sun *et al*., 2021[85]	Anti-pGlu3 Aβ	APP/PS1dE9 mouse	Lab-mad US device; 2 Hz, 10 ms bursts, for 100 s	Hippocampus	Optison® MBs (100 μL/kg)	1 sonication per week for 3 weeks
Bathini *et al*., 2022[86]	Anti-pGlu3 Aβ	APP/PS1dE9 mouse	Lab-mad US device; 2 Hz, 10 ms bursts, for 100 s	One or two hemispheres	Lab-made lipid-shelled MBs	1 sonication
Kong *et al*., 2022[61]	Aducanumab	5×FAD mouse	Lab-mad US device; 1 Hz burst, 0.25 MPa, 10 ms bursts, for 120 s	Hippocampus	Definity® MBs (0.04 mL/kg)	1 sonication every 2 weeks for a total of 3
Bajracharya *et al*., 2022[93]	RNF5	K3 mouse	Lab-made US device; 1 MHz, 10 Hz PRF, 0.7 MPa, 10 ms pulse duration, DC 10%, for 6s;	Whole brain	Lab-made lipid-shelled MBs (1 μL/g)	1 sonication per week for 12 weeks
Gouveia *et al*., 2023[62]	Pentobarbital	TgCRND8 mouse	Lab-made US device; 2 MPa, 10 ms bursts, 1 Hz, for 180 s	Amygdala	Lab-made NDs (0.1 mL/injection)	1 sonication
Antoniou *et al*., 2024[90]	Anti-Aβ1 – 40	5×FAD mouse	Lab-made US device; 1 MHz, 0.5 MPa *in situ*, 10 ms bursts, DF 1%, for 100 s	Left hemisphere	SonoVue® MBs (5 μL)	1 sonication

Abbreviations: DC: Duty cycle; MB: Microbubble; MRgFUS: Magnetic resonance imaging-guided focused ultrasound; ND: Nanodroplet; PRF: Pulse repetition frequency; US: Ultrasound.

reversibility of repeated BBB opening in the frontal lobe[74] and hippocampus[94,95] of early-stage AD patients using the ExAblate Neuro® Type 2 and Definity® MBs. In a study by Rezai *et al.,*[96] aducanumab was delivered through this US device, resulting in a significant reduction in Aβ plaque load. However, no neurological, cognitive, or behavioral changes were observed during the follow-up phase. The authors explained that the study primarily assessed safety due to insufficient statistical power to detect clinical changes. The study reported one case of cognitive decline following aducanumab treatment and at least one case of severe adverse effects, which were deemed unrelated to

the trial intervention. Headaches were the most frequently reported adverse events. Interestingly, the effects of the US in this study might be pleiotropic, involving actions of the therapeutic molecule, blood-borne factors entering cerebral tissue due to BBB opening, and neuromodulatory effects of the US itself through associated radiation forces.[97]

In addition, a pilot study demonstrated the safety and repeatability of BBB opening in the left supramarginal gyrus of mild AD patients using the SonoCloud®-1 device and SonoVue® MBs [69]. Recently, Bae *et al.* [98] designed and validated a portable clinical neuronavigation-guided US device for BBB opening using Definity® MBs. This device successfully opened the BBB in the right frontal lobe of AD patients without severe side effects (Table 5)

6. Applications in PD

6.1. PD

PD is the second most common neurodegenerative disease after AD. It affects approximately 4 million people worldwide, with an average onset age of 60 years. While rare cases occur in individuals under 40 years, 3% of people over 80 years are affected by PD.[99] The disease has a prevalence of 1 – 2/1000 and an incidence of 13.5/100,000 people/year.[100] PD is an idiopathic neurodegenerative disorder primarily characterized by the degeneration of dopaminergic neurons in the pars compacta of the substantia nigra in the midbrain, leading to impaired motor control. A hallmark of PD is the presence of Lewy bodies, which are intracellular aggregates of misfolded proteins, including α-synuclein (synucleinopathy).

The clinical presentation of PD primarily includes motor symptoms, such as bradykinesia, cogwheel rigidity, resting tremor, a slow shuffling gait, and imbalance. However, non-motor symptoms are also present and include orthostatic hypotension, rapid eye movement sleep behavioral disorder, and hallucinations.[101,102] Present pharmacologic treatments focus on increasing dopamine levels to address the dopamine deficiency observed in PD patients. The most common treatment is levodopa (L-DOPA), a dopamine pre-cursor that crosses the BBB, unlike dopamine itself. Dopamine agonists and enzyme inhibitors, such as DOPA decarboxylase inhibitor (carbidopa), catechol-O-methyltransferase inhibitors, and monoamine oxidase B (MAO-B) inhibitors, are often prescribed as adjuvants to levodopa to manage motor complications. In addition, numerous molecules with therapeutic potential are under investigation for the treatment of PD.[103,104]

6.2. Pre-clinical phase

MB-assisted US has been demonstrated to effectively deliver therapeutics to neurotoxic-lesioned (i.e., 6-hydroxydopamine, 6-OHDA; 1-methyl-4-phenyl-1,2,3,6-tetrahydropyridine,

Table 5. Drug delivery with MB-assisted US for clinical studies in Alzheimer's disease

References	Drug, dye, particle	Patients	US devices/parameters	Targeted area	MBs	Therapy duration
Lipsman *et al.*, 2018[74]	Gadolinium	5 patients with early AD	ExAblate Neuro® Type 2 300 ms burst length, repetition interval of 2.7 s, DC 0.74%, for 50 s	Frontal lobe	Definity® MBs (4 μL/kg)	2 sonications separated by 1 month
Rezai *et al.*, 2020[95]	Gadolinium	6 patients with early AD	ExAblate Neuro® Type 2	Hippocampus	Definity® MBs	3 sonications separated by 2 weeks
Mehta *et al.*, 2021[94]	Gadolinium	3 patients with early AD	ExAblate Neuro® Type 2 2.6 ms pulses spaced by 30.4 ms, 10 cycles, 1550 ms rest period, 4 – 11.5 W, for 90 s	Hippocampus	Definity® MBs	3 sonications separated by 2 weeks
Epelbaum *et al.*, 2022[69]	Gadolinium	9 patients with mild AD	SonoCloud-1® device 25,000-cycle pulse, every second, for 4 min	Left supra-marginal gyrus	SonoVue® MBs (0.1 mL/kg)	1 sonication every 2 weeks for a total of 7
Bae *et al.*, 2024[98]	Gadolinium	6 patients	Portable clinical neuronavigation-guided US device PNP 200 kPa, MI 0.4, center frequency 0.25 MHz, pulse length 10 ms, 2 Hz PRF, for 2 min	Right frontal lobe	Definity® MBs (0.1 mL/kg)	1 sonication
Rezai *et al.*, 2024[96]	Aducanumab	3 patients	ExAblate Neuro® Type 2	Left frontal, parietal, temporal lobes, hippocampus	Definity® MBs	1 sonication per month for 6 months

Abbreviations: AD: Alzheimer's disease; DC: Duty cycle; MB: Microbubble; PRF: Pulse repetition frequency; US: Ultrasound.

MPTP)[105-112] and transgenic (i.e., overexpression of α-synuclein gene).[113-116] rodent or non-human primate models of PD. These therapies primarily aim to protect dopaminergic neurons from neurotoxicity by activating cell growth and survival, autophagy, clearance of alpha-synuclein, or by inhibiting oxidative stress, neuroinflammation, and apoptosis. Therapeutics tested include glial cell line-derived neurotrophic factor (GDNF),[105-107,109] brain-derived neurotrophic factor,[110] neurturin,[109] curcumin,[108] triptolide (T10),[113] gastrodin,[112] and a short hairpin RNA (shRNA) against α-synuclein.[114]

Preclinical studies have investigated MB-assisted MRgUS protocols for delivering the *GDNF* gene (through plasmid DNA or AAV vectors) to various brain regions including the striatum, substantia nigra, caudate-putamen, and ventral midbrain in rodent models of PD.[105-107,109,110] Plasmids encoding GDNF were generally loaded onto MBs to protect them from enzymatic degradation in the bloodstream.[105-107,110] In contrast, the AAV-GDNF vector was co-administered with MBs before US exposure.[109] These studies demonstrated successful GDNF expression in targeted brain regions, attenuating damage to nigrostriatal dopaminergic pathways[109] and even rescuing dopaminergic neuronal loss.[107,109,110] This neuroprotective strategy also improved motor-related behavioral deficits.[105-107,109,110]

Due to its critical role in PD pathology, α-synuclein has been a primary target for therapeutic strategies such as shRNA against α-synuclein[114] and triptolide.[113] Xhima *et al.*[114] used MB-assisted US to deliver an AAV9 vector encoding shRNA targeting α-synuclein into the hippocampus, substantia nigra, olfactory bulb, and dorsal motor nucleus in a transgenic PD mouse model. After i.v. administration of Definity® MBs (0.02 mL/kg), the targeted brain regions were exposed to US waves (lab-made MRgFUS device; 10 ms bursts, 1 Hz PRF) for 120 s. This approach significantly reduced α-synuclein expression in the targeted areas, although no changes were observed in other neuronal biomarkers (e.g., tyrosine hydroxylase, synaptophysin), glial activation, or cell death. However, this study did not analyze behavioral or cognitive outcomes, which warrants further investigation. As for the tripolide treatment, Feng *et al.*[113] explored MB-assisted FUS for delivering this drug to the substantia nigra in a transgenic PD mouse model. Triptolide, an autophagy inducer, alleviates autophagic dysfunction associated with the accumulation of α-synuclein in PD. MBs loaded with triptolide targeted the BBB and accumulated at the endothelial wall of cerebral vessels. US waves (lab-made US device; 10 ms burst length, 0.3, 0.45, and 0.8 MPa, 1 Hz PRF) were applied to the substantia nigra for 60 s after i.v. MB injection. This resulted in increased triptolide concentrations in the targeted brain region, facilitating the clearance of various forms of α-synuclein, reducing neuronal loss, restoring dopamine secretion, and improving motor deficits in PD mice (Table 6).

In conclusion, MB-assisted MRgFUS is an effective and safe modality for delivering innovative therapeutics for the treatment of PD.

6.3. Clinical phase

The first two clinical studies investigated the feasibility and safety of BBB opening in PD patients using a bolus of Luminity® MBs (4 μL/kg) and the ExAblate Neuro® MRgFUS system.[117,118] In the study of Gasca-Salas *et al.*,[117] patients underwent two treatments, separated by a 3 – 3-week interval, to permeabilize the BBB at the level of the right parieto-occipito-temporal cortex. BBB opening was monitored through DCE-MRI for 24 h and 7 days post-treatment. Neuropsychological and motor evaluations, as well as 18F-FDG and 18F-FMT PET imaging, were conducted 3 – 4 weeks after the final treatment. This study demonstrated that BBB opening in PD patients was both reversible and safe, with no reported side effects. Similarly, Pineda-Pardo *et al.*[118] investigated uni- and bilateral BBB opening in the posterior putamen using the same MB-assisted MRgFUS protocol as Gasca-Salas *et al*. Similar conclusions were drawn, confirming the safety and feasibility of the approach.[117]

In 2024, Gasca-Salas *et al.*[119] expanded on their earlier work by demonstrating that BBB opening in the substantia nigra and putamen in PD patients was well tolerated, reversible, and feasible. In this study, Luminity® MBs (2.5 mL/min) were infused using the same protocol. In addition, Huang *et al.*[120] further evaluated the ExAblate Neuro® MRgFUS system's cavitation feedback controller for active power modulation during unilateral targeting of the putamen in PD patients. Definity® MBs (4 μL/kg/5 min) were infused, and a cavitation emission-based feedback controller automatically adjusted the acoustic power to maintain the desired cavitation dose levels. The efficacy of BBB opening was assessed with DCE-MRI and hemorrhages were monitored with T2*-weighted MRI. Results demonstrated that such a device enabled efficient and safe BBB opening by dynamically modulating acoustic power.

In another study, Meng *et al.*[121] investigated the safety and feasibility of delivering recombinant glucocerebrosidase (GCase) to the putamen of PD patients with *GBA1* mutations using MB-assisted MRgFUS. The GCase enzyme, encoded by the *GBA1* gene, is inversely related to α-synuclein oligomer accumulation. Its cerebral deficit in *GBA1*-related and idiopathic PD is associated with disease severity. In this study, patients underwent

Table 6. Drug delivery with MB-assisted US for pre-clinical studies in Parkinson's disease

References	Drug, dye, particle	Animal model	US devices/ parameters	Targeted area	MBs	Therapy duration
Fan *et al*., 2016[105]	GDNF	6-OHDA rat	Lab-made US device; 1-MHz, 1 Hz PRF, 0.7 MPa, 5,000 cycles)	Substantia nigra and striatum	Lab-made lipid-shelled MBs	1 sonication
Lin *et al*., 2016[107]	GDNF	MPTP mouse	Lab-made US device; 0.3 – 0.8 MPa, 10 ms burst length, 1 Hz PRF, for 60 s	Substantia nigra	Lab-made lipid-shelled MBs	Sonication twice a week for 3 weeks
Zhang *et al*., 2018[108]	Curcumin	MPTP mouse	Lab-made US device; 60s	Corpus striatum in medial forebrain bundle (MFB)	Lab-made lipid-shelled MBs	1 sonication every 2 days for 4 times
Xhima *et al*., 2018[114]	shRNA against α-synuclein	Transgenic mouse overexpression α-synuclein gene	Lab-made US device; 10 ms bursts, 1 Hz PRF, for 120 s	Hippocampus, substantia nigra, olfactory bulb, and dorsal motor nucleus)	Definity® MBs (0.02 mL/kg)	1 sonication
Yue *et al*., 2018[106]	GDNF	6-OHDA rat	Lab-made US device; 1 MHz, DC 20%, 2 W/cm^2 intensity	Right substantia nigra	Lab-made lipid-shelled MBs (0.01 mL/kg)	Once every 3 days, sacrificed at 3 weeks after treatment
Karakatsani *et al*., 2019[109]	GDNF	MPTP mouse	Lab-made US device; 10 Hz PRF, 0.45 MPa, for 60 s	Caudate-putamen and ventral midbrain region	Lab-made lipid-shelled MBs (0.1 μL/g)	1 sonication
Lin *et al*., 2020[110]	BDNF	MPTP mouse	Lab-made US device; 1 MHz, 10 ms burst length, 10 Hz PRF, for 3 min	Substantia nigra	Lab-made lipid-shelled MBs (10 μL)	Sonication twice a week for 3 weeks
Feng *et al*., 2022[113]	Triptolide	Transgenic mouse overexpression α-synuclein gene	Lab-made US device; 10 ms burst length, 1 Hz PRF, 0.3 – 0.8 MPa, for 60 s	Substantia nigra	Lab-made lipid-shelled MBs (100 μL)	Sonication twice a week for 3 weeks
Wang *et al*., 2022[112]	Gastrodin	MPTP mouse	Lab-made US device; 10 ms pulse width, 1 Hz, PRF, for 60 s	Left striatum	SonoVue® MBs (1.125 μL/g)	Sonication once every 3 days for 6 times
Blesa *et al*., 2023[111]	AAV9-hSyn -GFP	6 male macaque monkeys	Lab-made US device; for 60 s	Striatum and midbrain	Luminity® MBs (4 μL/kg/mL, 0.02 mL/s)	1 sonication

Abbreviations: DC: Duty cycle; MB: Microbubble; PRF: Pulse repetition frequency; US: Ultrasound; BDNF: brain-derived neurotrophic factor.

three treatment sessions every 2 weeks over 5 weeks. GCase was administered at escalating doses (15, 30, and 60 lU/kg) through i.v. infusion over 1 h, followed by the infusion of Definity® MBs (4 μL/kg/5 min). US waves were applied using the ExAblate Neuro® MRgFUS system (10 ms pulses, DC 1%, 0.5 MPa, for 2 min). The efficacy of acoustically mediated BBB opening was monitored using DCE-MRI. Motor performance was evaluated between treatments and 1, 3, and 6 months post-treatment, with 18F-FDG PET imaging and mental examination performed 1 month and 3 months after the final treatment. Results supported the safety and feasibility of this approach. BBB opening facilitated the targeted delivery of GCase, leading to reduced putaminal hypermetabolism 1 month after treatment, reflecting improved striatal dopaminergic metabolism, as well as significant improvement in movement disorders in PD patients (Table 7).

7. Applications in ALS

7.1. ALS

ALS, also known as Charcot's disease, is a neurodegenerative disease that affects both upper and lower motor neurons (UMN and LMN) in the motor cortex, brainstem, and spinal cord. This degeneration is irreversible and progressive, leading to a relentless decline in motor functions. The prevalence of ALS is approximatively 1 – 2/100,000 individuals and the incidence is 6 – 8/100,000 people/year.[76,122] ALS manifests in different forms depending on the location of the

Table 7. Drug delivery with MB-assisted US for clinical studies in Parkinson's disease

References	Drug, Dye, Particle	Patients	US devices/ parameters	Targeted area	MBs	Therapy duration
Gasca-Salas *et al.*, 2021[117]	Gadolinium	5 patients	ExAblate Neuro® MRgFUS system	Right parieto-occipito-temporal cortex	Luminity® MBs (4 µL/kg)	2 sonications separated by 2 – 3 weeks
Pineda-Pardo *et al.*, 2022[118]	Gadolinium	7 patients	ExAblate Neuro® MRgFUS system	Posterior putamen	Luminity® MBs (4 µL/kg)	2 sonications separated by 2 – 4 weeks
Huang *et al.*, 2022[120]	Glucocerebrosidase (GCase)	4 patients with GBA1 mutations	ExAblate Neuro® MRgFUS system; 10 ms pulses, DC 1%, 0.5 MPa, for 2 min	Putamen	Definity® MBs (4 µL/kg/5 min)	1 sonication every 2 weeks for a total of 3 sonications
Meng *et al.*, 2022[121]	Glucocerebrosidase (GCase)	4 patients with GBA1 mutations	ExAblate Neuro® MRgFUS system; 10 ms pulses, DC 1%, 0.5 MPa, for 2 min	Putamen	Definity® MBs (4 µL/kg/ 5 min)	1 sonication every 2 weeks for a total of 3 sonications
Gasca-Salas *et al.*, 2024[119]	Gadolinium	3 patients	ExAblate Neuro® MRgFUS system	Substantia nigra and putamen	Luminity® MBs (2.5 mL/min)	2 sonications separated by 2 – 3 weeks

Abbreviations: DC: Duty cycle; MB: Microbubble; MRgFUS: Magnetic resonance imaging-guided focused ultrasound; US: Ultrasound.

initial symptoms: (1) bulbar-onset ALS, characterized by dysarthria and dysphagia; (2) spinal-onset ALS, marked by spasticity, muscle weakness, and progressive atrophy of the limbs. About 90% of ALS cases are sporadic, while 10% are familial, involving at least two affected family members. Up to 50% of ALS patients experience cognitive and/or behavioral impairments, and 13% develop frontotemporal lobar dementia.[123]

To date, more than 30 causal genes have been implicated in the disease.[124,125] The most frequently involved genes are *C9ORF72*, Superoxide dismutase 1 (*SOD1*), *TARDBP* (TDP-43), and *FUS*. A key neuropathological hallmark of ALS is the accumulation and aggregation of TDP-43 in the cytoplasm of motor neurons, which is observed in nearly all ALS patients. However, it remains unclear how pathogenic variants in different genes converge to result in the same TDP-43 aggregation.[126] The pathophysiology of ALS involved multiple mechanisms, including neuroinflammation, glutamate-mediated excitotoxicity, oxidative stress, mitochondrial dysfunction, and alterations in mRNA metabolism and protein homeostasis.[126-128] These processes represent critical targets for the development of therapeutic molecules aimed a mitigating the disease's progression.[129-131]

7.2. Pre-clinical phase

Recently, Shen *et al.*[132] explored the use of edaravone in the *SOD1*^{G93A} mouse model of ALS, leveraging the MB-assisted US for enhancing drug delivery. SOD1 is a key antioxidant enzyme that protects cells from the deleterious effects of superoxide radicals. Dysfunction or aggregation of SOD1 protein contributes to the pathogenesis of ALS. The *SOD1*^{G93A} transgenic mouse model typically develops severe motor impairments by approximately 120 days of age and succumbs to the disease around 160 days.[133] In this study, Shen *et al.* targeted the motor cortex of *SOD1*^{G93A} mice with a US sequence (1.1 MHz, 1 Hz PRF, 9.09 ms burst length, 0.52 MPa) for 60 s using a lab-made US device after an i.v. injection of lab-made lipid-shelled MBs (0.2 µL/g). The treatment involved four intermittent, non-overlapping FUS exposures, with a 15-min interval between each application. Edaravone was administered alternately through i.v. and intraperitoneal routes (15 mg/kg) every 2 days, starting when the mice were 13 weeks old, for a duration of 6 weeks. The results demonstrated that the MB-assisted US achieved a two-fold increase in edaravone concentration within the motor cortex compared to the control condition. This acoustically mediated drug delivery significantly improved neuromuscular function and reduced muscle atrophy compared to ALS mice treated with edaravone without US. Importantly no tissue damage was observed, underscoring the safety of this approach. This proof-of-concept study highlights the potential of MB-assisted US for targeted drug delivery in the treatment of ALS (Table 8).[132]

7.3. Clinical phase

At present, a single clinical trial is investigating the feasibility, reversibility, and safety of transient BBB opening using transcranial MRgFUS in ALS patients.[76] Abrahao *et al.*[76] targeted the primary motor cortex, specifically the precentral gyrus, marking the first attempt to target subcortical white matter regions in humans. The study involved four right-handed participants (two women and

two men, with a median age of 61 years), assigned to either the arm ($n = 2$) or leg ($n = 2$) target groups based on which limb exhibited greater weakness on the left side. On the day of the experiment, patients temporarily discontinued their usual ALS treatment (riluzole or edaravone) but resumed them immediately after the procedure. Definity® MBs (4 μL/kg) were administered intravenously, followed by exposure of the target region to US waves (center frequency: 220 kHz) using the ExAblate Neuro® 4000 system. An acoustic power ramp test was conducted, followed by one to two 90-s sonication cycles to achieve BBB opening. During each cycle, the targeted brain tissue received a US sequence (center frequency of 220 kHz, pulse repetition period of 300 ms, DC 0.88%) for each of the four spots within the target region. Each cycle coincided with an i.v. injection of MBs. Abrahao *et al.,* successfully demonstrated the transient and safe acoustically mediated BBB opening in ALS patients. Importantly, no serious adverse effects (i.e., hemorrhage, edema, inflammation, or tissue damage) were observed 30- or 60-day post-treatment.

However, to date, no study has explored whether combining the US with therapeutic molecules could improve motor symptoms in ALS. Similarly, research on the therapeutic impact of US/therapeutic molecule combinations in AD and PD has yet to address symptom improvement comprehensively. This promising clinical trial lays the foundation for further investigations into MB-assisted US for therapeutic delivery in ALS treatment (Table 9).[76]

8. Applications in Huntington's disease (HD)

8.1. HD

HD, also known as Huntington's chorea, is a progressive dominantly inherited neurodegenerative disorder. Its prevalence is 5 – 10/100,000 in North America and Europe, with a higher rate observed in Western Europe.[136] The disease typically begins between the fourth to fifth decades of life and progressively worsens over 10 – 20 years, ultimately leading to death; however, it can also manifest before the age of 20.[136-138]

HD is characterized by a combination of psychiatric, cognitive, and motor symptoms. Clinical signs include involuntary movement disorders (e.g., chorea and dystonia) and voluntary movement impairments (e.g., clumsiness, dysarthria, swallowing disorders, falls, bradykinesia, rigidity). Cognitive impairments often involve issues with memory, attention, judgment, reasoning, and comprehension, with dementia frequently developing over time. The hallmark symptom of HD is Huntington's chorea, which involves involuntary jerking and muscle twitching.

Neuropathological findings reveal significant neurodegeneration, with the selective loss of neurons in the caudate and putamen of the basal ganglia. The disease is caused by an abnormal expansion of a CAG trinucleotide repeat in the coding region of the *HTT* gene.[137] This mutation leads to an expanded polyglutamine stretch in the N-terminal region of the Huntingtin protein, resulting in a toxic gain of function.[134,136] Despite the clear understanding of the genetic basis of HD, no curative treatment is currently available. Existing therapeutic approaches focus primarily on managing chorea, but several novel treatments are under active investigation.[103,139,140]

8.2. Pre-clinical phase

Despite the lack of a clinically approved treatment for HD, promising pharmacological approaches aimed at reducing HTT protein levels have been explored to increase neuronal

Table 8. Drug delivery with MB-assisted US for pre-clinical studies in amyotrophic lateral sclerosis

References	Drug, dye, particle	Animal model	US devices/parameters	Targeted area	MBs	Therapy duration
Shen *et al.*, 2023[132]	Edaravone	*SOD1*^{G93A} mouse	Lab-made US device; 1.1 MHz, 1 Hz PRF, 9.09 ms burst length, 0.52 MPa for 60 s	Motor cortex	Lab-made lipid-shelled MBs (0.2 μL/g)	4 intermittent non-overlapping sonication with a 15-min interval between each other

Abbreviations: DC: Duty cycle; MB: Microbubble; PRF: Pulse repetition frequency; US: Ultrasound.

Table 9. Drug delivery with MB-assisted US for clinical studies in amyotrophic lateral sclerosis

References	Drug, Dye, Particle	Patients	US devices/parameters	Targeted area	MBs	Therapy duration
Abrahao *et al.*, 2019[76]	Gadolinium	2 women and 2 men	ExAblate Neuro® 4000 system; center frequency of 220 kHz, pulse repetition period of 300 ms, DC of 0.88% for 90 s	Primary motor cortex	Definity® MBs (4 μL/kg)	1 sonication

Abbreviations: DC: Duty cycle; MB: Microbubble; US: Ultrasound.

survival and improve motor functions.[141] To date, there are three pre-clinical studies and no clinical trials investigating i.c. drug delivery using MB-assisted US for HD. Burgess *et al.*[134] examined the therapeutic potential of delivering cholesterol-conjugated anti-Htt siRNA (cc-siRNA-Htt) into the striatum of an HD mouse model through MB-assisted US (lab-made MRgFUS device; center frequency of 558 kHz, burst length of 10 ms, PRF of 1 Hz, 0.3 MPa). Definity® MBs (0.02 mL/kg) were administered intravenously, followed by immediate US exposure to the striatum for 120 s. Then, cc-siRNA-Htt was injected through either a tail vein catheter or an intra-carotid catheter. BBB opening was monitored using DCE-MRI. This protocol involved two US exposures separated by a 1-h interval, and the mice were sacrificed 48 h later. The results demonstrated that MRgFUS successfully delivered the cc-siRNA-Htt to the striatum, resulting in a significant 32% reduction in *Htt* gene expression, regardless of the route of administration.[134] However, this pre-clinical study did not assess whether the enhanced bioavailability of cc-siRNA-Htt led to increased neuronal survival or improved motor functions in HD mice.

In another study, Lin *et al.*[115] utilized the MB-assisted US to boost i.c. production of GDNF in the R6/2 mouse model of HD. A liposomal formulation of GDNF-encoding pDNA was administered intravenously, followed by the injection of SonoVue® MBs (0.1 mg/kg). The striatum was then exposed to a US sequence (lab-made US device; 1Hz PRF, 10 ms burst length, DC 1%, 0.33 MPa) for 30 s in the contralateral hemisphere and for 60 s in the ipsilateral hemisphere. This approach significantly increased i.c. GDNF protein levels, enhancing neuronal plasticity and cell numbers. It also delayed symptom onset and improved motor impairments in the treated group compared to the control group.[115] Similarly, Owusu-Yaw *et al.*[135] investigated the efficacy of MB-assisted US for the delivery of an AAV9 viral vector encoding the miR10150, a microRNA targeting HTT transcripts for degradation, along with green fluorescent protein (GFP) as a reporter gene. Following the i.v. injection of Optison® MBs (100 µL/kg), US waves (1 Hz, 10 ms, 0.34 MPa) were applied to the striatum (right caudate putamen) of zQ175 mice for 120 s using a lab-made US device. The AAV9 viral vectors were administered intravenously immediately after US exposure. Analysis of GFP expression in brain tissue confirmed the feasibility and efficiency of MB-assisted US for delivering AAV9 viral vector in both HD and wild-type mice at ages 2, 6, and 12 months. However, Owusu-Yaw *et al.* did not evaluate the i.c. production of miR10150 or its therapeutic benefit (Table 10).

Altogether, these findings demonstrate that MB-assisted US is a promising modality for the delivery of therapeutics in the treatment of HD.

9. Discussion

Accessing the brain for drug delivery remains a significant challenge in the treatment of neurodegenerative diseases. BBB opening is a rapidly expanding field, as evidenced by the growing number of publications on this topic. This method first emerged in the early 2000s with Hynynen's publications on BBB disruption in a rabbit model,[26] and a new momentum has been achieved thanks to advances in the understanding of the mechanisms and composition of MB/ND, the development of new transducer models, and the emergence of clinically approved devices in the 2010s. Many pre-clinical studies have demonstrated the safety, feasibility, and reversibility of opening the BBB. Among these, two studies have focused on the delivery of gadolinium in animal models of neurodegenerative diseases,[63,87] while others have investigated the delivery of therapeutic molecules to assess their effects on behavior.[112,115,132] A few

Table 10. Drug delivery with MB-assisted US for pre-clinical studies in Huntington's disease

References	Drug, dye, particle	Animal model	US devices/parameters	Targeted area	MBs	Therapy duration
Burgess *et al.*, 2012[134]	cc-siRNA-Htt	Rat	Lab-made MRgFUS device; center frequency of 558 kHz, burst length of 10 ms, 1 Hz PRF, 0.3 MPa	Striatum	Definity® MBs (0.02 mL/kg)	2 sonications at 1-h interval
Lin *et al.*, 2019[115]	GDNF	R6/2 mouse	Lab-made US device; 1Hz PRF, 10 ms burst length, DC 1%, 0.33 MPa for 30s at the contralateral hemisphere and for 60s	Striatum	SonoVue® MBs (0.1 mg/kg)	1 sonication
Owusu-Yaw *et al.*, 2024[135]	AAV9 viral vector encoding the microRNA, miR10150	zQ175 mouse	Lab-made US device; 1 Hz, 10 ms, 0.34 MPa for 120 s	Striatum	Optison® MBs (100 µL/kg)	1 sonication, sacrifice 3 weeks later

Abbreviations: DC: Duty cycle; MB: Microbubble; MRgFUS: Magnetic resonance imaging-guided focused ultrasound; PRF: Pulse repetition frequency; US: Ultrasound.

studies achieved both objectives, with most demonstrating enhanced i.c. delivery of therapeutics and improvements in cognitive functions. There is a notable preference for using MRgFUS in pre-clinical studies; however, the majority has been conducted on small animals, primarily rodents such as mice and rats. Only one study to date has utilized a large animal model, specifically a non-human primate, within the context of PD.[111] Expanding pre-clinical research to include large animals could significantly enhance the understanding of BBB opening and lend greater weight to the results. In addition, rodent models, whether transgenic or induced through neurotoxic lesions such as MPTP or 6-OHDA, have inherent limitations, posing challenges in interpreting results and extrapolating findings to humans.

Compared to pre-clinical trials, most clinical studies involving BBB disruption do not focus on drug delivery. Instead, they primarily assess the feasibility, safety, and reproducibility of BBB opening in patients with neurodegenerative disease.[74,76,119] Notably, one study in PD investigated glucocerebrosidase (GCase),[120,121] while another in AD evaluated the delivery of aducanumab.[96] These recent studies are promising for the advancement of BBB opening techniques in neurodegenerative diseases. However, all clinical trials conducted thus far have involved a very small number of participants, typically ranging from 3 to 9, which is surprising given the high prevalence of these conditions. To reliably evaluate the efficacy of therapeutics in humans, future studies need to include larger patient cohorts to determine whether BBB opening significantly enhances therapeutic effects compared to treatment alone. It is worth noting that no standardized treatment exists for neurodegenerative diseases, and therapeutic responses vary widely among patients. If a significant effect is not observed with BBB opening, it may not necessarily reflect a limitation of the technique but rather resistance to the treatment itself. Future studies should therefore not only focus on the feasibility of the technology but also prioritize clinical outcomes such as preserving memory, cognition, or motor functions in patients with neurodegenerative diseases.

One of the key challenges in slowing the progression of these diseases lies in their neurobiological characteristics. Diseases such as PD and ALS are more localized, whereas conditions, such as AD are diffusive. Targeted diseases are seemingly easier to treat, as neurodegeneration is confined to a specific or limited region in the brain, allowing the US to be focused on these areas. In contrast, treating diffuse diseases is more complex, as all affected regions would require treatment with FUS.

There is also a noticeable preference for clinically approved devices in this field. For instance, the NaviFUS® system has not been used in clinical trials for neurodegenerative diseases and has only been used for brain tumors, such as glioblastoma.[72,142] Similarly, the SonoCloud® system has only been tested in one clinical trial for AD as of 2022.[69] ExAblate Neuro® remains the most widely used system, including in a pre-clinical trial involving a non-human primate.[111] The non-invasive nature of MRgFUS and its relatively short intervention times (2 – 4 h) make it an attractive option for research. However, its use entails significant logistical challenges, particularly due to the reliance on MRI. An MRI system must be on-site, available for the procedure, and operated by experienced personnel, all of which contribute to the high costs associated with this approach.

A major limitation across these studies is the variation in protocols. Both in the pre-clinical and clinical phases, the use of MBs/NDs, US devices, and parameters lack consistency, resulting in limited reproducibility between studies. Differences are evident in the type of MBs used (i.e., lab-made, SonoVue®, Definity®, Optison®, and Sonazoid®) as well as in their method of administration. MBs are sometimes injected as a bolus and at other times as an infusion. O'Reilly *et al.*[143] compared BBB disruption *in vivo* using a long infusion (2 min) versus a bolus injection (15 s) of Definity® MBs at the same dose. Their findings revealed better BBB disruption with bolus injection, attributed to the higher peak concentration of MBs in the circulation during bolus administration. The method of administering therapeutics alongside MBs also varies. In clinical practice, sequential administration – infusion of the therapeutic treatment followed by bolus injection and sonication – is often preferred for the convenience of both healthcare staff and patients.[96,121] This method is similarly adopted in pre-clinic phases, with MBs typically administered as a bolus rather than an infusion. Additional protocol variations include the use of loaded or unloaded MBs, as well as targeted versus non-targeted MBs. At present, there is insufficient data to compare the therapeutic efficacy of drug-loaded versus unloaded MBs in neurodegenerative diseases. Few pre-clinical studies explore this comparison, and no drug-loaded MBs have been clinically approved, making such comparisons impossible in clinical trials.

Another challenge is the small sample size in clinical trials, which limits the ability to draw rigorous or generalized conclusions about the therapeutic efficacy of molecules delivered through sonoporation. In pre-clinical studies, researchers often use ab-made MBs, allowing greater flexibility in loading or tagging MBs. In contrast, clinical trials must use clinically approved MBs, which restricts this flexibility. Beyond MB characteristics, US parameters also vary widely between studies. Sonication duration may range from 30 s to 2 min, with acoustic

pressure varying between 0.4 MPa and 0.5 MPa. Parameters such as time, acoustic pressure, and frequency are tailored to each study. Pre-clinical protocols further differ across research laboratories, often due to the use of lab-made US devices. The number of sonication session also varies, with some studies employing a single treatment while others span 3 weeks with 2 sessions per week, for example. Despite these variations, all methods demonstrate success in BBB opening, suggesting the need for standardized protocols. It would be beneficial to establish defined parameters tailored to specific species (e.g., mice, rats, non-human primates, and humans) and target areas (e.g., striatum, motor cortex, hippocampus).

Regarding NDs, only one pre-clinical study has employed them for BBB opening in neurodegenerative diseases.[62] One reason for this limited use is the relative novelty of NDs, which are still being optimized despite the known advantages of ADV since 1998.[44] In addition, no NDs are clinically approved, making their use in clinical settings impossible. The greater familiarity and clinical approval of MBs make them a more accessible option. Nonetheless, studies using NDs have validated BBB opening in wild-type animals, such as with dextran in mice[57] and Evan's blue in rats.[108] Chen *et al.*[57] demonstrated that NDs are more effective than MBs in delivering drugs. While only one study has used NDs for neurodegenerative diseases (specifically AD[62]), other studies have focused on cancer therapy. These include *in vivo* studies on ovarian cancer,[144] hepatocellular carcinoma,[145] and glaucoma,[146] as well as anticancer drug delivery (lung and breast cancer cells)[147] and *in vitro* studies on breast and lung cancer.[148] These studies have shown significant tumor progression slowdown.

10. Conclusion

MB/ND-assisted US offers a promising approach for improving the i.c. delivery of therapeutic molecules by enabling BBB opening in both animal models and humans. While the studies reviewed here focus primarily on neurodegenerative diseases, this approach could also be applied to other conditions requiring barrier-crossing treatments. This approach holds great promise for advancing patient care by providing less invasive alternatives in the future.

Acknowledgments

None.

Funding

We would like to thank the Agence Nationale de la Recherche (ANR) for funding (ANR-22-CE19-0031) and the Région Centre-Val de Loire for the funding of PhD students (K.E.).

Conflict of interest

The authors declare no conflict of interest.

Author contributions

Conceptualization: Karen Ea, Patrick Vourc'h, Jean- Michel Escoffre

Writing – original draft: Karen Ea, Patrick Vourc'h, Jean-Michel Escoffre

Writing – review & editing: Nicolas Taulier, Christiane Contino-Pépin, Wladimir Urbach, Stéphane Desgranges, Hélène Blasco, Yara Al-Ojaimi, Philippe Corcia

Ethics approval and consent to participate

Not applicable.

Consent for publication

Not applicable.

Availability of data

Not applicable.

References

1. *Maladies Neurologiques : Une Approche Intégrée*. Available from: https://www.elsevier.com/fr-fr/connect/les-maladies-neurodegeneratives-et-maladies-apparentees-en-pratique [Last accessed on 2024 Sep 11].

2. Abbott NJ, Rönnbäck L, Hansson E. Astrocyte-endothelial interactions at the blood-brain barrier. *Nat Rev Neurosci*. 2006;7(1):41-53.

   doi: 10.1038/nrn1824

3. Abbott NJ, Patabendige AAK, Dolman DEM, Yusof SR, Begley DJ. Structure and function of the blood-brain barrier. *Neurobiol Dis*. 2010;37(1):13-25.

   doi: 10.1016/j.nbd.2009.07.030

4. Pardridge WM. The blood-brain barrier: Bottleneck in brain drug development. *NeuroRx*. 2005;2(1):3-14.

   doi: 10.1602/neurorx.2.1.3

5. Hawkins BT, Davis TP. The blood-brain barrier/ neurovascular unit in health and disease. *Pharmacol Rev*. 2005;57(2):173-185.

   doi: 10.1124/pr.57.2.4

6. Löscher W, Potschka H. Blood-brain barrier active efflux transporters: ATP-binding cassette gene family. *NeuroRx*. 2005;2(1):86-98.

   doi: 10.1602/neurorx.2.1.86

7. Mizee MR, Nijland PG, van der Pol SMA, *et al*. Astrocyte-derived retinoic acid: A novel regulator of blood-brain barrier function in multiple sclerosis. *Acta Neuropathol*. 2014;128(5):691-703.

doi: 10.1007/s00401-014-1335-6

8. Korczyn AD. Vascular parkinsonism--characteristics, pathogenesis and treatment. *Nat Rev Neurol*. 2015;11(6):319-326.

doi: 10.1038/nrneurol.2015.61

9. Drouin-Ouellet J, Sawiak SJ, Cisbani G, *et al*. Cerebrovascular and blood-brain barrier impairments in Huntington's disease: Potential implications for its pathophysiology. *Ann Neurol*. 2015;78(2):160-177.

doi: 10.1002/ana.24406

10. Wijesuriya HC, Bullock JY, Faull RLM, Hladky SB, Barrand MA. ABC efflux transporters in brain vasculature of Alzheimer's subjects. *Brain Res*. 2010;1358:228-238.

doi: 10.1016/j.brainres.2010.08.034

11. Palmer AM. The role of the blood-CNS barrier in CNS disorders and their treatment. *Neurobiol Dis*. 2010;37(1):3-12.

doi: 10.1016/j.nbd.2009.07.029

12. Alarcan H, Al Ojaimi Y, Lanznaster D, *et al*. Taking advantages of blood-brain or spinal cord barrier alterations or restoring them to optimize therapy in ALS? *J Pers Med*. 2022;12(7):1071.

doi: 10.3390/jpm12071071

13. Pardridge WM, Boado RJ. Reengineering biopharmaceuticals for targeted delivery across the blood-brain barrier. *Methods Enzymol*. 2012;503:269-292.

doi: 10.1016/B978-0-12-396962-0.00011-2

14. Chacko AM, Li C, Pryma DA, Brem S, Coukos G, Muzykantov V. Targeted delivery of antibody-based therapeutic and imaging agents to CNS tumors: Crossing the blood-brain barrier divide. *Expert Opin Drug Deliv*. 2013;10(7):907-926.

doi: 10.1517/17425247.2013.808184

15. Han L. Modulation of the blood-brain barrier for drug delivery to brain. *Pharmaceutics*. 2021;13(12):2024.

doi: 10.3390/pharmaceutics13122024

16. Al Ojaimi Y, Blin T, Lamamy J, *et al*. Therapeutic antibodies - natural and pathological barriers and strategies to overcome them. *Pharmacol Ther*. 2022;233:108022.

doi: 10.1016/j.pharmthera.2021.108022

17. Piper K, Kumar JI, Domino J, Tuchek C, Vogelbaum MA. Consensus review on strategies to improve delivery across the blood-brain barrier including focused ultrasound. *Neuro Oncol*. 2024;26(9):1545-1556.

doi: 10.1093/neuonc/noae087

18. Zhang Y, Liu Q, Zhang X, *et al*. Recent advances in exosome-mediated nucleic acid delivery for cancer therapy. *J Nanobiotechnology*. 2022;20(1):279.

doi: 10.1186/s12951-022-01472-z

19. Bouakaz A, Michel Escoffre J. From concept to early clinical trials: 30 years of microbubble-based ultrasound-mediated drug delivery research. *Adv Drug Deliv Rev*. 2024;206:115199.

doi: 10.1016/j.addr.2024.115199

20. Hynynen K. Focused ultrasound for blood-brain disruption and delivery of therapeutic molecules into the brain. *Expert Opin Drug Deliv*. 2007;4(1):27-35.

doi: 10.1517/17425247.4.1.27

21. Konofagou EE, Tung YS, Choi J, Deffieux T, Baseri B, Vlachos F. Ultrasound-induced blood-brain barrier opening. *Curr Pharm Biotechnol*. 2012;13(7):1332-1345.

doi: 10.2174/138920112800624364

22. Hynynen K, McDannold N, Vykhodtseva N, *et al*. Focal disruption of the blood-brain barrier due to 260-kHz ultrasound bursts: A method for molecular imaging and targeted drug delivery. *J Neurosurg*. 2006;105(3):445-454.

doi: 10.3171/jns.2006.105.3.445

23. Marquet F, Tung YS, Teichert T, Ferrera VP, Konofagou EE. Noninvasive, transient and selective blood-brain barrier opening in non-human primates *in vivo*. *PLoS One*. 2011;6(7):e22598.

doi: 10.1371/journal.pone.0022598

24. McDannold N, Arvanitis CD, Vykhodtseva N, Livingstone MS. Temporary disruption of the blood-brain barrier by use of ultrasound and microbubbles: Safety and efficacy evaluation in rhesus macaques. *Cancer Res*. 2012;72(14):3652-3663.

doi: 10.1158/0008-5472.CAN-12-0128

25. Rapoport N. Drug-loaded perfluorocarbon nanodroplets for ultrasound-mediated drug delivery. *Adv Exp Med Biol*. 2016;880:221-241.

doi: 10.1007/978-3-319-22536-4_13

26. Hynynen K, McDannold N, Vykhodtseva N, Jolesz FA. Noninvasive MR imaging-guided focal opening of the blood-brain barrier in rabbits. *Radiology*. 2001;220(3):640-646.

doi: 10.1148/radiol.2202001804

27. Hynynen K, McDannold N, Vykhodtseva N, Jolesz FA. Non-invasive opening of BBB by focused ultrasound. *Acta Neurochir Suppl*. 2003;86:555-558.

doi: 10.1007/978-3-7091-0651-8_113

28. Ibsen S, Schutt CE, Esener S. Microbubble-mediated ultrasound therapy: A review of its potential in cancer

treatment. *Drug Des Devel Ther*. 2013;7:375-388.

doi: 10.2147/DDDT.S31564

29. Tung YS, Vlachos F, Choi JJ, Deffieux T, Selert K, Konofagou EE. *In vivo* transcranial cavitation threshold detection during ultrasound-induced blood-brain barrier opening in mice. *Phys Med Biol*. 2010;55(20):6141-6155.

doi: 10.1088/0031-9155/55/20/007

30. Bettinger T, Tranquart F. Design of microbubbles for gene/drug delivery. *Adv Exp Med Biol*. 2016;880:191-204.

doi: 10.1007/978-3-319-22536-4_11

31. Becher H, Lofiego C, Mitchell A, Timperley J. Current indications for contrast echocardiography imaging. *Eur J Echocardiogr*. 2005;6(Suppl 2):S1-S5.

doi: 10.1016/s1525-2167(05)80722-x

32. Klibanov AL. Ultrasound molecular imaging with targeted microbubble contrast agents. *J Nucl Cardiol*. 2007;14(6):876-884.

doi: 10.1016/j.nuclcard.2007.09.008

33. McMahon D, O'Reilly MA, Hynynen K. Therapeutic agent delivery across the blood-brain barrier using focused ultrasound. *Annu Rev Biomed Eng*. 2021;23:89-113.

doi: 10.1146/annurev-bioeng-062117-121238

34. Yang FY, Fu WM, Yang RS, Liou HC, Kang KH, Lin WL. Quantitative evaluation of focused ultrasound with a contrast agent on blood-brain barrier disruption. *Ultrasound Med Biol*. 2007;33(9):1421-1427.

doi: 10.1016/j.ultrasmedbio.2007.04.006

35. McDannold N, Vykhodtseva N, Hynynen K. Effects of acoustic parameters and ultrasound contrast agent dose on focused-ultrasound induced blood-brain barrier disruption. *Ultrasound Med Biol*. 2008;34(6):930-937.

doi: 10.1016/j.ultrasmedbio.2007.11.009

36. van Rooy I, Mastrobattista E, Storm G, Hennink WE, Schiffelers RM. Comparison of five different targeting ligands to enhance accumulation of liposomes into the brain. *J Control Release*. 2011;150(1):30-36.

doi: 10.1016/j.jconrel.2010.11.014

37. Kucharz K, Kristensen K, Johnsen KB, *et al*. Post-capillary venules are the key locus for transcytosis-mediated brain delivery of therapeutic nanoparticles. *Nat Commun*. 2021;12(1):4121.

doi: 10.1038/s41467-021-24323-1

38. Shpak O, Verweij M, de Jong N, Versluis M. Droplets, Bubbles and ultrasound interactions. *Adv Exp Med Biol*. 2016;880:157-174.

doi: 10.1007/978-3-319-22536-4_9

39. Chen H, Konofagou EE. The size of blood-brain barrier opening induced by focused ultrasound is dictated by the acoustic pressure. *J Cereb Blood Flow Metab*. 2014;34(7):1197-1204.

doi: 10.1038/jcbfm.2014.71

40. Schutt EG, Klein DH, Mattrey RM, Riess JG. Injectable microbubbles as contrast agents for diagnostic ultrasound imaging: The key role of perfluorochemicals. *Angew Chem Int Ed Engl*. 2003;42(28):3218-3235.

doi: 10.1002/anie.200200550

41. Klibanov AL. Microbubble contrast agents: Targeted ultrasound imaging and ultrasound-assisted drug-delivery applications. *Invest Radiol*. 2006;41(3):354-362.

doi: 10.1097/01.rli.0000199292.88189.0f

42. Solans C, Izquierdo P, Nolla J, Azemar N, Garcia-Celma MJ. Nano-emulsions. *Curr Opin Colloid Interface Sci*. 2005;10(3):102-110.

doi: 10.1016/j.cocis.2005.06.004

43. Rapoport N, Nam KH, Gupta R, *et al*. Ultrasound-mediated tumor imaging and nanotherapy using drug loaded, block copolymer stabilized perfluorocarbon nanoemulsions. *J Control Release*. 2011;153(1):4-15.

doi: 10.1016/j.jconrel.2011.01.022

44. Apfel RE. *Activatable Infusable Dispersions Containing Drops of Superheated Liquid for Methods of Therapy and Diagnosis*. Patent Number: 5,840,276; 1998

45. Kripfgans OD, Fowlkes JB, Miller DL, Eldevik OP, Carson PL. Acoustic droplet vaporization for therapeutic and diagnostic applications. *Ultrasound Med Biol*. 2000;26(7):1177-1189.

doi: 10.1016/s0301-5629(00)00262-3

46. Vlatakis S, Zhang W, Thomas S, *et al*. Effect of phase-change nanodroplets and ultrasound on blood-brain barrier permeability *in vitro*. *Pharmaceutics*. 2023;16(1):51.

doi: 10.3390/pharmaceutics16010051

47. Wasielewska JM, White AR. Focused ultrasound-mediated drug delivery in humans - a path towards translation in neurodegenerative diseases. *Pharm Res*. 2022;39(3):427-439.

doi: 10.1007/s11095-022-03185-2

48. Song R, Zhang C, Teng F, *et al*. Cavitation-facilitated transmembrane permeability enhancement induced by acoustically vaporized nanodroplets. *Ultrason Sonochem*. 2021;79:105790.

doi: 10.1016/j.ultsonch.2021.105790

49. Husseini GA, Diaz de la Rosa MA, Richardson ES, Christensen DA, Pitt WG. The role of cavitation in acoustically activated drug delivery. *J Control Release*. 2005;107(2):253-261.

doi: 10.1016/j.jconrel.2005.06.015

50. Meijering BDM, Juffermans LJM, van Wamel A, *et al*.

Ultrasound and microbubble-targeted delivery of macromolecules is regulated by induction of endocytosis and pore formation. *Circ Res*. 2009;104(5):679-687.

doi: 10.1161/CIRCRESAHA.108.183806

51. Tran TA, Roger S, Le Guennec JY, Tranquart F, Bouakaz A. Effect of ultrasound-activated microbubbles on the cell electrophysiological properties. *Ultrasound Med Biol*. 2007;33(1):158-163.

doi: 10.1016/j.ultrasmedbio.2006.07.029

52. Sheikov N, McDannold N, Vykhodtseva N, Jolesz F, Hynynen K. Cellular mechanisms of the blood-brain barrier opening induced by ultrasound in presence of microbubbles. *Ultrasound Med Biol*. 2004;30(7):979-989.

doi: 10.1016/j.ultrasmedbio.2004.04.010

53. Sheeran PS, Matsuura N, Borden MA, *et al*. Methods of generating submicrometer phase-shift perfluorocarbon droplets for applications in medical ultrasonography. *IEEE Trans Ultrason Ferroelectr Freq Control*. 2017;64(1):252-263.

doi: 10.1109/TUFFC.2016.2619685

54. Ramesh R, Thimonier C, Desgranges S, *et al*. Acoustic droplet vaporization of perfluorohexane emulsions induced by heterogeneous nucleation at an ultrasonic frequency of 1.1 MHz. *Langmuir*. 2023;39(44):15716-15729.

doi: 10.1021/acs.langmuir.3c02272

55. Zhou Y. Application of acoustic droplet vaporization in ultrasound therapy. *J Ther Ultrasound*. 2015;3:20.

doi: 10.1186/s40349-015-0041-8

56. Almarghalani DA, Boddu SHS, Ali M, *et al*. Small interfering RNAs based therapies for intracerebral hemorrhage: Challenges and progress in drug delivery systems. *Neural Regen Res*. 2022;17(8):1717-1725.

doi: 10.4103/1673-5374.332129

57. Chen CC, Sheeran PS, Wu SY, Olumolade OO, Dayton PA, Konofagou EE. Targeted drug delivery with focused ultrasound-induced blood-brain barrier opening using acoustically-activated nanodroplets. *J Control Release*. 2013;172(3):795-804.

doi: 10.1016/j.jconrel.2013.09.025

58. Maghsoudinia F, Akbari-Zadeh H, Aminolroayaei F, Birgani FF, Shanei A, Samani RK. Ultrasound responsive Gd-DOTA/doxorubicin-loaded nanodroplet as a theranostic agent for magnetic resonance image-guided controlled release drug delivery of melanoma cancer. *Eur J Pharm Sci*. 2022;174:106207.

doi: 10.1016/j.ejps.2022.106207

59. Amir N, Green D, Kent J, *et al*. ^{18}F-Labeled perfluorocarbon droplets for positron emission tomography imaging. *Nucl Med Biol*. 2017;54:27-33.

doi: 10.1016/j.nucmedbio.2017.07.001

60. Cheng X, Li H, Chen Y, *et al*. Ultrasound-triggered phase transition sensitive magnetic fluorescent nanodroplets as a multimodal imaging contrast agent in rat and mouse model. *PLoS One*. 2013;8(12):e85003.

doi: 10.1371/journal.pone.0085003

61. Kong C, Yang EJ, Shin J, *et al*. Enhanced delivery of a low dose of aducanumab via FUS in 5×FAD mice, an AD model. *Transl Neurodegener*. 2022;11(1):57.

doi: 10.1186/s40035-022-00333-x

62. Gouveia FV, Lea-Banks H, Aubert I, Lipsman N, Hynynen K, Hamani C. Anesthetic-loaded nanodroplets with focused ultrasound reduces agitation in Alzheimer's mice. *Ann Clin Transl Neurol*. 2023;10(4):507-519.

doi: 10.1002/acn3.51737

63. Choi JJ, Wang S, Brown TR, Small SA, Duff KEK, Konofagou EE. Noninvasive and transient blood-brain barrier opening in the hippocampus of Alzheimer's double transgenic mice using focused ultrasound. *Ultrason Imaging*. 2008;30(3):189-200.

doi: 10.1177/016173460803000304

64. Zhang DY, Dmello C, Chen L, *et al*. Ultrasound-mediated delivery of paclitaxel for glioma: A comparative study of distribution, toxicity, and efficacy of albumin-bound versus cremophor formulations. *Clin Cancer Res*. 2020;26(2):477-486.

doi: 10.1158/1078-0432.CCR-19-2182

65. Ahmed MH, Hernández-Verdin I, Quissac E, *et al*. Low-intensity pulsed ultrasound-mediated blood-brain barrier opening increases anti-programmed death-ligand 1 delivery and efficacy in Gl261 mouse model. *Pharmaceutics*. 2023;15(2):455.

doi: 10.3390/pharmaceutics15020455

66. Carpentier A, Canney M, Vignot A, *et al*. Clinical trial of blood-brain barrier disruption by pulsed ultrasound. *Sci Transl Med*. 2016;8(343):343re2.

doi: 10.1126/scitranslmed.aaf6086

67. Idbaih A, Canney M, Belin L, *et al*. Safety and feasibility of repeated and transient blood-brain barrier disruption by pulsed ultrasound in patients with recurrent glioblastoma. *Clin Cancer Res*. 2019;25(13):3793-3801.

doi: 10.1158/1078-0432.CCR-18-3643

68. Sonabend AM, Gould A, Amidei C, *et al*. Repeated blood-brain barrier opening with an implantable ultrasound device for delivery of albumin-bound paclitaxel in patients with recurrent glioblastoma: A phase 1 trial. *Lancet Oncol*. 2023;24(5):509-522.

doi: 10.1016/S1470-2045(23)00112-2

69. Epelbaum S, Burgos N, Canney M, *et al*. Pilot study of repeated blood-brain barrier disruption in patients with mild Alzheimer's disease with an implantable ultrasound device. *Alzheimers Res Ther*. 2022;14(1):40.

doi: 10.1186/s13195-022-00981-1

70. Wei KC, Chu PC, Wang HYJ, *et al*. Focused ultrasound-induced blood-brain barrier opening to enhance temozolomide delivery for glioblastoma treatment: A preclinical study. *PLoS One*. 2013;8(3):e58995.

doi: 10.1371/journal.pone.0058995

71. Chen KT, Wei KC, Liu HL. Focused ultrasound combined with microbubbles in central nervous system applications. *Pharmaceutics*. 2021;13(7):1084.

doi: 10.3390/pharmaceutics13071084

72. Chen KT, Lin YJ, Chai WY, *et al*. Neuronavigation-guided focused ultrasound (NaviFUS) for transcranial blood-brain barrier opening in recurrent glioblastoma patients: Clinical trial protocol. *Ann Transl Med*. 2020;8(11):673.

doi: 10.21037/atm-20-344

73. Huang Y, Hynynen K. MR-guided focused ultrasound for brain ablation and blood-brain barrier disruption. *Methods Mol Biol*. 2011;711:579-593.

doi: 10.1007/978-1-61737-992-5_30

74. Lipsman N, Meng Y, Bethune AJ, *et al*. Blood-brain barrier opening in Alzheimer's disease using MR-guided focused ultrasound. *Nat Commun*. 2018;9(1):2336.

doi: 10.1038/s41467-018-04529-6

75. Mainprize T, Lipsman N, Huang Y, *et al*. Blood-brain barrier opening in primary brain tumors with non-invasive MR-guided focused ultrasound: A clinical safety and feasibility study. *Sci Rep*. 2019;9(1):321.

doi: 10.1038/s41598-018-36340-0

76. Abrahao A, Meng Y, Llinas M, *et al*. First-in-human trial of blood-brain barrier opening in amyotrophic lateral sclerosis using MR-guided focused ultrasound. *Nat Commun*. 2019;10(1):4373.

doi: 10.1038/s41467-019-12426-9

77. Soria Lopez JA, González HM, Léger GC. Alzheimer's disease. *Handb Clin Neurol*. 2019;167:231-255.

doi: 10.1016/B978-0-12-804766-8.00013-3

78. Wimo A, Winblad B, Aguero-Torres H, von Strauss E. The magnitude of dementia occurrence in the world. *Alzheimer Dis Assoc Disord*. 2003;17(2):63-67.

doi: 10.1097/00002093-200304000-00002

79. Cummings J, Lee G, Ritter A, Sabbagh M, Zhong K. Alzheimer's disease drug development pipeline: 2020. *Alzheimers Dement* (*N Y*). 2020;6(1):e12050.

doi: 10.1002/trc2.12050

80. Choi JJ, Pernot M, Small SA, Konofagou EE. Noninvasive, transcranial and localized opening of the blood-brain barrier using focused ultrasound in mice. *Ultrasound Med Biol*. 2007;33(1):95-104.

doi: 10.1016/j.ultrasmedbio.2006.07.018

81. Burns S, Selman A, Sehar U, Rawat P, Reddy AP, Reddy PH. Therapeutics of Alzheimer's disease: Recent developments. *Antioxidants* (*Basel*). 2022;11(12):2402.

doi: 10.3390/antiox11122402

82. Khan T, Waseem R, Shahid M, *et al*. Recent advancement in therapeutic strategies for Alzheimer's disease: Insights from clinical trials. *Ageing Res Rev*. 2023;92:102113.

doi: 10.1016/j.arr.2023.102113

83. Raymond SB, Treat LH, Dewey JD, McDannold NJ, Hynynen K, Bacskai BJ. Ultrasound enhanced delivery of molecular imaging and therapeutic agents in Alzheimer's disease mouse models. *PLoS One*. 2008;3(5):e2175.

doi: 10.1371/journal.pone.0002175

84. Liu Y, Gong Y, Xie W, *et al*. Microbubbles in combination with focused ultrasound for the delivery of quercetin-modified sulfur nanoparticles through the blood brain barrier into the brain parenchyma and relief of endoplasmic reticulum stress to treat Alzheimer's disease. *Nanoscale*. 2020;12(11):6498-6511.

doi: 10.1039/c9nr09713a

85. Sun T, Shi Q, Zhang Y, *et al*. Focused ultrasound with anti-pGlu3 Aβ enhances efficacy in Alzheimer's disease-like mice via recruitment of peripheral immune cells. *J Control Release*. 2021;336:443-456.

doi: 10.1016/j.jconrel.2021.06.037

86. Bathini P, Sun T, Schenk M, Schilling S, McDannold NJ, Lemere CA. Acute effects of focused ultrasound-induced blood-brain barrier opening on anti-pyroglu3 A beta antibody delivery and immune responses. *Biomolecules*. 2022;12(7):951.

doi: 10.3390/biom12070951

87. Burgess A, Dubey S, Yeung S, *et al*. Alzheimer disease in a mouse model: MR imaging-guided focused ultrasound targeted to the hippocampus opens the blood-brain barrier and improves pathologic abnormalities and behaviour. *Radiology*. 2014;273(3):736-745.

doi: 10.1148/radiol.14140245

88. Jordão JF, Ayala-Grosso CA, Markham K, *et al*. Antibodies targeted to the brain with image-guided focused ultrasound reduces amyloid-beta plaque load in the TgCRND8 mouse model of Alzheimer's disease. *PLoS One*. 2010;5(5):e10549.

doi: 10.1371/journal.pone.0010549

89. Dubey S, Heinen S, Krantic S, *et al*. Clinically approved

IVIg delivered to the hippocampus with focused ultrasound promotes neurogenesis in a model of Alzheimer's disease. *Proc Natl Acad Sci U S A*. 2020;117(51):32691-32700.

doi: 10.1073/pnas.1908658117

90. Antoniou A, Stavrou M, Evripidou N, *et al*. FUS-mediated blood-brain barrier disruption for delivering anti-Aβ antibodies in 5XFAD Alzheimer's disease mice. *J Ultrasound*. 2024;27(2):251-262.

doi: 10.1007/s40477-023-00805-4

91. Nisbet RM, Van der Jeugd A, Leinenga G, Evans HT, Janowicz PW, Götz J. Combined effects of scanning ultrasound and a tau-specific single chain antibody in a tau transgenic mouse model. *Brain*. 2017;140(5):1220-1230.

doi: 10.1093/brain/awx052

92. Janowicz PW, Leinenga G, Götz J, Nisbet RM. Ultrasound-mediated blood-brain barrier opening enhances delivery of therapeutically relevant formats of a tau-specific antibody. *Sci Rep*. 2019;9(1):9255.

doi: 10.1038/s41598-019-45577-2

93. Bajracharya R, Cruz E, Götz J, Nisbet RM. Ultrasound-mediated delivery of novel tau-specific monoclonal antibody enhances brain uptake but not therapeutic efficacy. *J Control Release*. 2022;349:634-648.

doi: 10.1016/j.jconrel.2022.07.026

94. Mehta RI, Carpenter JS, Mehta RI, *et al*. Blood-brain barrier opening with mri-guided focused ultrasound elicits meningeal venous permeability in humans with early Alzheimer disease. *Radiology*. 2021;298(3):654-662.

doi: 10.1148/radiol.2021200643

95. Rezai AR, Ranjan M, D'Haese PF, *et al*. Noninvasive hippocampal blood-brain barrier opening in Alzheimer's disease with focused ultrasound. *Proc Natl Acad Sci U S A*. 2020;117(17):9180-9182.

doi: 10.1073/pnas.2002571117

96. Rezai AR, D'Haese PF, Finomore V, *et al*. Ultrasound blood-brain barrier opening and aducanumab in Alzheimer's disease. *N Engl J Med*. 2024;390(1):55-62.

doi: 10.1056/NEJMoa2308719

97. Götz J, Padmanabhan P. Ultrasound and antibodies - a potentially powerful combination for Alzheimer disease therapy. *Nat Rev Neurol*. 2024;20(5):257-258.

doi: 10.1038/s41582-024-00943-1

98. Bae S, Liu K, Pouliopoulos AN, *et al*. Transcranial blood-brain barrier opening in Alzheimer's disease patients using a portable focused ultrasound system with real-time 2-D cavitation mapping. *medRxiv* [Preprint]. 2024.

doi: 10.1101/2023.12.21.23300222

99. Hayes MT. Parkinson's disease and parkinsonism. *Am J Med*. 2019;132(7):802-807.

doi: 10.1016/j.amjmed.2019.03.001

100. Tysnes OB, Storstein A. Epidemiology of Parkinson's disease. *J Neural Transm* (*Vienna*). 2017;124(8):901-905.

doi: 10.1007/s00702-017-1686-y

101. Beitz JM. Parkinson's disease: A review. *Front Biosci* (*Schol Ed*). 2014;6(1):65-74.

doi: 10.2741/s415

102. Reich SG, Savitt JM. Parkinson's disease. *Med Clin North Am*. 2019;103(2):337-350.

doi: 10.1016/j.mcna.2018.10.014

103. Pérez-Arancibia R, Cisternas-Olmedo M, Sepúlveda D, Troncoso-Escudero P, Vidal RL. Small molecules to perform big roles: The search for Parkinson's and Huntington's disease therapeutics. *Front Neurosci*. 2022;16:1084493.

doi: 10.3389/fnins.2022.1084493

104. Prasad EM, Hung SY. Current therapies in clinical trials of Parkinson's disease: A 2021 update. *Pharmaceuticals* (*Basel*). 2021;14(8):717.

doi: 10.3390/ph14080717

105. Fan CH, Ting CY, Lin CY, *et al*. Noninvasive, targeted, and non-viral ultrasound-mediated GDNF-plasmid delivery for treatment of Parkinson's disease. *Sci Rep*. 2016;6:19579.

doi: 10.1038/srep19579

106. Yue P, Miao W, Gao L, Zhao X, Teng J. Ultrasound-triggered effects of the microbubbles coupled to GDNF plasmid-loaded PEGylated liposomes in a rat model of Parkinson's disease. *Front Neurosci*. 2018;12:222.

doi: 10.3389/fnins.2018.00222

107. Lin CY, Hsieh HY, Chen CM, *et al*. Non-invasive, neuron-specific gene therapy by focused ultrasound-induced blood-brain barrier opening in Parkinson's disease mouse model. *J Control Release*. 2016;235:72-81.

doi: 10.1016/j.jconrel.2016.05.052

108. Zhang N, Yan F, Liang X, *et al*. Localized delivery of curcumin into brain with polysorbate 80-modified cerasomes by ultrasound-targeted microbubble destruction for improved Parkinson's disease therapy. *Theranostics*. 2018;8(8):2264-2277.

doi: 10.7150/thno.23734

109. Karakatsani ME, Wang S, Samiotaki G, *et al*. Amelioration of the nigrostriatal pathway facilitated by ultrasound-mediated neurotrophic delivery in early Parkinson's disease. *J Control Release*. 2019;303:289-301.

doi: 10.1016/j.jconrel.2019.03.030

110. Lin CY, Lin YC, Huang CY, Wu SR, Chen CM, Liu HL. Ultrasound-responsive neurotrophic factor-loaded

microbubble- liposome complex: Preclinical investigation for Parkinson's disease treatment. *J Control Release*. 2020;321:519-528.

doi: 10.1016/j.jconrel.2020.02.044

111. Blesa J, Pineda-Pardo JA, Inoue KI, *et al*. BBB opening with focused ultrasound in nonhuman primates and Parkinson's disease patients: Targeted AAV vector delivery and PET imaging. *Sci Adv*. 2023;9(16):eadf4888.

doi: 10.1126/sciadv.adf4888

112. Wang Y, Luo K, Li J, *et al*. Focused ultrasound promotes the delivery of gastrodin and enhances the protective effect on dopaminergic neurons in a mouse model of Parkinson's disease. *Front Cell Neurosci*. 2022;16:884788.

doi: 10.3389/fncel.2022.884788

113. Feng Y, An R, Zhang Y, *et al*. AHNAK-modified microbubbles for the intracranial delivery of triptolide: *In-vitro* and *in-vivo* investigations. *Int J Pharm*. 2022;629:122351.

doi: 10.1016/j.ijpharm.2022.122351

114. Xhima K, Nabbouh F, Hynynen K, Aubert I, Tandon A. Noninvasive delivery of an α-synuclein gene silencing vector with magnetic resonance-guided focused ultrasound. *Mov Disord*. 2018;33(10):1567-1579.

doi: 10.1002/mds.101

115. Lin CY, Tsai CH, Feng LY, *et al*. Focused ultrasound-induced blood brain-barrier opening enhanced vascular permeability for GDNF delivery in Huntington's disease mouse model. *Brain Stimul*. 2019;12(5):1143-1150.

doi: 10.1016/j.brs.2019.04.011

116. Lin CY, Huang CY, Chen CM, Liu HL. Focused ultrasound-induced blood-brain barrier opening enhanced α-synuclein expression in mice for modeling Parkinson's disease. *Pharmaceutics*. 2022;14(2):444.

doi: 10.3390/pharmaceutics14020444

117. Gasca-Salas C, Fernández-Rodríguez B, Pineda-Pardo JA, *et al*. Blood-brain barrier opening with focused ultrasound in Parkinson's disease dementia. *Nat Commun*. 2021;12(1):779.

doi: 10.1038/s41467-021-21022-9

118. Pineda-Pardo JA, Gasca-Salas C, Fernández-Rodríguez B, *et al*. Striatal blood-brain barrier opening in Parkinson's disease dementia: A pilot exploratory study. *Mov Disord*. 2022;37(10):2057-2065.

doi: 10.1002/mds.29134

119. Gasca-Salas C, Pineda-Pardo JA, Del Álamo M, *et al*. Nigrostriatal blood-brain barrier opening in Parkinson's disease. *J Neurol Neurosurg Psychiatry*. 2024;95:1089-1092.

doi: 10.1136/jnnp-2023-332967

120. Huang Y, Meng Y, Pople CB, *et al*. Cavitation feedback control of focused ultrasound blood-brain barrier opening for drug delivery in patients with Parkinson's disease. *Pharmaceutics*. 2022;14(12):2607.

doi: 10.3390/pharmaceutics14122607

121. Meng Y, Pople CB, Huang Y, *et al*. Putaminal recombinant glucocerebrosidase delivery with magnetic resonance-guided focused ultrasound in Parkinson's disease: A phase I study. *Mov Disord*. 2022;37(10):2134-2139.

doi: 10.1002/mds.29190

122. Lu H, Le WD, Xie YY, Wang XP. Current therapy of drugs in amyotrophic lateral sclerosis. *Curr Neuropharmacol*. 2016;14(4):314-321.

doi: 10.2174/1570159x14666160120152423

123. Hardiman O, Al-Chalabi A, Chio A, *et al*. Amyotrophic lateral sclerosis. *Nat Rev Dis Primers*. 2017;3:17071.

doi: 10.1038/nrdp.2017.71

124. Al-Chalabi A, Andrews J, Farhan S. Recent advances in the genetics of familial and sporadic ALS. *Int Rev Neurobiol*. 2024;176:49-74.

doi: 10.1016/bs.irn.2024.04.007

125. Van Daele SH, Moisse M, van Vugt JJFA, *et al*. Genetic variability in sporadic amyotrophic lateral sclerosis. *Brain*. 2023;146(9):3760-3769.

doi: 10.1093/brain/awad120

126. Nijs M, Van Damme P. The genetics of amyotrophic lateral sclerosis. *Curr Opin Neurol*. 2024;37(5):560-569.

doi: 10.1097/WCO.0000000000001294

127. Maurel C, Dangoumau A, Marouillat S, *et al*. Causative genes in amyotrophic lateral sclerosis and protein degradation pathways: A link to neurodegeneration. *Mol Neurobiol*. 2018;55(8):6480-6499.

doi: 10.1007/s12035-017-0856-0

128. Bradford D, Rodgers KE. Advancements and challenges in amyotrophic lateral sclerosis. *Front Neurosci*. 2024;18:1401706.

doi: 10.3389/fnins.2024.1401706

129. Corcia P, Lunetta C, Vourc'h P, Pradat PF, Blasco H. Time for optimism in amyotrophic lateral sclerosis. *Eur J Neurol*. 2023;30(5):1459-1464.

doi: 10.1111/ene.15738

130. Sun Z, Zhang B, Peng Y. Development of novel treatments for amyotrophic lateral sclerosis. *Metab Brain Dis*. 2024;39(3):467-482.

doi: 10.1007/s11011-023-01334-z

131. Wei Y, Zhong S, Yang H, *et al*. Current therapy in amyotrophic lateral sclerosis (ALS): A review on past and future therapeutic strategies. *Eur J Med Chem*.

2024;272:116496.

doi: 10.1016/j.ejmech.2024.116496

132. Shen Y, Zhang J, Xu Y, *et al*. Ultrasound-enhanced brain delivery of edaravone provides additive amelioration on disease progression in an ALS mouse model. *Brain Stimul*. 2023;16(2):628-641.

doi: 10.1016/j.brs.2023.03.006

133. Peggion C, Scalcon V, Massimino ML, *et al*. SOD1 in ALS: Taking stock in pathogenic mechanisms and the role of glial and muscle cells. *Antioxidants* (*Basel*). 2022;11(4):614.

doi: 10.3390/antiox11040614

134. Burgess A, Huang Y, Querbes W, Sah DW, Hynynen K. Focused ultrasound for targeted delivery of siRNA and efficient knockdown of Htt expression. *J Control Release*. 2012;163(2):125-129.

doi: 10.1016/j.jconrel.2012.08.012

135. Owusu-Yaw BS, Zhang Y, Garrett L, *et al*. Focused ultrasound-mediated disruption of the blood-brain barrier for AAV9 delivery in a mouse model of Huntington's disease. *Pharmaceutics*. 2024;16(6):710.

doi: 10.3390/pharmaceutics16060710

136. Vonsattel JP, DiFiglia M. Huntington disease. *J Neuropathol Exp Neurol*. 1998;57(5):369-384.

doi: 10.1097/00005072-199805000-00001

137. A novel gene containing a trinucleotide repeat that is expanded and unstable on Huntington's disease chromosomes. The Huntington's Disease Collaborative Research Group. *Cell*. 1993;72(6):971-983.

doi: 10.1016/0092-8674(93)90585-e

138. Rosenblatt A. Neuropsychiatry of Huntington's disease. *Dialogues Clin Neurosci*. 2007;9(2):191-197.

doi: 10.31887/DCNS.2007.9.2/arosenblatt

139. Saade J, Mestre TA. Huntington's disease: Latest frontiers in therapeutics. *Curr Neurol Neurosci Rep*. 2024;24(8):255-264.

doi: 10.1007/s11910-024-01345-y

140. Singh K, Jain D, Sethi P, *et al*. Emerging pharmacological approaches for Huntington's disease. *Eur J Pharmacol*. 2024;980:176873.

doi: 10.1016/j.ejphar.2024.176873

141. DiFiglia M, Sena-Esteves M, Chase K, *et al*. Therapeutic silencing of mutant huntingtin with siRNA attenuates striatal and cortical neuropathology and behavioral deficits. *Proc Natl Acad Sci U S A*. 2007;104(43):17204-17209.

doi: 10.1073/pnas.0708285104

142. Chen KT, Chai WY, Lin YJ, *et al*. Neuronavigation-guided focused ultrasound for transcranial blood-brain barrier opening and immunostimulation in brain tumors. *Sci Adv*. 2021;7(6):eabd0772.

doi: 10.1126/sciadv.abd0772

143. O'Reilly MA, Waspe AC, Ganguly M, Hynynen K. Focused-ultrasound disruption of the blood-brain barrier using closely-timed short pulses: Influence of sonication parameters and injection rate. *Ultrasound Med Biol*. 2011;37(4):587-594.

doi: 10.1016/j.ultrasmedbio.2011.01.008

144. Baghbani F, Moztarzadeh F. Bypassing multidrug resistant ovarian cancer using ultrasound responsive doxorubicin/curcumin co-deliver alginate nanodroplets. *Colloids Surf B Biointerfaces*. 2017;153:132-140.

doi: 10.1016/j.colsurfb.2017.01.051

145. Yang T, Ming X, Jie L, *et al*. Ultrasound-triggered nanodroplets for targeted co-delivery of sorafenib/doxorubicin for hepatocellular carcinoma therapy. *J Biomed Nanotechnol*. 2019;15(9):1881-1896.

doi: 10.1166/jbn.2019.2823

146. Silverman RH, Urs R, Burgess M, Ketterling JA, Tezel G. High-frequency ultrasound activation of perfluorocarbon nanodroplets for treatment of glaucoma. *IEEE Trans Ultrason Ferroelectr Freq Control*. 2022;69(6):1910-1916.

doi: 10.1109/TUFFC.2022.3142679

147. Cao Y, Chen Y, Yu T, *et al*. Drug release from phase-changeable nanodroplets triggered by low-intensity focused ultrasound. *Theranostics*. 2018;8(5):1327-1339.

doi: 10.7150/thno.21492

148. Lee JY, Crake C, Teo B, *et al*. Ultrasound-enhanced siRNA delivery using magnetic nanoparticle-loaded chitosan-deoxycholic acid nanodroplets. *Adv Healthc Mater*. 2017;6(8):1601246.

doi: 10.1002/adhm.201601246

ACCSCIENCE PUBLISHING

Journal of Clinical and Translational Research

REVIEW ARTICLE

A comprehensive review of clinical advances in the antifibrotic role of micro-RNA in pneumonia and pulmonary fibrosis

Bhaskar Pal[1,2*], Said Afredi[1], Krishan Maity[3], and Kushal Roychoudhuri[1]

[1]Department of Pharmaceutical Technology, Charaktala College of Pharmacy, Debipur, West Bengal, India

[2]Department of Pharmaceutical Technology, Maulana Abul Kalam Azad University of Technology, Kolkata, West Bengal, India

[3]Department of Pharmaceutical Technology, Bengal College of Pharmaceutical Science and Research, Durgapur, West Bengal, India

Abstract

Background: Pneumonia is a common respiratory infection affecting millions of people worldwide and often leads to serious complications such as pulmonary fibrosis – a progressive disorder recognized by persistent scarring, alveolar thickening, impaired gas exchange, and reduced lung capacity. The pathogenesis of pulmonary fibrosis remains complex and poorly understood. A hallmark feature is the buildup of extracellular matrix disrupting the normal architecture and function of the lung parenchyma, ultimately causing irreversible lung damage. At present, there is no known remedy for pulmonary fibrosis, and the existing treatments are often limited in efficacy and associated with adverse effects. This underscores the urgent need to identify novel molecular targets and therapeutic approaches for this debilitating condition. **Aim:** This review summarizes recent advances in understanding the pharmacotherapeutic potential of microRNAs (miRNAs) in reducing fibrosis associated with pneumonia and pulmonary fibrosis. It highlights the signaling mechanisms through which miRNAs regulate gene expression, as well as their role in maintaining lung development and homeostasis. The review also identifies the specific miRNAs with antifibrotic effects as demonstrated in experimental models and clinical settings. Finally, it discusses the key challenges in developing miRNA-based therapies, including delivery strategies and off-target effects. **Methods:** The study entailed a thorough literature review on antifibrotic effect of mi-RNA in pneumonia and lung fibrosis, conducted through the electronic searches on Google, Google Scholar, and PubMed databases. **Results:** In his study we provide a recent finding on antifibrotic activity of miRNA in pulmonary complications. Moreover, the evidences from animal and clinical researches are also discussed. This may further help scholars, practitioners, and legislators who are interested to do the research on mi-RNA therapies in clinical practice. **Conclusion:** In conclusion, miRNA-based diagnostics and therapies represent a promising frontier for the management of pneumonia and pulmonary fibrosis. Further research is warranted to deepen our understanding of miRNA mechanisms in the therapeutic context. **Relevance for patients:** Advances in therapies for pneumonia and pulmonary fibrosis can enhance treatment efficacy, aiding in the mitigation and treatment of the disease.

Keywords: Pneumonia; Pulmonary fibrosis; Myofibroblasts; Pharmacotherapeutics; MicroRNA

***Corresponding author:**
Bhaskar Pal
(palbhaskar96@gmail.com)

Citation: Pal B, Afredi S, Maity K, Roychoudhuri K. A comprehensive review of clinical advances in the antifibrotic role of micro-RNA in pneumonia and pulmonary fibrosis. *J Clin Transl Res*. 2025;11(2):28-40. doi: 10.36922/JCTR025080009

Received: February 17, 2025

Revised: March 5, 2025

Accepted: April 3, 2025

Published online: April 24, 2025

1. Introduction

Diagnosing childhood pneumonia is difficult due to the absence of a universally accepted definition. The term "pneumonia" typically denotes a lower respiratory tract infection (LRTI) characterized by fever, respiratory manifestations, and clinical or radiological evidence of parenchymal engagement. Pathologically, it signifies lung inflammation involving various structures such as the airways, alveoli, connective tissues, visceral pleura, and vasculature. Radiographically, pneumonia is identified by the presence of infiltrates on chest imaging in children exhibiting symptoms of an acute respiratory ailment.[1] Pneumonia is a common condition encountered by emergency and primary care physicians and remains a leading cause of illness and death among children in developing countries. However, new vaccines, antibiotics, and advances in diagnostics and surveillance have reduced mortality rates in developed countries.

It is essential to define several frequently used in the clinical context. "Walking pneumonia" typically refers to school-aged children and young individuals who exhibit both radiographic and clinical indications of pneumonia. However, these individuals experience only mild respiratory symptoms that do not disrupt their daily routines. Typically, *Mycoplasma pneumoniae* is the most commonly associated pathogen with walking pneumonia. Community-acquired pneumonia (CAP) refers to acute lung infections acquired outside hospital settings, whereas hospital-acquired pneumonia develops within 48 h of hospital admission. The latter also includes pneumonia in residents of long-term care homes and those who have recently undergone surgery. Although not exclusive to older children, the incidence of pneumonia increases between the ages of 5 and 20 years.[2,3] Most cases occur in isolation, but further investigation reveals that other family members suffer from the same disease and symptoms appear 1 – 3 weeks apart, consistent with the typical incubation period. *Legionella pneumophila* is considered the most virulent strain, causing rapid and severe illness. The incubation period generally ranges from 4 to 6 days but may extend up to 28 days. Transmission typically occurs through inhalation of infectious aerosol generated from water mist sources.[4]

Idiopathic pulmonary fibrosis (IPF), a common type of interstitial lung disease, is a chronic, progressive, and usually fatal condition, with a median survival of only 3 – 5 years. In the United States, no treatment has been conclusively proven effective; however, pirfenidone has been approved for use in Europe, Canada, and Japan.[5] IPF is most common in middle-aged and older males, with a prevalence of 14 – 42.7 cases/100,000 people. Pulmonary fibrosis may be triggered by environmental exposures, such as asbestos, silica, and ionizing radiation, as well as by connective tissue disorders and specific drugs. IPF's root etiology, however, remains largely unknown.[6] A number of lung insults – including toxic, autoimmune, drug-induced, viral, or traumatic damage – can lead to pulmonary fibrosis. It represents an exaggerated tissue response to injury. Host response factors such as age, genetic susceptibility, and environmental factors may influence disease development.[7] MicroRNAs (miRNAs) are tiny RNA molecules that do not code for proteins, though they are crucial in various biological processes and developmental pathways. They are usually about 19 – 25 nucleotides long. miRNA regulates gene expression through post-transcriptional signaling mechanisms, resulting in the repression of target genes. Their mechanism of action is similar to that of endogenous small interfering RNAs.[8] miRNAs are isolated from plants, animals, and viruses through molecular cloning and bioinformatics approaches.[9] Their repressive mechanisms vary. In some cases, miRNA induces mRNA cleavage by attaching to complementary sequences, particularly in the seed region, and then base-pairing in the central region. This targeted degradation based on RNA hydrolysis results in potent gene silencing.[10] miRNAs are a promising field of research due to their involvement in regulating several allergy disorders.[8] Specific miRNAs have been implicated in key pathogenic pathways underlying allergic inflammation, highlighting their potential as novel therapeutic targets.[11] Moreover, extensive studies have revealed miRNAs' dual role in cancer, either by suppressing tumor suppressor genes or by modulating oncogenes.[11] The intricate nature of miRNA-mediated gene expression regulation is also crucial for neuronal development, function, and survival. Most miRNA genes are transcribed by RNA polymerase II, forming a long primary transcript, known as pri-miRNA, which adopts a hairpin structure.[12] Many are encoded within introns of protein-coding genes, though others exist as independent units or within long non-coding RNAs.[12,13] Recent findings suggest that miRNAs act as direct regulators of immune processes contributing to fibrosis. Beyond mRNA regulation, certain miRNAs exhibit cytokine-like behavior and are referred to as "mirokines" due to their immunomodulatory functions.[14]

In this review, we summarize the current understanding of the potential pharmacotherapeutic role of miRNAs in preventing fibrosis, particularly in the context of pneumonia and pulmonary fibrosis. We discuss the molecular mechanisms by which miRNAs modulate the genes and lung homeostasis, highlight miRNAs with demonstrated antifibrotic effect, and address the challenges in developing miRNA-based therapies, including delivery strategies and off-target effects. A deeper understanding of these molecular mechanisms may help medical

practitioners in improving treatment approaches and researchers in developing novel therapeutic strategies.

2. Evidence from current literature

Randomized controlled trials comparing commonly used antibiotics for pneumococci infections with placebo or other classes of antibiotics in children under 18 years with community-acquired LRTI secondary to pneumococci have demonstrated the effectiveness of antibiotics in treating pediatric LRTI.[1] Although atypical pneumonia has been known for more than a century, its main causative pathogens are generally *Chlamydia pneumoniae*, *M. pneumoniae*, and *L. pneumophila*. The atypical pathogens are estimated to account for 22% of pneumonia cases worldwide, with diagnosis largely dependent on laboratory-based identification methods. Therapy with either macrolide antibiotics or fluoroquinolones is recommended, but more data are though further evidence is required to establish optimal treatment strategies. Combination therapy may be considered in severe patients.[4]

Padilla has described IPF as a chronic liver disease characterized by interstitial fibrosis, leading to a progressive decline in respiratory function and shortened life expectancy. Treatment strategies generally range from disease-modifying interventions to symptomatic relief. Significant advances have been made in understanding its pathogenesis, leading to the development of evidence-based therapeutic guidelines.[6] In October 2014, the U.S. Food and Drug Administration approved pirfenidone and nintedanib for the treatment of IPF. These agents provide clinicians with validated therapeutic options, although their use requires careful consideration of safety profiles and monitoring.[15]

Lu and Rothenberg demonstrated that miRNAs – tiny, naturally occurring RNA molecules – play critical roles in post-transcriptional gene regulation. In allergy research, there is a growing interest in miRNAs owing to their potential as biomarkers. miRNA mimics and inhibitors have emerged as promising candidates for innovative therapeutic approaches. Advanced technological tools have been devised for various miRNA-related tasks, including isolation, quantification, profiling, target identification, and manipulation of mRNA levels in both laboratory settings and within living organisms.[8]

miRNAs play a major role in cellular communication by binding to complementary sequences in mRNA, leading to the suppression of protein synthesis. However, their function is more complex than simply turning genes on or off.[10] miRNAs act as post-transcriptional regulators, playing pleiotropic roles in various biological functions and diseases, including cancer.[16] Catalanotto *et al.* highlighted the importance of miRNAs in controlling post-transcriptional gene silencing in an S-S manner. They highlight the vast network of regulatory RNAs formed by the miRNAs with multiple targets, which enables flexible control of mRNA expression, especially in the mammalian nervous system.[17]

Precursor miRNAs are processed in the nucleus and cytoplasm by the endoribonucleases Drosha and Dicer. The modulation of mature miRNA levels is essential for physiological processes such as development, differentiation, and disease pathogenesis. Post-transcriptional mechanisms include both cis-acting sequences in precursor miRNAs and trans-acting factors that interact with these precursors, affecting their processing. RNA-binding proteins (RBPs) play the principal role in controlling the processing of miRNAs. Recent investigations suggest that innate immune responses, particularly involving estrogen-mediated signaling pathways, may contribute significantly to systemic lupus erythematosus (SLE). Estrogen has been shown to lower the activation threshold of immune cells and boost the expression of toll-like receptor 8 (TLR8). Notably, miR-21 has been detected in exosomes derived from SLE patient serum and *in vitro* experiments have shown that pseudoexosomes can stimulate immune cells to increase TLR8 expression.[13]

3. Biogenesis of miRNA

miRNAs are typically located in the exonic or intronic regions of protein-coding genes, as well as in intergenic areas. Their production begins with transcription mediated by RNA polymerase II or III, resulting in a primary transcript called pri-miRNA. These pri-miRNAs usually have a 33-bp hairpin structure, a terminal loop, and a flanking single-stranded sequence. They are also capped at the 5' end and polyadenylated at the 3' end. In the nucleus, the microprocessor complex, consisting of the ribonuclease Drosha and the RBP DGCR8, processes the pri-miRNA by cutting 11 base pairs from the junction of the hairpin stem and single-stranded RNA. This produces a pre-miRNA, which is then transported to the cytoplasm by Exportin-5, a protein that depends on Ran-GTP. In the cytoplasm, the enzyme Dicer further processes the pre-miRNA by cutting near the terminal loop to generate the mature miRNA and its complementary strand (miRNA*) acting as the passenger strand. Other associated proteins, such as HIV-1 TAR RNA-binding protein (TRBP) and protein activator of PKR kinase (PACT), enhance the stability and processing efficiency of Dicer. In plants such as Arabidopsis, miRNA maturation also proceeds in a stepwise fashion, primarily through the action of Dicer-like 1 (DCL1). Other Dicer-like proteins (DCL2, DCL3, and DCL4) contribute to the generation of miRNAs of differing lengths.[18]

After the formation of miRNA duplex (miRNA/miRNA*), the strands separate in an ATP-independent manner. The guide strand of miRNA duplexes is incorporated into the RNA-induced silencing complex (RISC) through the Argonaute (Ago2) protein. The RISC assembly consists of Dicer, TRBP, PACT, and usually a combination of Ago2 and GW182, which stabilizes Ago2. The PAZ and MID domains of Ago protein promote the binding of miRNA to RISC, forming the miRISC complex. The passenger strand (miRNA*) is normally released and destroyed. The choice of the guide strand is influenced by the thermodynamic reliability of the 5' end, which affects AGO binding. Ultimately, miRISC serves as a guide to recognize complementary sequences on target mRNAs, leading to translational repression or mRNA degradation. This post-transcriptional gene silencing involves interactions between Ago2, GW182, cytoplasmic poly(A)-binding protein, and deadenylase complexes such as PAN2 – PAN3 and CCR4 – NOT, all of which contribute to effective miRNA-mediated mRNA silencing.[11]

4. Pathogenesis of pneumonia

Acute pneumonia is an inflammatory disorder that primarily affects the alveoli – the tiny air sacs of the lungs. Pneumonia usually occurs when people at risk are exposed to certain microorganisms, such as bacteria or viruses, though fungi and parasites can also cause the disease. CAP refers to a lung infection with acute infiltrates evident on chest radiographs in patients who have not been hospitalized or admitted to a long-term care facility within the preceding 14 days. In contrast, nosocomial or nosocomial pneumonia (also known as hospital-acquired pneumonia) develops more than 48 h after hospital admission and is not latent at the time of admission. *Streptococcus pneumoniae* is the most commonly identified causative agent for CAP and represents a unique disease spectrum among Gram-positive bacteria. This spectrum is also characteristic of two Gram-negative microorganisms – *Haemophilus influenzae* and *Neisseria meningitidis*. *M. pneumoniae* causes a significant proportion of atypical pneumonia cases and is transmitted by airborne droplets. Although it can affect any age group, it primarily affects young people aged 5 – 20 years. *L. pneumophila* is particularly serious due to its rapid onset and severe clinical course.[4] *Pseudomonas aeruginosa* rarely causes pulmonary disease in healthy individuals, though it is a significant pathogen in immunocompromised hosts, including neonates and patients with human immunodeficiency virus (HIV) infection.[19] Other relevant pathogens include *Staphylococcus aureus*, *Chlamydia psittaci*, *C. pneumoniae*, *Coxiella burnetii*, and *Pneumocystis carinii*, all of which are potential etiological agents of pneumonia.[20]

Many of these pathogens share distinct structural features, such as a rigid surface containing a polysaccharide capsule and phosphorylcholine (Figure 1). They also exhibit unique biological behaviors, including natural DNA transformation and quorum sensing-induced autolysis.[21] The classic lung lesion associated with pneumococcal infection is lobar pneumonia, which typically begins with peribronchial inflammation and progresses to full alveolar involvement. The pathological progression has been divided into four overlapping stages: engorgement, red hepatization, gray hepatization, and resolution.[22] The engorgement phase is marked by congestion of the alveolar capillaries, secretion of serous fluid into the alveolar space (Figure 1), and the existence of pneumococci in this fluid. In the red hepatization phase, continued vascular leakage leads to the accumulation of erythrocytes and macrophages within the alveoli, giving the lung a liver-like appearance. This is followed by gray hepatization, in which white blood cells infiltrate the lesion, and phagocytosis (opsonization) occurs. Grossly, the lung appears gray due to the dissolution of red cells, deposition of fibrin, and collapse of capillaries.[23] The final resolution stage involves the enzymatic breakdown of fibrin and clearance of cellular debris, ultimately restoring normal lung architecture.[21] The characteristic symptoms of pneumonia include cough with purulent sputum, fever, chills, pleuritic chest pain, confusion, headache, dyspnea, or difficulty in breathing.[24]

5. miRNA in the diagnosis of pneumonia

Bronchoalveolar lavage fluid (BALF) can be collected by bronchoscopy-assisted infusion of physiological saline into the alveoli, followed by aspiration under negative pressure. This procedure allows for the acquisition of lower respiratory tract cells and fluid for cytological analysis, microbial culture, and genetic diagnostics. A significant constituent of BALF is exosomes (EXOs), which have emerged as novel intravascular signaling effectors implicated in a number of lung illnesses.[25]

Serum miR-483-3p and miR-29c can be employed as biological markers in the diagnosis of severe pneumonia in children. Blood samples from kids who had *M. pneumoniae*-associated pneumonia showed a lower concentration of miR-1323 compared to healthy controls. Additionally, in whole blood miRNA profiling, the three most upregulated miRNAs – hsa-miR-127-3p, hsa-miR-493-5p, and hsa-miR-409-3p – effectively distinguished between healthy individuals and children with adenovirus-induced pneumonia. Furthermore, miR-146b has been shown to reduce inflammatory injury in pediatric pneumonia by inhibiting the MyD88/NF-κB signaling pathway.[25] miR-181b is both a diagnostic and prognostic biomarker for severe community-acquired pneumonia.[26]

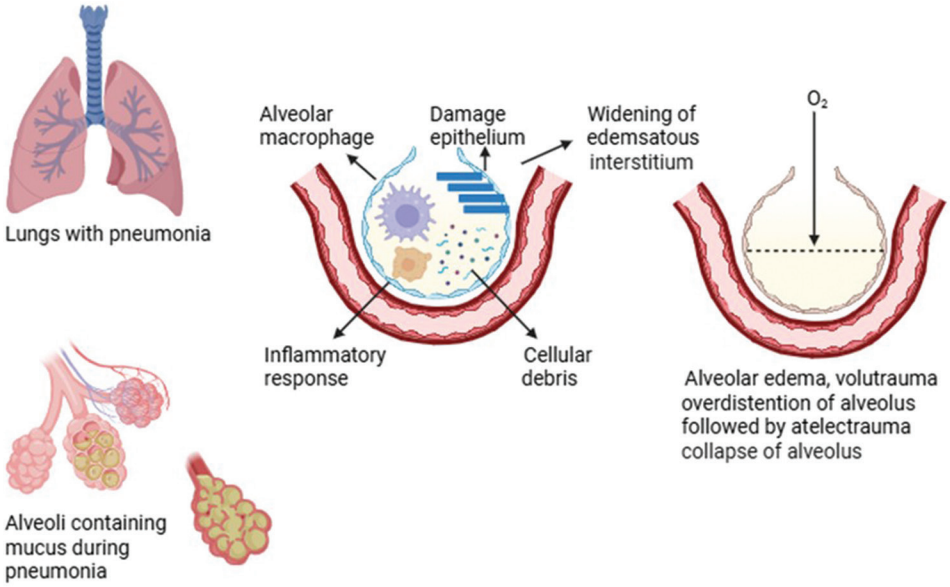

Figure 1. Alveolar alteration in pneumonia. Activation of macrophage and other oxidative stress leads to the release of inflammatory mediators, which further causes epithelial cell damage and cellular debris production. Moreover, during an acute injury in the lungs degradation of the capillary barrier occurs that can cause alveolar edema.[69]

These lines of evidence are established based on the easy fragmentation of free miRNAs in the blood.

6. miRNA in the treatment of pneumonia

Due to their ability to regulate gene expression at the post-transcriptional level, miRNAs play a significant part in the intricate interaction between host and pathogen during infection. To combat pathogen infection, miRNAs function as part of the host immune response. However, they can also collaborate with bacteria to spread the infection further.[27] The identification, defense, and clearance of the host as well as the entry, virulence, and immunological diversion of the pathogen can be regulated by specific miRNAs via inhibition and replacement therapy, according to a number of recent experimental investigations.[28] It has been reported that miRNAs have a role in controlling how pathogen-associated molecular patterns are recognized by TLRs, triggering the early modification of the host's resistance to infection incursion. miRNAs participate in the control of innate and adaptive immunity in the host. They also affect the polarization of macrophages, which in turn impacts the host's ability to clear microbial infections. Moreover, miRNAs regulate bacterial invasion, virulence factor expression, and even host cell apoptosis, thereby enabling bacterial persistence and immune escape.[29]

miRNA-based approaches are frequently employed in the study of bacteria-induced pneumonia. Multiple miRNAs have been identified for their potential in diagnosis, therapy, and prognosis of pneumonia.[30] For instance: in *P. aeruginosa*-induced pneumonia, miR-301b increased the proinflammatory response of the bacterial infection; in *S. pneumoniae*-induced pneumonia, miR-155 increased macrophage phagocytosis; in *K. pneumoniae*-induced pneumonia, miR-155 and miR-23a modulated bacterial adhesion; and in *L. pneumophila*-associated pneumonia, miR-125a-3p controlled bacterial replication. Additionally, miR-302 and miR-221/222 in pneumonia caused by *S. pneumoniae* and lipopolysaccharide, respectively, may encourage the growth of alveolar epithelial cells (AECs). The early and late phases of bacteria-associated infection showed significantly different miR-29b-2-5p expression levels. In the fight against bacteria-associated infection, these two miRNAs served dual regulatory functions.[31] By controlling IL-6, miR-217 may have a significant impact on the onset and progression of interstitial pneumonia. For interstitial pneumonia, this miRNA can be used as a marker for diagnosis and prognosis.[32]

The miRNAs are important targets for understanding the mechanisms of bacteria-induced pneumonia. Overall, several studies highlight the potential of miRNA techniques in the prediction and therapeutic management of bacteria-associated pneumonia, especially for extremely critical cases.[33] Given the significant health risks posed by drug-resistant and refractory bacterial pneumonia, identifying reliable miRNA-based diagnostic and predictive markers could significantly reduce mortality rates. The increasing focus on miRNAs in

pneumonia research reflects their growing importance in pathogenesis elucidation, disease assessment, and therapeutic intervention.[34]

However, most of these research findings were obtained from laboratory experiments. Only a small subset of miRNAs have been examined in clinical trials, with nearly none of them showing substantial improvement and most of them still waiting to be approved. Challenges include low sensitivity and specificity of some miRNA biomarkers, issues related to nucleic acid delivery, *in vivo* stability, cellular uptake, and off-target effects due to hybridization.[31] Overcoming these obstacles – such as improving site-specific intracellular transport and reducing adverse interactions – will be crucial for the widespread use of miRNA-based approaches for the therapeutic management of pneumonia.[31]

7. miRNAs in bacterial infection

In recent years, widespread overuse of antibiotics has significantly contributed to the emergence of bacterial resistance, a problem exacerbated by the stagnation in the development of new antibiotics due to outdated drug discovery methodologies.[35] Thus, serious bacterial infections continue to pose one of the most significant challenges to global public health, highlighting the urgent need for alternative antimicrobial strategies.[36] Recent studies have extensively explored the roles of miRNA in bacterial infections. miRNAs have been found to be crucial in post-transcriptional gene regulation, significantly influencing the interactions between host cells and bacterial pathogens. By regulating the expression of specific genes, miRNAs can affect the host's immune activity and the ability of pathogens to evade or counter that response.[29] These results suggest that miRNAs may serve as potential targets for novel therapeutic approaches and open new avenues for fighting bacterial infections. Developing miRNA-based therapies could provide a means to circumvent traditional antibiotic resistance and improve treatment outcomes for bacterial diseases. Therefore, further research into the role of miRNAs in bacterial infections is essential for the development of these innovative antibacterial strategies.[31]

8. RNA-sequencing and bioinformatics analysis

Recent research has increasingly focused on identifying miRNA biomarkers to facilitate the development of targeted therapy for pneumonia. In an effort to uncover such biomarkers, RNA was extracted from plasma samples of patients classified into three groups: Severe pneumonia (n=9), non-severe pneumonia (n=9), and healthy control (n=9). In this study, 11 significantly differentially expressed miRNAs were identified: six (including hsa-miR-34a and hsa-miR-455) were upregulated and five (including hsa-let-7f-1) were desensitized. These miRs retained their expression patterns in control, non-severe, and severe pneumonia samples.[37] Analysis of predicted differentially expressed miR target genes – such as kalirin (*KALRN*), Ras homolog family member A (*RHOA*), beta-catenin (*CTNNB1*), RNA polymerase II subunit K (*POLR2K*), and amyloid precursor protein (*APP*) – revealed enrichment in pathways associated with adherens junctions and Wnt signaling. Specifically, hsa-miR-200b was identified to target *KALRN*, whereas hsa-let-7f-1 was predicted to target *RHOA*, *CTNNB1*, *POLR2K*, and *APP*. Hsa-let-7f-1 was involved in carcinoma and the Notch signaling mechanisms, indicating its role in the development of pneumonia. Conversely, hsa-miR-455 was found to suppress pneumonia, while hsa-miR-200b was found to promote the development of pneumonia by targeting KALRN. This study identifies potential miRNA biomarkers and therapeutic targets for pneumonia management.[37]

9. Pathogenesis of pulmonary fibrosis

Pulmonary fibrosis represents the terminal stage of several diffuse parenchymal lung diseases and is characterized by extracellular matrix fibrosis, which ultimately leads to the eradication of normal lung architecture and respiratory insufficiency.[38] A key feature of interstitial fibrosis is the deposition of excess extracellular matrix (ECM) components within lung tissues. These include elastic fibers, laminin, fibronectin, and nidogen, with collagens being the most abundant. The most common type of pulmonary fibrosis is IPF, which is characterized by impaired AECs function and stimulation of wound healing signaling pathway in response to lung tissue injury.[39] Immune responses are also implicated in the IPF pathogenesis. The uncontrolled cytokines production (Figure 2) contributes to altered cellular behavior and immune imbalance, promoting a profibrotic microenvironment.[40] The pathogenesis begins with endothelial and epithelial injuries, triggering inflammation and edema. Chemical mediators enter the interstitium of the infected regions, activating fibroblasts. This causes the cells to migrate, proliferate, or generate excess collagen.[39] In patients with pulmonary fibrosis, interleukin concentration in blood, lung tissue, and/or BLF are affected. Interleukin level changes also occur between different stages of pulmonary fibrosis. These changes in interleukin concentration may reflect and influence the inflammatory state and are also useful for evaluating disease progression and severity.[40]

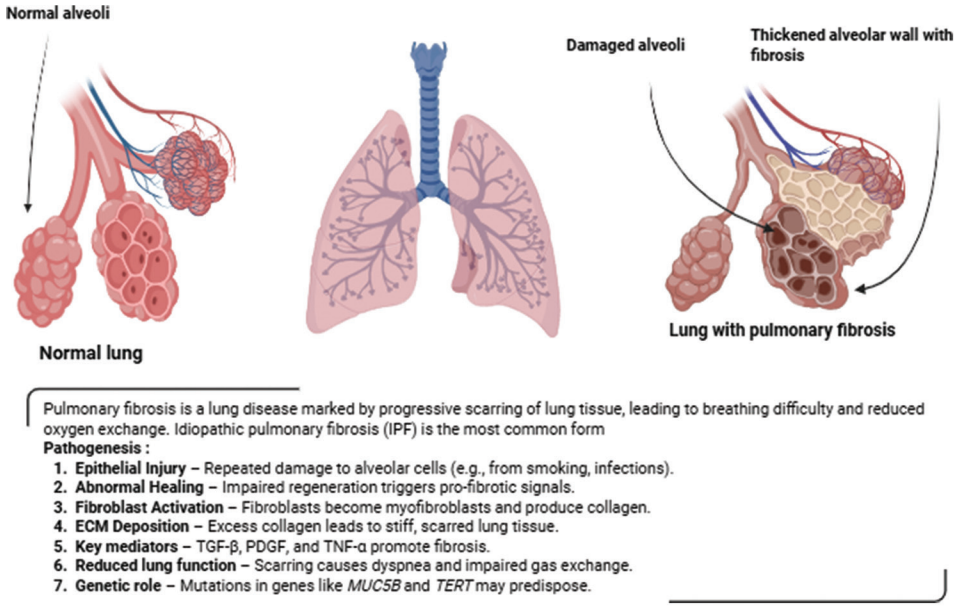

Figure 2. Pathogenic alteration of alveoli in pulmonary fibrosis. Uncontrolled cytokines production, platelet activation, and fibroblast differentiation may result in pulmonary fibrosis. Inflammatory mediators are also triggered by epithelial and endothelial tissue damage. Angiogenesis leads to fibrin reaching clot formation and eventually pulmonary fibrosis.[68]
Abbreviations: MUC5B: Gel-forming mucin protein encoded by MUC5B gene, PDGF: Platelet-derived growth factor, TERT: Telomerase reverse transcriptase, TGF-β; Transforming growth factor beta; TNF-α: Tumor necrosis factor-alpha.

Environmental exposures are significant risk factors for IPF. Epidemiological data reveal strong associations between IPF and cigarette smoke and metal dust exposure, although evidence for a dose-response relationship remains limited.[41] Notably, the harmful effects of smoking persist even after cessation, partly due to its capacity to induce epithelial injury and epigenetic modifications, such as DNA methylation and chromatin remodeling.[42]

Lysophosphatidic acid (LPA) is a growth factor-like phospholipid mediator found in almost all cell types such as epithelial cells, fibroblasts, and stem cells. LPA concentrations were found at elevated levels in the BALFs of IPF patients and they were associated with fibroblast recruitment and vascular leakage.[43] Prostaglandin E2 (PGE2) is a bioactive eicosanoid that regulates many important biological processes. PGE2 signaling has multiple inhibitory effects on lung cells, including limiting fibroblast proliferation, migration, and collagen production, all of which potentially suppress fibrosis. IPF patients often show a reduced production of prostaglandins.[44] Transforming growth factor (TGF)-β, a highly conserved cytokine family, has a significant impact on fibroblasts, contributing to the pathogenesis of pulmonary fibrosis (Figure 2).[28] TGF-β facilitates epithelial cell migration, synthesis of collagen, proliferation of fibroblast, and myofibroblast transdifferentiation.[45]

10. Significance of epithelial-mesenchymal transition (EMT) in the pathology of IPF

EMT is a biological process that plays a vital role during embryonic development and tissue remodeling in adults. However, EMT is also implicated in the pathogenesis of various diseases, including organ fibrosis and cancer.[46] EMT is regulated by key transcription factors such as Snail1/2, ZEB1/2, and members of the basic helix-loop-helix family, which repress epithelial markers such as E-cadherin and activate mesenchymal gene expression. In IPF, subepithelial fibroblast foci near damaged AECs promote aberrant epithelial-mesenchymal interactions, increasing fibroblast proliferation and excessive synthesis of collagen and ECM.[47] The origin and activation of fibroblasts and myofibroblasts in IPF remain controversial. Studies have shown that AECs can transform into myofibroblasts via EMT under the action of TGF-β, with the ECM being a key regulator.[48] EMT contributes to the fibrotic cascade in IPF by altering AEC characteristics – morphology, adhesion, migration, and resistance to apoptosis – while increasing matrix metalloproteinase expression and ECM degradation.[49]

11. miRNA in the diagnosis of IPF

miRNAs are crucial players not only in the biological development and cell differentiation processes but also

in the pathophysiology of IPF. In recent years, miRNA mimics and inhibitors have been explored as potential therapeutic tools for a wide range of human disorders. In the context of lung pathology, many miRNAs have been identified as promising diagnostic biomarkers. For instance, miRNA-320e and miRNA-320c were recognized as candidate biomarkers for diagnosing patients with chronic obstructive pulmonary disease (COPD) at risk of developing lung carcinoma. Moreover, desensitization of miRNA-339-5p and upregulation of miRNA-21 in plasma have shown diagnostic potential for early-stage lung adenocarcinoma. In cases of silica-induced pulmonary fibrosis (SPF), miRNA-19a downregulation can be a useful indicator. The functional variant of miRNA-4508 (rs6576457) may exert a major role in the emergence of SPF and act as a possible marker for diagnosis. However, the molecular mechanisms by which these miRNAs influence disease progression remain to be fully elucidated.[50] In smoking-related pulmonary fibrosis, several circulating miRNAs – miR-125b-5p, miR-20b, miR-128, and miR-30e – were significantly altered in both pulmonary tissue and plasma of mouse models. Forced vital capacity and radiologic tests showed an upregulation of blood miR-21 levels in IPF patients compared to controls and it was linked to severe tissue damage.[51] Reduced miR-30a-5p levels in BALF EXOs may serve as a potential biomarker for IPF diagnosis, while artificially boosting their levels may serve as a potential IPF management strategy.[52]

In addition, few plasma miRNAs were found to be prospective indicators of COPD. Given the significance of miRNAs in IPF, the utilization of miRNAs as possible markers for early disease detection will facilitate the identification and validation of additional circulating miRNAs.[53] Recent studies have even identified miRNA signatures in sputum-derived EXOs that are associated with disease severity in IPF. These composite signatures, comprising several miRNAs, offer promising avenues for non-invasive diagnosis with high specificity and sensitivity.[54]

12. miRNA in the treatment of IPF

Targeting specific miRNAs offers promising therapeutic potential for the treatment of IPF. Theoretically, molecular targeted therapies, such as miRNA-based treatments, can effectively minimize damage to healthy tissue by precisely targeting affected cells. However, before the introduction of miRNA-based treatment for IPF, numerous issues, including their reported flaws, must be resolved.[55,56]

Advances in genome-wide miRNA profiling have provided critical insights into the pathophysiology, prognosis, and potential therapeutic interventions for various human disorders, including IPF. For instance, miR-199a-5p, let-7d, and miR-21 have been identified to play critical roles in pulmonary fibrosis.[57] The importance of dysregulation of miRNAs in the pathology of both silica- and bleomycin-associated lung fibrosis was demonstrated in a study, where the authors discovered a unique miRNA profile for the disease.[58] In mouse fibrotic lung tissues, miR-21, miR-3107, miR-151-3p, miR-455, and miR-486-5p showed differential expression. Furthermore, lung tissue and serum samples of patients with silicosis or IPF showed lower levels of miR-486-5p expression compared to healthy donors.[59] Thus, miR-486-5p might be a key pathogenic factor underpinning the emergence of lung fibrosis. miR-486-5p is produced by processing the intronic RNA derived from the *ANK1* gene. Based on the cell and tissue types, this gene produces either a short (enriched in skeletal and heart muscle) or a long (enriched in erythroid) variant of the acute respiratory distress protein that connects the cytoskeleton to the plasma membrane.[60] Although *ANK1* is conserved across vertebrates, miR-486-5p is highly conserved among mammals but absent in non-mammalian species such as birds and fish. Located on chromosome 8p11, a region frequently deleted in various cancers, miR-486-5p and its counterpart miR-486-3p are involved in tumor suppression.[60] Reduced miR-486-5p expression has been observed in lung, colorectal, melanoma, and gastrointestinal cancers, whereas miR-486-3p dysregulation has been reported in pancreatic and esophageal cancers.[61]

In both animal models and clinical samples, decreased miR-486-5p expression has been associated with pathogenic induction of pulmonary fibrosis. Silica and BLM-associated pulmonary fibrosis animal models showed decreased miR-486-5p expression, similar to the tissue samples from silicosis and IPF patients.[62] Notably, the higher miR-486-5p expression inhibits the TGF-1-associated fibrogenesis in NIH/3T3 cells and reduces pulmonary fibrosis in mice. These results show that miR-486-5p has a potent anti-fibrotic effect in lung tissues and therefore represents a novel pharmacotherapeutic target for the management of pulmonary fibrosis.[59]

Another miRNA of interest is miR-770-5p, which has been found to be significantly downregulated in both silicosis patients and mice exposed to silica. miR-770-5p exhibited *in vivo* anti-fibrotic effects and *in vitro* inhibition of fibroblast activation via suppression of TGF-β1 signaling.[63] Specifically, it targets TGFBR1, a key receptor in the TGF-β/Smad pathway, thereby interfering with fibroblast activation and extracellular matrix deposition. These findings identify the miR-770-5p/TGFBR1/Smads axis as a novel regulatory mechanism in silica-associated pulmonary fibrosis, providing a scientific basis for multi-target therapeutic development.

13. Evidence from human and animal research

Few agents, including bleomycin, silica, and viral vectors, are used to simulate the fibrotic processes observed in human IPF.[64] Each model has distinct advantages and limitations, but among them, the bleomycin-induced model is the most well-characterized and widely utilized model in elucidating molecular mechanisms of fibrogenesis and aiding in therapy development.[65] This model closely resembles human IPF, particularly in collagen deposition and myofibroblast differentiation, making it ideal for studying miRNAs in experimental settings.

The let-7 miRNA family was one of the first to be discovered and has been well-studied in the context of metastasis. Specifically, let-7d was found to be downregulated in IPF lung tissue, and experimental studies using bleomycin-induced models demonstrated that decreased let-7d expression contributed to the suppression of epithelial markers and upregulation of mesenchymal markers, indicating its role in promoting EMT.[66] miR-21, initially identified as an oncogenic miRNA, is significantly upregulated in myofibroblasts and epithelial cells around fibrotic lesions, with antisense probes reducing fibrosis markers in mouse models. The miR-200 family, known to promote EMT in cancer, is downregulated in IPF, with the administration of miR-200c reducing fibrosis in mice.[67] Similarly, miR-154, a component of highly expressed miRNA cluster in IPF lungs, has been shown to exhibit profibrotic activity in *in vitro* assay.[68] Other miRNAs with confirmed involvement in IPF pathogenesis include: miR-29 family (exhibits therapeutic potential), miR-29b (gene transfer prevents fibrosis in mice), miR-375, miR-199-5p (overexpressed in fibrotic lesions; downregulated in IPF), the miR-17~92 cluster (downregulated in IPF), miR-145, miR-326, miR-96, miR-30a/d, miR-92, miR-26a, miR-210, and miR-98.[51]

14. Clinical use of miRNAs in pulmonary infections

Extracellular miRNAs (ex-miRNAs) are promising biomarkers for infectious diseases because they are present in body fluids and can be quantified by real-time PCR, a method already used in clinical practice.[69] A comprehensive review of 57 studies investigated ex-miRNAs in infectious diseases, such as hepatitis B, hepatitis C, HIV, and tuberculosis, using mainly serum and plasma samples, though cerebrospinal fluid, saliva, and sputum were also explored.[27] Most studies compared the miRNA profiles of infected individuals with healthy controls to identify disease-specific signatures. For instance, Zhang *et al.* reported that miR-378, miR-483-5p, miR-22, miR-29c, miR-101, and miR-320b could accurately distinguish patients with pulmonary tuberculosis TB from healthy individuals.[70] However, such comparisons to healthy controls may limit clinical utility, as the observed ex-miRNA changes could reflect general inflammatory responses rather than disease-specific alterations.

Ex-miRNA biomarkers can also distinguish viral and bacterial infections, predict sepsis outcomes, and monitor response to treatment. For instance, miR-223, miR-499, miR-15a/b, and miR-16 have been associated with sepsis diagnosis and mortality, though discrepancies between studies exist. miR-122 has consistently emerged as a biomarker of viral load and therapeutic response in hepatitis studies, highlighting its clinical relevance.[71] Although results are promising, variability in study design, miRNA isolation methods, profiling platforms, and data standardization complicate the interpretation. Standardization of methodology and validation of study findings are essential to realize the potential of identified miRNAs as reliable biomarkers of infection. Furthermore, analysis of miRNAs in EXOs, which are actively secreted and reflect cell-specific molecular changes, may improve both the sensitivity and specificity of miRNA-based biomarkers.[27]

15. Conclusion

Pneumonia and pulmonary fibrosis are two serious respiratory diseases that affect millions of people worldwide. While current treatment options can slow the progression of these diseases, they often have limited efficacy and can cause unwanted side effects. miRNAs are small non-coding RNAs that modulate gene expression by attaching to target mRNAs, thereby inhibiting translation or promoting degradation. miRNAs exert a crucial role in different biological activities, including cell division, differentiation, inflammation, apoptosis, and metabolism. Accumulating evidence highlights the regulatory role of miRNAs in inflammation, fibrosis, and immune responses in the lungs, making them a potential pharmacotherapeutic target for the management of pneumonia and pulmonary fibrosis. Several studies have shown that miRNAs can either promote or inhibit fibrosis by targeting key mediators of the fibrotic process, including TGF-β. In addition, miRNAs regulate the activation and differentiation of fibroblast and myofibroblast, which are the main effector cells of fibrosis. These findings suggest that miRNAs may serve not only as diagnostic and prognostic biomarkers but also as therapeutic targets for pulmonary fibrosis and pneumonia.

Preclinical studies have demonstrated that miRNA-based therapies can reduce inflammation, prevent fibrosis progression, and improve lung function in animal models with pneumonia and pulmonary fibrosis. Furthermore, some miRNAs have already been recognized as potential

biological markers for the diagnosis and prognosis of these diseases. Despite their potential, several challenges must be addressed before miRNA-based therapies can be translated into clinical practice. A major hurdle is the lack of target specificity, as miRNAs can modulate multiple genes, raising the risk of off-target effects. Furthermore, efficient and targeted delivery of miRNA therapeutics to lung tissues remains technically challenging due to issues related to stability, uptake, and biodistribution.

In conclusion, miRNA-based diagnostics and therapies represent a promising frontier for the management of pneumonia and pulmonary fibrosis. Further research is warranted to deepen our understanding of miRNA mechanisms in the therapeutic context. These efforts may pave the way for novel, targeted treatment strategies that significantly improve outcomes in patients with these serious respiratory diseases.

Acknowledgments

The authors would like to acknowledge the Department of Pharmaceutical Technology, Maulana Abul Kalam Azad University of Technology, India, and Charaktala College of Pharmacy, India, for providing them with the opportunity and resources to write this review.

Funding

None.

Conflict of interest

The authors declare that there is no conflict of interest.

Author contributions

Conceptualization: Bhaskar Pal, Said Afredi, Krishan Maity
Writing – original draft: Bhaskar Pal, Said Afredi, Krishan Maity
Writing – review & editing: All authors

Ethics approval and consent to participate

Not applicable.

Consent for publication

Not applicable.

Availability of data

Not applicable.

References

1. Gardiner SJ, Gavranich JB, Chang AB. Antibiotics for Community-Acquired Lower Respiratory Tract Infections Secondary to *Mycoplasma pneumoniae* in Children. Cochrane Database Syst Rev 2015;1:CD004875.
doi: 10.1002/14651858.cd004875.pub5
2. Steinhoff MC. Viral Vaccines for the Prevention of Childhood Pneumonia in Developing Nations: Priorities and Prospects. Rev Infect Dis 1991;13:S562-70.
doi: 10.1093/clinids/13.supplement-6.s562
3. Gereige RS, Laufer PM. Pneumonia Published Correction Appears in Pediatr Rev. 2014 Jan;35(1):29. Dosage Error in Article Text. Pediatr Rev 2013;34:438-56.
doi: 10.1542/pir.34-10-438
4. Arnold FW, Summersgill JT, Ramirez JA. Role of Atypical Pathogens in the Etiology of Community-Acquired Pneumonia. Semin Respir Crit Care Med 2016;37:819-28.
doi: 10.1055/s-0036-1592121
5. Pardo A, Selman M. Idiopathic Pulmonary Fibrosis: New Insights in its Pathogenesis. Int J Biochem Cell Biol 2002;34:1534-8.
doi: 10.1016/s1357-2725(02)00091-2
6. Padilla M. Idiopathic Pulmonary Fibrosis: The Role of Pathobiology in Making A Definitive Diagnosis. Am J Manag Care 2015;21:s276-83.
7. Thannickal VJ, Toews GB, White ES, Lynch JP 3rd, Martinez FJ. Mechanisms of Pulmonary Fibrosis. Annu Rev Med 2004;55:395-417.
doi: 10.1146/annurev.med.55.091902.103810
8. Lu TX, Rothenberg ME. MicroRNA. J Allergy Clin Immunol 2018;141:1202-7.
doi: 10.1016/j.jaci.2017.08.034
9. Bushati N, Cohen SM. Microrna Functions. Annu Rev Cell Dev Biol 2007;23:175-205.
doi: 10.1146/annurev.cellbio.23.090506.123406
10. Mohr AM, Mott JL. Overview of MicroRNA Biology. Semin Liver Dis 2015;35:3-11.
doi: 10.1055/s-0034-1397344
11. Romero-Cordoba SL, Salido-Guadarrama I, Rodriguez-Dorantes M, Hidalgo-Miranda A. MiRNA Biogenesis: Biological Impact in the Development of Cancer. Cancer Biol Ther 2014;15:1444-55.
doi: 10.4161/15384047.2014.955442
12. O'Carroll D, Schaefer A. General Principals of MiRNA Biogenesis and Regulation in the Brain. Neuropsychopharmacology 2013;38:39-54.
doi: 10.1038/npp.2012.87
13. Michlewski G, Cáceres JF. Post-Transcriptional Control of MiRNA Biogenesis. RNA 2019;25:1-16.
doi: 10.1261/rna.068692.118

14. Young NA, Valiente GR, Hampton JM, Wu LC, Burd CJ, Willis WL, *et al.* Estrogen-Regulated STAT1 Activation Promotes TLR8 Expression to Facilitate Signaling Via MicroRNA-21 in Systemic Lupus Erythematosus. Clin Immunol 2017;176:12-22.

doi: 10.1016/j.clim.2016.12.005

15. Dempsey TM, Payne S, Sangaralingham L, Yao X, Shah ND, Limper AH. Adoption of the Antifibrotic Medications Pirfenidone and Nintedanib for Patients with Idiopathic Pulmonary Fibrosis. Ann Am Thorac Soc 2021;18:1121-8.

doi: 10.1513/AnnalsATS.202007-901OC

16. Allegra A, Ettari R, Innao V, Bitto A. Potential Role of MicroRNAs in Inducing Drug Resistance in Patients with Multiple Myeloma. Cells 2021;10:448.

doi: 10.3390/cells10020448

17. Catalanotto C, Cogoni C, Zardo G. MicroRNA in Control of Gene Expression: An Overview of Nuclear Functions. Int J Mol Sci 2016;17:1712.

doi: 10.3390/ijms17101712

18. Budak H, Akpinar BA. Plant MiRNAs: Biogenesis, Organization and Origins. Funct Integr Genomics 2015;15:523-31.

doi: 10.1007/s10142-015-0451-2

19. Tang HB, DiMango E, Bryan R, Gambello M, Iglewski BH, Goldberg JB, *et al.* Contribution of Specific *Pseudomonas aeruginosa* Virulence Factors to Pathogenesis of Pneumonia in a Neonatal Mouse Model of Infection. Infect Immun 1996;64:37-43.

doi: 10.1128/iai.64.1.37-43.1996

20. Rider AC, Frazee BW. Community-Acquired Pneumonia. Emerg Med Clin North Am 2018;36:665-83.

doi: 10.1016/j.emc.2018.07.001

21. McCullers JA, Tuomanen EI. Molecular Pathogenesis of Pneumococcal Pneumonia. Front Biosci 2001;6:D877-89.

doi: 10.2741/mccullers

22. Song Y, Li X, Du X. Exposure to Nanoparticles is Related to Pleural Effusion, Pulmonary Fibrosis and Granuloma. Eur Respir J 2009;34:559-67.

doi: 10.1183/09031936.00178308

23. López A, Martinson SA. Respiratory System, Mediastinum, and Pleurae. In: Pathologic Basis of Veterinary Disease. Amsterdam, Netherlands: Elsevier; 2017. p. 471-560.e1.

doi: 10.1016/B978-0-323-35775-3.00009-6

24. Arshad H, Fasanya A, Cheema T, Singh AC. Acute Pneumonia. Crit Care Nurs Q 2016;39:148-60.

doi: 10.1097/CNQ.0000000000000108

25. Chugh K, Talwar N. Bronchoscopy in Pediatric Critical Care. J Pediatr Crit Care. 2015;2:100.

doi: 10.21304/2015.0201.00057

26. Sun Y, Xian Y, Duan Z, Wan Z, Li J, Liao Y, *et al.* Diagnostic Potential of MicroRNAs in Extracellular Vesicles Derived from Bronchoalveolar Lavage Fluid for Pneumonia-a Preliminary Report. Cells 2022;11:2961.

doi: 10.3390/cells11192961

27. Drury RE, O'Connor D, Pollard AJ. The Clinical Application of MicroRNAs in Infectious Disease. Front Immunol 2017;8:1182.

doi: 10.3389/fimmu.2017.01182

28. Abu-Izneid T, AlHajri N, Ibrahim AM, Javed N, Salem KM, Pottoo FH, *et al.* Micro-RNAs in the Regulation of Immune Response Against SARS CoV-2 and Other Viral Infections. J Adv Res 2021;30:133-45.

doi: 10.1016/j.jare.2020.11.013

29. Zhou X, Li X, Wu M. MiRNAs Reshape Immunity and Inflammatory Responses in Bacterial Infection. Signal Transduct Target Ther 2018;3:14.

doi: 10.1038/s41392-018-0006-9

30. Ojha R, Nandani R, Pandey RK, Mishra A, Prajapati VK. Emerging Role of Circulating MicroRNA in the Diagnosis of Human Infectious Diseases. J Cell Physiol 2019;234:1030-43.

doi: 10.1002/jcp.27127

31. Zhang F, Zhou Y, Ding J. The Current Landscape of MicroRNAs (MiRNAs) in Bacterial Pneumonia: Opportunities and Challenges. Cell Mol Biol Lett 2022;27:70.

doi: 10.1186/s11658-022-00368-y

32. Ayoub SE, Ahmed AM, Abdelwahed MY, Khalefa AA, Awaji AA, Zekry SS, *et al.* Biochemical Analysis of MiR-217 and MiR-532 in Patients with Fibromyalgia. Eur J Med Res 2025;30:85.

doi: 10.1186/s40001-025-02330-y

33. Podsiad A, Standiford TJ, Ballinger MN, Eakin R, Park P, Kunkel SL, *et al.* MicroRNA-155 Regulates Host Immune Response to Postviral Bacterial Pneumonia Via IL-23/IL-17 Pathway. Am J Physiol Lung Cell Mol Physiol 2016;310:L465-75.

doi: 10.1152/ajplung.00224.2015

34. Mowery NT, Terzian WT, Nelson AC. Acute Lung Injury. Curr Probl Surg 2020;57:100777.

doi: 10.1016/j.cpsurg.2020.100777

35. Torres A, Serra-Batlles J, Ferrer A, Jiménez P, Celis R, Cobo E, *et al.* Severe Community-Acquired Pneumonia. Epidemiology and Prognostic Factors. Am Rev Respir Dis 1991;144:312-8.

doi: 10.1164/ajrccm/144.2.312

36. Adhanom G, Gebreegziabiher D, Weldu Y, Wasihun AG, Araya T, Legese H, *et al.* Species, Risk Factors, and Antimicrobial Susceptibility Profiles of Bacterial Isolates from HIV-Infected Patients Suspected to Have Pneumonia in Mekelle Zone, Tigray, Northern Ethiopia. Biomed Res Int 2019;2019:8768439.

doi: 10.1155/2019/8768439

37. Huang S, Feng C, Zhai YZ, Zhou X, Li B, Wang LL, *et al.* Identification of MiRNA Biomarkers of Pneumonia using RNA-Sequencing and Bioinformatics Analysis. Exp Ther Med 2017;13:1235-44.

doi: 10.3892/etm.2017.4151

38. Wuyts WA, Agostini C, Antoniou KM, Bouros D, Chambers RC, Cottin V, *et al.* The Pathogenesis of Pulmonary Fibrosis: A Moving Target. Eur Respir J 2013;41:1207-18.

doi: 10.1183/09031936.00073012

39. Marshall RP, McAnulty RJ, Laurent GJ. The Pathogenesis of Pulmonary Fibrosis: Is there a Fibrosis Gene? Int J Biochem Cell Biol 1997;29:107-20.

doi: 10.1016/s1357-2725(96)00141-0

40. She YX, Yu QY, Tang XX. Role of Interleukins in the Pathogenesis of Pulmonary Fibrosis. Cell Death Discov 2021;7:52.

doi: 10.1038/s41420-021-00437-9

41. Sgalla G, Iovene B, Calvello M, Ori M, Varone F, Richeldi L. Idiopathic Pulmonary Fibrosis: Pathogenesis and Management. Respir Res 2018;19:32.

doi: 10.1186/s12931-018-0730-2

42. Bellaye PS, Kolb M. Why Do Patients Get Idiopathic Pulmonary Fibrosis? Current Concepts in the Pathogenesis of Pulmonary Fibrosis. BMC Med 2015;13:176.

doi: 10.1186/s12916-015-0412-6

43. Oikonomou N, Mouratis MA, Tzouvelekis A, Kaffe E, Valavanis C, Vilaras G, *et al.* Pulmonary Autotaxin Expression Contributes to the Pathogenesis of Pulmonary Fibrosis. Am J Respir Cell Mol Biol 2012;47:566-74.

doi: 10.1165/rcmb.2012-0004OC

44. Bozyk PD, Moore BB. Prostaglandin E_2 and the Pathogenesis of Pulmonary Fibrosis. Am J Respir Cell Mol Biol 2011;45:445-52.

doi: 10.1165/rcmb.2011-0025RT

45. Goodwin A, Jenkins G. Role of Integrin-Mediated TGFbeta Activation in the Pathogenesis of Pulmonary Fibrosis. Biochem Soc Trans 2009;37:849-54.

doi: 10.1042/BST0370849

46. Radisky DC. Epithelial-Mesenchymal Transition. J Cell Sci 2005;118:4325-6.

doi: 10.1242/jcs.02552

47. Selman M, Thannickal VJ, Pardo A, Zisman DA, Martinez FJ, Lynch JP 3rd. Idiopathic Pulmonary Fibrosis: Pathogenesis and Therapeutic Approaches. Drugs 2004;64:405-30.

doi: 10.2165/00003495-200464040-00005

48. Kim KK, Kugler MC, Wolters PJ, Robillard L, Galvez MG, Brumwell EN, *et al.* Alveolar Epithelial Cell Mesenchymal Transition Develops *in vivo* During Pulmonary Fibrosis and is Regulated by the Extracellular Matrix. Proc Natl Acad Sci U S A 2006;103:13180-5.

doi: 10.1073/pnas.0605669103

49. Cadena-Suárez AR, Hernández-Hernández HA, Alvarado-Vásquez N, Rangel-Escareño C, Sommer B, Negrete-García MC. Role of MicroRNAs in Signaling Pathways Associated with the Pathogenesis of Idiopathic Pulmonary Fibrosis: A Focus on Epithelial-Mesenchymal Transition. Int J Mol Sci 2022;23:6613.

doi: 10.3390/ijms23126613

50. Condrat CE, Thompson DC, Barbu MG, Bugnar OL, Boboc A, Cretoiu D, *et al.* MiRNAs as Biomarkers in Disease: Latest Findings Regarding Their Role in Diagnosis and Prognosis. Cells 2020;9:276.

doi: 10.3390/cells9020276

51. Rajasekaran S, Rajaguru P, Sudhakar Gandhi PS. MicroRNAs as Potential Targets for Progressive Pulmonary Fibrosis. Front Pharmacol 2015;6:254.

doi: 10.3389/fphar.2015.00254

52. Liu B, Jiang T, Hu X, Liu Z, Zhao L, Liu H, *et al.* Downregulation of MicroRNA-30a in Bronchoalveolar Lavage Fluid from Idiopathic Pulmonary Fibrosis Patients. Mol Med Rep 2018;18:5799-806.

doi: 10.3892/mmr.2018.9565

53. Wang M, Huang Y, Liang Z, Liu D, Lu Y, Dai Y, *et al.* Plasma MiRNAs Might Be Promising Biomarkers of Chronic Obstructive Pulmonary Disease. Clin Respir J 2016;10:104-11.

doi: 10.1111/crj.12194

54. Njock MS, Guiot J, Henket MA, Nivelles O, Thiry M, Dequiedt F, *et al.* Sputum Exosomes: Promising Biomarkers for Idiopathic Pulmonary Fibrosis. Thorax 2019;74:309-12.

doi: 10.1136/thoraxjnl-2018-211897

55. O'Reilly S. MicroRNAs in Fibrosis: Opportunities and Challenges. Arthritis Res Ther 2016;18:11.

doi: 10.1186/s13075-016-0929-x

56. Li H, Zhao X, Shan H, Liang H. MicroRNAs in Idiopathic Pulmonary Fibrosis: Involvement in Pathogenesis and Potential use in Diagnosis and Therapeutics. Acta Pharm Sin B 2016;6:531-9.

doi: 10.1016/j.apsb.2016.06.010

57. Chen X, Shi C, Wang C, Liu W, Chu Y, Xiang Z, *et al.* The Role

of MiR-497-5p in Myofibroblast Differentiation of LR-MSCs and Pulmonary Fibrogenesis. Sci Rep 2017;7:40958.

doi: 10.1038/srep40958

58. Gao X, Xu D, Li S, Wei Z, Li S, Cai W, *et al.* Pulmonary Silicosis Alters MicroRNA Expression in Rat Lung and miR-411-3p Exerts Anti-fibrotic Effects by Inhibiting MRTF-A/SRF Signaling. Mol Ther Nucleic Acids 2020;20:851-65.

doi: 10.1016/j.omtn.2020.05.005

59. Ji X, Wu B, Fan J, Han R, Luo C, Wang T, *et al.* The Anti-fibrotic Effects and Mechanisms of MicroRNA-486-5p in Pulmonary Fibrosis. Sci Rep 2015;5:14131.

doi: 10.1038/srep14131

60. Nath A, Rayabaram J, Ijee S, Bagchi A, Chaudhury AD, Roy D, *et al.* Comprehensive Analysis of MicroRNAs in Human Adult Erythropoiesis. Cells 2021;10:3018.

doi: 10.3390/cells10113018

61. Leng Q, Lin Y, Jiang F, Lee CJ, Zhan M, Fang H, *et al.* A Plasma MiRNA Signature for Lung Cancer Early Detection. Oncotarget 2017;8:111902-11.

doi: 10.18632/oncotarget.22950

62. Han R, Ji X, Rong R, Li Y, Yao W, Yuan J, *et al.* MiR-449a Regulates Autophagy to Inhibit Silica-Induced Pulmonary Fibrosis through Targeting Bcl2. J Mol Med (Berl) 2016;94:1267-79.

doi: 10.1007/s00109-016-1441-0

63. Yuan J, Li P, Pan H, Xu Q, Xu T, Li Y, *et al.* MiR-770-5p Inhibits the Activation of Pulmonary Fibroblasts and Silica-Induced Pulmonary Fibrosis Through Targeting TGFBR1. Ecotoxicol Environ Saf 2021;220:112372.

doi: 10.1016/j.ecoenv.2021.112372

64. Degryse AL, Lawson WE. Progress toward Improving Animal Models for Idiopathic Pulmonary Fibrosis. Am J Med Sci 2011;341:444-9.

doi: 10.1097/MAJ.0b013e31821aa000

65. Murchison EP, Hannon GJ. MiRNAs on the Move: MiRNA Biogenesis and the RNAi Machinery. Curr Opin Cell Biol 2004;16:223-9.

doi: 10.1016/j.ceb.2004.04.003

66. Pandit KV, Milosevic J, Kaminski N. MicroRNAs in Idiopathic Pulmonary Fibrosis. Transl Res 2011;157:191-9.

doi: 10.1016/j.trsl.2011.01.012

67. Gregory PA, Bert AG, Paterson EL, Barry SC, Tsykin A, Farshid G, *et al.* The MiR-200 Family and MiR-205 Regulate Epithelial to Mesenchymal Transition by Targeting ZEB1 and SIP1. Nat Cell Biol 2008;10:593-601.

doi: 10.1038/ncb1722

68. Chao CM, Carraro G, Rako ZA, Kolck J, Sedighi J, Zimmermann V, *et al.* Failure to Down-Regulate MiR-154 Expression in Early Postnatal Mouse Lung Epithelium Suppresses Alveologenesis, with Changes in Tgf-β Signaling Similar to those Induced by Exposure to Hyperoxia. Cells 2020;9:859.

doi: 10.3390/cells9040859

69. Boon RA, Vickers KC. Intercellular Transport of MicroRNAs. Arterioscler Thromb Vasc Biol 2013;33:186-92.

doi: 10.1161/ATVBAHA.112.300139

70. Zhang X, Guo J, Fan S, Li Y, Wei L, Yang X, *et al.* Screening and Identification of Six Serum MicroRNAs as Novel Potential Combination Biomarkers for Pulmonary Tuberculosis Diagnosis. PLoS One 2013;8:e81076.

doi: 10.1371/journal.pone.0081076

71. Jin BX, Zhang YH, Jin WJ, Sun XY, Qiao GF, Wei YY, *et al.* MicroRNA Panels as Disease Biomarkers Distinguishing Hepatitis B Virus Infection Caused Hepatitis and Liver Cirrhosis. Sci Rep 2015;5:15026.

doi: 10.1038/srep15026

ACCSCIENCE PUBLISHING

Journal of Clinical and Translational Research

ORIGINAL ARTICLE

Secular trends in cytomegalovirus risk and outcomes by race: A 10-year longitudinal study in adult kidney transplant recipients

Karim Soliman[1,2,3], Ahmed Daoud[2,3], Amy Perry[1]*, Morgan Overstreet[3], Erika Andrade[3], Isabel K. Calimlim[3], Courtney E. Harris[4], and David J. Taber[3,5]

[1]Department of Medicine Service, Ralph H. Johnson VA Healthcare System, Charleston, South Carolina, United States of America

[2]Department of Medicine, Division of Nephrology, Medical University of South Carolina, Charleston, South Carolina, United States of America

[3]Department of Surgery, Division of Transplant Surgery, Medical University of South Carolina, South Carolina, United States of America

[4]Department of Medicine, Division of Infectious Diseases, Medical University of South Carolina, South Carolina, United States of America

[5]Department of Pharmacy Service, Ralph H. Johnson VA Healthcare System, Charleston, South Carolina, United States of America

Abstract

Background and aim: Cytomegalovirus (CMV) remains a critical post-transplant opportunistic infection despite significant advancements in monitoring and therapy. The impact of African-American (AA) race on CMV risk and outcomes has been insufficiently studied. This study aimed to determine secular trends in the incidence of CMV D+/R– mismatching and evaluate their association with AA race and clinical outcomes. **Methods:** This single-center longitudinal cohort study involved adult kidney recipients transplanted between January 2012 and June 2021, with follow-up through June 2022. Univariate and multivariate statistics were performed to analyze the data. **Results:** Of 2392 kidney transplant recipients, 2,261 were included in the final analysis after applying exclusion criteria. The mean age was 52 years, 41% were female, and 57% were black. In addition, 19% were classified as CMV high-risk. Secular trend analysis revealed an increase in CMV D+/R– rates over time. AAs had 51% lower odds of being CMV D+/R– (p<0.001), which remained stable over the study period (p=0.80). In adjusted models, AAs had a 50% higher risk of developing CMV infection (Hazard ratio [HR] = 1.49, confidence interval [CI]: 1.1 – 2.0) and late CMV infection (HR = 1.5, CI: 1.03 – 2.3), with no significant change over time (p>0.20). AA race was also a risk factor for acute rejection and death-censored graft loss, with no notable changes observed over the study period. **Conclusion:** In kidney transplant recipients, the incidence of CMV D+/R– serostatus has increased over the past decade. AAs are 50% less likely to be CMV D+/R– but have higher normalized rates of other complications, which remained relatively stable over the study period. Future studies should explore the underlying mechanisms contributing to the higher rates of CMV infection in AAs, which could facilitate the development of targeted interventions. Factors such as immunosenescence and genetic polymorphisms warrant further exploration. **Relevance for patients:** CMV risk, outcomes, racial disparities in kidney transplant.

Keywords: Cytomegalovirus; Kidney transplant; Racial disparities; Outcomes; Immunosuppression; Infections

***Corresponding author:**
Amy Perry
(amy.perry2@va.gov)

Citation: Soliman K, Daoud A, Perry A, *et al*. Secular trends in cytomegalovirus risk and outcomes by race: A 10-year longitudinal study in adult kidney transplant recipients. *J Clin Transl Res*. 2025;11(2):41-51. doi: 10.36922/jctr.24.00067

Received: October 14, 2024

1st revised: December 3, 2024

2nd revised: December 9, 2024

Accepted: February 20, 2025

Published online: March 20, 2025

1. Introduction

Kidney transplantation stands as the cornerstone treatment for individuals with end-stage kidney disease[1] Compared to those who remain on dialysis, recipients of both living and deceased donor kidneys exhibit enhanced long-term survival rates and improved quality of life.[2] However, this therapeutic approach necessitates lifelong immunosuppression to mitigate the risk of cellular and antibody-mediated rejection, consequently predisposing recipients to a heightened susceptibility to infections.[3] Among these infectious risks, cytomegalovirus (CMV) infection emerges as a common concern in kidney transplant recipients, with a remarkable 70 – 90% of adults anticipated to be CMV seropositive.[4-6]

The impact of African-American (AA) race on access to and outcomes associated with kidney transplantation has been well-studied.[7-9] AAs have significantly reduced access to kidney transplantation, with delayed referrals and lower rates of evaluation, listing, and transplantation compared to Caucasians.[10-12] Post-transplant, AAs experience higher rates of acute rejection and graft loss,[13-15] with allografts lasting about half as those in Caucasians.[9] However, studies assessing the influence of AA race on CMV serostatus, infection risk, access to anti-CMV prophylaxis, and associated outcomes are lacking, particularly in D+/R– patients.[16-19] AAs are underrepresented in clinical trials related to kidney transplantation and CMV research.[16-19] CMV serostatus is correlated with geography and living conditions, which differ by race,[17] suggesting that AAs might have higher rates of CMV seropositivity (R+) and thus lower CMV infection and disease risks, but this is not well-studied.[20] A small single-center study demonstrated CMV infection rates of 7.5% in 80 AA kidney transplant recipients, with 15% being D+/R–, all receiving induction and valganciclovir prophylaxis.[15] However, without comparisons to other racial or ethnic groups, the implications are unclear.[15] Beyond this, studies assessing the risk and outcomes of CMV infection by AA race in contemporary kidney transplantation are also lacking.[16-19] Given the current focus on health equities and racial justice within healthcare and society, conducting studies that better understand the influence of AA race on CMV serostatus, anti-CMV prophylaxis use and access, infection rates, and associated outcomes is crucial.

Thus, the study aims to elucidate the secular trends in the incidence of CMV D+/R– mismatching and assess whether these trends are influenced by AA race, with significant implications for clinical outcomes such as rejection rates, BK virus infection, and death-censored graft loss.

2. Methods

2.1. Study design and patients

This single-center, longitudinal cohort study included kidney transplant recipients who underwent transplantation between January 2012 and June 2021. Eligible patients were those identified as kidney recipients at the study institution transplanted within the study timeframe and excluded if they received liver, heart, lung, intestine, or bone marrow transplants. Exclusion criteria included age under 18 years at the time of transplant, inability to link to the institution's corporate data warehouse to gather clinical information from the electronic health record, and repeat transplant recipients during the study timeframe. Patients were longitudinally followed until graft loss, death, or the study endpoint (June 2022), providing a minimum of 1 year of post-transplant follow-up.

2.2. Primary exposure, outcomes, and definitions

The primary dependent exposure variable in this study was race, defined as AA versus non-AA. The main outcomes of interest were CMV D+/R– serostatus and CMV infection. CMV serostatus was determined using qualitative CMV immunoglobulin G results from both donor and recipient at the time of transplant. The following outcomes definitions were used for this study:

(i) CMV infection: Defined as plasma CMV polymerase chain reaction (PCR) ≥1,000 IU/mL, with nucleic acid amplification techniques calibrated to the World Health Organization's International Standard for Human CMV.

(ii) CMV disease: Defined as the presence of organ dysfunction in the setting of CMV infection with biopsy-proven presence of CMV in the affected organ using DNA hybridization.

(iii) Probable or likely refractory CMV infection: Defined as CMV viremia that increases more than 1 $\log_{10}$ in CMV DNA levels from initial viral load after at least 2 weeks of appropriately dosed antiviral therapy.

(iv) CMV antiviral drug resistance: Defined as viral genetic alteration that decreases susceptibility to one or more antiviral drugs.

(v) Acute rejection: Defined as a renal allograft biopsy showing at least borderline grade according to Banff criteria.

(vi) BK infection: Defined as BK viremia of at least 2,000 copies/mL.

(vii) Severe BK infection: Defined as BK viremia of at least 10,000 copies/mL.

(viii) BK nephropathy: Defined based on the pathology report from the kidney allograft biopsy.

(ix) Non-CMV and non-BK infections: Defined as

any diagnosed and treated infection leading to hospitalization. Opportunistic infections were also sub-classified for this study.

(x) Graft loss: Defined as a return to chronic dialysis, re-transplantation, or death. Death-censored graft loss was also assessed for this study.

2.3. Data collection and covariates

Data collection included baseline donor/recipient demographics and transplant characteristics, validated from the transplant center-specific Standard Transplant Analysis Research files. These included age, sex, race, weight, history of diabetes, dialysis vintage, wait time, calculated panel reactive antibody (PRA) score at transplant, human leukocyte antigen mismatches, cold ischemic time, delayed graft function, and pancreas transplant status. Donor characteristics included age, sex, race, donor type, and kidney donor risk index in deceased donors. Longitudinal data were collected through a combination of electronic record data extractions from the institution's data warehouse and manual chart abstraction. Electronic data extractions included medications, laboratory data, and clinical events, such as hospitalizations, emergency department visits, graft loss, and death, occurring during the post-transplant period. Chart abstraction was used to assess biopsy findings, causes of hospitalizations, type of CMV infection, confirmation of CMV disease (and organ[s] affected), CMV treatments, and other relevant medications of interest for future analyses.

2.4. Statistical analysis

Data are presented as percentages for nominal variables, with univariate comparisons using Fisher's exact test or Pearson's Chi-squared test, as appropriate. For continuous variables with normal distribution, results are reported as means and standard deviations, with comparisons performed using Student's *t*-test for two independent samples. For non-normally distributed variables, results were reported using medians and interquartile ranges, with univariate statistical comparison conducted using the Mann-Whitney U-test. Normal distribution was assessed using normality plots and the Shapiro-Wilk test. Multivariable analysis for secular trend assessments was conducted using generalized linear models (GLM) with a logit link for the binary outcome (CMV D+/R− yes/no), with race as the primary independent variable and transplant quarter as a covariate. The GLM accounted for time correlations within patients. Time-dependent Cox regression analysis was employed for multivariable survival analyses involving all time-to-event outcomes. In these Cox models, a three-way interaction term was added to assess differences in temporal trends by CMV serostatus by race on clinical outcomes (serostatus × transplant quarter × race). All analyses were conducted using Statistical Analysis System (SAS) version 9.4 (SAS Institute, United States [US]). $p<0.05$.

3. Results

During the 10-year study period, a total of 2,392 kidney transplants were performed at the study institution. After excluding 79 pediatric patients and 53 patients with missing data or second transplants, the final cohort consisted of 2,261 patients. Among these patients, 1,287 patients (57%) were AA, with 185 (14.4%) having high-risk CMV serostatus, and 974 patients (43%) were non-AA, with 25.4% being high-risk. The Consolidated Standards of Reporting Trials diagram is provided in Figure 1. Table 1 compares baseline characteristics between AA versus non-AA patients. The average age was 51 years for AAs and 53 years for non-AAs, with females comprising 43.4% and 37.6%, respectively. There was no significant difference in weight, body mass index, kidney or pancreas transplant history, or donor characteristics between the AA and non-AA groups. History of diabetes mellitus, years on dialysis, and waitlist status were significantly higher in AAs compared to non-AAs. AAs also had higher PRA levels ($p<0.001$) and significantly lower rates of CMV D+/R− high-risk serostatus than the non-AA subjects ($p<0.001$). Delayed graft function rates were also significantly higher in AAs.

Table 2 shows unadjusted univariate analyses to compare AAs and non-AAs for CMV infections and other related outcomes. AAs had significantly higher rates of graft loss ($p=0.022$), death-censored graft loss ($p<0.001$), antibody-mediated rejections ($p=0.003$), acute cellular rejections ($p=0.007$), and hospitalizations for non-infection causes ($p=0.026$). There were no statistically significant differences in BK viremia ($p=0.10$), BK nephropathy ($p=0.205$), CMV infection rates ($p=0.125$), CMV disease ($p=0.848$), resistance ($p=0.844$), or breakthrough ($p=0.234$) between AAs and non-AAs. The sequential Cox regression model assessing the impact of AA race, either unadjusted or adjusted, on relevant clinical outcomes is illustrated in Table 3. AA had a 68% higher risk of CMV infection after adjustment for CMV serostatus (adjusted hazard ratio [aHR] = 1.68, confidence interval [CI]: 1.30 – 2.17), with a reduced risk after controlling for acute rejection (aHR = 1.21, CI: 0.94 – 1.56). It was significant in the fully adjusted model, whereby AA had a 41% higher risk of CMV infection than non-AAs (aHR = 1.41, CI: 1.05 – 1.86). The risk of developing late CMV infection, graft loss, and death-censored graft loss were significantly higher in AAs versus non-AAs. In contrast, the risk of BK infection, CMV disease, and breakthrough prophylaxis CMV infection were similar based on race (Table 4).

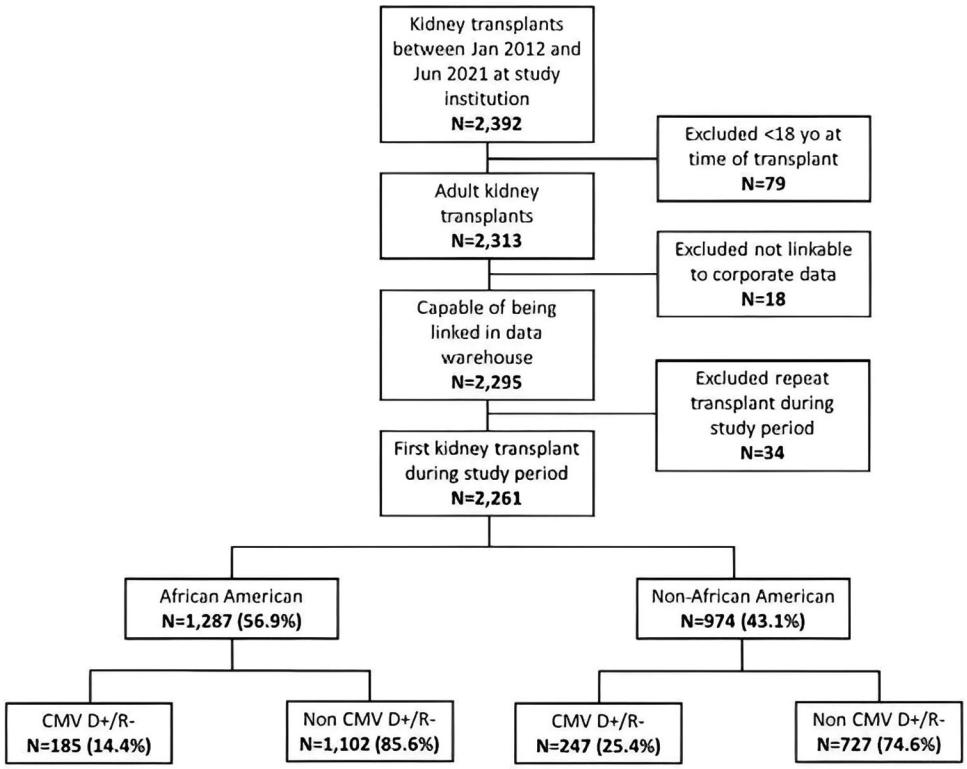

Figure 1. Consolidated standards of reporting trials diagram. The diagram details how the cohort was formed, including exclusion reasons and number of patients.
Abbreviations: CMV: Cytomegalovirus; yo: Years old.

Temporal trend analysis demonstrated increasing CMV D+/R− rates over time, with AAs having 51% lower odds of being CMV D+/R− (odds ratio = 0.49, CI: 0.40 – 0.61, $p<0.001$), which remained stable over the 10-year study period ($p=0.80$ for AA * kidney transplant year interaction) (Figure 2). Sequential Cox modeling also demonstrated that in adjusted models, the higher risk of developing CMV infection and late CMV infection in AAs did not change significantly over time (three-way interaction: D+/R− * AA * transplant year, $p>0.20$). Similarly, risks of acute rejection, graft loss, and death-censored graft loss in AAs remained relatively stable over the 10-year study period (three-way interaction: D+/R− * AA * transplant year, $p>0.20$).

4. Discussion

This study, involving 2,261 transplanted kidney recipients from January 2012 to June 2021, revealed a secular trend for rising CMV D+/R− rates over time. Notably, AAs had 51% lower odds of being CMV D+/R− compared to non-AAs, a trend that has remained stable over the 10-year study period. After adjusting for CMV serostatus, AAs had a 41 – 68% higher risk of developing CMV infection and a 50 – 63% higher risk of late CMV infection. This increased risk is partially explained by higher acute rejection rates in AAs. In addition, AA race was associated with increased risks of graft loss and death-censored graft loss, which have not changed appreciably over the past decade.

Early studies dating back to the 1980s and 1990s consistently reported a higher prevalence of CMV infections among AAs compared to Caucasians, a pattern that persists.[20,21] Studies conducted in the first decade of the 21st century reported CMV seropositivity rates of 84% among AA adults.[22] Our findings align with these trends, demonstrating a 50% higher risk of CMV infection and late CMV infection in AAs after controlling for their lower likelihood of being D+/R−. This underscores the significance of race as a robust risk factor for CMV infection in kidney transplant recipients. Sequential modeling demonstrated that the higher rates of acute rejection in AAs may partially explain this higher risk. However, in fully adjusted models, including baseline characteristics and acute rejection, the risk of CMV infection in AAs was 41% higher than that of non-AAs, indicating that other unmeasured or unknown factors are likely involved.

Our study also highlights continued poorer outcomes in AA kidney transplant recipients, consistent with previous

Table 1. Baseline characteristics for the overall cohort and comparison between African-American and non-African-American groups

Baseline variable	Non-AA (*n*=974)	AA (*n*=1,287)	*p*-value
Age (mean±SD)	53.3±13.8	51.6±12.8	0.002
Female	37.6%	43.4%	0.005
Weight (kg, mean±SD)	87.2±19.9	88.9±18.1	0.039
BMI (kg/m^2, mean±SD)	29.6±8.6	30.2±5.5	0.071
History of diabetes	38.5%	49.2%	<0.001
History of dialysis	61.4%	87.3%	<0.001
Years on dialysis	2.0±2.4	4.1±3.0	<0.001
Years on the waiting list (mean±SD)	1.4±1.8	1.6±1.9	<0.001
Education high school or less	35.4%	52.4%	<0.001
History pancreas transplant	6.5%	7.1%	0.573
Primary insurance			<0.001
Private	34.8%	16.2%	
Medicare	62.9%	81.0%	
Medicaid	1.5%	2.3%	
Other	0.9%	0.6%	
Working at transplant	33.6%	22.3%	<0.001
Previous kidney transplant	10.5%	6.9%	0.003
Kidney pumped	45.6%	56.7%	<0.001
CMV D+/R−serostatus	25.4%	14.4%	<0.001
Median HLA mismatches (IQR)	4 (3, 5)	5 (4, 5)	<0.001
Median PRA (IQR)	17 (0, 64)	37 (2, 83)	<0.001
Cold ischemic time (hours, mean±SD)	14.2±9.1	16.3±7.7	<0.001
Donor type			<0.001
Living	24.1%	4.7%	
Deceased brain death	65.5%	82.3%	
Deceased cardiac death	10.4%	13.0%	
Donor female	43.3%	35.8%	0.003
Donor hepatitis C+	3.4%	2.7%	0.357
Donor diabetes	5.4%	6.9%	0.130
Donor terminal creatinine (mean±SD)	1.3±1.0	1.4±1.5	0.162
Donor BMI (kg/m^2, mean±SD)	27.2±6.1	27.6±6.4	0.104
KDPI (%, mean±SD)	39.3±25.2	39.9±24.9	0.643
Delayed graft function	17.2%	28.3%	<0.001

Abbreviations: AA: African Americans; BMI: Body mass index; CMV: Cytomegalovirus; HLA: Human leukocyte antigen; IQR: Interquartile range; KDPI: Kidney donor profile index; PRA: Panel reactive antibody; SD: Standard deviation.

literature. Isaacs *et al.*[23] conducted a large prospective analysis utilizing the United Network for Organ Sharing renal transplant registry, involving 14,617 patients who received living-related donor kidney transplants in the US between 1988 and 1996.[23] Their findings revealed that, after adjusting for potential confounding variables, AAs were 1.7 times more likely than whites to experience graft failure during the research period. Purnell *et al.*[17] analyzed all-cause graft loss in 63,910 AAs and 145,482 whites who received kidney transplants from living or deceased donors between 1990 and 2012.[17] Over the study period, 5-year graft loss after living donation decreased from 37.4% to 22.2% for AAs and from 20.8% to 13.9% for whites, whereas 5-year graft loss following deceased donation decreased from 51.4% to 30.6% for AAs and 37.3% – 25.0% for whites. These findings revealed that the 5-year graft loss difference between AAs and whites narrowed from 16.6% to 8.3% after living donation and 14.1% to

Table 2. Univariate comparisons between African Americans and non-African Americans for cytomegalovirus infections and other relevant outcomes

Outcomes	Non-AA (*n*=974) (%)	AA (*n*=1,287) (%)	*p*-value
CMV infection	10.1	12.1	0.125
CMV disease	1.3	1.2	0.848
CMV refractory infection	0.3	0.5	0.554
CMV resistance	0.4	0.5	0.844
CMV infection after 3 months	9.6	10.8	0.331
CMV infection after 6 months	6.1	6.1	0.937
CMV infection after 1 year	0.9	1.6	0.187
CMV breakthrough patient infection	1.2	1.9	0.234
Rejection≥borderline	4.9	7.8	**0.007**
Rejection 1A or worse	4.7	7.3	**0.012**
AMR rejection	0.5	1.9	**0.003**
BK nephropathy	0.3	0.7	0.205
BK viremia>2,000 copies	19.3	22.1	0.100
BK viremia>10,000 copies	14.3	16.4	0.167
Hospitalized for OI	14.4	16.8	0.119
Hospitalized non-OI infection	21.1	21.0	0.969
Hospitalized for other reasons	52.2	56.9	**0.026**
Death	19.7	18.7	0.555
Death-censored graft loss	6.5	12.1	**<0.001**
Graft loss	22.9	27.1	**0.022**

Note: Statistical significance determined at $p<0.05$ (bolded).
Abbreviations: AA: African American; AMR: Antibody-mediated rejection; CMV: Cytomegalovirus; OI: Opportunistic infection.

Table 3. Sequential Cox regression modeling assessing the impact of African-American race on relevant clinical outcomes

Outcome	Unadjusted risk	Adjusted for CMV D+/R− status	Adjusted for CMV D+/R−status and acute rejection	Adjusted for baseline characteristics	Adjusted for baseline and acute rejection
	HR (95% CI)	HR (95% CI)	HR (95% CI)	HR (95% CI)	HR (95% CI)
CMV infection	1.24 (0.96 – 1.60)	1.68 (1.30 – 2.17)	1.21 (0.94 – 1.56)	1.46 (1.08 – 1.96)	1.41 (1.05 – 1.89)
CMV disease	0.95 (0.46 – 1.98)	1.28 (0.60 – 2.71)	1.14 (0.53 – 2.44)	1.21 (0.50 – 2.91)	1.06 (0.43 – 2.62)
Late CMV infection (more than 6 months)	1.06 (0.75 – 1.48)	1.63 (1.16 – 2.30)	1.50 (1.06 – 2.13)	1.59 (1.06 – 2.37)	1.50 (1.01 – 2.24)
Breakthrough prophylaxis CMV infection	1.53 (0.77 – 3.07)	2.20 (1.09 – 4.43)	1.95 (0.95 – 3.99)	1.34 (0.60 – 3.01)	1.27 (0.56 – 2.87)
BK viremia>2,000 copies	1.16 (0.96 – 1.39)	1.17 (0.97 – 1.41)	1.15 (0.95 – 1.40)	1.25 (1.01 – 1.55)	1.21 (0.97 – 1.51)
Graft loss	1.30 (1.10 – 1.54)	1.31 (1.11 – 1.56)	1.28 (1.08 – 1.51)	1.09 (0.90 – 1.33)	1.07 (0.88 – 1.31)
Death-censored graft loss	2.02 (1.51 – 2.71)	2.10 (1.56 – 2.82)	1.87 (1.39 – 2.52)	1.67 (1.19 – 2.33)	1.52 (1.08 – 2.15)

Abbreviations: CI: Confidence interval; CMV: Cytomegalovirus; HR: Hazard ratio.

5.6% after deceased donation. The study concluded that the disparity in outcomes between AAs and white races reduced over time.[17] Despite some improvements, the magnitude of this disparity has not substantially changed over the past half-century. Nevertheless, study results from the United Kingdom suggest that while outcomes may be poorer in the black population, the black race itself may not be a significant risk factor for death or graft loss; other correlated factors in the US population are likely to contribute to this disparity.[24] This concept has far-reaching implications for future CMV management and the development of future therapeutic and investigational strategies. In tandem with previous studies, this hypothesis highlights the importance of exploring a more tailored

Table 4. Sequential hazard ratios for CMV Infection and transplant outcomes by race

Sequential model	Hazard ratios (95% confidence interval) for the outcomes											
	CMV infection	CMV disease	CMV resistance	CMV refractory infection	CMV infection>6 months	Acute rejection	Hosp for OI	Hosp for non-OI infection	Hosp for other reasons	BK viremia >2,000	Graft loss	Death	Death-censored graft loss
Only CMV D+/R− (ref=No)	5.7 (4.5 – 7.3)	8.4 (3.9 – 18.0)	17.9 (3.8 – 84.2)	35 (4 – 280)	12.0 (8.3 – 17.1)	1.4 (1.0 – 2.1)	1.4 (1.1 – 1.8)	1.3 (1.04 – 1.7)	0.9 (0.8 – 1.2)	1.06 (0.8 – 1.3)	1.0 (0.8 – 1.3)	0.86 (0.66 – 1.11)	1.22 (0.9 – 1.7)
Only African-American race	1.24 (0.96 – 1.60)	0.95 (0.5 – 1.98)	1.15 (0.3 – 4.08)	1.53 (0.4 – 6.1)	1.06 (0.8 – 1.48)	1.76 (1.23 – 2.51)	1.2 (0.95 – 1.51)	1.0 (0.8 – 1.2)	1.21 (1.02 – 1.43)	1.16 (0.96 – 1.39)	1.3 (1.1 – 1.54)	1.01 (0.9 – 1.22)	2.02 (1.51 – 2.7)
Only transplantation year (ref=2012)	1.1 (1.05 – 1.15)	0.8 (0.7 – 0.9)	1.3 (1.0 – 1.8)	1.3 (0.8 – 2.1)	1.1 (1.04 – 1.18)	0.9 (0.86 – 0.97)	0.94 (0.9 – 0.97)	0.95 (0.92 – 0.99)	0.9 (0.8 – 0.9)	0.95 (0.92 – 0.99)	1.05 (1.01 – 1.09)	1.08 (1.04 – 1.13)	1.0 (0.95 – 1.06)
D+/R− race * time interaction	0.98 (0.92 – 1.05)	1.01 (0.8 – 1.28)	1.4 (0.95 – 2.01)	0.7 (0.3 – 1.3)	0.99 (0.9 – 1.1)	1.02 (0.91 – 1.15)	0.99 (0.92 – 1.1)	0.99 (0.92 – 1.06)	1.0 (0.94 – 1.06)	0.98 (0.92 – 1.05)	1.02 (0.95 – 1.1)	1.07 (0.98 – 1.15)	1.0 (0.91 – 1.11)
CMV D+/R−fully adjusted	6.8 (5.1 – 8.9)	13.9 (5.6 – 34.5)	26.9 (4.3 – 170)	100 (6 – 1800)	15.4 (10 – 23)	1.4 (0.9 – 2.0)	1.7 (1.3 – 2.3)	1.5 (1.1 – 1.9)	1.02 (0.8 – 1.3)	1.08 (0.8 – 1.4)	1.2 (0.95 – 1.5)	1.1 (0.82 – 1.46)	1.28 (0.9 – 1.82)
African-American race fully adjusted	1.49 (1.1 – 2.02)	1.23 (0.5 – 3.1)	1.69 (0.3 – 8.7)	5.5 (0.6 – 48.4)	1.5 (1.03 – 2.3)	1.85 (0.2 – 2.9)	1.12 (0.8 – 1.5)	1.03 (0.8 – 1.3)	1.11 (0.9 – 1.37)	1.25 (1.0 – 1.57)	1.08 (0.9 – 1.33)	0.8 (0.6 – 1.04)	1.60 (1.1 – 2.3)

Abbreviations: CMV: Cytomegalovirus; OI: Opportunistic infection.

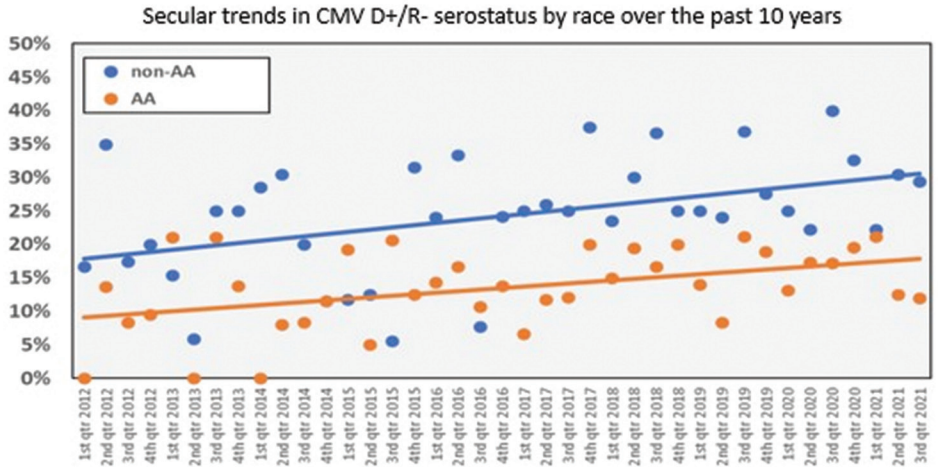

Figure 2. Temporal trends in the incidence of CMV D+/R− serostatus based on recipient race
Abbreviations: AA: African American; CMV: Cytomegalovirus; qtr: Quarter.

approach to immunosuppression and CMV prophylactic agents in the AA cohort.[24,25] Future efforts should account for racial disparities and their individualized risks, with the ultimate goal of achieving a more favorable outcome than conventional therapeutic options. Novel alternatives of traditional therapies in racial disparities, such as the utilization of letermovir – the most recently Food and Drug Administration-approved prophylactic drug in high-risk CMV cohorts situated in areas where standard practices yielded unfavorable outcomes – merit exploration.[26,27] In the context of racial disparities, leukopenia – which is often brought on by immunosuppression and routine CMV prophylactic agents – needs additional research to avoid introducing therapies that can inadvertently exacerbate pre-existing health disparities.[28] Therefore, forthcoming efforts should prioritize comprehensive assessments of risk variables in AA and tailor therapies accordingly, emphasizing the underlying mechanisms that influence clinical outcomes in CMV management.

There are several limitations to this study that merit discussion. Despite the relatively large size of this cohort, multicenter and/or national registry data are required to substantiate the external validity of these findings. Although we used the Scientific Registry of Transplant Recipients (SRTR) data to validate these CMV D+/R− trends within the same period, further rigorous research is warranted. The retrospective nature of the present study precludes causal inference due to concerns related to unmeasured and residual confounding. Nevertheless, considerable effort and diligence were devoted to reducing the occurrence of missing values through electronic and manual chart abstraction and longitudinal modeling, which also ensured temporality in the relationships between risk factors and outcomes. Evolving patient demographics and clinical practices could constitute potential residual or unmeasured confounding over the 10 years. To address this, we selected a time frame with minimal modifications to immunosuppression and infectious disease prophylaxis protocols. However, donor and recipient characteristics evolved considerably during this period, mirroring national SRTR trends.[29] In addition, our CMV DNA PCR methodology changed during the study, coinciding with the emergence of the COVID-19 pandemic. While dummy variables of patients transplanted during these periods were used to account for these changes, residual confounding may not be minimized.

Future studies should explore genetic polymorphisms to understand their impact on racial disparities in CMV infection risk. Research has implicated racial differences in gene expression as a factor for survival outcomes in non-kidney transplant settings,[30] which could be extrapolated to other organs for future study. As genetic testing for medication administration is becoming more prevalent, the results of these tests could facilitate the identification of alleles associated with CMV serostatus and infection risk.

Another area for investigation is immunosenescence, which may contribute to the increased risk of infection in AAs. This phenomenon may provide an environment for new infections and reactivation of latent CMV,[31] warranting further research.

5. Conclusion

Although the incidence of CMV D+/R− serostatus has significantly increased in kidney transplantation over the past decade, AAs exhibit a 50% lower likelihood of being

CMV D+/R– while experiencing significantly higher normalized rates of CMV infection, late CMV infection, acute rejection, and death-censored graft loss. Notably, these risks among AAs have shown no significant improvement over this 10-year study period. Additional research should focus on the underlying factors contributing to the elevated incidence of CMV infection among AAs. This would facilitate the development of targeted interventions to alleviate this disparity. Immunosenescence, which has documented correlations with CMV, is one phenomenon to consider in further research. In addition, studying genetic polymorphisms could provide additional insights into racial disparities in transplant outcomes, potentially informing strategies to mitigate these disparities.

Acknowledgments

None.

Funding

Research presented in this manuscript was conducted through the support of a grant provided by Merck Pharmaceuticals.

Conflict of interest

David J Taber reports financial support was provided by Merck & Co Inc. David J Taber reports a relationship with Veloxis Pharmaceuticals Inc., that includes board membership and funding grants. David J Taber reports a relationship with CareDx Inc., that includes board membership and funding grants. If there are other authors, they declare that they have no known competing financial interests or personal relationships that could have appeared to influence the work reported in this paper.

Author contributions

Conceptualization: All authors
Investigation: All authors
Methodology: David J. Taber
Visualization: David J. Taber
Writing – original draft: All authors
Writing – review & editing: All authors

Ethics approval and consent to participate

The study conforms to the ethical guidelines of the 1975 Declaration of Helsinki, as reflected in the prior approval by the institution's human research committee. This study was approved by the Medical University of South Carolina (MUSC) Institutional Review Board (IRB) under protocol number Pro00118675. All research procedures were conducted in accordance with MUSC ethical committee guidelines.

Consent for publication

This is a retrospective study utilizing data available in the MUSC data system. As all data were de-identified and analyzed anonymously, patient consent was not required for publication in accordance with institutional and ethical guidelines.

Availability of data

Data are available from the corresponding author upon reasonable request.

References

1. Suthanthiran M, Strom TB. Renal transplantation. *N Engl J Med*. 1994;331(6):365-376.
   doi: 10.1056/NEJM199408113310606
2. Wolfe RA, Ashby VB, Milford EL, *et al*. Comparison of mortality in all patients on dialysis, patients on dialysis awaiting transplantation, and recipients of a first cadaveric transplant. *N Engl J Med*. 1999;341(23):1725-1730.
   doi: 10.1056/NEJM199912023412303
3. Szumilas K, Wilk A, Wiśniewski P, *et al*. Current status regarding immunosuppressive treatment in patients after renal transplantation. *Int J Mol Sci*. 2023;24(12):10301.
   doi: 10.3390/ijms241210301
4. Agrawal A, Ison MG, Danziger-Isakov L. Long-term infectious complications of kidney transplantation. *Clin J Am Soc Nephrol*. 2022;17(2):286-295.
   doi: 10.2215/CJN.15971020
5. Kasiske BL, Zeier MG, Chapman JR, *et al*. KDIGO clinical practice guideline for the care of kidney transplant recipients: A summary. *Kidney Int*. 2010;77(4):299-311.
6. Kuo HT, Ye X, Sampaio MS, Reddy P, Bunnapradist S. Cytomegalovirus serostatus pairing and deceased donor kidney transplant outcomes in adult recipients with antiviral prophylaxis. *Transplantation*. 2010;90(10):1091-1098.
   doi: 10.1097/TP.0b013e3181f7c053
7. Patzer RE, McClellan WM. Influence of race, ethnicity and socioeconomic status on kidney disease. *Nat Rev Nephrol*. 2012;8(9):533-541.
   doi: 10.1038/nrneph.2012.117
8. Ciancio G, Burke GW, Suzart K, *et al*. The use of daclizumab, tacrolimus and mycophenolate mofetil in african-american and Hispanic first renal transplant recipients. *Am J Transplant*. 2003;3(8):1010-1016.
   doi: 10.1034/j.1600-6143.2003.00181.x
9. Neylan JF. Racial differences in renal transplantation after immunosuppression with tacrolimus versus cyclosporine. FK506 Kidney Transplant Study Group. *Transplantation*.

1998;65(4):515-523.

doi: 10.1097/00007890-199802270-00011

10. Podder H, Podbielski J, Hussein I, Katz S, Van Buren C, Kahan BD. Sirolimus improves the two-year outcome of renal allografts in African-American patients. *Transpl Int*. 2001;14(3):135-142.

doi: 10.1007/s001470100315

11. Weber M, Deng S, Arenas J, *et al.* Decreased rejection episodes in African-American renal transplant recipients receiving mycophenolate mofetil/tacrolimus therapy. *Transplant Proc*. 1997;29(8):3669-3670.

doi: 10.1016/s0041-1345(97)01067-1

12. Branson RD, Davis K Jr., Butler KL. African Americans' participation in clinical research: Importance, barriers, and solutions. *Am J Surg*. 2007;193(1):32-39, discussion 40.

doi: 10.1016/j.amjsurg.2005.11.007

13. Lantos PM, Permar SR, Hoffman K, Swamy GK. The excess burden of cytomegalovirus in African American communities: A geospatial analysis. *Open Forum Infect Dis*. 2015;2(4):ofv180.

doi: 10.1093/ofid/ofv180

14. Zuhair M, Smit GSA, Wallis G, *et al*. Estimation of the worldwide seroprevalence of cytomegalovirus: A systematic review and meta-analysis. *Rev Med Virol*. 2019;29(3):e2034.

doi: 10.1002/rmv.2034

15. Gruber SA, Garnick J, Morawski K, *et al*. Cytomegalovirus prophylaxis with valganciclovir in African-American renal allograft recipients based on donor/recipient serostatus. *Clin Transplant*. 2005;19(2):273-278.

doi: 10.1111/j.1399-0012.2005.00337.x

16. Taber DJ, Gebregziabher M, Hunt KJ, *et al*. Twenty years of evolving trends in racial disparities for adult kidney transplant recipients. *Kidney Int*. 2016;90(4):878-887.

doi: 10.1016/j.kint.2016.06.029

17. Purnell TS, Luo X, Kucirka LM, *et al*. Reduced racial disparity in kidney transplant outcomes in the United States from 1990 to 2012. *J Am Soc Nephrol*. 2016;27(8): 2511-2518.

doi: 10.1681/ASN.2015030293

18. Hart A, Smith JM, Skeans MA, *et al.* OPTN/SRTR 2017 annual data report: Kidney. *Am J Transplant*. 2019;19(Suppl 2): 19-123.

doi: 10.1111/ajt.15274

19. Patzer RE, Gander J, Sauls L, *et al*. The RaDIANT community study protocol: Community-based participatory research for reducing disparities in access to kidney transplantation. *BMC Nephrol*. 2014;15:171.

doi: 10.1186/1471-2369-15-171

20. White NH, Yow MD, Demmler GJ, *et al*. Prevalence of cytomegalovirus antibody in subjects between the ages of 6 and 22 years. *J Infect Dis*. 1989l;159(6):1013-1017.

doi: 10.1093/infdis/159.6.1013

21. Helanterä I, Kyllönen L, Lautenschlager I, Salmela K, Koskinen P. Primary CMV infections are common in kidney transplant recipients after 6 months valganciclovir prophylaxis. *Am J Transplant*. 2010;10(9):2026-2032.

doi: 10.1111/j.1600-6143.2010.03225.x

22. Staras SA, Dollard SC, Radford KW, Flanders WD, Pass RF, Cannon MJ. Seroprevalence of cytomegalovirus infection in the United States, 1988-1994. *Clin Infect Dis*. 2006;43(9):1143-1151.

doi: 10.1086/508173

23. Isaacs RB, Nock SL, Spencer CE, *et al*. Racial disparities in renal transplant outcomes. *Am J Kidney Dis*. 1999;34(4):706-712.

doi: 10.1016/S0272-6386(99)70397-5

24. Williams A, Richardson C, McCready J, *et al*. Black ethnicity is not a risk factor for mortality or graft loss after kidney transplant in the United Kingdom. *Exp Clin Transplant*. 2018;16(6):682-689.

doi: 10.6002/ect.2018.0241

25. Harding K, Mersha TB, Pham PT, *et al*. Health disparities in kidney transplantation for African Americans. *Am J Nephrol*. 2017;46(2):165-175.

doi: 10.1159/000479480

26. Limaye AP, Budde K, Humar A, *et al*. Letermovir vs valganciclovir for prophylaxis of cytomegalovirus in high-risk kidney transplant recipients: A randomized clinical trial. *JAMA*. 2023;330(1):33-42.

doi: 10.1001/jama.2023.9106

27. Raglow Z, Kaul DR. A new antiviral option for cytomegalovirus prevention after kidney transplant. *JAMA*. 2023;330(1):27-29.

doi: 10.1001/jama.2023.9100

28. Brum S, Nolasco F, Sousa J, *et al*. Leukopenia in kidney transplant patients with the association of valganciclovir and mycophenolate mofetil. *Transplant Proc*. 2008;40(3): 752-754.

doi: 10.1016/j.transproceed.2008.02.048

29. Lentine KL, Smith JM, Miller JM, *et al*. OPTN/SRTR 2021 annual data report: Kidney. *Am J Transplant*. 2023;23(2 Suppl 1):S21-S120.

doi: 10.1016/j.ajt.2023.02.004

30. Moayedi Y, Fan CS, Miller RJ. Gene expression profiling and

racial disparities in outcomes after heart transplantation. *J Heart Lung Transplant.* 2019;38(8):820-829.

doi: 10.1016/j.healun.2019.05.008

31. Müller L, Di Benedetto S. Immunosenescence and cytomegalovirus: Exploring their connection in the context of aging, health, and disease. *Int J Mol Sci*. 2024;25(2):753.

doi: 10.3390/ijms25020753

ACCSCIENCE PUBLISHING

Journal of Clinical and Translational Research

ORIGINAL ARTICLE

Retrospective comparative study of CT-guided needle localization versus medical glue localization for preoperative management of pulmonary nodules

Zhanyu Xu†, Yihua Huang†, Zehao Huang†, Huajian Peng, Jun Liu, Xu Feng*, Nuo Yang*, and Jianji Guo*

Department of Thoracic and Cardiovascular Surgery, The First Affiliated Hospital of Guangxi Medical University, Nanning, Guangxi Zhuang Autonomous Region, China

Abstract

Background: Video-assisted thoracoscopic surgery (VATS) is the preferred treatment for pulmonary nodules, making preoperative localization crucial. **Aim**: This study compared the effectiveness and complications of two computed tomography (CT)-guided localization methods for pulmonary nodules: localization needle and medical glue. **Methods**: This retrospective study included 86 patients with pulmonary nodules undergoing preoperative localization at the First Affiliated Hospital of Guangxi Medical University (July 2023 – April 2024). The patients were divided into two groups: the localization needle group (n=64) and the medical glue group (n=22). Clinical data, including baseline characteristics, localization-related data, complications, and surgical outcomes, were collected and analyzed, and subgroup analyses were done to identify risk factors for pneumothorax and pulmonary hemorrhage. **Results**: Both methods achieved a 100% localization success rate, with all nodules successfully resected. The needle group had longer localization time (17.19 vs. 15.36 min, p<0.05) and higher pneumothorax incidence (23.4% vs. 4.5%, p<0.05). The needle group also had a lower cough incidence (1.6% vs. 22.7%, p<0.05) but higher pain scores (2.89 vs. 2.36, p<0.05). No significant differences were observed in intrapulmonary hemorrhage, operative time, surgical approach, or postoperative pathology (p>0.05) between the two groups. However, subgroup analysis revealed significant differences in puncture times, localization methods, nodule size, lung history, and puncture depth related to pneumothorax and hemorrhage (p<0.05). **Conclusion**: Both CT-guided localization methods are safe and effective for VATS. The number of punctures is a key risk factor for complications such as pneumothorax and intrapulmonary hemorrhage, emphasizing the importance of careful planning and technique during localization. **Relevance for patients**: Identifying the most effective localization methods for pulmonary nodules ensures a higher success rate in surgeries, with fewer complications, ultimately leading to better patient outcomes and faster recovery. Proper preoperative localization helps reduce the risk of adverse events like pneumothorax, ensuring safer procedures and improved overall care for patients.

Keywords: CT-guided localization; Pulmonary nodules; Needle localization; Medical glue; Video-assisted thoracoscopic surgery

†*These authors contributed equally to this work.*

***Corresponding authors:**
Jianji Guo
(guojianji@gxmu.edu.cn)
Nuo Yang
(yangnuo@gxmu.edu.cn)
Xu Feng
(fengxu@sr.gxmu.edu.cn)

Citation: Xu Z, Huang Y, Huang Z, *et al*. Retrospective comparative study of CT-guided needle localization versus medical glue localization for preoperative management of pulmonary nodule. *J Clin Transl Res*. 2025;11(2):52-61. doi: 10.36922/JCTR025070007

Received: February 14, 2025

Revised: February 28, 2025

Accepted: March 12, 2025

Published online: March 27, 2025

1. Introduction

Lung cancer, despite its global incidence ranking as the second highest among cancers, remains the leading cause of cancer-related mortality worldwide.[1] In China, lung cancer is the most prevalent cancer in terms of both incidence and mortality.[2] Advances in low-dose spiral computed tomography (CT) and routine health screenings have improved early detection of lung cancer, increasing the identification of small pulmonary nodules (SPNs), many of which represent early-stage cancer.[3] SPNs can be classified into solid and subsolid types, with the latter subclassified into pure and mixed ground-glass nodules.[4]

Early-stage lung cancer is generally treated with surgical intervention, and video-assisted thoracoscopic surgery (VATS) has become the preferred method for resecting high-risk nodules due to its advantages over open thoracotomy, including reduced trauma, faster recovery, fewer complications, and the ability to obtain definitive pathological diagnoses.[5] However, accurately localizing small or deeply situated nodules during VATS remains a significant challenge. Traditional methods using preoperative CT have a low success rate of approximately 30%,[6,7] which can lead to extended surgical times, conversion to open thoracotomy, or even surgical failure. This highlights the need for more reliable preoperative localization methods.[8,9]

Accurate preoperative localization is crucial for achieving successful VATS outcomes, reducing the need for conversion to open thoracotomy, and improving resection rates. Various techniques have been developed to aid in preoperative localization, including the use of medical glue, localization needles, iodized oil, indocyanine green, and autologous blood.[10] Among there, medical glue and localization needles are commonly used due to their simplicity, high success rates, and low complication rates. However, there is limited comparative research evaluating the efficacy and safety of these two methods.

This study aims to comprehensively evaluate and compare CT-guided needle localization and CT-guided medical glue localization in terms of success rates, localization times, and complication rates. The goal is to provide insights into selecting optimal preoperative localization techniques for SPNs, ultimately improving the safety and success of VATS.

2. Materials and methods

2.1. Study subjects

This retrospective study analyzed 86 patients who underwent preoperative lung nodule localization prior to VATS at the First Affiliated Hospital of Guangxi Medical University from July 2023 to April 2024. Patients were divided into two groups: the localization needle group (n=64) and the medical glue group (n=22). The allocation was based on specific medical criteria, including the nodule's size, location, and imaging characteristics, all of which could impact the feasibility and safety of the localization technique. The preoperative surgeon evaluated these factors and determined the most appropriate method for each patient in order to optimize procedural outcomes. All cases involved solitary nodules, meaning only one pulmonary nodule was localized in each patient. The research received ethics committee approval, and informed consent was obtained from all participants.

2.2. Inclusion and exclusion criteria

The inclusion criteria of this study were as follows:

(1) Lung nodule with a maximum diameter of ≤30 mm;
(2) A high likelihood of malignancy in the lung nodule, as indicated by nodule enlargement or an increase in solid components during follow-up and imaging features such as lobulation, cavitation, or spiculation;
(3) The preoperative surgeon determined that accurate localization via visual inspection or palpation during surgery would be challenging (here, "palpation" refers to the intraoperative use of a single finger during VATS to approximate the nodule's location);
(4) The nodule does not involve the pleura, hilum, or mediastinum; and
(5) The patient is in a suitable condition for thoracoscopic surgery.

The exclusion criteria of this study were as follows:

(1) Lung nodule with a maximum diameter of <5 mm or >30 mm;
(2) Lesion located more than 40 mm from the visceral pleura;
(3) Contraindications to puncture or surgical intervention;
(4) Patients with a history of thoracic surgeries, pleural effusion, or suspected pleural malignancy; and
(5) Patients have a poor general condition, inability to tolerate surgery, or other severe illnesses.

2.3. Puncture equipment

The puncture equipment used in this study included: GE Lightspeed VCT 64-slice spiral CT scanner (GE Healthcare, IL, USA), lung nodule localization needle (20G × 100 mm, model SS50-10) (Ningbo Shengjiekang Biotechnology Co., Ltd, China), medical glue (endoscopic type/1.5 mL) (Compont, China); TSK semi-automatic percutaneous lung biopsy needle (18G × 160 mm) (Tokyo Seimitsu Kogyo K.K., Japan).

2.4. Localization procedure

Prior to the procedure, each patient and his/her family were explained about the localization process, objectives, risks, and precautions. Informed consent was obtained from the patient and he/she was instructed to maintain a stable position and smooth breathing during the procedure.

2.4.1. Localization needle group

The patient was positioned based on the nodule's location (supine, lateral, or prone position). CT scan was performed to confirm the nodule's position and metal markers were used to define the puncture area. Laser guidance was employed to pinpoint the puncture site, and local infiltration anesthesia with 2% lidocaine was applied to the planned puncture site. The localization needle was inserted through the skin into the lung, ensuring the tip was adjacent to the lesion but not within it to avoid seeding. The localization needle tail wire was pushed to the chest wall, and then the cannula was withdrawn. Any complications, such as pneumothorax, pulmonary hemorrhage, or coughing, were monitored and documented during the procedure (Figure 1A-C). The complication monitoring protocol was implemented using a multi-step approach. First, an immediate CT scan was performed on completion of the procedure to detect early complications, such as pneumothorax and pulmonary hemorrhage. Approximately 4 h post-procedure, the patient underwent routine clinical assessments; if new symptoms emerged, follow-up imaging via chest X-ray or CT scan was conducted to further evaluate potential complications. Additionally, during the interval prior to the VATS procedure – typically within 24 h – any new or emerging patient symptoms were promptly assessed, with additional imaging studies performed as necessary. All identified complications were meticulously documented for subsequent analysis.

2.4.2. Medical glue group

Literature reports vary on the dose of medical glue used for pulmonary nodule localization. Some studies suggest an injection volume of 0.5 – 1.0 mL,[11] while others recommend 0.2 – 0.3 mL.[12] To determine the medical glue dose in this study, various doses of medical glue were tested in experiments on *ex vivo* pig lungs (Figure 1D-G): 0.3 mL, 0.5 mL, 0.7 mL, and 0.9 mL. These experiments found that injecting 0.7 mL of medical glue through the puncture needle formed a hard gel particle approximately 15 mm in size in pig lungs. The variations in recommended doses may be attributed to differences in the diameter and length of the puncture needle used.

In the specific procedure, the puncture needle was inserted into the lung until it was 10 mm from the nodule. After confirming there was no bleeding, 0.7 mL of medical glue was injected, followed by the aspiration of 0.1 mL of air to ensure the glue fully entered the lung tissue and rapidly formed a hard mass. A CT scan was then performed to confirm the glue mass position and to check for any complications (Figure 1H-J).

2.5. VATS surgical procedure

Surgery is typically performed using single-port or double-port VATS. After administering anesthesia with a double-lumen endotracheal tube, the patient was placed in the lateral decubitus position. The surgical area was disinfected, and an incision was made at the fifth intercostal space along the mid-axillary line. The thoracoscope was inserted, and the nodule was identified using the localization needle tail wire, or, in the case of medical glue localization, by using instruments or palpation to detect the hardened glue mass. Once the target nodule was identified, a partial lung resection (wedge resection or segmentectomy) was performed if the nodule is more than 20 mm from the lesion's edge. Intraoperative frozen section analysis of the resected specimen was conducted to guide further surgical decisions. For malignant nodules larger than 20 mm, a lobectomy and lymph node dissection were performed. If the nodule was undetected during thoracoscopic surgery, conversion to open thoracotomy may be necessary. If the resected lung tissue showed no nodule, lobectomy or conversion to open thoracotomy may be required.

2.6. Data collection and evaluation metrics

Clinical data were collected from patients, including baseline information (general information, imaging data), localization operation and complications, and surgical details. General information included gender, age, smoking history, and history of lung disease. Imaging data included distance from the nodule to the pleura, nodule characteristics, nodule location, and size. Localization operation and complications covered localization time (from the start of CT scanning to the completion of localization), puncture depth, number of punctures (1/>1), localization success rate (defined as the final CT image showing the localization needle or medical glue mass adjacent to the nodule, with successful visualization during VATS or no displacement of the needle or detachment), and post-localization complications including pneumothorax (small, moderate, or large), pulmonary hemorrhage (defined as[13] no hemorrhage when CT imaging showed <1 cm^2 of patchy shadow around the needle; minor hemorrhage when CT imaging showed increased density of ground-glass shadow ≥1 cm^2 without irritating cough or hemoptysis; major hemorrhage when CT imaging showed ground-glass shadow ≥3 cm^2 or the

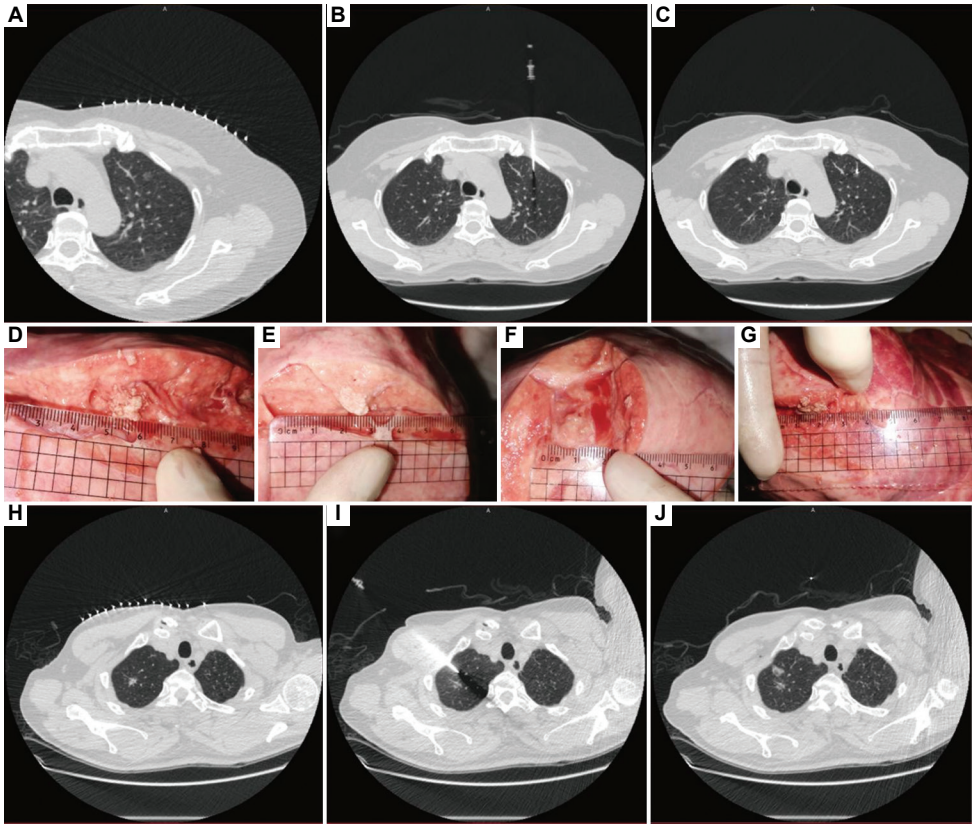

Figure 1. CT-guided localization needle placement and medical glue injection for pulmonary nodule management. (A) Patient 1; pre-localization CT scans show an 8 mm nodule, (B) localization needle adjacent to the nodule without penetration, and (C) needle anchored near the nodule with no complications like pneumothorax or hemorrhage. (D-G) Formation of hard masses after medical glue injection; 9 mm (D, 0.3 mL), 12 mm (E, 0.5 mL), 14 mm (F, 0.7 mL), and 15 mm (G, 0.9 mL). (H) Patient 2; pre-localization CT scans show a 15 mm nodule and (I) needle adjacent to the nodule without penetration, (J) while post-injection CT scan shows the position of the nodule and glue, with no complications like cough or pneumothorax.
Abbreviation: CT: Computed tomography.

patient exhibits imaging signs along with irritating cough or hemoptysis), pain [assessed using the Numeric Rating Scale]. Surgical details included surgical success rate (defined as complete nodule resection, with the nodule at least 20 mm from the resection margin), surgical time (from skin incision to skin closure), surgical approach used (wedge resection, segmentectomy, or lobectomy), and pathological results.

2.7. Statistical methods

Data analysis was conducted using SPSS version 26.0. Normally distributed data were summarized as mean ± standard deviation and analyzed using t-tests. Non-normally distributed data were expressed as median values and analyzed using rank-sum tests. Descriptive statistics for count data included percentages and frequencies, with inter-group comparisons analyzed using Fisher's exact test or chi-square tests. A $p<0.05$ was considered statistically significant.

3. Results

3.1. Baseline characteristics of patients and pulmonary nodules

A total of 86 patients with SPNs were included in the study and divided into two groups based on the preoperative localization method: 64 patients in the localization needle group and 22 patients in the medical glue group. The baseline characteristics of the two groups were as follows: There were no statistically significant differences between the groups in terms of gender distribution, mean age, smoking history, or history of pulmonary disease ($p>0.05$). The distance from the nodule to the pleura and the size of the nodules also showed no significant difference between the groups ($p>0.05$). Additionally, the distribution of nodule types (solid nodules, mixed ground-glass nodules, and pure ground-glass nodules) and their locations in the lungs exhibited no statistically significant differences between the two groups ($p>0.05$). Detailed statistical results are shown in Table 1.

Table 1. Baseline characteristics of patients and pulmonary nodules in the localization needle group and medical glue group

	Localization needle group (*n*=64)	Medical glue group (*n*=22)	*p*-value
Gender (male/female)	18/46	6/16	0.939
Age (years)	52.45±12.43	52.35±10.55	0.922
Smoking history (yes/no)	10/54	3/19	0.822
Pulmonary disease history (yes/no)	10/54	4/18	0.748
Nodule size (mm)	12.40±4.33	13.77±5.41	0.235
Distance to pleura (mm)	13.247±10.01	11.159±7.89	0.381
Nodule location			0.661
Right upper lobe	24	9	
Right middle lobe	3	1	
Right lower lobe	9	5	
Left upper lobe	18	3	
Left lower lobe	10	4	
Nodule characteristics			0.725
Pure ground-glass nodules	22	5	
Mixed ground-glass nodules	34	12	
Solid nodules	8	5	

3.2. Comparison of localization time, complications, and surgical outcomes between localization needle and medical glue groups

Localization time was significantly longer in the localization needle group (17.19 ± 2.56 min) compared to the medical glue group (15.36 ± 2.06 min, $p<0.05$). Both groups had a 100% localization success rate, with no significant differences noted. No pleural reactions were observed. The needle group reported more complications, including 15 cases of pneumothorax, 11 cases of pulmonary hemorrhage, and 1 case of cough, compared to the glue group with 1 case of pneumothorax, 2 cases of pulmonary hemorrhage, and 5 cases of cough. There was no significant difference in pulmonary hemorrhage ($p>0.05$), but differences in pneumothorax, cough, and pain scores were significant ($p<0.05$). Pain scores averaged 2.89 ± 0.95 in the needle group and 2.36 ± 0.79 in the glue group ($p<0.05$). All complications were mild, with pneumothorax and pulmonary hemorrhage not requiring emergency treatment, and coughs relieved by antitussives. No severe complications occurred. The average VATS time was similar between the groups ($p>0.05$), and all procedures achieved 100% nodule resection, with no significant differences in surgical approach or conversion to open surgery ($p>0.05$). Surgical approaches (wedge resection, segmentectomy, lobectomy) and pathology results (benign lesions, *in situ* adenocarcinoma, microinvasive adenocarcinoma, invasive adenocarcinoma) were distributed similarly between the groups ($p>0.05$). Detailed statistical results are shown in Table 2.

3.3. Subgroup analysis of pneumothorax and pulmonary hemorrhage

Patients were divided into subgroups based on the presence or absence of pneumothorax and pulmonary hemorrhage after the procedure. The pneumothorax group showed significant differences compared to the nonpneumothorax group in terms of the number of punctures, localization method, nodule size, and history of pulmonary disease ($p<0.05$). However, there were no significant differences in age, gender, smoking history, nodule location, distance from pleura, puncture depth, or localization time ($p>0.05$). Similarly, the pulmonary hemorrhage group revealed significant differences in history of pulmonary disease, puncture depth, localization time, and number of punctures ($p<0.05$), while no significant differences were observed in age, gender, smoking history, nodule location, nodule size, distance from pleura, or localization method ($p>0.05$). Detailed statistical results are shown in Table 3.

4. Discussion

The localization of pulmonary nodules can be achieved through various methods, categorized into preoperative and intraoperative localization based on the timing of the procedure. Currently, the most commonly used preoperative localization techniques include CT-guided percutaneous localization, bronchoscopy-assisted localization, and CT virtual three-dimensional (3D) localization.[14,15] CT-guided percutaneous localization involves placing a marker near the pulmonary nodule under CT guidance before surgery. The nodule is then located by searching for the marker, making this the most widely used localization method in clinical practice. This technique can be further classified based on the materials used, including medical adhesive, lipiodol, autologous blood, and others.[16-18]

The pulmonary nodule localization needle is a modified version of the hook-wire and is designed for single use. It features a quadruple-barbed structure at the tip and a three-color soft thread at the tail, allowing for secure anchorage within the lung tissue and marking the depth of localization. This method has a high success rate and a low incidence of complications, as supported by existing studies.[19] A study indicates that, compared to the hook-wire, the pulmonary nodule localization needle has a higher success rate (100% vs. 84.0%, $p<0.05$) and fewer complications (12.9% vs. 40.0%, $p<0.05$).[20] Wang *et al.* reported that using a CT-guided novel pulmonary nodule

Table 2. Comparison of localization time, complications, surgical approach, and pathology results between the localization needle group and medical glue group

	Localization needle group (*n*=64)	Medical glue group (*n*=22)	*p*-value
Localization time (min)	17.19±2.56	15.36±2.06	0.003
Number of punctures (1/>1)	44/20	4/18	0.238
Complications			
Pneumothorax (yes/no)	15/49	1/21	0.049
Pulmonary hemorrhage (yes/no)	11/53	2/20	0.501
Cough (yes/no)	1/63	5/17	0.004
Pain score	2.89±0.95	2.36±0.79	0.021
Vats time (min)	114.6±35.1	116.6±34.2	0.819
Surgical approach			0.086
Wedge resection	41	14	
Segmentectomy	16	2	
Lobectomy	7	6	
Pathology results			0.315
Benign lesions	11	2	
In situ adenocarcinoma	5	4	
Microinvasive adenocarcinoma	11	6	
Invasive adenocarcinoma	37	10	

localization needle before thoracoscopic resection of SPNs effectively reduces the risk of displacement or dislodgement of the hook-wire and alleviates postoperative pain.[21]

Medical glue, a type of medical adhesive product, enables rapid solidification, with cyanoacrylate being its main component. Scholars first described its use for preoperative localization of pulmonary nodules in the late 20th century, using CT guidance.[22] When medical glue comes into contact anionic substances such as blood, it undergoes anionic polymerization and rapidly forms a clump.[23] During localization, CT guidance is used to inject the medical glue near the pulmonary nodule. After injection, a hard mass forms, which can be palpated to confirm its position, thereby completing the localization. Medical glue acts as a tissue sealant that rapidly solidifies upon injection into the lung parenchyma, sealing the puncture tract and preventing pneumothorax and bleeding to some extent. CT-guided medical glue localization has a high success rate and low complication rate, making it a safe and effective preoperative localization method. Studies have reported localization success rates of up to 100% and low complication rates, including asymptomatic pneumothorax (11.9%) and mild intrapulmonary hemorrhage (13.1%), with no other complications observed.[24]

Each pulmonary nodule localization method has its advantages and disadvantages. Due to their simplicity,

Table 3. Subgroup analysis of risk factors for pneumothorax and pulmonary hemorrhage

	Pneumothorax group (*n*=16)	Non-pneumothorax group (*n*=70)	*p*-value	Pulmonary hemorrhage group (*n*=13)	Non-pulmonary hemorrhage group (*n*=73)	*p*-value
Age (years)	53.73±13.61	52.18±11.61	0.65	54.15±8.79	52.15±12.41	0.58
Gender (male/female)	3/13	21/49	0.539	6/7	18/55	0.111
Smoking history (yes/no)	1/15	12/58	0.446	4/9	9/64	0.103
Pulmonary disease history (yes/no)	6/10	8/62	0.011	5/8	9/64	0.019
Nodule location			0.105			0.434
Right upper lobe	2	31		5	28	
Right middle lobe	2	2		0	4	
Right lower lobe	4	10		4	10	
Left upper lobe	5	16		3	18	
Left lower lobe	3	11		1	13	
Nodule size (mm)	10.63±2.12	13.24±4.91	0.002	13.15±5.09	12.68±4.58	0.739
Distance to pleura (mm)	14.03±10.93	12.44±9.32	0.561	15.80±11.73	12.163±9.12	0.209
Puncture depth (mm)	18.89±10.54	18.22±7.58	0.773	23.07±9.41	17.49±7.61	0.021
Localization time (min)	17.00±2.20	16.66±2.63	0.644	18.46±1.85	16.41±2.55	0.007
Localization method (needle/glue)	1/15	49/21	0.049	11/2	53/20	0.499
Number of punctures (1/>1)	6/10	56/14	0.001	6/7	56/17	0.04

high success rates, and low complication rates, CT-guided pulmonary nodule localization needle and medical glue localization are commonly used in clinical practice. However, comparative analyses of these two methods are currently limited. This study included 86 cases, with 64 cases using the pulmonary nodule localization needle and 22 cases using medical glue. No pleural reactions or severe complications were observed in either group post-localization. Even when complications such as coughing or pneumothorax occurred, the symptoms were mild and did not require intervention, suggesting that both the pulmonary nodule localization needle and medical glue are safe and effective preoperative localization methods for pulmonary nodules. However, significant differences were observed between the two groups in terms of localization time and complication rates ($p<0.05$). In analyzing the complications, 1 case of pneumothorax occurred in the medical glue group, while 15 cases were reported in the localization needle group, indicating a statistically significant difference ($p<0.05$). The medical glue, primarily composed of cyanoacrylate, rapidly solidifies upon injection into the lung parenchyma. When the puncture needle is withdrawn, the solidified adhesive seals the puncture tract, preventing air entry into the pleural cavity and reducing the incidence of pneumothorax. Therefore, medical glue is recommended for elderly patients with conditions such as emphysema, bullae, or compromised lung function.

In this study, patients in the medical glue group reported lower pain scores than those in the localization needle group, with a statistically significant difference ($p<0.05$). This difference is likely attributed to the localization needle moving with the patient's breathing, coughing, or positional changes, causing traction and stimulation of the lung tissue and pleura, which leads to pain. In contrast, medical glue, being a liquid material, rapidly forms a solid mass upon injection into the lung parenchyma, securing firmly without direct pleural contact, resulting in less pain. Studies have shown that the pain associated with medical glue localization is primarily due to the puncture injury and gradually diminishes over time.[25] Reducing pain can help prevent pleural reactions, which is particularly beneficial for patients with low pain tolerance.[26] If a pulmonary nodule localization needle is used, adequate analgesia should be provided. In this study, 5 patients in the medical glue group experienced coughing, compared to 1 patient in the localization needle group, showing a significant difference ($p<0.05$). Researchers such as Tao *et al.*[27] noted that the strong odor of medical glue could trigger irritation-induced coughing, and rapid injection may also cause coughing. Our findings are consistent with previous published report. Potential strategies to mitigate this issue include: carefully controlling the injection volume and speed to minimize glue diffusion; refining the glue formulation to reduce its irritative properties; administering antitussive or anti-inflammatory medications preoperatively; and providing prophylactic nebulization with budesonide post-procedure to reduce glue-induced bronchial inflammation. Moreover, for patients with chronic obstructive pulmonary disease (COPD) or asthma, preoperative localization using the pulmonary nodule localization needle is preferred to minimize the risk of exacerbating primary diseases due to medical adhesive-induced coughing.

Literature indicates that postlocalization with a needle may limit patient mobility; insufficient immobilization, excessive movement during transfer, or prolonged lung collapse can increase the risk of dislodgement. A longer interval between localization and VATS resection is associated with a higher rate of localization-related complications. In contrast, medical adhesive offers better safety and stability, allowing for a longer interval between localization and surgery, thereby providing more flexible scheduling.[28,29] Patients also tolerate cyanoacrylate markers well following medical glue localization.[30] Thus, medical glue is preferred when there is a long interval between localization and surgery.

Furthermore, a potential area for future improvement involves the development of a decision-making algorithm that integrates patient-specific pulmonary comorbidities and anatomical factors to optimize the choice of localization technique. For example, needle localization may be prone to marker displacement due to lung mobility, particularly in patients with conditions such as COPD or asthma. Recent advances in respiratory monitoring and control, as illustrated by a portable, noninvasive ventilator system[31] demonstrate that incorporating sophisticated algorithms and real-time monitoring into medical devices is feasible. Such technological innovations could be adapted to refine pulmonary nodule localization by tailoring the choice between needle and medical glue based on individual patient characteristics. Future studies should explore the clinical utility of these decision-making tools to further enhance the safety and efficacy of localization procedures.

Analysis of this study suggests significant differences between the pneumothorax and non-pneumothorax groups in terms of lung disease history, nodule size, localization method, and puncture attempts. Patients with a history of pulmonary diseases, such as COPD and emphysema, may exhibit compromised pleural integrity due to the destruction of alveolar elastic fibers and the formation of pulmonary bullae.[32,33] Consequently, these patients are more susceptible to pleural rupture and subsequent pneumothorax during puncture or

localization procedures. Moreover, in patients with small nodules, the increased technical difficulty often necessitates multiple adjustments in needle angle or depth, thereby elevating the number of pleural punctures. Yao *et al*.[34] found that an increased number of puncture attempts during hook-wire localization is an independent risk factor for pneumothorax. Multiple punctures may create more holes in the visceral pleura, compromising its integrity and increasing the risk of air entering the pleural cavity, leading to pneumothorax. Similarly, analysis in this study shows significant differences between the intrapulmonary hemorrhage and non-hemorrhage groups concerning puncture attempts, lung disease history, and localization time. These findings align with other studies.[35] Intrapulmonary hemorrhage likely occurs due to the rich vascularity of the lungs, with puncture needles potentially damaging small pulmonary vessels. An increased number of punctures raises the risk of vascular injury, thereby elevating the risk of hemorrhage. Proper lesion assessment and route planning before puncture can minimize failure and reduce the incidence of pneumothorax and intrapulmonary hemorrhage. Patients with a history of lung diseases may be more prone to hemorrhage during puncture procedures due to reduced alveolar wall elasticity and abnormal vascular distribution.[32,33] Additionally, prolonged puncture times may induce increased anxiety and stress in patients, which can compromise the stability of the localization process and further elevate the risk of pulmonary hemorrhage.

Our study has several limitations. First, our adhesive protocol was standardized based on previous literature, and we did not systematically evaluate modifications—such as reducing the injected volume or altering the formulation—to minimize the adhesive's irritative reaction. Although the glue group exhibited lower pain scores compared to the needle group, further optimization of the adhesive parameters may enhance the safety and tolerability of the localization technique. Second, while the use of localization markers ensured that all lesions were readily identified during surgery, thereby achieving our localization objectives, the retrospective design precluded the collection of quantitative data to assess differences in marker stability between the localization procedure and surgery. This limitation represents a promising direction for future research. Finally, the retrospective nature of our study introduces inherent limitations, including potential selection bias and confounding factors that may affect the generalizability of our findings. Future prospective studies with standardized protocols are warranted to validate these results and further mitigate potential biases.

5. Conclusion

For preoperative localization of pulmonary nodules, both CT-guided pulmonary nodule localization needles and medical glue are safe and effective, but it is crucial to note the distinctive set of advantages and disadvantages of each method. Medical glue is preferable for patients with emphysema, bullae, poor pain tolerance, long puncture paths, or longer intervals between localization and surgery. In contrast, the pulmonary nodule localization needle is more suitable for patients with COPD or asthma. Intrapulmonary hemorrhage is associated with localization time, puncture depth, lung disease history, and puncture attempts, while pneumothorax is related to lung disease history, nodule size, localization method, and puncture attempts.

Acknowledgments

We are deeply grateful to the medical team (physicians, nurses, and anesthesiology staff) at the First Affiliated Hospital of Guangxi Medical University for their professional expertise and tireless efforts in supporting this research.

Funding

This work was supported in part by Self-financed Scientific Research of Guangxi Zhuang Autonomous Region Health Commission (Z20211032), Guangxi Medical and Health Appropriate Technology Development and Popularization Application Project (S2022070), the Joint Project on Regional High-Incidence Diseases Research of Guangxi Natural Science Foundation (2024GXNSFBA010032), the Youth Science Foundation of Guangxi Medical University (GXMUYSF202420), the National Key Clinical Specialty Construction Project, Guangxi Medical and Health Key Discipline Construction Project and Guangxi Key Clinical Specialty Construction Project.

Conflict of interest

There are no conflicts of interest.

Author contributions

Conceptualization: Zhanyu Xu, Jianji Guo
Formal analysis: Zehao Huang, Nuo Yang
Investigation: Yihua Huang, Zehao Huang, Huajian Peng, Xu Feng
Methodology: Zhanyu Xu, Yihua Huang
Supervision: Xu Feng, Nuo Yang, Jianji Guo
Writing – original draft: Zhanyu Xu
Writing – review & editing: Jun Liu, Xu Feng, Nuo Yang, Jianji Guo

Ethics approval and consent to participate

The authors are accountable for all aspects of the work in ensuring that questions related to the accuracy or integrity of any part of the work are appropriately investigated and resolved. The study was conducted in accordance with the Declaration of Helsinki (as revised in 2013). This study was approved by the Ethics Committee of the First Affiliated Hospital of Guangxi Medical University (NO.2023-S775-01). Requirement to obtain individual consent for this retrospective analysis was waived.

Consent for publication

All human participants in this study provided verbal informed consent for the publication of anonymized data. All identifiable information has been rigorously removed or altered to protect participant privacy.

Availability of data

Data are available from the authors upon reasonable request, subject to ethics approval.

References

1. Siegel RL, Miller KD, Wagle NS, Jemal A. Cancer Statistics, 2023. CA Cancer J Clin 2023;73:17-48.

   doi: 10.3322/caac.21763

2. Han B, Zheng R, Zeng H, Wang S, Sun K, Chen R, *et al.* Cancer Incidence and Mortality in China, 2022. J Natl Cancer Cent 2024;4:47-53.

   doi: 10.1016/j.jncc.2024.01.006

3. Lancaster HL, Heuvelmans MA, Oudkerk M. Low-dose Computed Tomography Lung Cancer Screening: Clinical Evidence and Implementation Research. J Intern Med 2022;292:68-80.

   doi: 10.1111/joim.13480

4. Mazzone PJ, Lam L. Evaluating the Patient with A Pulmonary Nodule: A Review. JAMA 2022;327:264-73.

   doi: 10.1001/jama.2021.24287

5. Feray S, Lubach J, Joshi GP, Bonnet F, Van De Velde M. PROSPECT Guidelines for Video-assisted Thoracoscopic Surgery: A Systematic Review and Procedure-specific Postoperative Pain Management Recommendations. Anaesthesia 2022;77:311-25.

   doi: 10.1111/anae.15609

6. Keating J, Singhal S. Novel Methods of Intraoperative Localization and Margin Assessment of Pulmonary Nodules. Semin Thorac Cardiovasc Surg 2016;28:127-36.

   doi: 10.1053/j.semtcvs.2016.01.006

7. Tang L, Zhang Y, Wang Y. Intraoperative Identification of Pulmonary Nodules During Minimally Invasive Thoracic Surgery: A Narrative Review. Quant Imaging Med Surg 2022;12:5271-87.

   doi: 10.21037/qims-22-309

8. Li CD, Huang ZG, Sun HL, Wang LT, Wang YL, Gao BX, *et al.* Marking Ground Glass Nodules with Pulmonary Nodules Localization Needle Prior to Video-assisted Thoracoscopic Surgery. Eur Radiol 2022;32:4699-706.

   doi: 10.1007/s00330-022-08597-7

9. Wang Y, Chen E. Advances in the Localization of Pulmonary Nodules: A Comprehensive Review. J Cardiothorac Surg 2024;19:396.

   doi: 10.1186/s13019-024-02911-8

10. Wang L, Sun D, Gao M, Li C. Computed Tomography-guided Localization of Pulmonary Nodules Prior to Thoracoscopic Surgery. Thorac Cancer 2023;14:119-26.

    doi: 10.1111/1759-7714.14754

11. McDaniel JD, Racadio JM, Patel MN, Johnson ND, Kukreja K. CT-guided Localization of Pulmonary Nodules in Children Prior to Video-Assisted Thoracoscopic Surgical Resection Utilizing A Combination of two Previously Described Techniques. Pediatr Radiol 2018;48:626-31.

    doi: 10.1007/s00247-018-4069-0

12. Ye W, Dong C, Lin C, Wu Q, Li J, Zhou Z, *et al.* Medical Adhesive VS Hookwire for Computed Tomography-guided Preoperative Localization and Risk Factors of Major Complications. Br J Radiol 2021;94:20201208.

    doi: 10.1259/bjr.20201208

13. Rothman A, Lim S, Hasegawa D, Steiger D, Patel R, Lee YI. Abnormal Pulmonary Function Testing as an Independent Risk Factor for Procedural Complications During Transthoracic Needle Biopsies. J Bronchology Interv Pulmonol 2022;29:213-9.

    doi: 10.1097/LBR.0000000000000819

14. Xin N, Wu X, Chen Z, Wei R, Saito Y, Lachkar S, *et al.* A New Preoperative Localization of Pulmonary Nodules Guided by Mixed Reality: A Pilot Study of an Animal Model. Transl Lung Cancer Res 2023;12:150-7.

    doi: 10.21037/tlcr-22-884

15. Anayama T, Yamamoto M, Hirohashi K, Miyazaki R, OkadaH, Doi A, *et al.* The Accuracy of Cone-beam Computed Tomography and Augmented Fluoroscopy-guided Bronchoscopic Marking of Multiple Small-sized Pulmonary Nodules in a Hybrid Operating Room: A Retrospective Cohort Study. Quant Imaging Med Surg 2021;11:725-36.

    doi: 10.21037/qims-20-781

16. Rho J, Lee JW, Quan YH, Choi BH, Shin BK, Han KN, *et al.* Fluorescent and Iodized Emulsion for Preoperative Localization

of Pulmonary Nodules. Ann Surg 2021;273:989-96.

doi: 10.1097/SLA.0000000000003300

17. Zhang H, Zhang X, Li Y, Huang Z, Liu H, Chen X. The Efficacy and Safety of CT-guided Localization of Pulmonary Nodules by Medical Adhesives Containing Methylene Blue Before Surgery. Heliyon 2024;10:e31404.

doi: 10.1016/j.heliyon.2024.e31404

18. Xu J, Si T, Zheng M, Guan J, Li Z, Xu Z. CT Guided Autologous Blood Localization of Pulmonary Ground Glass Nodules for Video Assisted Thoracoscopic Surgery Compared to Micro-Coil Localization. J Cardiothorac Surg 2022;17:183.

doi: 10.1186/s13019-022-01934-3

19. Kong J, Guo J, Zhang H, Li Y, Wang G, Zhang Y. CT-Guided Localization Techniques of Small Pulmonary Nodules: A Prospective Non-randomized Controlled Study on Pulmonary Nodule Localization Needle and Methylene Blue Staining with Surgical Glue. J Thorac Dis 2020;12:6826-35.

doi: 10.21037/jtd-20-3147

20. Kleedehn M, Kim DH, Lee FT, Lubner MG, Robbins JB, Ziemlewicz TJ, *et al.* Preoperative Pulmonary Nodule Localization: A Comparison of Methylene Blue and Hookwire Techniques. AJR Am J Roentgenol 2016;207:1334-9.

doi: 10.2214/AJR.16.16272

21. Wang Z, Li B, Hu Z, Zhao Q, Zhang X, Zhao H, *et al.* Comparison of Different Localization Needles and Postures in Localization of Pulmonary Nodules. J Cardiothorac Surg 2024;19:668.

doi: 10.1186/s13019-024-03144-5

22. Yoshida J, Nagai K, Nishimura M, Takahashi K. Computed Tomography-fluoroscopy Guided Injection of Cyanoacrylate to Mark A Pulmonary Nodule for Thoracoscopic Resection. Jpn J Thorac Cardiovasc Surg 1999;47:210-3.

doi: 10.1007/BF03217996

23. Mazur M, Zakrzewski W, Szymonowicz M, Rybak Z. Medical Adhesives and Their Role in Laparoscopic Surgery-A Review of Literature. Materials (Basel) 2022;15:5215.

doi: 10.3390/ma15155215

24. Zhang H, Li Y, Chen X, He Z. Comparison of Hook-wire and Medical Glue for CT-guided Preoperative Localization of Pulmonary Nodules. Front Oncol 2022;12:922573.

doi: 10.3389/fonc.2022.922573

25. Yu S, Li W, Liu X, Chen X, He X, Duan X, *et al.* Application Value of CT-guided Localization Using A Coil in Combination with Medical Adhesive in Sublobar Resection. Clin Transl Oncol 2023;25:2931-7.

doi: 10.1007/s12094-023-03156-y

26. Du A, Hannan L, Muruganandan S. A Narrative Review on Pain Control Interventions for Non-Surgical Pleural Procedures. Respir Med 2023;207:107119.

doi: 10.1016/j.rmed.2023.107119

27. Tao G, Jingying Y, Tan G, Xiaotao D, Min C. A Novel CT-guided Technique Using Medical Adhesive for Localization of Small Pulmonary Ground-glass Nodules and Mixed Ground-Glass Nodules (≤20 mm) Before Video-assisted Thoracoscopic Surgery. Diagn Interv Radiol 2018;24:209-12.

doi: 10.5152/dir.2018.17315

28. Pezeshkian F, McAllister M, Singh A, Jaklitsch MT, Gill RR, Bueno R, *et al.* Image-guided Video-assisted Thoracoscopic Surgery (iVATS): A Single Center Experience and Review. J Thorac Dis 2023;15:7035-41.

doi: 10.21037/jtd-23-1461

29. Huang Y, Zhao Z, Wang T, Yang J, Lu Z, Wang B, *et al.* A Comparison between Prethoracoscopy Localization of Small Pulmonary Nodules by Means of Medical Adhesive versus Hookwire. J Vasc Interv Radiol 2018;29:1547-52.

doi: 10.1016/j.jvir.2018.05.013

30. Liu Y, Hou Z, Wu K, Zhu Y, Wang H, Han Y. α-Cyanoacrylate Rapid Medical Adhesive (Medical EC Glue) Localization of Pulmonary Nodules Guided by Computed Tomography before Thoracoscopic Surgery. Curr Med Imaging 2023;19:382-8.

doi: 10.2174/1573405618666220920113257

31. Menniti M, Laganà F, Oliva G, Bianco M, Fiorillo AS, Pullano SA. Development of Non-invasive Ventilator for Homecare and Patient Monitoring System. Electronics 2024;13:790.

doi: 10.3390/electronics13040790

32. Ferrera MC, Labaki WW, Han MK. Advances in Chronic Obstructive Pulmonary Disease. Annu Rev Med 2021;72:119-34.

doi: 10.1146/annurev-med-080919-112707

33. Janssen R, Piscaer I, Franssen FM, Wouters EF. Emphysema: Looking Beyond Alpha-1 Antitrypsin Deficiency. Expert Rev Respir Med 2019;13:381-97.

doi: 10.1080/17476348.2019.1580575

34. Yao F, Wang J, Yao J, Xu L, Wang J, Gao L. Reevaluation of the Efficacy of Preoperative Computed Tomography-guided Hook Wire Localization: A Retrospective Analysis. Int J Surg 2018;51:24-30.

doi: 10.1016/j.ijsu.2018.01.014

35. Chiu JH, Chang YY, Weng CY, Lee YC, Yeh YC, Chen CK. Risk Factors for Pneumothorax and Pulmonary Hemorrhage Following Computed Tomography-guided Transthoracic Core-needle Biopsy of Subpleural Lung Lesions. J Chin Med Assoc 2022;85:500-6.

doi: 10.1097/JCMA.0000000000000705

ACCSCIENCE PUBLISHING

Journal of Clinical and Translational Research

ORIGINAL ARTICLE

Understanding fetal posterior fossa abnormalities: Insights from MRI and ultrasound imaging

Deniz Delibaş*, Arzu Gülşah Yalçın, Zafer Yumak, and Elif Ergün

Department of Radiology, TC Saglik Bakanligi Ankara Egitim ve Arastirma Hastanesi, Ankara, Turkey

Abstract

Background: The posterior fossa is a critical brain region housing essential structures such as the cerebellum and brainstem, crucial for coordination, balance, and autonomic functions. Abnormalities in this area significantly impact fetal development and postnatal outcomes, necessitating accurate diagnosis and characterization of fetal posterior fossa abnormalities. **Aims:** This review aims to analyze the diagnostic role of ultrasound, the primary imaging modality due to its accessibility and safety, and magnetic resonance imaging, which provides enhanced diagnostic accuracy in identifying central nervous system anomalies, particularly those involving the posterior fossa. A comprehensive approach is proposed to address the diagnostic complexities of cerebellar malformations, including ambiguous terminology and overlapping clinical features, which pose notable challenges. **Relevance for patients:** The complexity and lack of consensus regarding cerebellar malformations across medical disciplines can hinder accurate diagnosis and timely intervention. By advancing interdisciplinary research and refining diagnostic approaches, this study aims to enhance clinical management strategies and improve patient outcomes in cases of posterior fossa pathologies, ultimately fostering a more integrated and effective approach to diagnosis and treatment.

Keywords: Fetal imaging; Fetal magnetic resonance imaging; Fetal ultrasound; Posterior fossa

***Corresponding author:**
Deniz Delibaş
(deniz.delibas@saglik.gov.tr)

Citation: Delibaş D, Yalçın AG, Yumak Z, Ergün E. Understanding fetal posterior fossa abnormalities: Insights from MRI and ultrasound imaging. *J Clin Transl Res*. 2025;11(2):62-77.
doi: 10.36922/jctr.6240

Received: November 19, 2024

1st revised: February 10, 2025

2nd revised: March 14, 2025

Accepted: March 17, 2025

Published online: April 4, 2025

1. Introduction

The posterior cranial fossa houses the brainstem and cerebellum, essential parts of the central nervous system (CNS). The hindbrain, also known as the rhombencephalon, is the embryonic precursor of the posterior fossa structures. During embryonic days 17 – 21, the notochord induces the overlying ectoderm, which ultimately gives rise to the neural tube and neural crest. Initially, three primary brain vesicles form: the forebrain, midbrain, and hindbrain. By the 4th week, these develop into five secondary vesicles: The telencephalon, diencephalon, mesencephalon, metencephalon, and myelencephalon. The hindbrain further differentiates into the metencephalon (pons and cerebellum) and the myelencephalon (medulla oblongata), whereas its cavity develops into the fourth ventricle and central canal. Throughout this process, the midbrain (mesencephalon) undergoes comparatively minimal alterations.[1,2]

Transabdominal ultrasound, a key component of fetal imaging, is complemented by fetal magnetic resonance imaging (MRI) as a crucial adjunct. Guidelines from reputable organizations such as American College of Obstetricians and Gynecologists (ACOG), American Institute of Ultrasound in Medicine (AIUM), Australasian Society for Ultrasound in Medicine (ASUM), National Health Service (NHS), and International Society of Ultrasound in Obstetrics and Gynecology (ISUOG) emphasize the importance of posterior fossa assessment during second-trimester pregnancy imaging.[3-7] MRI, when performed without contrast media, has no known adverse fetal effects at any stage of pregnancy.[7] Over the past decade, MRI has improved prenatal diagnosis of CNS anomalies, especially in the posterior fossa.[8] Despite some controversy in terminology, diagnosing posterior fossa malformations can significantly aid parental counseling and pregnancy management.

The primary aim of this review is to evaluate and compare the roles of ultrasound and MRI in diagnosing fetal posterior fossa anomalies, with a focus on cerebellar malformations. It seeks to clarify diagnostic criteria, address ambiguous terminology, and propose standardized protocols that could improve parental counseling and clinical decision-making.

2. Methods

A comprehensive literature search was conducted using PubMed to identify relevant articles published up to (2024). Search terms included "fetal posterior fossa," "fetal ultrasound," "fetal MRI," and terms related to posterior fossa pathologies. Studies were selected based on their relevance to prenatal imaging of the posterior fossa and associated pathologies. Both original research articles and review papers were considered, with a focus on those that provided detailed imaging protocols, diagnostic criteria, and outcome analyses. Reference lists of selected articles were also reviewed to identify additional sources. Data were synthesized to critically assess the diagnostic performance, advantages, and limitations of ultrasound and MRI in this context.

3. Fetal posterior fossa

3.1. Normal anatomy of the fetal posterior fossa on MRI and ultrasound

At approximately 8 weeks of gestation, the rhombencephalon appears as a cystic structure and is the first identifiable feature in the posterior fossa (Figure 1). By 11 – 13 weeks, the brainstem and fourth cerebral ventricle become visible in the mid-sagittal view, which is commonly used for measuring nuchal translucency and assessing the nasal bone. The fourth ventricle appears as an intracranial

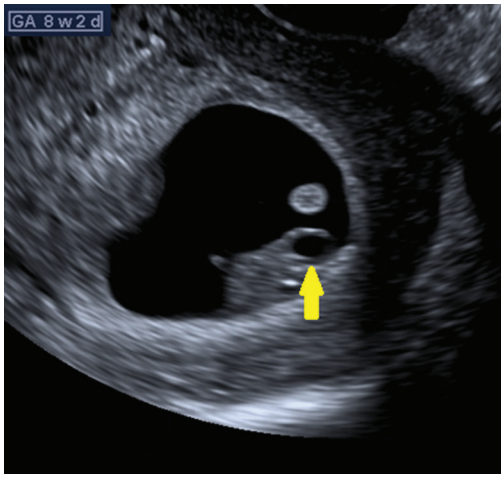

Figure 1. The fetal rhombencephalon, observed as an anechoic structure in the posterior brain (yellow arrow), is a normal finding at 8 – 10 weeks of gestation and is not indicative of developmental issues.
Abbreviation: GA: Gestational age.

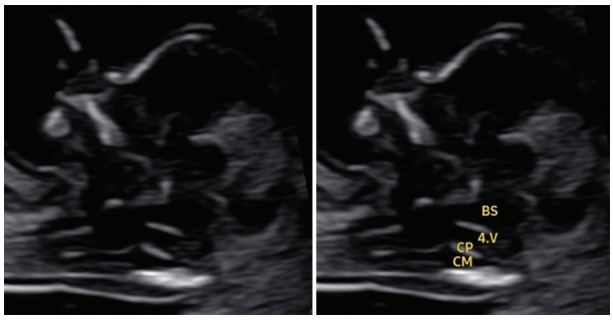

Figure 2. Sagittal ultrasound images of a 13-week fetus, displaying a comprehensive view of key structures within the developing brain. The left image presents an unmarked scan, while the right image includes labelled anatomical structures, such as the BS, the 4.V, the CP, and the CM, helping in the identification of critical posterior fossa components.
Abbreviations: BS: Brainstem; 4.V: Fourth ventricle; CP: Choroid plexus; CM: Cisterna magna.

translucency with echogenic borders, located between the brainstem and the cisterna magna, with the choroid plexus of the fourth ventricle visible posteriorly[9] (Figure 2).

A routine mid-trimester ultrasound includes a transcerebellar plane to evaluate the posterior fossa[7] (Figure 3). This plane assesses the cerebellum, cerebellar vermis, and cerebrospinal fluid (CSF) in the cisterna magna. Before 19 – 20 weeks of gestational, the cerebellar vermis may not fully cover the fourth ventricle, leading to an atypical appearance that could be mistakenly interpreted as a vermian defect.[10] While the evaluation primarily relies on the axial plane, the mid-sagittal plane serves as a problem-solving tool in cases of uncertainty. However, factors such as fetal presentation, maternal obesity, fetal skull ossification, and oligohydramnios may limit the feasibility

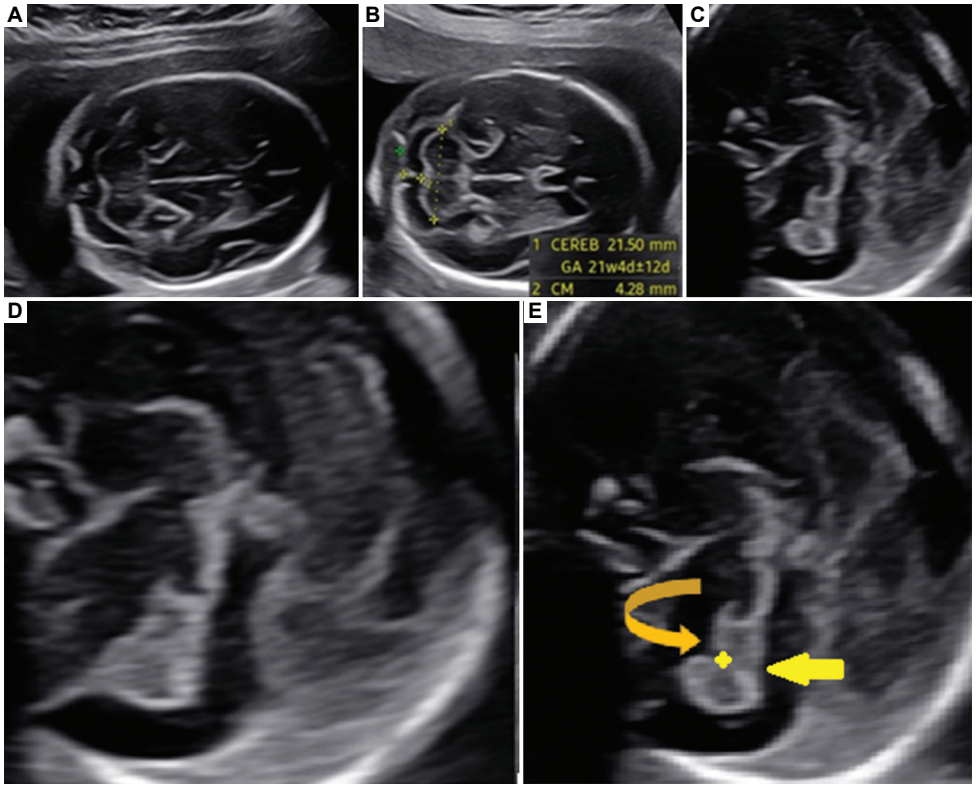

Figure 3. Ultrasound images of different 21-week fetuses illustrating posterior fossa structures. (A and B) Axial ultrasound images show a normal posterior fossa, including the CEREB and CM measurements. (C-E) Mid-sagittal ultrasound images demonstrate early vermian lobulation, highlighting key anatomical structures, such as the primary fissure (curved orange arrow), the fourth ventricle (straight yellow arrow), and the fastigium (yellow star), forming an angle close to 0º with the brainstem.
Abbreviations: CEREB: Cerebellum; CM: CM: Cisterna magna; GA: Gestational age.

and accuracy of ultrasound examination. Therefore, fetal MRI enables additional assessment of the fourth ventricle, cisterna magna, and vermian growth through multiplanar imaging. By 17.5 weeks, landmarks such as the fastigial point and primary fissure help in evaluating the vermis This assessment includes vermian lobulation, the tegmentovermian angle, and the craniocaudal diameter of the vermis[11] (Figure 4).

3.2. Magnetic resonance imaging

The use of MRI during pregnancy is increasing, although imaging quality, sequences, and operator expertise vary across centers.[12] MRI before 18 weeks usually does not provide additional information beyond ultrasound. Understanding brain development timelines is crucial for determining the optimal timing of MRI scans. As pregnancy progresses, maternal discomfort may increase during the scan, therefore, the left-lateral decubitus position is recommended for improved comfort.[13]

Most fetal MRIs use a 1.5 Tesla (T) field strength, with a growing trend towards 3T. Common sequences include T2-weighted fast spin-echo or steady-state free-precession (SSFP), as well as T1-weighted contrast via two-dimensional gradient echo (GRE) sequences and single-shot high-resolution (SSH) GRE echoplanar sequences. Additional sequences, include diffusion-weighted imaging, diffusion tensor imaging, dynamic SSFP sequences, and SSH magnetic resonance cholangiopancreatography sequences, provide three-dimensional-like images.[12] A targeted approach is often used to focus on specific pathologies, acquiring dedicated images tailored to the affected area using half-Fourier acquisition single-shot turbo spin-echo, true fast imaging with steady-state free precession, and T1-weighted sequences.

3.3. Pathologies of the fetal posterior fossa

3.3.1. Dandy-Walker malformation (DWM)

The existing literature lacks consensus on the terminology for pathologies associated with fourth ventricle enlargement. Traditionally, DWM is diagnosed based on vermian hypoplasia (VH) with enlargement of the fourth ventricle and posterior fossa.[14] Nonetheless, ongoing research is dedicated to establishing more objective diagnostic criteria, aiming to enhance the precision and reliability. A recent

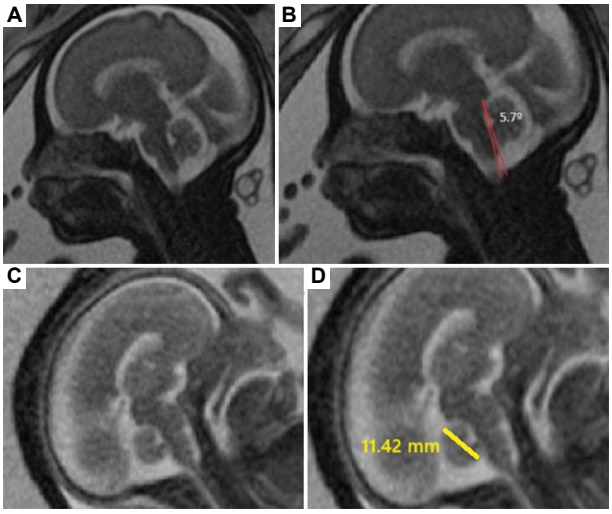

Figure 4. Normal MRI images. (A and B) Sagittal TRUFI MRI images of a 30-week fetus depicting the relationship between the brainstem and vermis, vermian lobulation, and the tegmentovermian angle. (C and D) Sagittal TRUFI MRI images of a 22-week fetus showing the craniocaudal diameter of the vermis.
Abbreviations: MRI: Magnetic resonance imaging; TRUFI: True fast imaging with steady-state precession.

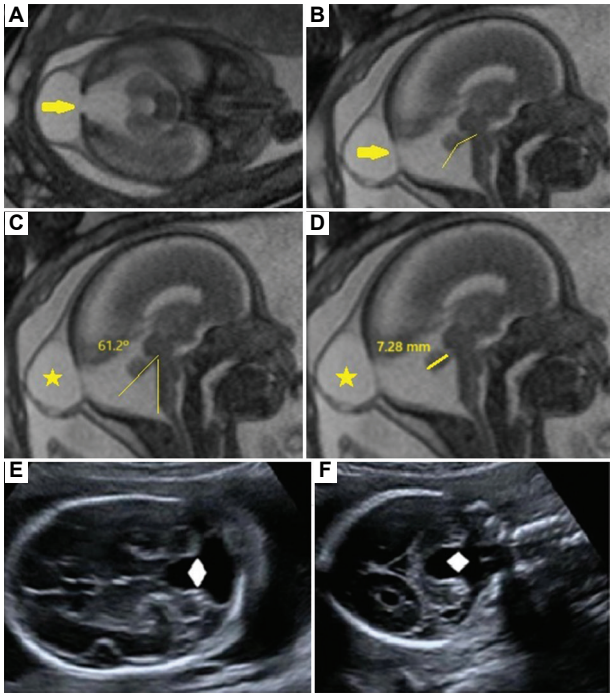

Figure 5. MRI and ultrasound images of different 21-week fetuses. (A-D) Axial TRUFI and sagittal HASTE images show DWM associated with an occipital bone defect-related (yellow arrow) encephalocele (yellow star). The images show vermian hypoplasia, an enlarged tegmentovermian angle, and an obtuse fastigial recess (thin line angle). (E and F) Axial and coronal ultrasound images show the fourth ventricle in relation to the cisterna magna, exhibiting cystic enlargement (white rhombus shape).
Abbreviations: TRUFI: True fast imaging with steady-state free precession; HASTE: Half-Fourier acquisition single-shot turbo spin-echo; DWM: Dandy-Walker malformation.

study proposes novel diagnostic criteria, including features such as inferior predominant VH, inferolateral displacement of the tela choroidea/choroid plexus, and the presence of an unpaired caudal lobule. Additional markers include an enlarged tegmentovermian angle and an obtuse fastigial recess (Figure 5). It is recommended that posterior fossa size and torcular location be excluded from the criteria.[15] Most DWM cases are sporadic, though rare familial cases linked to specific genes exist.[16,17] DWM can also be associated with syndromes such as Meckel–Gruber and Walker–Warburg.[18,19] Outcomes vary widely, with approximately 30% of individuals achieving normal development.[20] Severe MRI abnormalities, such as an extremely thin brainstem, have been associated with poor neonatal outcomes, including neonatal intensive care unit mortality. In addition, neurological deficits, including epilepsy, often emerge in early childhood. Prenatal counseling should address the potential need for ventilatory support at birth (typically not long-term), the low risk of long-term feeding support, and the high likelihood of requiring ventriculoperitoneal shunt placement and developing epilepsy.[21]

3.3.2. Vermian hypoplasia

Historically, terms like "Dandy–Walker variant," "Dandy–Walker complex," and "Dandy-Walker spectrum" have contributed to confusion in the literature. Recently, a consensus has emerged favoring the term "vermian hypoplasia" (VH) for a more precise anatomical definition. This shift enhances clarity in communication and better classification, thereby improving pregnancy counseling, prognosis assessment, and genetic evaluation.

VH is characterized by minimal upward rotation of the vermis due to a slightly enlarged fourth ventricle, without elevation of the tentorium cerebelli (Figure 6). The retro cerebellar fluid collection directly communicates with the fourth ventricle, resembling DWM but typically presenting with a smaller fluid collection.[22] While most cases of VH occur sporadically, instances of X-linked inheritance have been documented,[23] and various associated genes have been identified.[24] Isolated VH poses no risk of recurrence; however, cases with a genetic basis may be associated with a recurrence risk.[25] The prognosis of VH is highly variable and is strongly influenced by the presence of coexisting genetic syndromes and systemic anomalies rather than the cerebellar malformation itself. Studies have shown that patients with isolated VH generally exhibit favorable neurodevelopmental outcomes, whereas those with additional intra- and extracranial anomalies are consistently experienced poor prognosis.[26,27] Given

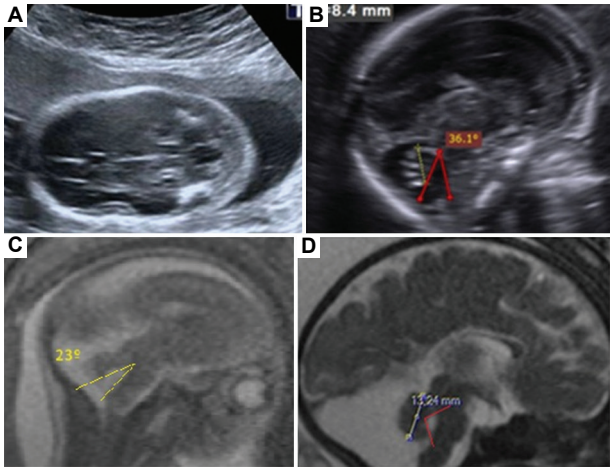

Figure 6. Ultrasound and MRI images of different patients. (A and B) Axial and sagittal ultrasound images show a slightly enlarged fourth ventricle, minimal upward rotation of the hypoplastic vermis, and an increased tegmentovermian angle. (C) A sagittal HASTE image of a 21-week fetus shows an increased tegmentovermian angle associated with vermian hypoplasia. (D) Sagittal TRUFI images of a 34-week fetus demonstrate a small vermis consistent with gestational age and an acute fastigial recess (thin line angle).

the strong correlation between VH, genetic syndromes, and cardiac anomalies, prenatal counseling should emphasize the importance of genetic evaluation and fetal echocardiography, as these findings can significantly impact clinical management and parental decision-making.[21]

3.3.3. Cerebellar hypoplasia/dysplasia

Cerebellar hypoplasia is defined by a transverse cerebellar diameter that is smaller than expected for the gestational age (Figure 7). Dysplasia, on the other hand, refers to abnormal cerebellar development, including white or gray matter anomalies and abnormal foliation patterns (Figure 7). These conditions may present independently or concurrently, adding complexity to both diagnosis and clinical intervention.

Cerebellar hypoplasia and dysplasia have diverse etiologies, including chromosomal abnormalities (e.g., trisomy 13 and 18), intracranial hemorrhage, intrauterine infections, and prenatal exposure to substances such as anticonvulsant drugs, alcohol, or cocaine. The cerebellum may be globally or unilaterally affected.[28] When cerebellar and pons hypoplasia occur together, it is termed pontocerebellar hypoplasia, which may also be associated with cerebral atrophy and delayed myelination.[29] Nonetheless, in muscular dystrophies, cerebellar cysts, dysplasia, and hypoplasia represent predominant features of brain involvement.[30] Previous studies have indicated that the simple dysplasia group has better postnatal outcomes compared to the group with associated

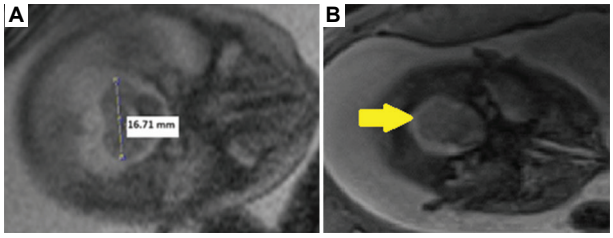

Figure 7. Cerebellar hypoplasia and dysplasia on fetal MRI. (A) Axial TRUFI image shows cerebellar hypoplasia based on TCD for this gestational age. (B) Axial HASTE image shows a dysmorphic cerebellum (yellow arrow).
Abbreviations: MRI: Magnetic resonance imaging; TRUFI: True fast imaging with steady-state free precession; TCD: transverse cerebellar diameter; HASTE: Half-Fourier acquisition single-shot turbo spin-echo.

cerebellar malformations. However, given the small sample sizes and short follow-up periods in these studies, such conclusions should be interpreted with caution.[28]

3.3.4. Blake's pouch cyst

At approximately the 10th week of gestation, the choroid plexus develops, which indents the thin roof plate of the fourth ventricle, creating the plica choroidalis. This process divides the roof into the anterior membranous area and the posterior membranous area (PMA). The PMA subsequently expands into Blake's pouch, which later gives rise to the foramen of Magendie, facilitating CSF flow into the cisterna magna subarachnoid space.[31] Failure of Blake's pouch to regress results in the formation of a Blake's pouch cyst. The key imaging finding is the presence of a normally sized and configured vermis. However, due to the mass effect on the underlying vermis, which is displaced upwards, there is an associated increase in the tegmentovermian angle (Figure 8).[32] When isolated, a Blake's pouch cyst is associated with a favorable prognosis, with a high likelihood of intrauterine resolution and normal neurodevelopment outcomes in nearly all cases.[33] Table 1 summarizes the key imaging features that help distinguish Blake's pouch cyst from other entities within the Dandy-Walker continuum.

3.3.5. Posterior fossa arachnoid cysts

Arachnoid cysts (AC) are intra-arachnoid lesions that expand by secreting CSF. Approximately 25% of these cysts occur in the posterior fossa.[34] They are in the extra-axial space and exert a mass effect, altering the shape of surrounding brain structures and often causing scalloping along the adjacent calvarium (Figure 9). The cysts consistently exhibit CSF signal intensity across all imaging sequences.[35] Although mostly sporadic, arachnoid cysts have been associated with syndromes such as Chudley-McCullough syndrome, acrocallosal syndrome, and autosomal recessive primary ciliary dyskinesia. It remains

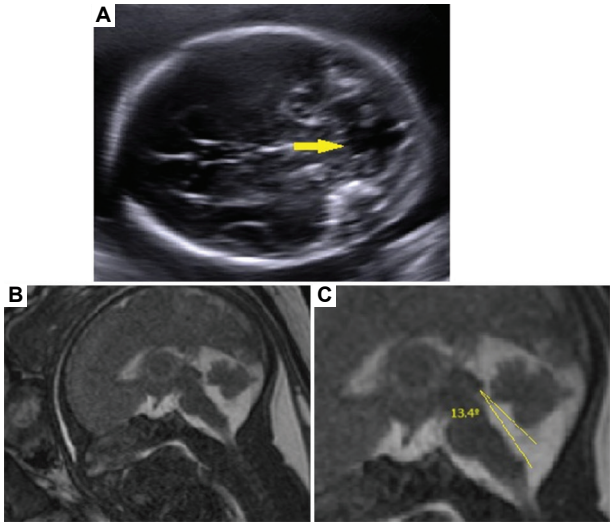

Figure 8. Blake's pouch cysts imaging in a 33-week fetus. (A) Axial ultrasound image shows Blake's pouch cyst (yellow arrow). (B and C) Sagittal HASTE and TRUFI images demonstrate a normal-sized and well-configured vermis with a slightly increased tegmentovermian angle. Abbreviations: TRUFI: True fast imaging with steady-state free precession; HASTE: Half-Fourier acquisition single-shot turbo spin-echo.

uncertain whether patients with AC and cognitive dysfunction, but without signs of mass effect or elevated intracranial pressure, would benefit from surgery. The relationship between these neurological symptoms and AC is not yet fully understood. Advances in human genetic research may offer deeper insights into the underlying pathogenic mechanisms.[36]

3.3.6. Mega cisterna magna

The cisterna magna, located posterior to the cerebellum, is a CSF-filled space with dimensions typically ranging from 2 – 10 mm.[37] When the distance between the posterior vermis and the occipital bone exceeds 10 mm, it is classified as a mega cisterna magna (Figure 10).

Mega cisterna magna may occur in isolation or association with neurodevelopmental conditions such as DWM, VH, and Blake's pouch cyst. Accurate diagnosis is crucial for proper parental counseling and clinical management. Unlike an arachnoid cyst, which exerts a mass effect, a mega cisterna magna is considered a normal variant.[38] It can be distinguished from DWM by the presence of a normal vermis and tegmentovermian angle.

3.3.7. Chiari II malformations

Chiari II malformation is characterized by a myelomeningocele accompanied by the displacement of posterior fossa contents into the foramen magnum. Over time, several theories have emerged to explain its pathogenesis. Fundamentally, Chiari II malformation

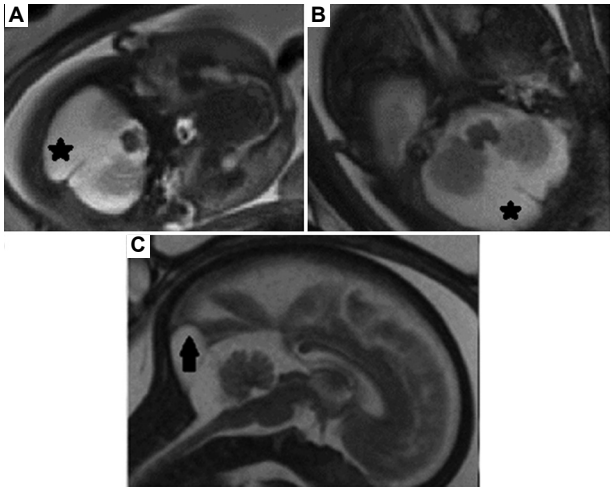

Figure 9. MRI findings of a posterior fossa arachnoid cyst. (A-C) MRI images of a 35-week fetus demonstrate extra-axial enlargement of the posterior fossa (black star), accompanied by indentation to the tentorium cerebelli (black arrow). The findings are consistent with an arachnoid cyst.

Table 1. Key imaging features of Dandy-Walker continuum

Diagnosis	Vermis	TVA	Fastigial recess
Dandy-Walker malformation	Hypoplastic	Increased	Obtuse
VH	Hypoplastic	Increased/Normal	Acute
BPC	Normal	Increased	Acute

Abbreviations: VH: Vermian hypoplasia; BPC: Blake's pouch cyst; TVA: Tegmentovermian angle.

is attributed to the failure of the neural plate to fold correctly, potentially leading to neural tube defects. Chiari II malformation is believed to result from abnormal fetal brain development caused by CSF leakage from an open neural tube defect, leading to intracranial hypotension. This leakage causes the collapse of the developing ventricular system and the downward displacement of posterior fossa structures, ultimately resulting in small posterior fossa and hindbrain abnormalities. The origins of other associated anomalies, such as callosal dysplasia and falcine deficiency, remain less understood but are also thought to be secondary to the neural tube defect.[39] Due to the obstruction of CSF flow, ventriculomegaly is commonly observed.[40]

Associations with both CNS and non-CNS anomalies are commonly observed in Chiari II malformation.[41] Imaging demonstrates effacement of the cisterna magna, the bilateral indentation of the frontal bones resulting in a "lemon-shaped" cranium, and a curved appearance of the cerebellum, known as the "banana sign" (Figure 11). In addition, the fourth ventricle is elongated and displaced downward[42] (Figure 12). While the anatomical level of

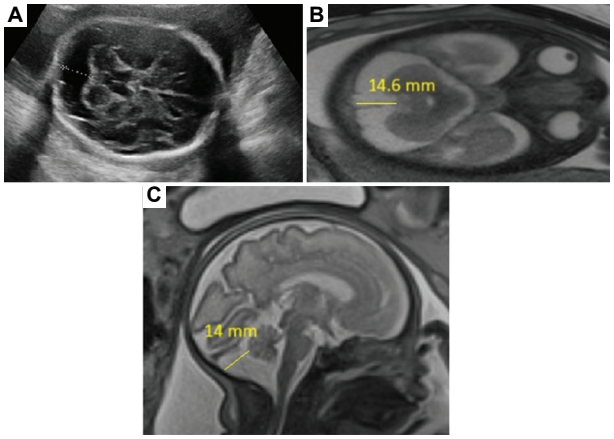

Figure 10. Imaging of mega cisterna magna. (A) Axial ultrasound image demonstrates the measurement of an enlarged cisterna magna. (B) Axial TRUFI and (C) Sagittal HASTE MRI images illustrate a n increased CSF posterior to the cerebellum, with no evidence of mass effect.
Abbreviations: CSF: Cerebrospinal fluid; TRUFI: True fast imaging with steady-state free precession; HASTE: Half-Fourier acquisition single-shot turbo spin-echo; MRI: Magnetic resonance imaging.

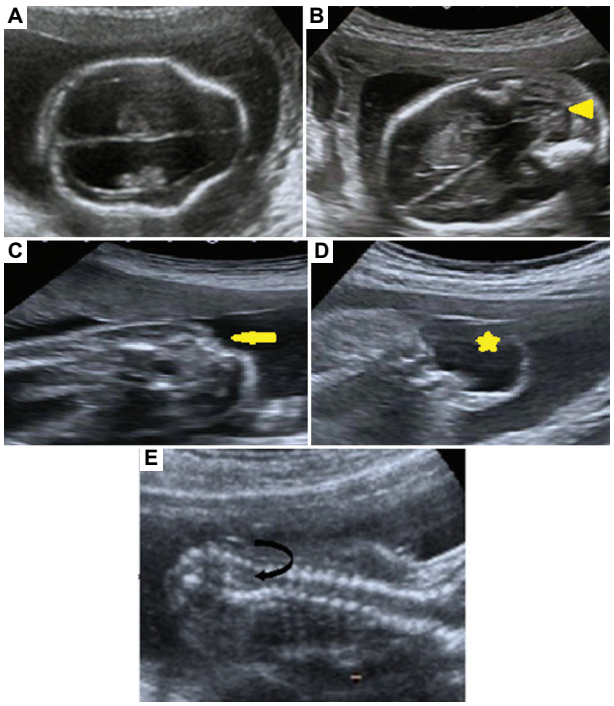

Figure 11. Multiplanar ultrasound images of a fetus with meningomyelocele. (A) A "lemon-shaped" cranium. (B) A curved appearance of the cerebellum, known as "banana-sign" (yellow arrowhead). (C-E) Ultrasound images show a skin defect (yellow arrow), a meningomyelocele sac (yellow star), and the separation of vertebral ossification centers (curved black arrow), respectively.

the lesion remains a key prognostic factor, the absence of vermian displacement is generally associated with a more favorable outcome. In contrast, vermian displacement

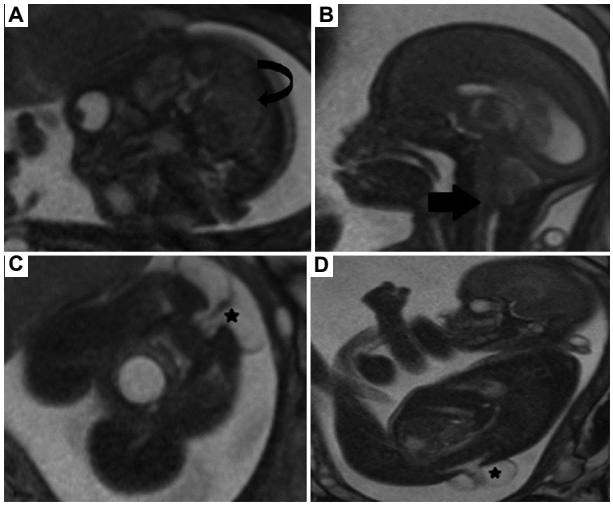

Figure 12. Multiplanar TRUFI images of a fetus. (A) Axial image demonstrates obliteration of cisterna magna (curved black arrow). (B) Sagittal image shows herniation of posterior fossa contents into the cervical canal through the foramen magnum (black arrow). (C and D) Axial and sagittal images of the torso show a meningomyelocele sac containing neural tissue (black star).
Abbreviations: TRUFI: True fast imaging with steady-state free precession.

and callosal dysgenesis may negatively impact long-term ambulatory status in some cases.[43] Given these considerations, optimal management requires lifelong multidisciplinary care, as regular follow-ups can help mitigate the risks of renal disease and shunt-related complications. In addition, some cases of cardiopulmonary arrest may be preventable, as they could be linked to Chiari II malformation decompensation.[44]

3.3.8. Occipital encephalocele

An encephalocele is a congenital defect characterized by the protrusion of meninges, CSF, and brain tissue through a cranial defect. These anomalies are categorized based on their location and can be either open or covered by skin. Most congenital encephaloceles are associated with intracranial abnormalities.[45] They may occur as isolated anomalies or as part of syndromes, chromosomal abnormalities, single-gene disorders, or due to teratogenic influences.[46]

Encephaloceles involve a bony defect in the skull and varying degrees of brain tissue displacement (Figure 13). Imaging shows diverse characteristics, including abnormal cortical folding, calcification, and hemorrhage within the externalized brain tissue. In severe cases, brainstem abnormalities, such as posterior bending and atypical configurations, may be present.[47] Surgical intervention remains the primary treatment option. Despite advancements in surgical management, morbidity

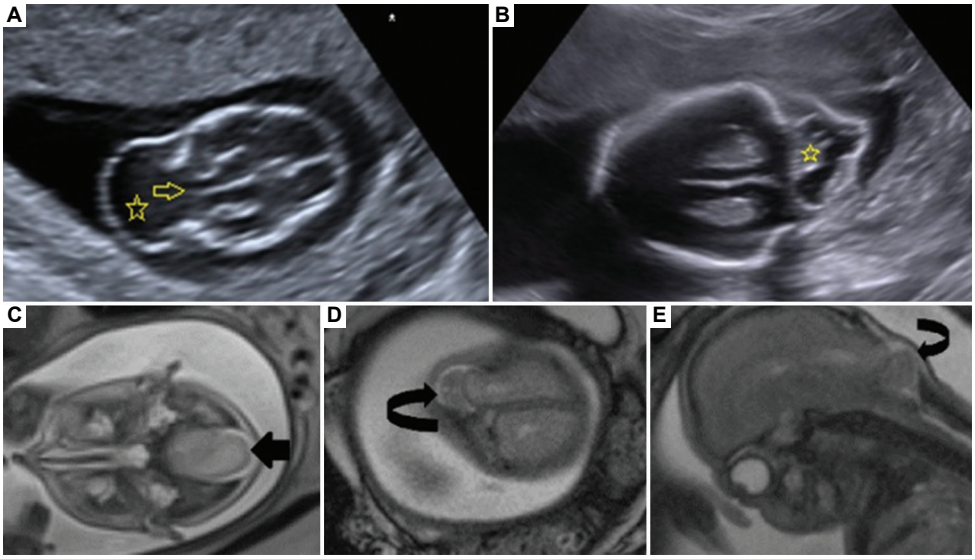

Figure 13. Ultrasound and MRI images of different patients. (A) Axial ultrasound image obtained in the first trimester demonstrates an occipital bone defect (yellow outlined arrow) with an accompanying encephalocele sac (yellow outlined star). (B) The encephalocele sac contains malformed brain structures (yellow outlined star). (C) Axial HASTE, (D) axial TRUFI and (E) sagittal TRUFI images show an occipital encephalocele (black arrow) with an occipital bone defect. The sac includes brain tissue (black curved arrow).
Abbreviations: MRI: Magnetic resonance imaging; TRUFI: True fast imaging with steady-state free precession; HASTE: Half-Fourier acquisition single-shot turbo spin-echo.

and mortality rates remain high. However, significant improvements have been achieved in recent years due to the development of high-resolution imaging techniques, refined surgical approaches, and enhanced postoperative care.[48]

3.3.9. Rhombencephalosynapsis

Rhombencephalosynapsis is a rare congenital malformation characterized by the fusion of the cerebellar hemispheres along the midline, which may be complete or partial.[49] While many patients do not exhibit syndromic features, rhombencephalon synapsis is a hallmark of Gómez-López-Hernández syndrome, which presents with parietal alopecia, trigeminal anesthesia, and craniofacial dysmorphisms.[50] It has also been associated with VACTERL syndrome, which includes vertebral, anal, cardiovascular, tracheoesophageal, renal, and limb anomalies.[51] The condition is sporadic and has a low recurrence risk.

Characteristic imaging findings include agenesis of the vermis, fusion of the cerebellar hemispheres, superior cerebellar peduncles, and dentate nuclei, creating a "keyhole" appearance of the fourth ventricle (Figure 14). The transverse folding of the fused cerebellum is best visualized on coronal T2-weighted images.[52] Rhombencephalosynapsis may also be associated with hydrocephalus, typically due to aqueductal stenosis, as well as other CNS anomalies such as absent olfactory bulbs, dysgenesis of the corpus callosum, and absent septum pellucidum.[53] Abnormalities of the cerebellar vermis—ranging from its absence to various pathologies—are linked to a spectrum of movement, balance, and emotional disturbances. These underscore the importance of early MRI-based diagnosis in guiding effective surgical and supportive management strategies to improve patient outcomes.[54]

3.3.10. Congenital aqueductal stenosis (CAS)

CAS is a leading cause of hydrocephalus,[55] resulting from the narrowing or obstruction of the cerebral aqueduct due to various factors. One severe form, X-linked hydrocephalus, can be detected *in utero* but remains poorly understood.[56] Secondary causes of CAS include infections or intraventricular hemorrhages, which lead to inflammation or bleeding that constricts the aqueduct. Additionally, tumors or vascular malformations may cause extrinsic compression.[57] Ventriculomegaly, often identified during routine mid-trimester fetal ultrasound scans, plays a key role in detecting CAS (Figure 15). While historically challenging to manage, recent advancements in imaging, patient selection, and fetal surgery techniques have renewed interest in evaluating and developing intrauterine therapies for hydrocephalus, with aqueductal stenosis being a significant consideration.[58]

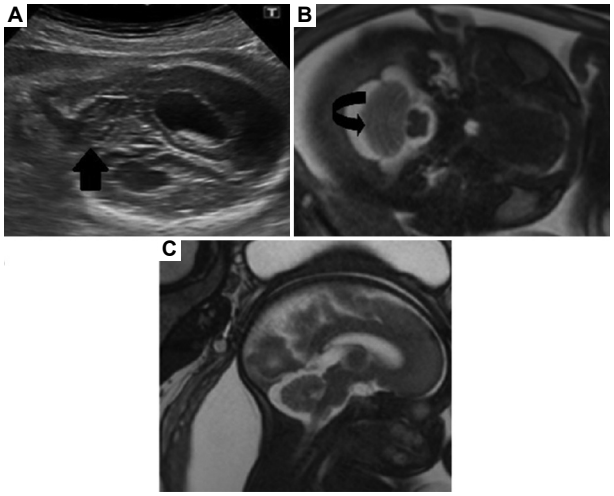

Figure 14. Imaging of rhombencephalosynapsis. (A) Coronal ultrasound image of a 30-week fetus demonstrates fusion of the cerebellar hemispheres (black arrow). Similar to MRI, the transverse folding of the fused cerebellum is a distinctive feature. (B) Axial TRUFI image demonstrates fused cerebellar hemispheres and continuous cerebellar folia (curved black arrow). (C) Sagittal TRUFI image shows midline sections revealing the absence of the vermis.
Abbreviations: MRI: Magnetic resonance imaging; TRUFI: True fast imaging with steady-state free precession.

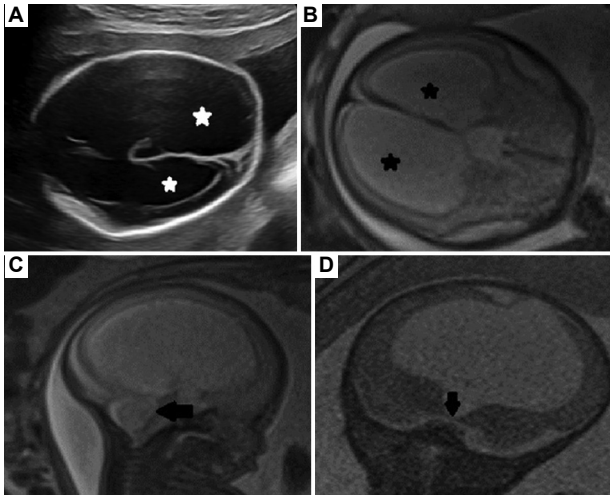

Figure 15. Imaging of congenital aqueductal stenosis. Severe ventriculomegaly is shown in (A) axial ultrasound and (B) axial HASTE image (white and black star). (C and D) The obstruction at the level of the cerebral aqueduct (black arrow) is visualized in sagittal HASTE and coronal TRUFI images.
Abbreviations: TRUFI: True fast imaging with steady-state free precession; HASTE: Half-Fourier acquisition single-shot turbo spin-echo.

3.3.11. Ciliopathies

Ciliopathies are a diverse group of genetic disorders caused by mutations in genes linked to the cilium-centrosome complex. These mutations can lead to conditions such as cystic kidney disease, blindness, neurological deficits, obesity, and diabetes.[59] Among the ciliopathies affecting the posterior fossa, notable examples include Joubert syndrome, Meckel-Gruber syndrome, orofaciodigital syndrome type VI (OFD-6), and COACH syndrome. Joubert syndrome, OFD-6, and COACH syndrome are particularly distinguished by the distinctive characteristic "molar tooth sign," a feature absent in Meckel-Gruber syndrome. In Joubert syndrome, key imaging findings include a deep interpeduncular fossa, VH, thickened superior cerebellar peduncle, and an enlarged fourth ventricle[60] (Figure 16). When additional abnormalities, such as cephaloceles and tectocerebellar dysraphia, including DWM, are present alongside the classic features, the condition is referred to as "Joubert plus."[61,62] Recent advances in understanding ciliopathies have paved the way for precision treatments, including antisense oligonucleotides for exon skipping, translational read-through drugs, small molecules targeting cilium-dependent pathways, and emerging gene therapies, all of which show promise in preclinical models.[63]

3.3.12. Pontocerebellar hypoplasia (PCH)

PCH is a congenital condition characterized by the underdevelopment of both the cerebellum and pons. To date, over twenty types have been identified, each linked to distinct genetic mutations.[64] While MRI remains the primary imaging method, ultrasound can also be used. Sagittal imaging plays a crucial role in distinguishing cerebellar hypoplasia from pontocerebellar hypoplasia[53] (Figure 17). A mid-sagittal view can show a non-lobulated cerebellar vermis. The "dragonfly pattern" in a coronal view shows flattened cerebellar hemispheres with a relatively preserved vermis, which resembles the wings and head of a dragonfly. In contrast, the "butterfly pattern" indicates a small but proportionate cerebellum. Axial MRI scans of the lower mesencephalon often show a "Figure 8" appearance, while dilated interfolial spaces suggest a reduction in parenchymal volume.[65] Although pontocerebellar hypoplasia is the primary feature, its clinical manifestation varies depending on the affected gene, ranging from neurological disorders to joint contractures. Accurate classification of PCH subtypes is essential for determining prognosis and guiding neurodevelopmental care.[66]

3.3.13. Walker-Warburg syndrome (WWS)

WWS is a lethal form of congenital muscular dystrophy that is associated with hydrocephalus, cobblestone lissencephaly, and retinal dysplasia.[67] WWS stands out noticeably on MRI due to its unique or characteristic appearance. The brainstem typically exhibits hypoplasia and a "kinked" or "Z" configuration, while the tectum demonstrates enlargement. Furthermore, the cerebellum presents as both small and dysmorphic, with abnormal

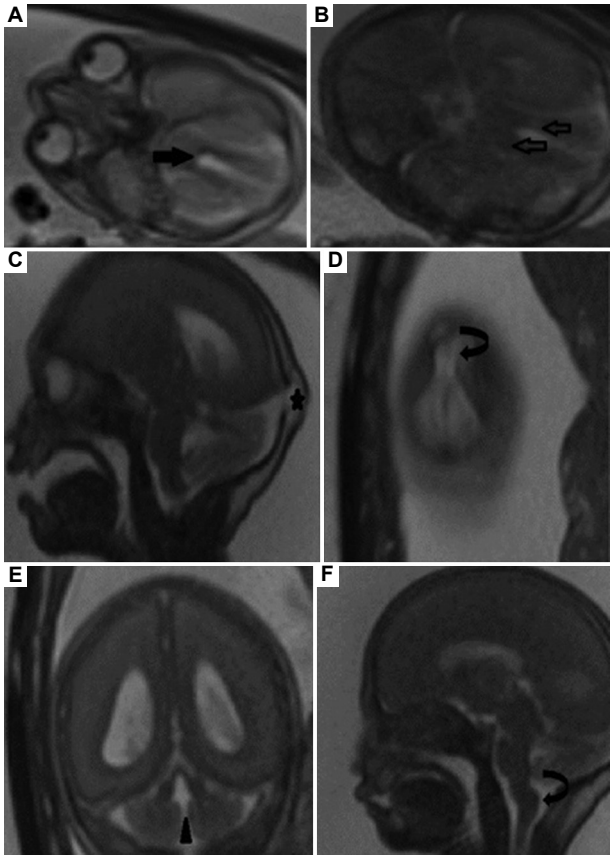

Figure 16. Multiplanar images of a 22-week fetus. (A and B) Axial HASTE and TRUFI images show the characteristic of "molar tooth sign" (black arrow) and thickening of the superior cerebellar peduncle (black outlined arrow). (C and D) Sagittal and coronal TRUFI İmages indicate an accompanying encephalocele (black star), with the cerebellar hemispheres observed to be drawn toward the encephalocele sac (black curved arrow). (E) Coronal TRUFI image shows agenesis of the vermis (black arrowhead). (F) Sagittal TRUFI image shows dorsal traction of the brainstem (black curved arrow).
Abbreviations: TRUFI: True fast imaging with steady-state free precession; HASTE: Half-Fourier acquisition single-shot turbo spin-echo.

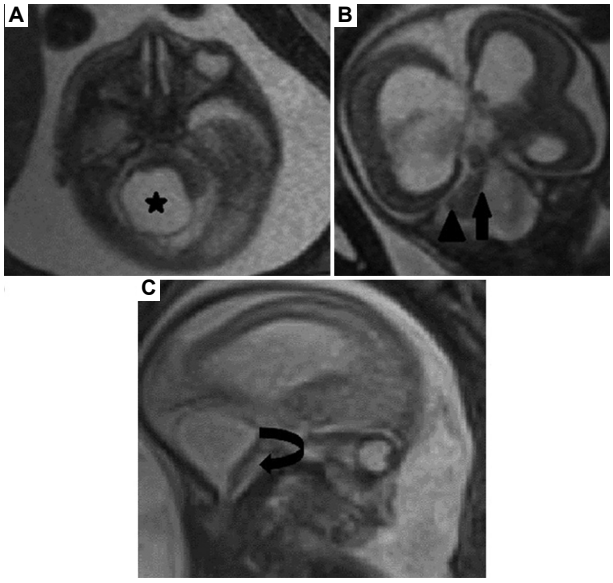

Figure 17. MRI images of (A) axial and (B) coronal TRUFI, as well as (C) sagittal HASTE images, demonstrate agenesis of the vermis (black arrow) and right cerebellar hemisphere (black star). Additionally, the left cerebellar hemisphere appears small and dysmorphic (black arrowhead). Notably, the pons is significantly hypoplastic for gestational age, with an absent ventral bulge (black curved arrow).
Abbreviations: MRI: Magnetic resonance imaging; TRUFI: True fast imaging with steady-state free precession; HASTE: Half-Fourier acquisition single-shot turbo spin-echo.

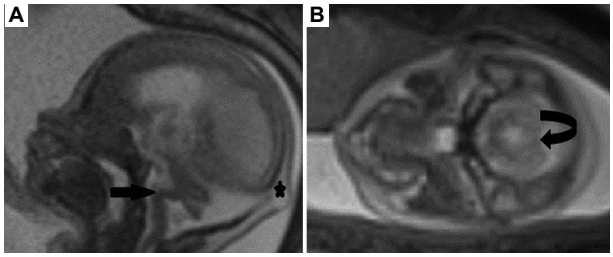

Figure 18. MRI of a 20-week fetus. (A) Sagittal TRUFI and (B) axial HASTE images show kinked pontomesencephalic junction (black arrow), an encephalocele sac (black star), and a dysmorphic, small cerebellum and vermis (black curved arrow).
Abbreviations: TRUFI: True fast imaging with steady-state free precession; HASTE: Half-Fourier acquisition single-shot turbo spin-echo.

foliation (Figure 18). Additinally, cobblestone lissencephaly can occur in all or part of the brain, resulting in an uneven, nodular, or "pebbly" brain surface, and hydrocephalus is often observed[68] (Figure 19).

3.3.14. Other pathologies

Focal cerebellar lesions diagnosed prenatally are relatively uncommon. In the posterior fossa, as in other brain regions, bleeding and masses can occur. The detection of a focal echogenic lesion in the cerebellum via ultrasound often suggests parenchymal hemorrhage. The imaging characteristics vary depending on the hemorrhage stage. Acute and subacute hemorrhages are characterized by global or partial hemispheric swelling, with T2-weighted signal abnormalities showing mixed hyper- or hypointensity, along with T1- and/or diffusion-weighted hyperintense signals (Figure 20). Conversely, chronic hemorrhages exhibit focal hemispheric volume reduction and distortion, often accompanied by areas or rims of T2-weighted signal decrease within the parenchyma.[69] The neurological outcome is determined by the specific areas of the cerebellum that are affected, with vermian involvement being associated with a poorer long-term outcome.[70]

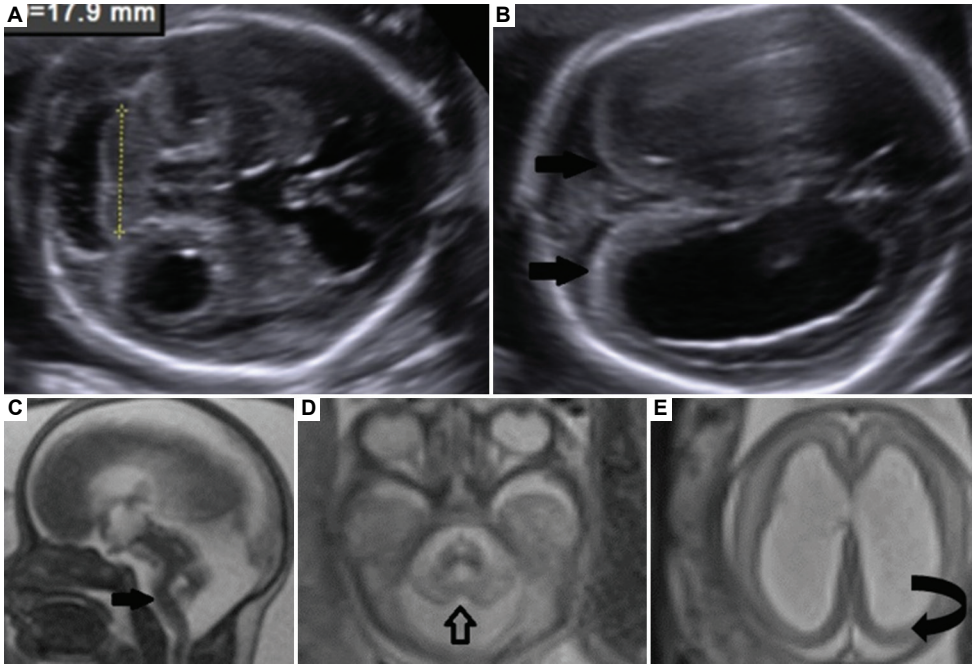

Figure 19. MRI and ultrasound images of a 22-week fetus. (A and B) Axial ultrasound images demonstrate a small cerebellum (yellow dotted lines), ventriculomegaly, and cobblestone lissencephaly (black arrow). (C-E) Sagittal TRUFI and axial HASTE images show kinked pontomesencephalic junction (black arrow) and a small vermis (black outlined arrow), which correspond to the ultrasound findings of a small cerebellum, ventriculomegaly, and cobblestone lissencephaly (black curved arrow).
Abbreviations: MRI: Magnetic resonance imaging; TRUFI: True fast imaging with steady-state free precession; HASTE: Half-Fourier acquisition single-shot turbo spin-echo.

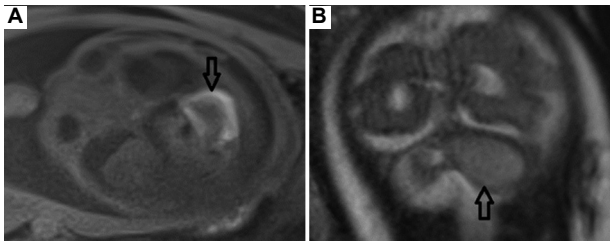

Figure 20. MRI characterization of subacute cerebellar hemorrhage is more convient. (A) Axial T1 and (B) coronal TRUFI images show a right cerebellar hematoma (black open arrow) involving the vermis.
Abbreviations: MRI: Magnetic resonance imaging; TRUFI: True fast imaging with steady-state free precession.

While most fetal brain tumors occur in supratentorial regions, posterior fossa mass lesions are less common.[71] One such pathology is heterotopia, or neuroglial hamartomas, which consist of disorganized yet mature cells, including neurons, glia, and blood vessels.[72] Imaging demonstrates mixed signals from gray and white matter, with minimal or no contrast enhancement and no infiltration into adjacent structures (Figure 21). These lesions do not grow over time.[73] Resection is the recommended management approach, and the overall prognosis following resection is excellent, with normal neurological development.[74]

4. Discussion

Fetal posterior fossa anomalies present diagnostic challenges due to complex anatomy, overlapping imaging features, and ambiguous terminology. While ultrasound remains the primary screening tool, MRI provides valuable supplementary information when ultrasound is limited by technical or patient-related factors.

This review indicates that both ultrasound and MRI possess distinct diagnostic strengths. Ultrasound is widely accessible and effective for initial screening; however, image quality may be compromised by factors, such as maternal obesity, oligohydramnios, unfavorable fetal positioning, or advanced gestational age. In such cases, MRI offers superior soft-tissue contrast and multiplanar imaging, making it an invaluable complementary tool. Under optimal imaging conditions, neither modality is inherently superior, yet their combined use significantly enhances overall diagnostic accuracy, ensuring a more comprehensive assessment of posterior fossa structures. Prognosis varies depending on the underlying etiology and associated anomalies. Isolated cerebellar malformations generally have more favorable outcomes, whereas additional structural or genetic abnormalities

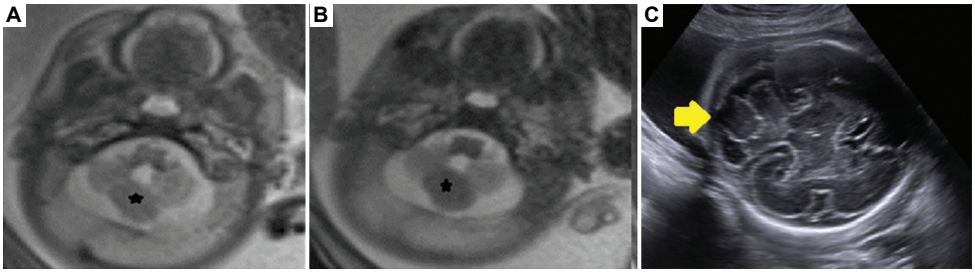

Figure 21. Multimodal imaging of a posterior fossa extra-axial mass-like lesion. (A) Axial HASTE and (B) TRUFI images demonstrate a posterior fossa extra-axial mass-like lesion with signal characteristics resembling G-ray matter (black star). (C) An ultrasound image confirms the presence of the same extra-axial lesion across different imaging modalities (yellow arrow).
Abbreviations: HASTE: Half-Fourier acquisition single-shot turbo spin-echo; TRUFI: True fast imaging with steady-state free precession.

often correlate with more severe neurodevelopmental impairments.

This review's comprehensive approach facilitates an integrated understanding of a wide spectrum of posterior fossa pathologies. Detailed imaging descriptions across multiple modalities have been instrumental in refining diagnostic criteria and supporting effective prenatal counseling. However, several limitations must be acknowledged. Variability in imaging protocols and operator expertise across centers may affect the generalizability of findings. Furthermore, the heterogeneity of the available literature—where some conditions are described only in isolated case reports or small series—coupled with a persistent lack of standardized diagnostic criteria in certain areas, poses significant challenges to the overall synthesis of evidence.

Further research is needed to establish standardized imaging protocols and diagnostic criteria, particularly for conditions with overlapping features, such as DWM and VH. Prospective multicenter and multidisciplinary studies would be instrumental in validating diagnostic measures, exploring advanced imaging techniques, and fostering a common language among professionals across specialties. Moreover, investigations into the correlation between prenatal imaging findings and long-term neurodevelopmental outcomes could further refine prenatal counseling and management strategies. Given the complexity of these disorders, an interdisciplinary approach is essential for improving diagnostic accuracy and guiding parental counseling. Collaboration among neurologists, radiologists, maternal-fetal medicine specialists, geneticists, and neonatologists is crucial for establishing standardized protocols for prenatal imaging, postnatal follow-up, and long-term patient care. A well-structured, multidisciplinary framework will streamline diagnosis, refine treatment strategies, and ultimately enhance clinical decision-making and patient outcomes.

5. Conclusion

Ultrasound and MRI play complementary roles in diagnosing fetal posterior fossa anomalies. While ultrasound is the primary screening tool, MRI enhances accuracy when ultrasound is limited. Standardized protocols and multidisciplinary collaboration are essential for improving diagnostic consistency and refining prenatal counseling and management strategies.

Acknowledgments

We sincerely appreciate Dr. Hasan Yiğit for his assistance in providing MRI reports, which significantly contributed to the study.

Funding

None.

Conflict of interest

The authors declare that they have no conflicts of interest.

Author contributions

Conceptualization: Deniz Delibaş,
Data curation: Arzu Gülşah Yalçın, Zafer Yumak
Investigation: Deniz Delibaş, Arzu Gülşah Yalçın, Zafer Yumak
Methodology: Deniz Delibaş
Supervision: Elif Ergün
Writing–original draft: Deniz Delibaş
Writing–review & editing: Elif Ergün

Ethics approval and consent to participate

Ethical approval for the collection of clinical data from patients was obtained from the Scientific Research Ethics Committee of the TC Sağlık Bakanlığı Ankara Eğitim ve Araştırma Hastanesi (Approval number: E-93471371 – 514.10 – 255038351, Approval date: September 25, 2024).

Informed consent was obtained from all patients involved in the study.

Consent for publication

Consent for publication was obtained from the hospital in accordance with institutional regulations.

Availability of data

Not applicable.

References

1. Moore KL, Persaud TVN, Torchia MG. *The Developing Human: Clinically Oriented Embryology*. 9th ed. Philadelphia, PA: Elsevier; 2019. p. 404-406.
2. Larsen WJ, Schoenwolf GC, Bleyl SB, Brauer PR. *Larsen's Human Embryology*. 5th ed. Philadelphia, PA: Churchill Livingstone/Elsevier; 2018. p. 95-9.
3. American College of Obstetricians and Gynecologists. ACOG practice bulletin No. 101: Ultrasonography in pregnancy. *Obstet Gynecol*. 2009;113(2 Pt 1):451-461.

   doi: 10.1097/AOG.0b013e31819930b0
4. American Institute of Ultrasound in Medicine. *Case Study Requirements for Accreditation*. Available from: https://www.aium.org/docs/default-source/accreditation/case-study-requirements/76811.pdf [Last accessed on 2024 Jan 19].
5. Australasian Society for Ultrasound in Medicine. *Guidelines for the Performance of Second (mid) Trimester Ultrasound*. Available from: https://www.asum.com.au/files/public/sop/curver/obs-gynae/guidelines-for-the-performance-of-second-mid-trimester-ultrasound.pdf [Last accessed on 2024 Jan 19].
6. UK Government. *Fetal Anomaly Screening Programme Handbook: 20-Week Screening Scan*. Available from: https://www.gov.uk/government/publications/fetal-anomaly-screening-programme-handbook/20-week-screening-scan [Last accessed on 2024 Jan 19].
7. International Society of Ultrasound in Obstetrics and Gynecology. *ISUOG Practice Guidelines: Routine Mid-trimester Fetal Ultrasound*. Available from: https://www.isuog.org/static/4e2ed89e-fa8a-42c2-9c0929cd89cb58ff/isuog-practice-guidelines-routine-mid-trimester-fetal-ultrasound.pdf [Last accessed on 2024 Jan 19].
8. Fileva N, Severino M, Tortora D, Ramaglia A, Paladini D, Rossi A. Second trimester fetal MRI of the brain: Through the ground glass. *J Clin Ultrasound*. 2023;51(2):283-299.

   doi: 10.1002/jcu.23423
9. Chaoui R, Benoit B, Mitkowska-Wozniak H, Heling KS, Nicolaides KH. Assessment of intracranial translucency (IT) in the detection of spina bifida at the 11-13-week scan. *Ultrasound Obstet Gynecol*. 2009;34(3):249-252.

   doi: 10.1002/uog.7329
10. International Society of Ultrasound in Obstetrics and Gynecology. ISUOG practice guidelines (updated): Sonographic examination of the fetal central nervous system. Part 1: Performance of screening examination and indications for targeted neurosonography. *Ultrasound Obstet Gynecol*. 2020;56(3):476-484.

    doi: 10.1002/uog.22145
11. Robinson AJ, Blaser S, Toi A, *et al*. The fetal cerebellar vermis: Assessment for abnormal development by ultrasonography and magnetic resonance imaging. *Ultrasound Q*. 2007;23(3):211-223.

    doi: 10.1097/RUQ.0b013e31814b162c
12. Malinger G, Lev D, Lerman-Sagie T. Is fetal magnetic resonance imaging superior to neurosonography for detection of brain anomalies? *Ultrasound Obstet Gynecol*. 2002;20(4):317-321.

    doi: 10.1046/j.1469-0705.2002.00825.x
13. International Society of Ultrasound in Obstetrics and Gynecology. ISUOG practice guidelines: Performance of fetal magnetic resonance imaging. *Ultrasound Obstet Gynecol*. 2017;49(5):671-680.

    doi: 10.1002/uog.17412
14. Barkovich AJ, Raybaud CA, editors. Congenital malformations of the brain and skull. In: *Pediatric Neuroimaging*. 6th ed. Philadelphia, PA: Wolters Kluwer; 2019. p. 724.
15. Whitehead MT, Barkovich MJ, Sidpra J, *et al*. Refining the neuroimaging definition of the dandy-walker phenotype. *AJNR Am J Neuroradiol*. 2022;43(10):1488-1493.

    doi: 10.3174/ajnr.A7659
16. Aldinger KA, Lehmann OJ, Hudgins L, *et al*. FOXC1 is required for normal cerebellar development and is a major contributor to chromosome 6p25.3 Dandy-Walker malformation. *Nat Genet*. 2009;41(9):1037-1042.

    doi: 10.1038/ng.422
17. Grinberg I, Northrup H, Ardinger H, *et al*. Heterozygous deletion of the linked genes ZIC1 and ZIC4 is involved in Dandy-Walker malformation. *Nat Genet*. 2004;36(10):1053-1055.

    doi: 10.1038/ng1420
18. Alsamal M, Zitoun OA, Abdulghani EA, Sula I. Meckel-Gruber syndrome together with Dandy-Walker malformation: An atypical case report of a 2nd recurrence in a consanguine marriage. *Childs Nerv Syst*. 2024;40(1):257-261.

    doi: 10.1007/s00381-023-06104-x
19. Spennato P, Mirone G, Nastro A, *et al*. Hydrocephalus in Dandy-Walker malformation. *Childs Nerv Syst*.

2011;27(10):1665-1681.

doi: 10.1007/s00381-011-1544-4

20. Bolduc ME, Limperopoulos C. Neurodevelopmental outcomes in children with cerebellar malformations: A systematic review. *Dev Med Child Neurol*. 2009;51(4): 256-267.

doi: 10.1111/j.1469-8749.2008.03224.x

21. Venkatesan C, Kline-Fath B, Horn PS, Poisson KE, Hopkin R, Nagaraj UD. Short- and long-term outcomes of prenatally diagnosed Dandy-Walker malformation, vermian hypoplasia, and Blake pouch cyst. *J Child Neurol*. 2021;36(12):1111-1119.

doi: 10.1177/08830738211049115

22. Parisi MA, Dobyns WB. Human malformations of the midbrain and hindbrain: Review and proposed classification scheme. *Mol Genet Metab*. 2003;80(1-2):36-53.

doi: 10.1016/j.ymgme.2003.08.010

23. Wakeling EL, Jolly M, Fisk NM, Gannon C, Holder SE. X-linked inheritance of Dandy-Walker variant. *Clin Dysmorphol*. 2002;11(1):15-18.

doi: 10.1097/00019605-200201000-00003

24. Cesaroni E, Matricardi S, Cappanera S, Marini C. First reported case of an inherited PACS2 pathogenic variant with variable expression. *Epileptic Disord*. 2022;24(3):572-576.

doi: 10.1684/epd.2022.1417

25. Bosemani T, Orman G, Boltshauser E, Tekes A, Huisman TA, Poretti A. Congenital abnormalities of the posterior fossa. *Radiographics*. 2015;35(1):200-220.

doi: 10.1148/rg.351140038

26. Patek KJ, Kline-Fath BM, Hopkin RJ, Pilipenko VV, Crombleholme TM, Spaeth CG. Posterior fossa anomalies diagnosed with fetal MRI: Associated anomalies and neurodevelopmental outcomes. *Prenat Diagn*. 2012;32(1):75-82.

doi: 10.1002/pd.2911

27. Tarui T, Limperopoulos C, Sullivan NR, Robertson RL, Du Plessis AJ. Long-term developmental outcome of children with a fetal diagnosis of isolated inferior vermian hypoplasia. *Arch Dis Child Fetal Neonatal Ed*. 2014;99(1):F54-F58.

doi: 10.1136/archdischild-2013-304678

28. Poretti A, Boltshauser E, Doherty D. Cerebellar hypoplasia: Differential diagnosis and diagnostic approach. *Am J Med Genet C Semin Med Genet*. 2014;166(2):211-226.

doi: 10.1002/ajmg.c.31398

29. Poretti A, Boltshauser E, Huisman TA. Cerebellar and brainstem malformations. *Neuroimaging Clin N Am*. 2016;26(3):341-357.

doi: 10.1016/j.nic.2016.03.005

30. Clement E, Mercuri E, Godfrey C, *et al*. Brain involvement in muscular dystrophies with defective dystroglycan glycosylation. *Ann Neurol*. 2008;64(5):573-582.

doi: 10.1002/ana.21482

31. Shekdar K. Posterior fossa malformations. *Semin Ultrasound CT MR*. 2011;32(3):228-241.

doi: 10.1053/j.sult.2011.02.003

32. Whitehead MT, Vezina G, Schlatterer SD, Mulkey SB, Du Plessis AJ. Taenia-Tela choroidea complex and choroid plexus location help distinguish Dandy-Walker malformation and Blake pouch cysts. *Pediatr Radiol*. 2021;51(8):1457-1470.

doi: 10.1007/s00247-021-04991-3

33. Gandolfi Colleoni G, Contro E, Carletti A, *et al*. Prenatal diagnosis and outcome of fetal posterior fossa fluid collections. *Ultrasound Obstet Gynecol*. 2012;39(6):625-631.

doi: 10.1002/uog.11071

34. Barkovich AJ, Raybaud CA, editors. Congenital malformations of the brain and skull. In: *Pediatric Neuroimaging*. 6th ed. Philadelphia, PA: Wolters Kluwer; 2019. p. 798.

35. Osborn AG, Preece MT. Intracranial cysts: Radiologic-pathologic correlation and imaging approach. *Radiology*. 2006;239(3):650-664.

doi: 10.1148/radiol.2393050823

36. Qureshi HM, Mekbib KY, Allington G, *et al*. Familial and syndromic forms of arachnoid cyst implicate genetic factors in disease pathogenesis. *Cereb Cortex*. 2023;33(6):3012-3025.

doi: 10.1093/cercor/bhac257

37. Mahony BS, Callen PW, Filly RA, Hoddick WK. The fetal cisterna magna. *Radiology*. 1984;153(3):773-776.

doi: 10.1148/radiology.153.3.6387792

38. Khan AN, Smirniotopoulos JG. *Arachnoid Cyst Imaging. eMedicine*; 2021. Available from: https://emedicine.medscape.com/article/336489-overview [Last accessed on 2024 Mar 03].

39. Osborn AG, Linscott LL, Salzman KL. *Osborn's Brain: Imaging, Pathology, and Anatomy*. Netherlands: Elsevier Health Sciences; 2024.

40. Bedei I, Krispin E, Sanz Cortes M, *et al*. Prenatal diagnosis and postnatal outcome of closed spinal dysraphism. *Prenat Diagn*. 2023;43(12):1521-1532.

doi: 10.1002/pd.6454

41. Bulas D. Fetal evaluation of spine dysraphism. *Pediatr Radiol*. 2010;40(6):1029-1037.

doi: 10.1007/s00247-010-1583-0

42. Kunpalin Y, Richter J, Mufti N, *et al*. Cranial findings detected by second-trimester ultrasound in fetuses with myelomeningocele: A systematic review. *BJOG*.

2021;128(2):366-374.

doi: 10.1111/1471-0528.16496

43. Khalaveh F, Seidl R, Czech T, *et al*. Myelomeningocele-Chiari II malformation-neurological predictability based on fetal and postnatal magnetic resonance imaging. *Prenat Diagn*. 2021;41(8):922-932.

doi: 10.1002/pd.5987

44. Talamonti G, Marcati E, Mastino L, Meccariello G, Picano M, D'Aliberti G. Surgical management of Chiari malformation type II. Childs *Nerv Syst*. 2020;36(8):1621-1634.

doi: 10.1007/s00381-020-04675-7

45. Osborn AG. Osborn's Brain: Imaging, Pathology, and Anatomy. 2nd ed. Netherlands: Elsevier; 2018. p. 1298.

46. Thompson DN. Postnatal management and outcome for neural tube defects including spina bifida and encephalocoeles. *Prenat Diagn*. 2009;29(4):412-419.

doi: 10.1002/pd.2199

47. Kasprian GJ, Paldino MJ, Mehollin-Ray AR, *et al*. Prenatal imaging of occipital encephaloceles. *Fetal Diagn Ther*. 2015;37(3):241-248.

doi: 10.1159/000366159

48. Markovic I, Bosnjakovic P, Milenkovic Z. Occipital encephalocele: Cause, incidence, neuroimaging and surgical management. *Curr Pediatr Rev*. 2020;16(3):200-205.

doi: 10.2174/1573396315666191018161535

49. Demaerel P, Morel C, Lagae L, Wilms G. Partial rhombencephalosynapsis. *AJNR Am J Neuroradiol*. 2004;25(1):29-31.

50. Schell-Apacik CC, Cohen M, Vojta S, *et al*. Gomez-Lopez-Hernandez syndrome (cerebello-trigeminal-dermal dysplasia): Description of an additional case and review of the literature. *Eur J Pediatr*. 2008;167(1):123-126.

doi: 10.1007/s00431-007-0478-z

51. Ishak GE, Dempsey JC, Shaw DW, *et al*. Rhombencephalosynapsis: A hindbrain malformation associated with incomplete separation of midbrain and forebrain, hydrocephalus and a broad spectrum of severity. *Brain*. 2012;135(Pt 5):1370-1386.

doi: 10.1093/brain/aws065

52. Guibaud L. Practical approach to prenatal posterior fossa abnormalities using MRI. *Pediatr Radiol*. 2004;34(9): 700-711.

doi: 10.1007/s00247-004-1248-y

53. Massoud M, Guibaud L. Prenatal imaging of posterior fossa disorders: A review. *Eur J Paediatr Neurol*. 2018;22(6): 972-988.

doi: 10.1016/j.ejpn.2018.07.007

54. Khaladkar SM, Jhala NA, Shukla A, Shah R, Durgi EC. Rhombencephalosynapsis: A rare hindbrain malformation. *Cureus*. 2024;16(7):e65400.

doi: 10.7759/cureus.65400

55. Stone SS, Warf BC. Combined endoscopic third ventriculostomy and choroid plexus cauterization as primary treatment for infant hydrocephalus: A prospective North American series. *J Neurosurg Pediatr*. 2014;14(5):439-446.

doi: 10.3171/2014.7.PEDS14152

56. Adle-Biassette H, Saugier-Veber P, Fallet-Bianco C, *et al*. Neuropathological review of 138 cases genetically tested for X-linked hydrocephalus: Evidence for closely related clinical entities of unknown molecular bases. *Acta Neuropathol*. 2013;126(3):427-442.

doi: 10.1007/s00401-013-1146-1

57. Emery SP, Narayanan S, Greene S. Fetal aqueductal stenosis: Prenatal diagnosis and intervention. *Prenat Diagn*. 2020;40(1):58-65.

doi: 10.1002/pd.5527

58. Peiro JL, Fabbro MD. Fetal therapy for congenital hydrocephalus-where we came from and where we are going. *Childs Nerv Syst*. 2020;36(8):1697-1712.

doi: 10.1007/s00381-020-04738-9

59. Hildebrandt F, Benzing T, Katsanis N. Ciliopathies. *N Engl J Med*. 2011;364(16):1533-1543.

doi: 10.1056/NEJMra1010172

60. Surisetti BK, Holla VV, Prasad S, *et al*. Clinical and imaging profile of patients with Joubert syndrome. *J Mov Disord*. 2021;14(3):231-235.

doi: 10.14802/jmd.21066

61. Al-Smair A, Younes S, Saadeh A, Kaoukji AR, Jaber O. Joubert-Plus syndrome with an atretic cephalocele: A case report. *Radiol Case Rep*. 2022;17(10):3630-3634.

doi: 10.1016/j.radcr.2022.07.038

62. Poretti A, Singhi S, Huisman TA, *et al*. Tecto-cerebellar dysraphism with occipital encephalocele: Not a distinct disorder, but part of the Joubert syndrome spectrum? *Neuropediatrics*. 2011;42(4):170-174.

doi: 10.1055/s-0031-1287763

63. Van De Weghe JC, Gomez A, Doherty D. The Joubert-Meckel-Nephronophthisis spectrum of ciliopathies. *Annu Rev Genomics Hum Genet*. 2022;23:301-329.

doi: 10.1146/annurev-genom-121321-093528

64. *Online Mendelian Inheritance in Man. Pontocerebellar Hypoplasia Search Results*. Available from: https://www.omim.org/search?index=entry&search=%22pontocerebellar+hypoplasia%22 [Last accessed on 2024 Apr 21.

65. Rüsch CT, Bölsterli BK, Kottke R, Steinfeld R, Boltshauser E.

Pontocerebellar hypoplasia: A pattern recognition approach. *Cerebellum*. 2020;19(4):569-582.

doi: 10.1007/s12311-020-01135-5

66. Accogli A, Addour-Boudrahem N, Srour M. Diagnostic approach to cerebellar hypoplasia. *Cerebellum*. 2021;20(4):631-658.

doi: 10.1007/s12311-020-01224-5

67. Zago S, Silvestri E, Arcangeli T, *et al*. Fetal presentation of Walker-Warburg syndrome with compound heterozygous POMT2 missense mutations. *Fetal Pediatr Pathol*. 2023;42(2):334-341.

doi: 10.1080/15513815.2022.2116620

68. Osborn AG. *Osborn's Brain: Imaging, Pathology, and Anatomy*. 2nd ed. Netherlands: Elsevier; 2018. p. 1218.

69. Scelsa B, Cutillo G, Lanna MM, *et al*. Prenatal diagnosis and neurodevelopmental outcome in isolated cerebellar hypoplasia of suspected hemorrhagic etiology: A retrospective cohort study. *Cerebellum*. 2022;21(6):944-953.

doi: 10.1007/s12311-021-01341-9

70. Simonazzi G, Bernabini D, Curti A, *et al*. Fetal cerebellar damage in fetuses with severe anemia undergoing intrauterine transfusions. *J Matern Fetal Neonatal Med*. 2016;29(3):389-392.

doi: 10.3109/14767058.2014.1001973

71. Feygin T, Khalek N, Moldenhauer JS. Fetal brain, head, and neck tumors: Prenatal imaging and management. *Prenat Diagn*. 2020;40(10):1203-1219.

doi: 10.1002/pd.5722

72. Barkovich AJ, Raybaud CA, editors. Congenital malformations of the brain and skull. In: *Pediatric Neuroimaging*. 6th ed. Netherlands: Wolters Kluwer; 2019. p. 1094.

73. Meoded A, Turan S, Harman C, *et al*. Pre- and postnatal ultrasound and magnetic resonance imaging of intracranial extra-axial glioneuronal heterotopia. *Fetal Diagn Ther*. 2011;30(4):314-316.

doi: 10.1159/000330859

74. Russler-Germain E, Majumdar S, Nguyen T, Hirose K, Yang PH, Dahiya S. Glioneuronal heterotopia in the right middle cranial fossa. *Free Neuropathol*. 2024;5:28.

doi: 10.17879/freeneuropathology-2024-5848

ACCSCIENCE PUBLISHING

Journal of Clinical and Translational Research

ORIGINAL ARTICLE

Impact of prenatal exposure to crude oil pollutants on newborn anthropometrics and thyroid hormone levels in Southern Nigeria

Mathias Abiodun Emokpae[1]*, Lawrence Ogana[1], and Adebayo Okikiola Uthman[2]

[1]Department of Medical Laboratory Science, School of Basic Medical Sciences, University of Benin, Benin City, Edo, Nigeria

[2]Department of Medical Laboratory Science, Achievers University Owo, Owo, Ondo, Nigeria

Abstract

Background: The search and extraction of crude oil produce harmful environmental compounds and expose individuals, particularly during crucial and vulnerable stages of development like pregnancy, to a variety of negative health impacts. **Aim:** This study aims to assess the effects of prenatal exposure to ambient crude oil pollutants on selected newborn anthropometric measurements and maternal/cord blood thyroid hormone levels in crude oil-producing communities. **Methods:** Fifty pregnant women were environmentally exposed to crude oil, along with their newborns, and 30 pregnant women who were not exposed, along with their infants, were enrolled in the study. Maternal blood was obtained between weeks 29 and 39 of pregnancy, while cord blood was collected after birth. Thyroid hormones (triiodothyronine [T3], thyroxine [T4], and thyroid-stimulating hormone [TSH]) were measured using an enzyme-linked immunosorbent assay. The newborn's weight, length, and head circumference were measured, and the ponderal index (PI) was calculated for all study neonates. **Results:** The results indicated that selected newborn health indicators (recumbent length, head circumference, and PI) were considerably lower in infants exposed before birth compared to non-exposed neonates. TSH in cord blood was much lower, but T3 and T4 levels were significantly greater in prenatally exposed newborns than in prenatally unexposed neonates. Serum TSH levels were notably higher, whereas T3 and T4 levels were reduced in women exposed to crude oil than in expectant mothers who were not. The difference in mean glucose levels between exposed and non-exposed expectant mothers was insignificant. Both mothers and newborns exposed to ambient crude oil toxicants displayed mild or silent changes in thyroid hormone levels. **Conclusion:** Silent hypothyroidism in crude oil-exposed mothers and hyperthyroidism in prenatally exposed neonates might be responsible for the changes in health indicators of neonates. Health education and awareness of the dangers associated with crude oil exposure, as well as preventive measures, should be intensified in these communities. **Relevance for patients:** Prenatal exposure to crude oil pollutants can impair growth and development and pose a threat to the health of newborn infants.

Keywords: Pregnancy; Newborn; Prenatal exposure; Thyroid hormones; Petroleum

***Corresponding author:**
Mathia A. Emokpae
(mathias.emokpae@uniben.edu)

Citation: Emokpae MA, Ogana L, Uthman AO. Impact of prenatal exposure to crude oil pollutants on newborn anthropometrics and thyroid hormone levels in Southern Nigeria. *J Clin Transl Res.* 2025;11(2):78-86.
doi: 10.36922/jctr.24.00083

Received: December 24, 2024

Revised: February 2, 2025

Accepted: March 27, 2025

Published online: April 14, 2025

1. Introduction

Crude oil comprises a variety of vaporous and semi-vaporous chemicals, including polycyclic aromatic hydrocarbons (PAHs), sulfur- and nitrogen-containing substances, and metal elements. The burning of crude oil releases additional PAH combustion by-products, including a wide range of vaporous gases and very small particulate matter, which could be inhaled or penetrate the epithelial cells of the body. Petroleum hydrocarbons behave differently in the environment and are readily released into the atmosphere, food chain, and environment that humans make contact with.[1] The discharge of crude oil pollutants into the environment is a serious concern. Fuel derived from petroleum hydrocarbons is widely utilized on a global scale. Contamination frequently arises from various activities, such as exploration, production, maintenance, transportation, storage, and accidental release of petroleum hydrocarbons, due to the high demand for it as an energy source. This contamination causes substantial ecological consequences. The advancement of contemporary society has exerted strain on the energy supply, particularly on petroleum hydrocarbons, which have borne the majority of this burden.[2,3] The ramifications of this event are both disastrous and catastrophic, impacting not only humans but also other living organisms within the ecosystem.

The search, mining, and processing of crude oil generate harmful environmental substances and expose individuals, particularly during crucial and vulnerable stages of development like pregnancy, to a wide range of health effects that can persist throughout life and potentially be passed on to future generations.[4] Crude oil toxicants can enter the human body via the oral route, nose, and skin, which can gradually stockpile or accumulate in the liver, blood, and epithelial tissues. Blood flow between the mother and fetus is very important to human development and needs to be investigated, especially in crude oil-producing communities due to their sensitivity to both mother and fetus.[5] Expectant mothers and their unborn babies are at risk when exposed to a combination of pollutants known as endocrine disruptors, as the fetus depends on the mother for nutrients, gasses, and waste exchange. The duration of exposure and dose of the toxicants absorbed are crucial factors that exert biological effects on the fetus. Prenatal exposure to crude oil and its derivatives through placental transfer may lead to adverse effects on fetal weight, recumbent length, head circumference, and ponderal index (PI).[6,7] Evidence has indicated that crude oil toxicants may actively participate in the transcription of thyroid-releasing hormones and may impede thyroid function,[6,8] thus affecting neonatal health and pregnancy outcomes by distorting growth and development.[5] Although the placenta acts as a selective barrier against several unwanted or toxic substances from the mother to the fetus, these substances can still damage the placenta, resulting in adverse consequences for pregnancy outcomes.[9-11]

The thyroid modulates important processes, such as neuronal stem cell multiplication, movement, and myelination in the fetus. The unborn child depends on the maternal thyroid hormone supply before 18 – 20 weeks of pregnancy. Therefore, the placental transfer of the expectant mothers' thyroid hormone throughout early pregnancy is critical. Hence, the iodine status of the pregnant woman is essential for the fetus's brain development. Evidence has demonstrated that exposure to environmental crude oil contaminants can impede thyroid hormone accessibility and action at several functional levels.[4,12,13] It was suggested that the exposure of the fetus to thyroid hormone-disrupting substances and iodine deficiency are major contributing factors to the increasing incidence of neurodevelopmental diseases in humans.[4] Iodine is a crucial component of the thyroid hormone and contributes to its biosynthesis. The role of environmental and genetic interactions in causing illness is now more evident than when the concept was first proposed.[14] There has been limited investigation into the potential influence of unborn babies' exposure to environmental crude oil toxicants on neonatal anthropometric indices in Southern Nigeria. This study seeks to determine how prenatal exposure to ambient crude oil toxicants affects neonatal anthropometric indices and maternal/cord blood thyroid hormone levels in crude oil-producing villages in Southern Nigeria.

2. Methods

2.1. Study design

This research was designed as a case-control study and was carried out at the Central Hospitals in Warri and Asaba, Nigeria, from July 2021 to June 2022. The study focused on adult expectant mothers in their third trimester who were permanent residents of the Warri South Local Government Area, an area characterized by active crude oil exploration and exploitation, as well as Asaba, a town devoid of such activities. Both locations are situated within Delta State, Nigeria.

2.2. Study population

The study subjects included adult expectant mothers who were in their third trimester of pregnancy and residing in Warri and Asaba (Delta State, Nigeria). They were between the ages of 18 and 41 years. Fifty healthy pregnant women living in Warri (cases) and 30 healthy pregnant women living in Asaba (controls) were enrolled in the research.

2.3. Ethical considerations

The research was conducted in accordance with ethics guidelines, and approval was obtained from the Ethics and Health Research Committee of the Central Hospital, Warri, Delta State, Nigeria (CHW/ECC VOL 1/168). Before collecting specimens, informed consent was given by all participants. Participants who did not provide informed consent were excluded. Absolute confidentiality was maintained throughout the study.

2.4. Inclusion and exclusion criteria

The study only included healthy expectant mothers who gave birth in the hospital, attended the antenatal clinic for care, and delivered their babies there. Expectant mothers who had lived in Warri South, the location of crude oil search and extraction, permanently for more than 5 years were also included. The control subjects were permanent residents of Asaba town who had never resided in Warri town or any other community where crude oil extraction takes place. Women who were expecting and had complex obstetric problems, hemoglobinopathies, thyroid abnormalities, or chronic disease were not included.

2.5. Questionnaire

To collect socio-anthropological data, an interview-administered questionnaire was employed, which included age, educational status, medical history, and family history of hypothyroidism. The hospital records provided information on medication use, due date of delivery, and maternal health and obstetrics. Anthropometric measurements (birth weight, head circumference, and recumbent length in the newborns) were made using standard procedures. PI was derived for all study individuals using Equation I:

$$\text{Ponderal index} = \frac{\text{Birth weight (g)}}{\text{Birth length (cm)}} \times 100 \quad \text{(I)}$$

A PI < 10 indicates fetal malnutrition, while a PI < 3 suggests severe fetal wasting.[14]

2.6. Sample size determination

The sample size (N) was obtained using Equation II:[15]

$$N = Z^2P(1-P)/d^2 \quad \text{(II)}$$

Where N = required sample size, Z = confidence level interval at 95% (standard value of 1.96), P = prevalence of newborn deaths due to crude oil spillage in Niger Delta, Nigeria, and d = margin of error at 5% (standard value of 0.05). The rate of newborn death due to crude oil spillage in the Niger-Delta region of Nigeria was 3.83%.[16] The sample size was calculated to be 56.59. Therefore, 57 expectant mothers were enrolled. However, only 50 crude oil-exposed expectant mothers (and their newborns) and 30 non-exposed expectant mothers (and their newborns) were finally evaluated, as seven participants had incomplete data.

2.7. Sample collection

Venous blood samples (approximately 5 mL) were obtained from expectant mothers during the gestational period of 29 – 39 weeks and subsequently transferred into a sterile sample container. The specimens were allowed to coagulate at a temperature range of 20 – 22°C. Upon completion of the coagulation process, the samples were subjected to centrifugation in a bucket centrifuge operating at 3,000 rpm for 10 min. The resulting serum was carefully decanted into a new container and stored at −80°C until further analysis. Following childbirth, the umbilical cord was immediately clamped at both ends and severed. Approximately 5 mL of cord blood was extracted from the umbilical vein and placed into a designated plain container, which was then properly labeled. The collected cord blood samples were allowed to clot and subsequently centrifuged at 2,500 rpm for 15 min after clot retraction. The serum was decanted and preserved at −80°C until further analysis.

2.8. Determination of thyroid hormones and thyroid-stimulating hormone (TSH)

Enzyme-linked immunosorbent assay test kits (Elabscience, United States of America [USA]) were used for the determination of thyroid hormones. Measuring the concentration of hormones in the blood is considered a useful method for diagnosing thyroid problems. The reagents, calibrators, and controls were equilibrated to room temperature, specifically between 20°C and 27°C. The wells of the microplates were arranged in duplicate for each calibrator, control, and patient specimen to be analyzed. The hormone levels were determined in batches according to the manufacturer's protocol, using 1 mL serum aliquot, which was kept frozen at −80°C. The serum aliquot was allowed to thaw at room temperature before analysis.

To avoid differences in reaction time between wells, the reagents were added in the same sequence. The plate was not shaken after adding the substrate. The incubation process occurred at ambient temperature for 15 min. The optical density in each well was measured at a wavelength of 450 nm using a microplate reader. The absorbance was measured within 30 min after the addition of the stop solution.

A calibration curve was utilized to determine the hormone levels in the specimens. The concentration for an unknown sample was estimated by extrapolating from the graph.[17,18]

2.9. Statistical analysis

The results obtained were systematically organized and subjected to appropriate statistical analysis. The gathered results were analyzed using Statistical Package for Social Science (version 26.0; IBM, Chicago, USA). Data were analyzed using independent Student's *t*-test, and values are presented as mean ± standard deviation. The significance level was established at $p<0.05$.

3. Results

Table 1 displays the sociodemographic variables of the subjects. The age distribution of study participants ranged from 18 to 41 years, and no notable difference was observed between the mean age of exposed and non-exposed expectant mothers. The educational status, employment status, and body mass index (BMI) were not significantly different between exposed and non-exposed expectant mothers.

Table 2 demonstrates that the gender of the newborn and birth weight were not significantly different between prenatally exposed and prenatally non-exposed infants.

Table 3 compares the anthropometric measurements of prenatally exposed and unexposed newborn infants. Prenatal exposure resulted in significantly smaller head circumferences ($p<0.005$), recumbent lengths ($p<0.001$), and PI ($p<0.001$) compared to unexposed newborn babies.

Table 1. Sociodemographic characteristics of pregnant women in the study

Parameters	*n* (%)	
	Exposed mothers	Unexposed mothers
Maternal age (years)		
18 – 23	8 (16)	6 (20)
24 – 29	14 (28)	12 (40)
30 – 35	20 (40)	10 (33.3)
36 – 41	8 (16)	2 (6.7)
Educational status		
Primary	3 (6)	2 (6.6)
Secondary	28 (56)	14 (46.7)
Tertiary	19 (38)	14 (46.7)
Employment status		
Yes	45 (90)	26 (86.7)
No	5 (10)	4 (13.3)
Body mass index (kg/m^2)		
Normal (18.5 – 25)	30 (60)	18 (60)
Overweight (>25)	20 (40)	12 (40)

Note: The maternal age of exposed mothers and unexposed mothers is 27.2±1.2 and 27.4±0.9 years, respectively.

There was no significant difference in birth weight between exposed and unexposed newborn babies.

Table 4 demonstrates that expectant moms who were exposed to crude oil pollution had similar thyroid hormone levels and glucose concentrations to those who were not exposed. Crude oil pollution-exposed mothers had considerably higher serum TSH levels ($p<0.03$) compared to unexposed mothers, but triiodothyronine (T3) and thyroxine (T4) levels were significantly lower ($p<0.001$ and $p<0.04$, respectively). There was a significant difference in mean glucose levels between exposed and unexposed pregnant women.

Table 2. Demographic characteristics of newborn infants in the study

Variables	*n* (%)	
	Prenatally exposed	Prenatally non-exposed
Gender of newborn		
Male	23 (46)	14 (46.7)
Female	27 (54)	16 (53.3)
Birth weight (kg; reference range: 2.5 – 4.0)		
Low (<2.5)	3 (6)	2 (6.7)
Normal (>2.5)	47 (94)	28 (93.3)

Table 3. Comparison of anthropometric measurements of prenatally exposed (*n*=50) and non-exposed (n=30) newborn infants

Anthropometric parameters	Prenatally exposed newborn infants	Non-exposed newborn infants	*p*
Birth weight (kg)	3.34±0.3	3.47±0.4	0.2
Head circumference (cm)	33.3±1.2	34.4±2.1	0.005
Recumbent length (cm)	52.8±0.2	54.4±0.2	0.001
Ponderal index (g/cm^3)	2.24±0.5	2.45±0.2	0.001

Table 4. Levels of thyroid hormone and glucose in exposed (*n*=50) and unexposed (*n*=30) expectant mothers to crude oil pollution

Parameters	Reference range	Crude oil-exposed mothers	Unexposed mothers	*p*
TSH (mIU/L)	0.39 – 4.16	2.83±0.84	2.46±0.83	0.034
T3 (ng/mL)	10.0 – 20.0	6.85±1.45	9.26±0.59	0.001
T4 (µg/dL)	4.8 – 11.6	11.12±0.86	12.08±1.54	0.046
Glu (mg/dL)	70 – 100	92.7±7.18	68.0±2.01	0.207

Note: The reference ranges are trimester-specific.
Abbreviations: TSH: Thyroid-stimulating hormone; T3: Triiodothyronine; T4: Thyroxine; Glu: Glucose.

Table 5 compares thyroid hormone levels in cord blood from prenatally exposed and unexposed newborns to crude oil toxicants. Prenatally exposed newborns had significantly reduced mean cord blood TSH (p<0.027), but significantly greater T3 (p<0.045) and T4 (p<0.001) levels compared to unexposed infants.

4. Discussion

Prenatal environmental exposure to crude oil contaminants may adversely impact the health of pregnant women and unborn babies. The specific mechanisms may be linked to the consumption of contaminated foods, water, dermal contact, and ambient air pollution. In this study, the effect of antepartum environmental exposure to crude oil toxicants on recumbent length, weight at delivery, head circumference, PI at birth, and thyroid hormone was investigated.

Data from this study indicated that the selected newborn health indicators (recumbent length, head circumference, and PI) were significantly lower among prenatally exposed newborns compared to unexposed infants. These observations did not agree with previous studies,[6,19-21] as there was no observed association between antenatal PAH exposure and statistically significant adverse effects on measured anthropometric indicators (recumbent length, head circumference, and birth weight) of PAH-exposed infants.

Our findings agreed with those of Perera *et al.*,[22] who observed that PAH-DNA adduct compounds were linked to a 3% decrease in head circumference. Perera *et al.*[23] observed a notable reduction in newborn height and head circumference in a different study, and they linked this to exposure to environmental PAHs and the transplacental transfer of contaminants. The disparity between previous literature and the present study may be attributable to changes in exposure conditions and levels between various study sites, unique vulnerability to these toxicants in different populations,[24] and differences in exposure pathways. In the crude oil-producing region of Nigeria, illegal or secret oil refining and ineffective pipeline maintenance have been recognized as contributors to a significant proportion of oil spills in most crude oil-producing communities.[25,26]

Table 5. Comparison of cord blood thyroid hormone levels in prenatally exposed newborns (n=50) and unexposed newborns (n=30) to crude oil pollution

Parameters	Prenatally exposed neonates	Prenatally unexposed neonates	p
TSH (mIU\L)	2.11±0.09	4.22±0.01	0.027
T3 (ng\dL)	1.57±0.03	1.44±0.80	0.045
T4 (µg\gL)	11.22±0.05	8.05±0.07	0.001

Abbreviations: TSH: Thyroid-stimulating hormone; T3: Triiodothyronine; T4: Thyroxine.

Reduced anthropometric measurements at birth have been linked to lower IQ levels, diminished cognitive abilities, and subpar academic performance during childhood.[27] However, the precise mechanisms by which crude oil toxicant exposure affects embryonic development are not fully understood. Fetal toxicity associated with PAHs can be attributed to various factors, including their anti-estrogenic properties,[28] which arise from their capacity to bind to human aryl-hydrocarbon receptors, thereby stimulating the production of P450 enzymes. In addition, inadequate detoxification processes, compromised DNA repair mechanisms, and elevated rates of cellular proliferation contribute to the heightened susceptibility of fetuses and infants to environmental pollutants compared to adults. Furthermore, the central nervous system is especially at risk during prenatal development, as PAHs can easily traverse the placental barrier.[21-24] Cell membrane dysfunction, defective enzyme systems, or inhibition of uteroplacental blood flow can cause cell death in the endothelium and syncytiotrophoblast cells.[6] In addition, PAHs may generate oxidative stress,[19] decrease placenta cell multiplication, and cause fetal growth retardation in prenatally exposed newborn babies.

However, the observed insignificant change in the infant birth weight was consistent with that of Dehghani *et al.*[6] An insignificant association was observed between antenatal exposure to PAH compound and newborn weight reduction following regression analysis.

The PI has been used widely in neonatology as a measure of fetal growth status, particularly to establish the symmetry of intrauterine growth restriction (IUGR). Evidence has demonstrated the impact of changed PI on short-term perinatal outcomes of acidosis, rise in perinatal mortality, and adverse neurological outcomes. It is also an indicator of long-term impact on the BMI of young males, glucose tolerance in children, blood pressure and coronary heart disease in adults, and the age of menopause in women.[29] In children with IUGR, the build-up of adipose tissue and muscle mass becomes smaller, resulting in a decreased PI. When birth weight is added to birth length, it can be used to differentiate between lean body weight and long babies (low PI) and fat body weight and short babies high PI.[14]

From this study, it was observed that the thyroid gland function was suppressed in mothers residing in crude oil-bearing communities compared to those living in non-crude oil-bearing communities. This observation aligns with the results obtained from research conducted on animals.[30] Zebrafish exposed to water contaminated with

Iranian heavy crude oil for 5 days displayed significantly lower levels of T3 and T4. In contrast, the examination of gross and histomorphology in rats exposed to crude oil did not reveal any evidence of treatment-related changes in the thyroid.[31] Furthermore, long-term exposure to bitumen fumes, specifically from a mixture of 70% air-rectified and 30% vacuum residue bitumen at a concentration of 100 mg/m^3, had only minor effects on the respiratory tract and did not exhibit any significant impact on the thyroid gland.[32] Thyroid hormones, notably T3 and T4, are crucial for the fetus's growth and neurological development.[33] Beginning from week 14 to the end of week 27 of pregnancy, the fetal hypothalamus-pituitary-thyroid axis activates and produces an increasing amount of thyroid hormones.[34]

The average concentration of T3 in crude oil-exposed mothers was noticeably lower compared to non-crude oil-exposed mothers in the present study, which aligned with the findings of Forhead and Fowden.[33] T3, a hormonally active compound, is synthesized from T4 and possesses greater potency than T4. It affects nearly all physiological processes within the body. Furthermore, a reduced concentration of T3 can lead to a decline in the metabolic rate of body tissues, which consequently hampers growth and maturation.[35] The decrease in serum T4 levels observed in individuals exposed to crude oil may be attributed to a shortened T4 degradation period. Several chemicals have been identified to reduce the serum degradation period of T4 by stimulating liver enzymes involved in T4 conjugation.[36] Chemicals found in the environment, such as polychlorinated biphenyls, bisphenol A, and brominated flame retardants, have been proven to influence hormone metabolism, leading to alterations in hormone-mediated reactions.[37]

In this study, it was also discovered that the average level of TSH was notably lower in the umbilical cord blood of newborns whose mothers were exposed to crude oil pollution compared to newborns whose mothers were not exposed. The average T3 and T4 concentrations in the umbilical cord blood of infants born to mothers exposed to crude oil pollution were significantly elevated compared to neonates born to non-exposed mothers. The levels of thyroid hormones in newborns are affected by changes in the thyroid function and iodine levels of the mother.[38] The remarkably lower TSH and increased T3 and T4 levels aligned with the findings in deer mice by Movasseghi *et al*.[39] The authors observed that deer mice raised in a reclaimed oil spill site exhibited a notable increase in follicular cell proliferation and a decrease in colloid levels in their thyroid glands compared to control mice. Animals experiencing higher levels of oxidative stress exhibited a notable increase in thyroid hormone levels. This could suggest an elevation in metabolic requirements resulting from subclinical toxicity associated with contaminants. T3 is the biologically active form of the thyroid hormone that binds to nuclear receptors to carry out the functions of the thyroid hormone, facilitating appropriate development of the brain, liver, and skeletal system.[40] Newborns with a deficit thyroid hormone may exhibit skeletal abnormalities as a result of insufficient endochondral ossification, a process by which the fetal cartilaginous model of bones contributes to longitudinal growth and skeletal maturation. In addition, the thyroid hormones control the activity of numerous genes that are crucial for the formation of the central nervous system in embryos.

The limitation of the study is its inability to quantify crude oil contaminants in the environment, as more than 1,300 different compounds may be produced as a result of oil and gas search and mining activities. Between 1976 and 1996, the Department of Petroleum Resources reported that close to two million barrels of petroleum had been dumped into the area. According to research by the United Nations Development Programme, there were 6,817 oil spills between 1976 and 2001, resulting in the spill of three million barrels of oil, more than 70% of which were not usually recovered.[41]

The assessment of prenatal exposure to crude oil pollutants through a single measurement may have its limitations; however, measurements taken during the second and third trimesters are regarded as a reliable indicator of exposure throughout the latter two trimesters of gestation. The urinary iodine of the babies was not controlled in this study. Urinary iodine concentration is regarded as a good marker for recent dietary iodine status, as more than 90% of dietary iodine is excreted in the urine.[42] However, a recent study among women of childbearing age in the study area indicated that a greater proportion of the women (44.2%) had more than adequate iodine nutrition, while 6.49% had excessive. The authors observed that the iodine status of women was adequate, as none of the women was deficient.[43] In addition, thyroid-binding globulin was not estimated in this study. Thyroid-binding globulin is one of the three transport proteins that transport thyroid hormones to the necessary tissues. It is not known whether crude oil contains dioxin, but a study has demonstrated that dioxin can originate from the regeneration of the catalytic reforming units during petroleum refining to produce gasoline. Dioxin has been reported in wastewaters and sludges that are contaminated with chlorinated dibenzo-dioxins and chlorinated dibenzofurans from petroleum refineries.[44]

5. Conclusion

This study found that neonatal health indices, such as recumbent length, head circumference, and PI, were

significantly lower in antenatally exposed babies than in unexposed infants. TSH in cord blood was lower, whereas T3 and T4 were greater in antenatally exposed infants compared to the unexposed infants. Mean serum TSH was higher, while T3 and T4 were lower in crude oil pollutant-exposed women compared to non-exposed women. Findings suggest that exposure to crude oil pollutants can influence the hypothalamic-pituitary-thyroid regulatory system. Health education and awareness of the dangers associated with environmental crude oil exposure, as well as preventive measures, should be intensified in these communities.

Acknowledgments

The authors appreciate the contributions of the doctors, nurses, medical laboratory scientists, and research assistants involved in the completion of this study.

Funding

None.

Conflict of interest

The authors declare no conflict of interest.

Author contributions

Conceptualization: Mathias Abiodun Emokpae
Investigation: All authors
Methodology: All authors
Writing–original draft: All authors
Writing–review & editing: Mathias Abiodun Emokpae

Ethics approval and consent to participate

The research was conducted following the ethics guidelines, and approval was obtained from the Ethics and Health Research Committee of the Central Hospital, Warri, Delta State (reference CHW/ECC VOL 1/168). Before collecting specimens, we obtained informed consent from all participants. Participants who did not provide informed consent were excluded. Absolute confidentiality was maintained throughout the study.

Consent for publication

Patients consented to the publication of their data.

Availability of data

The datasets generated and/or analyzed during this study are available from the corresponding author upon reasonable request.

References

1. United Nations Environment Programme. *Environmental Assessment of Ogoni Land*. Nairobi: UNEP; 2011. p. 8-17.
2. Foster WG, Gregorovich S, Morrison KM, *et al*. Human maternal and umbilical cord blood concentrations of polybrominated diphenyl ethers. *Chemosphere*. 2011;84(10):1301-1309.
   doi: 10.1016/j.chemosphere.2011.05.028
3. Zota AR, Park JS, Wang Y, Petreas M, Zoeller RT, Woodruff TJ. Polybrominated diphenyl ethers, hydroxylated polybrominated diphenyl ethers, and measures of thyroid function in second trimester pregnant women in California. *Environ Sci Technol*. 2011;45(18):7896-7905.
   doi: 10.1021/es200422b
4. Demeneix BA. Evidence for prenatal exposure to thyroid disruptors and adverse effects on brain development. *Eur Thyroid J*. 2019;8(6):283-292.
   doi: 10.1159/000504668
5. Dai Y, Xu X, Huo X, Faas MM. Effects of polycyclic aromatic hydrocarbons (PAHs) on pregnancy, placenta, and placental trophoblasts. *Ecotoxicol Environ Saf*. 2023;262:115314.
   doi: 10.1016/j.ecoenv.2023.115314
6. Dehghani S, Fararouei M, Rafiee A, Hoepner L, Oskoei V, Hoseini M. Prenatal exposure to polycyclic aromatic hydrocarbons and effects on neonatal anthropometric indices and thyroid-stimulating hormone in a Middle Eastern population. *Chemosphere*. 2022;286(Pt 1):131605.
   doi: 10.1016/j.chemosphere.2021.131605
7. Jiang L, Xiao Q, Zhang J, Zhao Y, Chen L, Lu S. Association between fetal exposure to polycyclic aromatic hydrocarbons and low birth weight: A case-control study in Shenzhen, China. *Environ Sci Pollut Res*. 2022;29:88779-88787.
   doi: 10.1007/s11356-022-21965-6
8. Adipah S. Introduction of petroleum hydrocarbons contaminants and its human effects. *J Environ Sci Public Health*. 2019;3:1-9.
   doi: 10.26502/jesph.96120043
9. Dong X, Wang Q, Peng J, Wu M, Pan B, Xing B. Transfer of polycyclic aromatic hydrocarbons from mother to fetus in relation to pregnancy complications. *Sci Total Environ*. 2018;636:61-68.
   doi: 10.1016/j.scitotenv.2018.04.274
10. Li P, Hua R, Li K, *et al*. Polycyclic aromatic hydrocarbons exposure and early miscarriage in women undergoing *in vitro* fertilization-embryo transfer. *Hum Fertil* (*Camb*). 2020;23:17-22.
    doi: 10.1080/14647273.2018.1479888
11. Li J, Sun X, Xu J, Tan H, Zeng EY, Chen D. Transplacental transfer of environmental chemicals: Roles of molecular descriptors and placental transporters. *Environ Sci Technol*. 2021;55:519-528.
    doi: 10.1021/acs.est.0c06778

12. Heindel JJ, Balbus J, Birnbaum L, *et al*. Developmental origins of health and disease: Integrating environmental influences. *Endocrinology*. 2015;156(10):3416-3421.

doi: 10.1210/EN.2015-1394

13. Barouki R, Melén E, Herceg Z, *et al*. Epigenetics as a mechanism linking developmental exposures to long-term toxicity. *Environ Int*. 2018;114:77-86.

doi: 10.1016/j.envint.2018.02.014

14. Hwang JK, Kang HN, Ahn JH, Lee HJ, Park HK, Kim CR. Effects of ponderal index on neonatal mortality and morbidities in extremely premature infants. *J Korean Med Sci*. 2022;37(24):e198.

doi: 10.3346/jkms.2022.37.e198

15. Jaykaran C, Tamoghna B. How to calculate sample size for different study designs in medical research? *Indian J Psychol Med*. 2013;35(2):121-126.

doi: 10.4103/0253-7176.116232

16. Bruederle A, Hodler R. Effect of oil spills on infant mortality in Nigeria. *Proc Natl Acad Sci U S A*. 2019;116(12):5467-5471.

doi: 10.1073/pnas.1818303116

17. Gharib H, Ryan RJ, Mayberry WE, Hockert T. Radioimmunoassay for triiodothyronine (T 3): I. Affinity and specificity of the antibody for T 3. *J Clin Endocrinol Metab Endocr*. 1971;33:509-516.

18. Hopton MR, Harrap JJ. Immunoradiometric assay of thyrotropin as a "first-line" thyroid-function test in the routine laboratory. *Clin Chem*. 1986;32:691-693.

19. Agarwal P, Anand M, Chakraborty P, Singh L, Masih J, Taneja A. Placental levels of polycyclic aromatic hydrocarbons (PAHs) and their association with birth weight of infants. *Drug Chem Toxicol*. 2022;45:868-877.

doi: 10.1080/01480545.2020.1783285

20. Lamichhane DK, Leem JH, Kim HC, *et al*. Impact of prenatal exposure to polycyclic aromatic hydrocarbons from maternal diet on birth outcomes: A birth cohort study in Korea. *Public Health Nutr*. 2016;19:2562-2571.

doi: 10.1017/S1368980016000550

21. Jedrychowski W, Perera FP, Tang D, *et al*. Impact of barbecued meat consumed in pregnancy on birth outcomes accounting for personal prenatal exposure to airborne polycyclic aromatic hydrocarbons: Birth cohort study in Poland. *Nutrition*. 2012;28(4):372-377.

doi: 10.1016/j.nut.2011.07.020

22. Perera, FP, Rauh V, Whyatt RM, *et al*. Molecular evidence of an interaction between prenatal environmental exposures and birth outcomes in a multiethnic population. *Environ Health Perspect*. 2004;112(5):626-630.

doi: 10.1289/ehp.6617

23. Perera FP, Rauh V, Tsai WY, *et al*. Effects of transplacental exposure to environmental pollutants on birth outcomes in a multiethnic population. *Environ Health Perspect*. 2003;111:201-205.

doi: 10.1289/ehp.5742

24. Wang B, Jin L, Ren A, *et al*. Levels of polycyclic aromatic hydrocarbons in maternal serum and risk of neural tube defects in offspring. *Environ Sci Technol*. 2015;49:588-596.

doi: 10.1021/acs.est.5b03471

25. Oghenetega OB, Ana GRE, Okunlola MA, Ojengbede OA. Oil spills, gas flaring and adverse pregnancy outcomes: A systematic review. *Open J Obstet Gynecol*. 2020;10(1):187-199.

doi: 10.4236/ojog.2020.1010016

26. Ewim DRE, Orikpete OF, Scott T, *et al*. Survey of wastewater issues due to oil spills and pollution in the Niger Delta area of Nigeria: A secondary data analysis. *Bull Natl Res Cent*. 2023;47:116.

doi: 10.1186/s42269-023-01090-1

27. Edwards SC, Jedrychowski W, Butscher M, *et al*. Prenatal exposure to airborne polycyclic aromatic hydrocarbons and children's intelligence at 5 years of age in a prospective cohort study in Poland. *Environ Health Perspect*. 2010;118(9):1326-1331.

doi: 10.1289/ehp.0901070

28. Boonen I, Van Heyst A, Van Langenhove K, *et al*. Assessing the receptor-mediated activity of PAHs using AhR-, ERα- and PPARγ- CALUX bioassays. *Food Chem Toxicol*. 2020;145:111602.

doi: 10.1016/j.fct.2020.111602

29. Kumar B P, Eregowda A, ManjunathS. Maternal nutritional status during pregnancy as a predictor of Ponderal index and body proportionality at birth, in term neonates. *Int J Adv Med*. 2020;7:1712-1716.

doi: 10.18203/2349-3933.ijam20204524

30. Kim S, Sohn JH, Ha SY, *et al*. Thyroid hormone disruption by water-accommodated fractions of crude oil and sediments affected by the Hebei spirit oil spill in zebrafish and GH3 Cells. *Environ Sci Technol*. 2016;50(11):5972-5980.

doi: 10.1021/acs.est.6b00751

31. API. *28-Day Dermal Toxicity Study in the Rabbit, Vacuum Residuum, API Sample 81-13. Testing Laboratory: Borriston Laboratories, Inc., Temple Hill, Maryland Report No.: 1703(1). Study Number: 30-32852. Report Date: 1983-09-09. Summary from REACH CSR for Bitumen*. Washington, DC: American Petroleum Institute; 2010.

32. Fowles JR, Banton MI, Boogaard PJ, Ketelslegers HB, Rohde AM. Assessment of petroleum streams for thyroid toxicity. *Toxicol Lett*. 2016;254:52-62.

doi: 10.1016/j.toxlet.2016.05.001

33. Forhead AJ, Fowden AL. Thyroid hormones in fetal growth and prepartum maturation. *J Endocrinol*. 2014;221:R87-R103.

doi: 10.1530/JOE-14-0025

34. Patel J, Landers K, Li H, Mortimer RH, Richard K. Delivery of maternal thyroid hormones to the fetus. *Trends Endocrinol Metab*. 2011;22:164-170.

doi: 10.1016/j.tem.2011.02.002

35. Kelly M, Gauthier MS, Saha AK, Ruderman NB. Activation of AMP-activated protein kinase by interleukin-6 in rat skeletal muscle: Association with changes in cAMP, energy state, and endogenous fuel mobilization. *Diabetes*. 2009;58:1953-1960.

doi: 10.2337/db08-1293

36. Glatt CM, Ouyang M, Welsh W, *et al*. Molecular characterization of thyroid toxicity: Anchoring gene expression profiles to biochemical and pathologic end points. *Environ Health Perspect*. 2005;113:1354-1361.

doi: 10.1289/ehp.7690

37. Boas M, Feldt-Rasmussen U, Skakkebaek NE, Main KM. Environmental chemicals and thyroid function. *Eur J Endocrinol*. 2006;154:599-611.

doi: 10.1530/eje.1.02128

38. Velasco I, Martin J, Gallego M, Gutierrez-Repiso C, Santiago P, Lopez-Siguero JP. Maternal-fetal thyroid function at the time of birth and its relation with iodine intake. *Thyroid*. 2013;23:1619-1626.

doi: 10.1089/thy.2013.0035

39. Movasseghi AR, Rodríguez-Estival J, Smits J. Thyroid pathology in deer mice (*Peromyscus maniculata*) from a reclaimed mine site on the athabasca oil sands. *Environ Pollut*. 2017;222:42-49.

doi: 10.1016/j.envpol.2017.01.008

40. Vancamp P, Darras VM. Dissecting the role of regulators of thyroid hormone availability in early brain development: Merits and potential of the chicken embryo model. *Mol Cell Endocrinol*. 2017;459:71-78.

doi: 10.1016/j.mce.2017.01.045

41. UNDP. *Niger Delta Human Development Report*. UNDP. 2006. p. 76. Available from: https://hdr.undp.org/content/human-development-report [Last accessed on 2024 May 09].

42. Rohner F, Zimmermann M, Jooste P, *et al*. Biomarkers of nutrition for development--iodine review. *J Nutr*. 2014;144(8):1322S-1342S.

doi: 10.3945/jn.113.181974

43. Orisa CA, Amadi AO, Oguzor GB. Assessment of the Iodine status of women of reproductive age (15-49 Years) in Rivers State, Nigeria. *Niger J Nutr Sci*. 2023;44(2):55-64.

doi: 10.4314/njns.v44i2.24

44. Elder JR, Prothro MG. *Interim Petroleum Refinery Dioxin Discharges Activities and Guidance Update*. 1987. Washington DC: United States Environmental Protection Agency; 1987. Available from: https://www.3.epa.gov [Last accessed on 2025 Jan 26].

ACCSCIENCE PUBLISHING

Journal of Clinical and Translational Research

SPECIAL ISSUE ARTICLE

Clinical applications of a novel, Food and Drug Administration -approved biomimetic matrix in refractory diabetic foot ulcers: An observational case series analysis

Sara Rose-Sauld[1,2], Jennifer Skolnik[1,2], and Adam Landsman[1,2*]

[1]Department of Orthopaedic Surgery, Division of Foot and Ankle Surgery, Massachusetts General Hospital, Boston, Massachusetts, United States of America

[2]Department of Orthopaedics, Foot and Ankle Research and Innovation Lab (FARIL), Boston, Massachusetts, United States of America

(This article belongs to the *Special Issue: Innovations in Wound Healing*)

Abstract

Background: Biomimetic matrix (BMM) is a fully synthetic matrix composed of self-assembling peptides, an emerging class of biomaterials, for the treatment of chronic wounds. **Aim:** This preliminary case series explores the potential clinical applications of BMM in eight patients with chronic diabetic foot ulcers. The patients were selected based on wound chronicity and a lack of response to standard of care and/or previous treatments with biologics, including amniotic-derived materials, decellularized collagen, and living cell/collagen-derived products. **Results:** A total of eight subjects were evaluated and monitored in this case series. All subjects had diabetes, and the comorbidities included venous stasis, Charcot neuroarthropathy, obesity, osteomyelitis, peripheral vascular disease, and a history of prior partial foot amputation. All subjects treated with BMM responded after one to three applications. Overall, treatment with BMM resulted in an average percent wound area reduction of 63.6% over 6 weeks for chronic wounds that had remained open for an average of 21.5 months. **Conclusion:** BMM treatment reduced the wound area and depth of complex, stalled chronic diabetic lower extremity wounds. **Relevance for patients:** BMM, a synthetic self-assembling peptide-based matrix, demonstrated progression in treating stalled diabetic wounds that were not responsive to human- or animal-derived products.

Keywords: Diabetic foot ulcer; Biomimetic matrix; Synthetic self-assembling peptide; Wound healing

***Corresponding author:**
Adam Landsman
(alandsman@mgh.harvard.edu)

Citation: Rose-Sauld S, Skolnik J, Landsman A. Clinical applications of a novel, food and drug administration -approved biomimetic matrix in refractory diabetic foot ulcers: An observational case series analysis. *J Clin Transl Res*. 2025;11(2):87-93.
doi: 10.36922/jctr.24.00063

Received: September 19, 2024

1st revised: November 11, 2024

2nd revised: January 13, 2025

Accepted: March 27, 2025

Published online: April 18, 2025

1. Introduction

Chronic wounds represent a significant challenge in clinical practice, particularly when traditional therapies fail to induce healing.[1] Advanced therapies for chronic wounds typically include the application of advanced wound dressings or tissue-harvested/engineered skin substitutes to reduce inflammation and accelerate the healing process,

with often controversial or limited results, including the risk of rejection, infection, and impaired healing.[2]

Biomimetic matrix (BMM) is a fully synthetic matrix composed of self-assembling peptides—an emerging class of biomaterials recently applied to wound care.[3] Self-assembling peptides are constructed from short chains of synthetically derived amino acids capable of self-assembling into nano- and micro-structures, forming a three-dimensional (3D) scaffold. Self-assembling is a naturally occurring process involving the formation of spontaneous peptide aggregates mediated by non-covalent intermolecular interactions.[4]

Self-assembling peptides can be synthesized in a laboratory to mimic intricate, naturally occurring structures, taking advantage of their functional and dynamic properties applicable to wound healing.[5] For instance, some synthetic peptides are capable of self-assembling into matrices or biomimetic structures to facilitate cellular migration, adhesion, and proliferation. They can also be engineered to mimic naturally occurring structures with targeted features to produce enhanced therapeutic effects.[6] Innovative materials derived from self-assembling peptides, such as BMM, have potent cidal effects against microbial pathogens while sparing desirable mammalian cells.[7,8] This antibacterial effect is achieved by introducing cationic peptides capable of interacting and disrupting negatively charged components present in the bacterial membrane.[9] Furthermore, through mimicking naturally occurring structures, such as the native extracellular matrix (ECM), synthetic self-assembling peptides are highly biocompatible, biodegradable, and capable of interacting with biological ligands.[5] By leveraging these advancements, self-assembling peptides open new venues for advanced wound care by integrating multiple therapeutic functions into a single, customizable biomimetic structure. BMM's self-assembling peptide sequence was specifically designed to provide a 3D scaffolding matrix that resembles the dermal native ECM while offering antibacterial protection, a unique combination that is highly advantageous for the healing of chronic and complex wounds.

In this study, we review a series of eight cases in which a novel self-assembling peptide-based BMM was used to treat stalled, chronic diabetic foot ulcers (wounds present for at least 3 months without any evidence of a decrease in wound area) in patients with various comorbidities that did not respond to other advanced wound care products and/or biologic skin substitutes.

2. Methods

2.1. Patient enrollment

This preliminary case series explores the potential clinical applications of a BMM (Gel4Med, Inc., MA, USA) synthesized to resemble the native ECM while maintaining antibacterial activities. Eight patients with stalled chronic wounds present for 3 – 56 months were enrolled in the study. The inclusion criteria were based on wound chronicity (i.e., having a wound that has not decreased in size for at least 3 months) and lack of response to previous standard of care and/or biologic treatments. All subjects also had diabetes but there were no exclusions based on hemoglobin A1C. In addition, all subjects failed previous treatment with advanced dressing materials and/or biologics including amniotic-derived materials, decellularized collagen, and living cell/collagen products, with no noticeable improvement. Subjects with purulent, draining wounds and active cellulitis were excluded. In addition, patients not able to comply with regular visits scheduled every 2 weeks and unable to change their dressings were excluded from the study.

All wounds were previously treated with topical antibiotics (bacitracin, silver sulfadiazine, mupirocin) and wound irrigation solutions designed to reduce or eliminate bioburden (hypochlorous acid, Dakins solution, povidone-iodine), in addition to appropriate off-loading of the wound site. Before enrollment, all patients were confirmed to have palpable dorsalis pedis and posterior tibial pulses on the wounded foot. A summary of the patients enrolled, including wound location and size, previous advanced treatments, and outcomes after BMM treatment, is provided in Table 1.

2.2. Wound bed preparation and treatment

Wounds were thoroughly debrided of all non-viable tissue, cleaned with alcohol or hypochlorous acid solution, and patted dry prior application of BMM. BMM is composed of synthetic self-assembling peptides that form a 3D scaffolding wound matrix. The BMM delivery system is supplied sterile in a pre-filled syringe with an optional flexible applicator tip, each individually packaged in a sterile peel pouch, ready to use for direct application to wounds. The flexible applicator tip allows precise delivery to the wound site, facilitating application to irregularly shaped and/or hard-to-access wounds, such as tunneling or undermining areas. BMM is stable at room temperature and does not require additional preparation. In this study, the supplied flexible applicator tip was attached directly to the BMM's sterile prefilled syringe for product application (Figure 1). BMM was applied across the entire wound surface until completely coated to a thickness of about a dime (approximately 1.3 mm).

After application, BMM and the entire wound surface were covered with a non-adhering and non-absorptive dressing (Adaptic 3M, St. Paul, MN, USA) and backed by sterile gauze. Patients were instructed to leave the dressing

Table 1. Patients' characteristics at the enrollment, including prior treatments, duration, wound location, wound depth, and comorbidities prior to BMM treatment

S. no.	Age (years)	Prior treatments	Wound duration (months)	Wound location	Wagner classification[14]	Comorbidities
Patient 1	37	A, C, E, HA, LC, O, S, SX, V	39	Heel	2	D, N, OS
Patient 2	37	A, C, HA, LC, O, S, VS	30	Forefoot	1	N, OS, PVD
Patient 3	67	E, HA, O	8	Heel	2	D, N
Patient 4	58	A, C, E, HA, LC, LCA, O, S, SX, V	56	Forefoot	1	A, D, N, O, OS
Patient 5	88	C, E, HA, LC, LCA, S, V	3	Ankle	3	D, N, OS, PVD
Patient 6	69	O, S	15	Lateral Foot	1	C, D, N, PVD
Patient 7	70	A, C, E, HA, LC, LCA, O, S	8	Heel	3	D, N, O
Patient 8	84	C, HA, LCA, O, S	13	Mid-arch	2	C, N

Notes: *Prior treatments*: A: Amniotic membrane; C: Collagen-decellularized; E: Enzymatic debridement; H: Hyperbaric oxygen; HA: Hypochlorous acid irrigation; LC: Living cell; LCA: Living cell amniotic; O: Off-loading shoe or boot; S: Silver dressing; SX: Surgery; V: Negative pressure wound therapy; VS: Vascular surgery. *Comorbidities*: A: Partial amputation; C: Charcot deformity; D: Diabetes; N: Neuropathy; O: Obesity; OS: Osteomyelitis; PVD: Peripheral vascular disease.
Abbreviation: BMM: Biomimetic matrix.

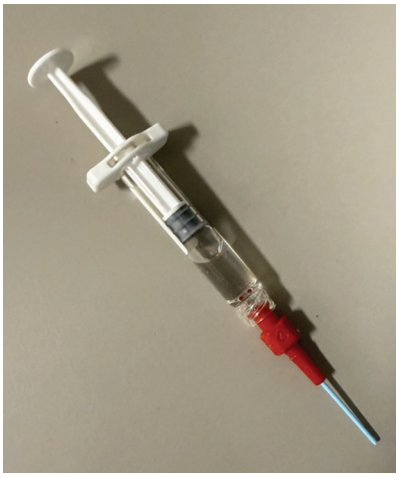

Figure 1. BMM is a transparent gel, and is provided in a sterile syringe. It can be applied to the surface of the wound, or by inserting the flexible tip into tunneling or undermined areas.
Abbreviation: BMM: Biomimetic matrix.

in place for 3 – 5 days, depending on the extent of drainage from the wound. The BMM was re-applied as needed for up to three applications per patient, and each application was normally 2 weeks apart. BMM is promptly integrated into the tissue and bioresorbed, and therefore, does not need to be removed from the wound site at dressing changes.

All patients received appropriate off-loading to protect the wound site. Wounds were measured and photographed just before the initial application and at subsequent visits. The wound area was calculated by tracing the wound perimeter to calculate the surface area. This was then compared to a standardized marker within the picture frame to calculate the wound surface area. These measurements were used to calculate changes in wound area. All measurements were taken following wound debridement.

3. Results

This study selected a small clinical sample of eight patients with stalled chronic diabetic foot wounds. The ulceration duration before BMM treatment ranged from 3 up to 56 months (average = 21.5 months). The wounds were located on weight-bearing surfaces of the foot, except for one venous stasis ulcer located on the ankle in a patient who was also diabetic. The wounds in this clinical case series consisted of Wagner Grade 3 (n = 2; 25%), Grade 2 (n = 3; 37.5%), and Grade 1 (n = 3; 37.5%) ulcers. All wounds had previously received standard of care, and, except for one patient, wounds had also been previously treated with multiple biologic products and failed to respond. Several wounds had also previously been treated with negative pressure therapy before treatment with BMM without achieving significant improvement. A summary including prior treatments, wound duration, wound location, wound depth, and comorbidities before BMM treatment of all the subjects enrolled in this study can be found in Table 1.

All patients treated with BMM experienced a substantial reduction in the percent wound area, with an average decrease of 63.6%, ranging from 22% to 100% wound closure. Patients received one to three applications of BMM. When considering similar wounds, it appears that the number of applications of BMM does have an impact on the percent change in wound area. For example, patients 1, 3, and 7 had similar comorbidities, and comparable location (heel). However, patient 1 received only two BMM treatments, while patients 3 and 7 each received three treatments. Our data shows that patients 3 and 7 had

a higher percent closure rate than patients 1, who received a lower number of BMM applications.

The treatment length ranged from 5 to 11 weeks, with one patient achieving full wound closure at 6 weeks following a single application of BMM. In this cohort of patients treated with BMM, a reduction in inflammation followed by the presence of granulation tissue was observed early in the healing process. This was followed by maturation of the granulation tissue leading to re-epithelialization. Furthermore, odor and drainage were noticeably improved with BMM treatment.

No adverse effects were observed during the treatment with BMM, and the product was well-tolerated by all subjects in this study. This is particularly important given the concern around potential immunogenicity and skin reactions associated with certain peptides.[10] BMM has been subjected to extensive safety testing including sensitization and skin irritation studies using relevant animal models as well as human subjects under "worst-case" conditions. As a result, BMM has been approved as a non-sensitizer and non-irritant by the U.S. Food and Drug Administration (FDA). In this small case series study, no signs of inflammation or irritation were observed, and, in fact, an improvement in the peri-wound skin appearance was noted.

The number of BMM applications, duration of treatment, initial and final wound size, initial and final wound depth, and percent change in wound area for each subject are tabulated in Table 2. Representative pictures of wounds before and after BMM treatment are also shown in Figure 2.

Although not intended to be part of our analysis, the outcomes from our initial patient cohort are of value added. The initial eight wounds showed significant progress for most part of the study. The wound of patient 1 closed by week 14, remained closed for 5 weeks, briefly opened for a week, and then closed again. This wound remained closed for >3 months. The wounds of patients 2, 3, and 8 closed completely in 8 – 9 weeks and remained closed for >3 months. The wound of patient 4 closed at week 11 and remained closed for >3 months. For patient 5, the wound remained open still, even after the wound had decreased further in the area to 13 cm^2, and thus the patient was subsequently scheduled for vascular intervention. Patient 6's wound was closed at week 6 and remained closed for >3 months. For patient 7, the wound area reduced to 3.5 cm^2 but then expanded again; this patient was lost to follow-up.

4. Discussion

In this clinical series, chronic, stalled diabetic lower extremity wounds were treated with a novel, FDA-approved BMM. Besides diabetes, all patients presented multiple comorbidities that can negatively impair wound healing, such as neuropathy, peripheral vascular disease, osteomyelitis, and prior partial amputation. Nearly all wounds were present for over a year without any progression toward healing despite the use of a variety of biologics, including living cell products, collagen, and amniotic-derived membranes, as well as regular debridement, negative pressure wound therapy, and off-loading when appropriate.

The wound area was calculated by tracing the wound perimeter to calculate the surface area. This was then

Table 2. Number of applications, treatment duration, initial and final wound size, and percent change in wound area of patients treated with BMM

S. no.	Number of BMM applications	Treatment follow-up (weeks)	Initial wound size (cm^2)	Initial wound depth (mm)*	Final wound size (cm^2)	Final wound depth (mm)*	Change in wound area (%)
Patient 1	2	7	2.72	3	2.12	2	−22.1
Patient 2	1	6	1.20	1	0.12	1	−91.7
Patient 3	3	5	0.44	1	0.08	1	−83.3
Patient 4	2	5	3.00	2	1.90	1	−36.7
Patient 5	1	11	40.5	3	18.2	1	−55.1
Patient 6	1	6	1.50	2	0.00	0	−100.0
Patient 7	3	5	9.80	4	5.77	3	−41.1
Patient 8	2	6	1.04	1	0.21	1	−79.1
Average	1.875	6.4	7.525	2.125	3.55	1.250	−63.6
SD	±0.835	±2.0	±13.652	+1.126	±6.2322	+0.886	±28.7

Note: *Wound depth is typically highly variable across the surface of the wound and is provided here as an average only, and not specific to any particular section of the wound.
Abbreviations: BMM: Biomimetic matrix; SD: Standard deviation.

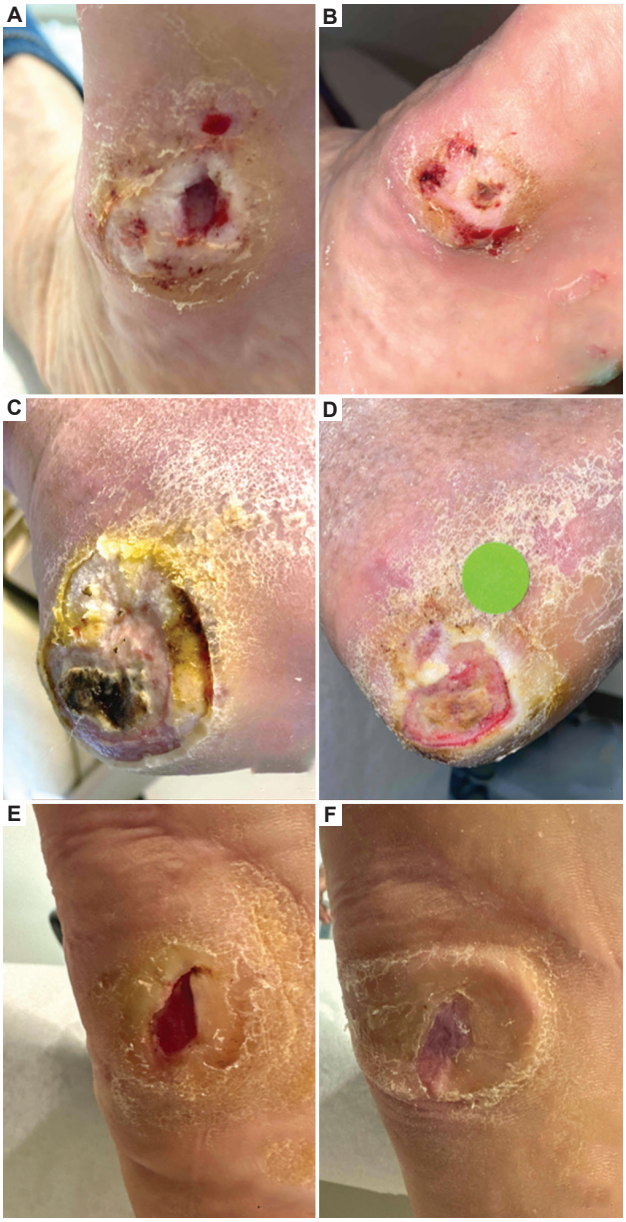

Figure 2. Representative images of chronic wounds before and after treatment with BMM. Charcot midfoot ulceration on day 1 (A) and after 6 weeks (B), with two applications of BMM. Heel ulcer on day 1 (C) and 5 weeks later (D), after three treatments with BMM. Midfoot ulcer beneath the fifth metatarsal base on day 1 (green marker is placed for size standardization) (E) and 6 weeks after (F) one treatment with BMM. Abbreviation: BMM: Biomimetic matrix.

compared to a standardized marker within the picture frame to calculate the wound surface area (Figure 2D). These measurements were used to calculate changes in wound area. All measurements were taken following wound debridement.

After one, two, or three applications of BMM, all wounds in this study demonstrated a measurable reduction in the percent wound area. When comparing similar wounds on patients with similar comorbidities, the investigators found that those wounds receiving more treatments showed a greater reduction in wound area. Odor, drainage, inflammation, and re-epithelization were also noticeably improved, with most wounds showing a reduction in depth within one or two BMM applications. In addition, no adverse effects during and after BMM application were observed. According to Sheehan *et al.*,[11] a reduction in wound area of diabetic foot ulcers observed for over 4 weeks can be used as a robust predictor for complete healing after 12 weeks, supporting the hypothesis that treatment with BMM may substantially increase the chances of full closure.

BMM achieved an average percent wound area reduction of 63.6% in wounds measuring 7.5 cm^2 on average after 6 weeks of treatment with one to three applications. In comparison, a meta-analysis study on the treatment of foot ulcers in patients with diabetes reports that an average percent area reduction of 48% was found in patients treated with advanced biologic products after 12 weeks, with an average wound size of 3.5 cm^2.[12] BMM achieved higher area reduction rates in larger wounds in about half the average time compared with advanced biologics.

In this study, the investigators relied on each patient's prior treatments to serve as their respective controls. All eight study subjects had been previously treated with off-loading and other advanced modalities, ranging from living cell treatments to advanced biologic wound care products. Many of these subjects also had prior treatments with negative pressure wound therapy. In each case, the patients were enrolled only after demonstrating a lack of progress or even worsening of their wounds for at least 3 months. (The average duration of wounds among the eight subjects was 21.5 months). Due to the small sample size, it was not practical to evaluate half the subjects with a placebo and half with BMM, and that is a limitation of the current study.

In this study, BMM, a fully synthetic matrix composed of self-assembling peptides, was evaluated in a variety of chronic, stalled diabetic wounds. The BMM used in this case series is shelf-stable at room temperature, supplied as a flowable matrix in a sterile, prefilled syringe system with a flexible applicator so that the material can be easily dispensed onto and can intimately contact the wound bed, including the hard-to-access areas. These features allow BMM to closely adhere to the wound surface and coat any defects or irregularities, providing superior contact compared to sheets and other form factors such as powders. In addition, unlike most biological wound care products,

which require thawing and/or additional manipulation such as cutting to size, rehydrating, or reconstituting, the BMM delivery system is ready to use and easy to apply.

Historically, other biomaterials used in wound management do not address some of the most critical factors to achieving wound closure. Collagen-based materials, for instance, provide a substrate for cellular migration and proliferation and may help reduce enzymatic degradation but do not control bioburden and are, in fact, prone to microbial colonization.[13] Living cell materials have been shown to stimulate wound healing by introducing growth factors in addition to an ECM, but they also fail to reduce bioburden during the healing process and are constrained by other limitations including low cell survival post-delivery or even adverse events such as immunogenicity.

BMM mimics the native ECM, which is critical in supporting cellular infiltration and revascularization while also functioning as an antibacterial barrier to contamination. The specifically designed delivery system enables precise application and intimate contact of the BMM with the wound bed, including hard-to-reach areas, and therefore eliminates dead space. The self-stable, sterile, ready, and easy-to-use system makes it a convenient product across different wound care settings. The fact that the matrix is resorbable and fully integrated with the tissue is also beneficial, as it does not require product removal at dressing changes, which could disrupt the newly developed tissue and delay the healing process. BMM was uniquely designed to address the specific clinical needs of a chronic wound and to address the shortcomings of other treatment options.

5. Conclusion

In this small case series, we explored the use of BMM, a novel class of self-assembling peptide-based biomaterial for wound care. The findings demonstrate that BMM treatment rapidly reduced wound area, improved overall appearance, and reduced the depth of complex diabetic lower extremity wounds. Considering the limitations of a case series, it is important to note that this study lacks the statistical rigor and appropriate methodology to support BMM's efficacy. However, these results provide insights into the potential use of this innovative product to treat and manage complex chronic wounds. Further studies, preferably randomized clinical trials, are needed to validate and expand the findings from this study.

Acknowledgments

The authors would like to thank Ana Tellechea, Brunno Caetano, Manav Mehta, Daljit Kaur, and Rebecca Salamone for their help and guidance with this study.

Funding

None.

Conflict of interest

The authors declare no conflict of interest.

Author contributions

Conceptualization: Adam Landsman
Investigation: All authors
Methodology: Adam Landsman
Writing – original draft: All authors
Writing – review & editing: All authors

Ethics approval and consent to participant

This work has been approved by Massachusetts General Brigham IRB, Protocol #2025P000269.

Consent for publication

Not applicable.

Availability of data

Data is available from the corresponding author upon reasonable request.

References

1. Darwin E, Tomic-Canic M. Healing chronic wounds: Current challenges and potential solutions. *Curr Dermatol Rep*. 2018;7(4):296-302.

   doi: 10.1007/s13671-018-0239-4

2. Vecin NM, Kirsner RS. Skin substitutes as treatment for chronic wounds: Current and future directions. *Front Med* (*Lausanne*). 2023;10:1154567.

   doi: 10.3389/fmed.2023.1154567

3. Singh AV, Chandrasekar V, Prabhu VM, *et al*. Sustainable bioinspired materials for regenerative medicine: Balancing toxicology, environmental impact, and ethical considerations. *Biomed Mater*. 2024;19(6):1-17.

   doi: 10.1088/1748-605X/ad85bb

4. Haines LA, Rajagopal K, Ozbas B, Salick DA, Pochan DJ, Schneider JP. Light-activated hydrogel formation via the triggered folding and self-assembly of a designed peptide. *J Am Chem Soc*. 2005;127:17025-17029.

   doi: 10.1021/ja054719o

5. Jafari A. Advancements in self-assembling peptides: Bridging gaps in 3D cell culture and electronic device fabrication. *J Biomater Appl*. 2024;38(10):1013-1035.

   doi: 10.1177/08853282241240139

6. La Manna S, Di Natale C, Onesto V, Marasco D. Self-

assembling peptides: From design to biomedical applications. *Int J Mol Sci*. 2021;22(23):12662.

doi: 10.3390/ijms222312662

7. Veiga AS, Schneider JP. Antimicrobial hydrogels for the treatment of infection. *Biopolymers*. 2013;100:637-644.

doi: 10.1002/bip.22412

8. Daphne A, Salick DJP. Design of an injectable b-hairpin peptide hydrogel that kills methicillin-resistant *Staphylococcus aureus*. *Adv Mater*. 2009;21:4120-2123.

doi: 10.1002/adma.200900189

9. Veiga AS, Sinthuvanich C, Gaspar D, Franquelim HG, Castanho MAR, Schneider J. Arginine-rich self-assembling peptides as potent antibacterial gels. *Biomaterials*. 2012;33:8907-8916.

doi: 10.1016/j.biomaterials.2012.08.046

10. Chandrasekar V, Panicker AJ, Dey AK, *et al*. Integrated approaches for immunotoxicity risk assessment: Challenges and future directions. *Discov Toxicol*. 2024;1:9.

doi: 10.1007/s44339-024-00010-w

11. Sheehan P, Jones P, Caselli A, Giurini JM, Veves A. Percent change in wound area of diabetic foot ulcers over a 4-week period is a robust predictor of complete healing in a 12-week prospective trial. *Diabetes Care*. 2003;26(6):1879-1882.

doi: 10.2337/diacare.26.6.1879

12. Santema TB, Poyck PP, Ubbink DT. Skin grafting and tissue replacement for treating foot ulcers in people with diabetes. *Cochrane Database Syst Rev*. 2016;2:CD011255.

doi: 10.1002/14651858.CD011255.pub2

13. Zheng L, Tseomashko N, Voronova A, Vasil'kov A, Hu X, Wang X. Recent advances of collagen composite biomaterials for biomedical engineering: Antibacterial functionalization and 3D-printed architecturalization. *Collagen Leather*. 2024;6:22.

doi: 10.1186/s42825-024-00164-8

14. Wagner FW Jr. The dysvascular foot: A system for diagnosis and treatment. *Foot Ankle*. 1981;2(2):64-122.

doi:10.1177/107110078100200202

ACCSCIENCE PUBLISHING

Journal of Clinical and Translational Research

MEDICAL HYPOTHESIS

A systematic review protocol of medical and clinical research landscapes and quality in Malaysia and Indonesia (REALQUAMI)

Boon-How Chew[1]*, Shaun Wen Huey Lee[2], Lim Poh Ying[3], Soo Huat Teoh[4], Aneesa Abdul Rashid[1], Navin Kumar Devaraj[1], Adibah Hanim Ismail[1], Abdul Hadi Abdul Manap[1], Fadzilah Mohamad[1], Aaron Fernandez[5], Hanifatiyah Ali[1], Puteri Shanaz Jahn Kassim[1], Nurainul Hana Shamsuddin[1], Noraina Muhamad Zakuan[6], Akiza Roswati Abdullah[7], and Indah S. Widyahening[8]

[1]Department of Family Medicine, Faculty of Medicine and Health Science, Universiti Putra Malaysia, Serdang, Selangor, Malaysia

[2]School of Pharmacy, Monash University Malaysia, Bandar Sunway, Selangor, Malaysia

[3]Department of Community Health, Faculty of Medicine and Health Science, Universiti Putra Malaysia, Serdang, Selangor, Malaysia

[4]Advanced Medical and Dental Institute (AMDI), Universiti Sains Malaysia, Kepala Batas, Penang, Malaysia

[5]Department of Psychiatry, Faculty of Medicine and Health Science, Universiti Putra Malaysia, Serdang, Selangor, Malaysia

[6]Department of Biomedical Sciences, Faculty of Medicine and Health Science, Universiti Putra Malaysia, Serdang, Selangor, Malaysia

[7]Medical and Health Sciences Library, Faculty of Medicine and Health Science, Universiti Putra Malaysia, Serdang, Selangor, Malaysia

[8]Department of Community Medicine, Faculty of Medicine, Universitas Indonesia, Jakarta, Indonesia

***Corresponding author:**
Boon-How Chew
(chewboonhow@upm.edu.my)

Citation: Chew B, Lee SWH, Ying LP, *et al*. A systematic review protocol of medical and clinical research landscapes and quality in Malaysia and Indonesia (REALQUAMI). *J Clin Transl Res*. 2025;11(2):94-105.
doi: 10.36922/jctr.24.00071

Received: October 22, 2024

1st Revised: December 11, 2024

2nd Revised: December 12, 2024

Accepted: March 11, 2025

Published online: April 4, 2025

Abstract

Background: The evolving landscape of clinical and biomedical research has raised concerns about waste and quality. Poorly conducted studies mislead clinical practice and compromise patient outcomes. Reliable data from past research are essential for research quality improvement. **Aim:** The aim of the study was to characterize and assess the quality of research in Malaysia and Indonesia. **Methods**: To establish the proposed systematic review protocol, we will search PubMed, Cochrane Library, CINAHL, and PsycINFO for studies published from 1962 to 2019, supplemented by MyMedR for Malaysian research. Two reviewers will independently screen studies, extract data, and assess quality. Phase 1 will descriptively report research characteristics, including researcher profiles and journal outlets. In Phase 2, a quality screening tool will be validated across three domains: relevance, methodological credibility, and result usefulness. Associations between research characteristics and quality will be analyzed through multivariable regression and longitudinal trends will be explored. **Results**: Findings from the proposed systematic review protocol will generate baseline data for national and international comparisons, guiding stakeholders, researchers, funders, and policymakers on research evolution and quality trends. Results may inform improvement initiatives and resource allocation for understudied areas. **Conclusion:** This review aims to establish a

comprehensive baseline of research outputs and the pattern of research quality in the participating countries and discipline. The findings may underscore the presence of a valid classification method to guide future research and enhance evidence-based practice in healthcare. **Relevance for patients**: By identifying research strengths and gaps, this proposed systematic review supports the development of robust study designs that generate reliable evidence, ultimately enhancing patient care and health outcomes.

Keywords: Systematic review; Clinical research; Biomedical research; Research characteristics; Research quality; Malaysia; Indonesia

1. Introduction

There is currently an increasing number of clinical and biomedical research and publications globally, especially those originating from Asia.[1] However, the increase in quantity does not correlate with the quality of research conducted. Instead, significant research waste has been reported due to irrelevancy,[2] poor research design,[3] inaccessible research data,[4] and incomplete reporting.[5,6] Moreover, John Ioannidis, one of the co-directors at the new Meta-Research Innovation Center at Stanford, admitted that "it was very easy to make errors" when discussing the challenges encountered throughout the research process, despite the noble intentions of the researchers.[7] The clinical and biomedical research landscape in Asia has been evolving throughout the past decades, beyond those reported from a few sources, with growth seen more in terms of quantity than quality.[1] Similarly, the quality of published research in a country such as Malaysia and Indonesia has not been examined over the past few decades. Comprehensive assessments and evidence are needed to inform existing researchers, research institutes, and stakeholders in these countries about the adequacy of current efforts or the need to improvise existing research practices.

An estimated 200 tools were previously available for evaluating research quality or biases in randomized and non-randomized studies.[8-10] A recent literature review up to April 2022 identified 417 appraisal tools for non-randomized studies of interventions.[11] These tools serve critical functions in ensuring that studies adhere to robust methodological standards, minimizing bias, and enhancing the reliability of results. Deeks *et al.*[8] evaluated non-randomized intervention studies, highlighting challenges like biases and confounding factors, and emphasized the need for tailored tools to address these complexities. Their work reviewed tools designed to standardize assessments and improve comparability, providing a framework for systematic quality evaluations. MacLehose *et al.*[9] compared effect sizes from randomized and non-randomized studies, identifying significant discrepancies due to biases in study designs, and underscored the importance of quality assessment tools for detecting and addressing these differences to ensure reliable comparisons and synthesis across diverse research designs. Zeng *et al.*[10] reviewed methodological quality assessment tools across preclinical, clinical, and systematic review domains, highlighting their strengths, gaps, and domain-specific challenges. Nevertheless, most tools available for assessing non-randomized studies are generally of poor methodological quality, making it consistently difficult or even impossible to assess the methodological quality and risk of bias across primary studies[12] Many different tools exist for different study designs, such as the Cochrane Risk of Bias tool for randomized trials,[13] the A Revised Tool for the Quality Assessment of Diagnostic Accuracy Studies 2 tool[14] for diagnostic test accuracy studies, the Assessment of Multiple Systematic Reviews[15] and Risk of Bias in Systematic Reviews tools[16] for systematic reviews, and the Risk of Bias In Non-Randomized Studies of Interventions[17] for non-randomized studies of the effects of interventions. In addition, there are a few web-based tools and checklists for different study designs: the National Institutes of Health Study Quality Assessment Tool for controlled intervention studies, systematic reviews and meta-analyses, observational cohort and cross-sectional studies, case–control, pre-post, and case series studies (https://www.nhlbi.nih.gov/health-topics/study-quality-assessment-tools); the Critical Appraisal Skills Program checklists by Oxford-based Better Value Healthcare Ltd. (https://casp-uk.net/casp-tools-checklists/); a web application Critical Appraisal Tools (FLC 2.0) developed by OSTEBA Spain to guide the critical appraisal process (http://www.lecturacritica.com/es/acerca.php).

Among some of the more widely used and recommended tools are the Newcastle-Ottawa scale (NOS),[18] the Downs and Black instrument,[19] and the latter RTI item bank (RTI-IB).[20] The NOS, which has been used to illustrate issues in data extraction from primary non-randomized

studies, has only eight items and is simpler to apply.[18] However, the items may require customization to the review question of interest. The Downs and Black instrument[19] has been modified for use in a methodological systematic review.[20] The reviewers found that some of the 29 items were difficult to apply to case–control studies. In addition, the instrument requires considerable epidemiological expertise and is time-consuming and difficult to operate.[21-24] The median observed inter-rater agreement for the RTI-IB was 75% (25th percentile [p25] = 61%; p75 = 89%). The median first-order agreement coefficient statistic was 0.64 (p25 = 0.51; p75 = 0.86). Although the RTI-IB facilitates a more complete quality assessment than the NOS, it is also more burdensome. In addition, there are different meanings for epidemiological terminologies across different countries. For example, the term "selection bias" describes what others may call "applicability" or "generalizability." Consequently, applying these tools presents challenges, as they require significant epidemiological expertise, are time-consuming to use, and often yield inconsistent results due to low inter-rater reliability. Thus, comprehensive manuals are required to accompany these tools to provide instructions for standardized interpretation by different users. However, this may pose a real challenge to users, as few tools have such comprehensive manuals. To the best of our knowledge, no existing tool serves as an all-rounded tool for assessing all types of study designs,[10] nor is there a recommended tool suitable for quickly screening the quality of published research.

In light of this, our research group has assimilated quality indicators used in existing tools, drawing from a series of user guides to the medical literature by the Evidence-Based Medicine Working Group,[25,26] systematic reviews,[27,28] and principles of clinical epidemiology,[29] and consequently, developed a comprehensive assessment tool based on the findings. In future work, the group will systematically assess the characteristics in research publications by researchers in Malaysia and Indonesia and subsequently identify quality indicators of these research publications.

2. Research design

The overall research design consists of two analytical phases:

(i) Phase 1 (research landscapes): Descriptive reporting of the research demographics and characteristics in each country to date.
(ii) Phase 2 (research quality): Quality assessment of research based on the published reports in journals.

2.1. Inclusion criteria and search strategy

Before data analysis, all clinical and biomedical research conducted in Malaysia or Indonesia, from January 1962 to December 2019, will be identified from various databases: PubMed, Cochrane Library, CINAHL, and PsycINFO (Figure 1); including all published peer-reviewed health and biomedical research papers from each country (Malaysia or Indonesia), or authored by citizens of each country (Malaysian or Indonesian) with an affiliation to an institution in either country. Additional literature will be extracted from the MyMedR (Malaysian Medical Repository) (http://mymedr.afpm.org.my/) database, as it specifically compiles published papers in health and biomedical research conducted in Malaysia or by authors who have a Malaysian affiliation. MyMedR also draws from MyJurnal, an online system used by the Malaysia Citation Centre of the Ministry of Higher Education Malaysia to collect and index all Malaysian journals. Grey literature will not be included, and there will be no exclusion based on language. Search results will be compiled into Endnote reference management software, where duplicates will be removed. If necessary, authors and institutions will be contacted. A medical librarian and a scientific officer at the Faculty of Medicine and Health Sciences, Universiti Putra Malaysia will assist with these tasks. The screening process for publications from both countries will be completed by two separate teams, each based in Malaysia and Indonesia, respectively.

2.2. Study selection and data extraction

The authors of the present article (i.e., physicians and medical professionals) will serve as reviewers of the identified articles and will be trained on the review protocol before commencing the paper screening. The articles will be screened by title and abstract. The full text of eligible articles will be retrieved and distributed to pairs of reviewers for screening; independently extracted information will be input into a standard data extraction template (Tables A1-4). This template has been pilot-tested on 10 articles among all the reviewers for clarity, and modification of the template was done accordingly. The final piloted template is available in Tables A1 and 3. Any discrepancy during article selection and data extraction will be solved by consensus between three or more reviewers. To ensure the inclusion of only high-quality data, B.H.C. will reassess 10 – 20% of the included articles.

In the event of duplicate publications or multiple reports of a research study, we will use the most complete data set aggregated across all known publications. Duplicate publications are defined as two or more published articles that report on the same research question.

2.3. Research landscapes

Phase 1 of the project will describe the following characteristics of the reported research (Table A1 for more details):

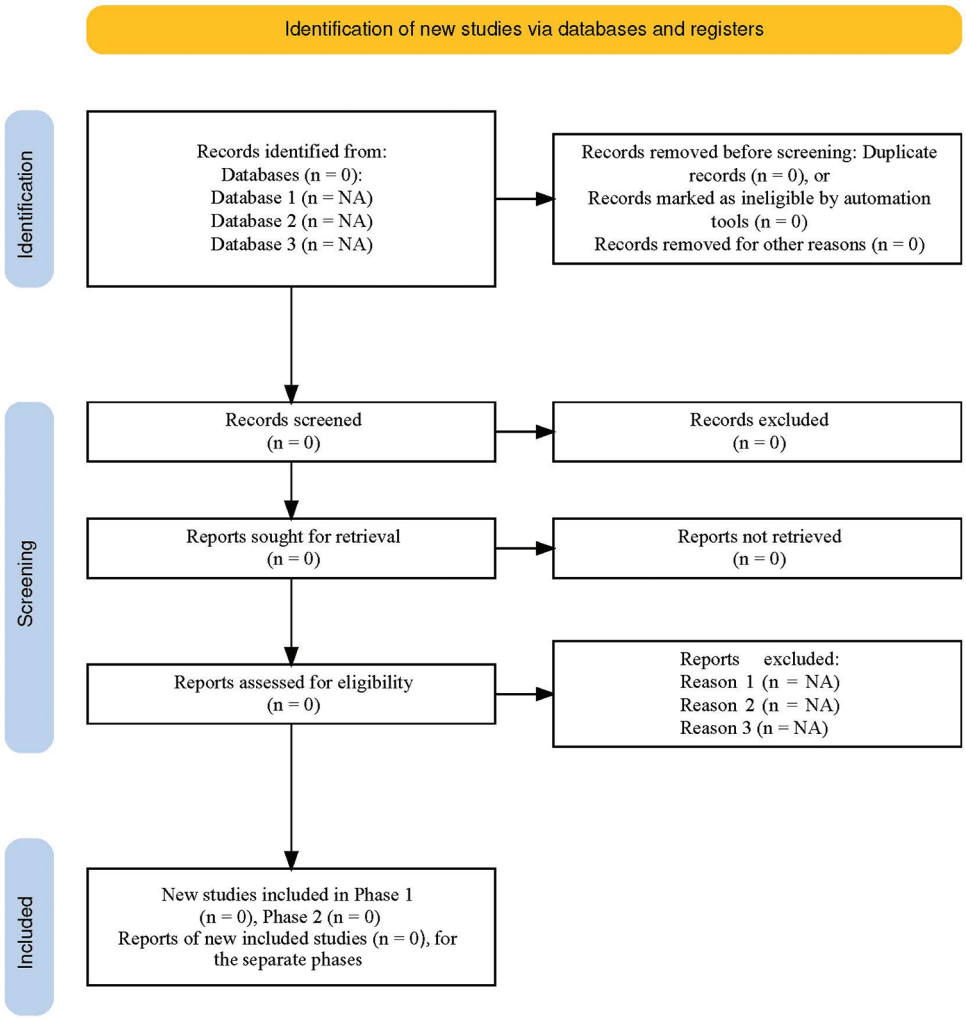

Figure 1. Outline of the flow of information through the two phases of the systematic review. Adapted from Haddaway *et al.*, (2022).[30]

(i) Institution and qualification of the corresponding author/s;
(ii) Number of authors, institutions, and expertise;
(iii) Numbers of international collaborating authors and institutions;
(iv) Numbers of study sites;
(v) Journal type: Local, regional, or international; open access or traditional subscription-based; general or discipline-specific;
(vi) Setting: Healthcare facility (hospital, clinic, etc.) or community;
(vii) Type of study: Audit versus research; secondary (reviews) or primary (diagnostic, prognostic, etiologic, or interventional); clinical or non-clinical (laboratory, public health, health service, etc.);
(viii) Data-collection design;
(ix) Date of study conducted, completed, and published;
(x) Health conditions studied, and/or organ systems involved;
(xi) Drugs, devices/tools, surgical, psychological, or health services. (Table A5)

2.4. Research quality

In Phase 2, the research quality will be assessed based on various criteria across three domains: relevance, credibility, and usefulness (Table 1). All reviewers will learn the principles of clinical epidemiology through a workshop and reach a consensual understanding of the terms used to represent research quality in this project. During the workshop, we will implement a training session for all reviewers, in which all reviewers will read and score the same articles. Each item will be scored 1 if present, and 0 when absent. This will be followed by a discussion on any similarities or differences in the quality assessment and scores to ensure uniformity in the understanding of the quality domains when applied to the actual screening process. We will also determine the

Table 1. Research quality domains and items to be used in the screening tool (total score: 0 – 10)

Relevance (3 items; subtotal score: 0 – 3)	Credibility (4 items; subtotal score: 0 – 4)	Usefulness (3 items; subtotal score: 0 – 3)
- Scientific relevance: Indicate this with an acceptable literature review or citing systematic reviews[a] - Societal relevance: Research area or involvement of end-users (e.g., patients) - Research team/experts: The research is led by experts in the relevant field or conducted with relevant experts	- Data-collection design: Appropriate for the research question[b]; experimental vs. non-experimental; time feature of variables considered - External validity: Representative of or generalizability to an important and relevant population; comparability between groups in randomized control trials - Internal validity: Validated instrument, measurement process, and performed by trained or blinded assessors - Precision: Appropriate sample size estimation and achievement	- Important outcomes used and reported[c] - Meaningful estimates: Practical numerical results, taking into consideration the response rate, missing data, proper statistical test, and analysis[d] - Conclusion: Accounts for study limitations[e]

Notes: [a]Set the right research priorities, clear research question/hypothesis; [b]Ethical conduct and patient safety/rights/priorities included; [c]Outcomes that truly matter to patients; [d]The study provides useful data for the intended end-users, unusual or unexpected analysis is explained and justified; [e]No over-claimed or misleading conclusion.

inter-rater reliability agreement using Cohen's kappa κ and intra-class correlation (ICC). The kappa κ is a measure of agreement between different observers beyond chance agreement.[31] The κ statistic will be computed separately for each domain's item (0 or 1). The ICC will be used to assess the three domains' subtotal (3, 4, and 3) and the total score (Table 1).

The kappa result will be interpreted as follows: Values ≤0 indicate no agreement; 0.01 – 0.20 indicate slight agreement; 0.21 – 0.40 indicate fair agreement; 0.4 – 0.60 indicate moderate agreement; 0.61 – 0.80 indicate substantial agreement; and 0.81 – 1.00 indicate almost perfect agreement.[32,33] For the ICC, values <0.40 indicate poor correlation; 0.40 – 0.59 indicate fair correlation; 0.60 – 0.74 indicate good correlation; and 0.75 – 1.0 indicate excellent correlation.[34,35] We specify that an a priori level of κ > 0.60 and ICC > 0.75 must be achieved before Phase 2 of the study begins. Retraining and reassessment of the reviewers on different articles will be conducted until the inter-rater agreement reaches the desirable levels. The expected lower bound of a 95% confidence limit for κ is no <0.60, with an assumed marginal prevalence of zero score of 30%. Using alpha and beta error rates of 0.05 and 0.2, respectively, a pair of reviewers will rate 20 papers each,[34,35] with five pairs of reviewers and 100 samples for the subtotal and total ICC estimation.[33]

2.5. Research quality domains for screening

2.5.1. Relevance

The relevance of research will be assessed from three perspectives: scientific relevance, the composition of the research team, and societal relevance. Research is considered scientifically relevant if it addresses a true and real scientific problem and provides the needed knowledge to understand an existing phenomenon. Scientific relevance also denotes that the research sets out on a justified scientific foundation and is informed by existing evidence. Thus, scientifically relevant research is usually globally relevant due to its highly generalizable topics and subjects.

Societal relevance refers to research that addresses a true and real societal problem. This relevancy may exist in smaller (e.g., a particular condition or disease in a unique population) or wider (e.g., global) populations. These two domains of scientific and societal relevance relate to having novelty in the research.

The last domain in the relevance category refers to the research team; that is, investigators and experts of relevant professional qualifications. This may include patients and the public in certain research areas when the opinions of end-users are considered important, such as in interventions or the experiences of patients or family members.

2.5.2. Credibility

This category is assessed after it is judged that the research is relevant. Four essential features are considered the minimum requirements for a research study to be credible and for its results to inform or contribute to practice change; that is, data collection design, precision, external validity, and internal validity.

The design of the data collection process has to align with the research objective or question. The approach used in data collection depends on whether the research is causal or non-causal, as well as whether the research is experimental or non-experimental, to provide more accurate data. The time feature or characteristics of the variables involved in the research should be collected in their intended phases or stages, such as a risk factor in the asymptomatic phase, or symptoms or biomarkers in the latent period.

Sampling and sample types are also important in the credibility domain. The sample of the participants should consist of the appropriate group from the population for the research, as they represent the population to which the results could later be generalized. However, in causal or experimental research, comparability between groups in research takes precedence over representativeness because confounding or prognostic factors between groups result in valid outcomes related to the exposure.

Quantitative research is essentially about measurements, measuring tools, and the measurement process. The measurement of variables is to be performed using validated tools through a standardized process, and if necessary, by trained and blinded assessors. Any query or suspicion on the methods of measurement in research will result in internal non-validity.

Credible research provides an appropriate and rational sample size estimation based on the research question and its primary objective, as well as previous research within the same discipline. Adequate sample size is required for sufficient precision in research. The achievement or non-achievement of the desired sample size should be reported or justified and discussed accordingly.

2.5.3. Usefulness

Credible research warrants attention due to the value of its results. The usefulness of research results lies in their importance, the provision of meaningful estimates, and the fair conclusion supported by the research design.

Important outcomes are of high priority and concern to the end-users. These generally refer to the hard outcomes, strong correlates, or intermediate markers to the research exposure, including condition diagnoses and surrogates (blood or serum markers).

Research results are meaningful when they are easily understood in the context of clinical practice or the daily lives of patients. Meaningful estimates are usually the direct results of the study, such as the actual numbers of occurrences, incidence and prevalence rates, and risk ratios. Indirect outcome measures, such as plasma glucose excursion, and transformed estimates, such as standardized or the logarithmic form of a unit of measurement, require a reverse transformation of the units for better clarity. Otherwise, they could complicate the translation and interpretation of results.

The conclusion of a research serves as a crucial complement to the readers' own judgment. As the final interpretation and remarks provided by the authors and investigators of the research, it is essential to present the results within the appropriate context and applicability, taking into account the study design constraints and any limitations encountered throughout the research process.

3. Data analysis

The principal investigator (B.H.C) bears the overall responsibility for the compilation, maintenance, and management of the review database. The database is stored on a password-protected computer and shared on a university server repository on completion.

Every eligible and included journal article will be assessed according to two main areas – research characteristics and quality of the research. The dataset will be checked for any missing data and errors. The data will then be reported descriptively; frequency and percentage for categorical data; mean and standard deviation (median and interquartile range) for normally distributed (and not normally distributed) continuous data. Time series plots will be used to investigate the trends and patterns of research characteristics, health conditions, and quality of research over the years. The geographic information system may also be plotted to evaluate the locations and areas of research conducted. Longitudinal trends in certain research characteristics, health conditions, or research areas across different settings and clinical or biomedical disciplines will be explored.

Associations between research characteristics and quality will be explored, and the independent effect of each determinant will be quantified using multiple linear regression analysis. In addition, research quality, as a categorical outcome, will be analyzed in tertiles. The highest tertile will be compared to the lowest tertile, and the determinants will be assessed using multiple logistic regression. Longitudinal trends in research quality will be explored, where a calculated 95% confidence interval and two-sided α of 0.05 will be used to test significance. Model checking will be conducted to get the best and most parsimonious final model that meets statistical assumptions. Estimates will be generated using PASW 25.0 (Statistical Package for the Social Sciences, United States of America) and MLwiN version 3.02 (Centre for Multilevel Modeling, University of Bristol, UK).

4. Discussion

Analytical results obtained will be informative to all stakeholders of clinical and biomedical research regarding the evolution of research conduct and performance from the past to the present. Research profiles throughout the past decades may be studied in relation to socioeconomic, political, or policy changes in specific years. The longitudinal and prospective trends in the research profiles, research quality, and the association between them could

provide suggestions for improvement initiatives or identify an institutional role model that has achieved a certain degree of success. In addition, analyzing health conditions or research areas across different settings and determining whether they are over- or under-studied may help guide future prioritization of research initiatives and resource allocation. Descriptive comparison between countries may also be possible if there are similar studies conducted in other countries. This provides meaningful benchmarking and insights into the effects of evolving historical events in clinical and biomedical research activities and quality in each country.

The research quality tool proposed in this article may be a useful screening tool for all quantitative study designs, except qualitative studies, case reports, and systematic reviews. We anticipate that it would be a useful tool for a quick critical appraisal of research quality. The sequence of Relevance-Credibility-Usefulness (acronymized as RECRUS) may enhance efficiency and empower tool users in the critical appraisal process. The main limitation of this tool would be the reporting quality of the research, including zero reporting or null publication of any completed study.[36] In addition, a relatively large number of graduate and postgraduate students' research projects that were published as thesis and not in journals[37] may not be accessible through the tool's search strategies. Reporting quality is not assessed using the research quality tool proposed in this article, as specific guides and checklists already exist for this purpose. While the quality and comprehensiveness of research reporting may not be as poor as methodological research quality, they can still affect its assessment.[38] The 10 items within the three domains of the research quality screening tool are considered fundamental minimums for most clinical and biomedical research and are expected to be available in most published articles. Missing information in the included articles may be recovered by contacting the corresponding authors via email or telephone.

5. Conclusion

This systematic review aims to provide a comprehensive overview of the clinical and biomedical research landscape in Malaysia and Indonesia from 1962 to 2019. By systematically identifying and characterizing research output over this period, the review will establish a baseline for evaluating research productivity, methodological rigor, and quality. The findings are expected to highlight both the progress made and the existing gaps in research, offering critical insights for researchers, funding bodies, and policymakers. Ultimately, this work will serve as a catalyst for future efforts to enhance research capacity, reduce waste, and promote evidence-based practices in the region. Continued monitoring and comparative evaluations over time will further support strategic planning and resource allocation to strengthen the research ecosystem in Malaysia and Indonesia.

Acknowledgments

The authors would like to thank the following colleagues for their helpful suggestions during the protocol development stage: Dr. Alfi Yasmina (Lambung Mangkurat University, Indonesia), Dr. Tan Kit-Aun, Dr. Sanjiv Rampal Lekhraj, Dr. Dhashani Sivaratnam, Dr. Maliza Mawardi, Associate Professor Dr. Cheong Ai Theng, Professor Dr. Lee Ping Yein, and Professor Dr. Ching Siew Mooi (Universiti Putra Malaysia, Malaysia).

Funding

None.

Conflict of interest

The authors declare that they have no competing interests.

Author contributions

Conceptualization: Boon-How Chew

Investigation: Boon-How Chew, Shaun Wen Huey Lee, Lim Poh Ying, Soo Huat Teoh, Aneesa Abdul Rashid, Navin Kumar Devaraj, Adibah Hanim Ismail, Abdul Hadi Abdul Manap, Fadzilah Mohamad, Aaron Fernandez, Hanifatiyah Ali, Puteri Shanaz Jahn Kassim, Nurainul Hana Shamsuddin,Noraina Muhamad Zakuan, Akiza Roswati Abdullah

Writing - original draft: Boon-How Chew, Shaun Wen Huey Lee

Writing - review & editing: Boon-How Chew, Shaun Wen Huey Lee, Lim Poh Ying, Soo Huat Teoh, Aneesa Abdul Rashid, Navin Kumar Devaraj, Adibah Hanim Ismail, Abdul Hadi Abdul Manap, Fadzilah Mohamad, Aaron Fernandez, Hanifatiyah Ali, Puteri Shanaz Jahn Kassim, Nurainul Hana Shamsuddin,Noraina Muhamad Zakuan, Indah S. Widyahening

Ethics approval and consent to participate

Not applicable.

Consent for publication

Not applicable.

Availability of data

The protocol proposed in this article has been registered in PROSPERO (CRD42020152907; 2020; https://www.crd.york.ac.uk/prospero/display_record.php?ID=CRD42020152907) and the Open Science Framework registry for Research on the Responsible Conduct of Research (https://osf.io/w85ce).

References

1. UNESCO. *UNESCO Science Report: Towards 2030*. Paris, France: United Nations Educational, Scientific and Cultural Organization; 2015. Available from: https://unesdoc.unesco.org/ark:/48223/pf0000235406 [Last accessed on 20 Mar 2025].

2. Chalmers I, Bracken MB, Djulbegovic B, *et al*. How to increase value and reduce waste when research priorities are set. *Lancet.* 2014;383(9912):156-165.

   doi: 10.1016/S0140-6736(13)62229-1

3. Ioannidis JP, Greenland S, Hlatky MA, *et al*. Increasing value and reducing waste in research design, conduct, and analysis. *Lancet.* 2014;383(9912):166-175.

   doi: 10.1016/S0140-6736(13)62227-8

4. Chan AW, Song F, Vickers A, *et al*. Increasing value and reducing waste: Addressing inaccessible research. *Lancet.* 2014;383(9913):257-266.

   doi: 10.1016/S0140-6736(13)62296-5

5. Macleod MR, Michie S, Roberts I, *et al*. Biomedical research: Increasing value, reducing waste. *Lancet.* 2014;383(9912):101-104.

   doi: 10.1016/S0140-6736(13)62329-6

6. Glasziou P, Altman DG, Bossuyt P, *et al*. Reducing waste from incomplete or unusable reports of biomedical research. *Lancet.* 2014;383(9913):267-276.

   doi: 10.1016/S0140-6736(13)62228-X

7. Ioannidis JPA. Why most published research findings are false. *PLoS Med.* 2005;2(8):e124.

   doi: 10.1371/journal.pmed.1004085

8. Deeks JJ, Dinnes J, D'Amico R, *et al*. Evaluating non-randomised intervention studies. *Health Technol Assess.* 2003;7(27):3-10, 1-173.

   doi: 10.3310/hta7270

9. MacLehose RR, Reeves BC, Harvey IM, Sheldon TA, Russell IT, Black AM. A systematic review of comparisons of effect sizes derived from randomised and non-randomised studies. *Health Technol Assess.* 2000;4(34):1-154.

10. Zeng X, Zhang Y, Kwong JS, *et al*. The methodological quality assessment tools for preclinical and clinical studies, systematic review and meta-analysis, and clinical practice guideline: A systematic review. *J Evid Based Med.* 2015;8(1):2-10.

    doi: 10.1111/jebm.12141

11. Jiu L, Hartog M, Wang J, *et al*. Tools for assessing quality of studies investigating health interventions using real-world data: A literature review and content analysis. *BMJ Open*. 2024;14(2):e075173.

    doi: 10.1136/bmjopen-2023-075173

12. Higgins JPT, Thomas J, Chandler J, Cumpston M, Li T, Page MJ, Welch VA, editors. *Cochrane Handbook for Systematic Reviews of Interventions version 6.5*, *Cochrane*; 2024. Available from https://www.training.cochrane.org/handbook

13. Higgins JP, Altman DG, Gotzsche PC, *et al*. The Cochrane Collaboration's tool for assessing risk of bias in randomised trials. *BMJ.* 2011;343:d5928.

    doi: 10.1136/bmj.d5928

14. Whiting PF, Rutjes AW, Westwood ME, *et al*. QUADAS-2: A revised tool for the quality assessment of diagnostic accuracy studies. *Ann Intern Med.* 2011;155(8):529-536.

    doi: 10.7326/0003-4819-155-8-201110180-00009

15. Shea BJ, Grimshaw JM, Wells GA, *et al*. Development of AMSTAR: A measurement tool to assess the methodological quality of systematic reviews. *BMC Med Res Methodol.* 2007;7:10.

    doi: 10.1186/1471-2288-7-10

16. Whiting P, Savovic J, Higgins JP, *et al*. ROBIS: A new tool to assess risk of bias in systematic reviews was developed. *J Clin Epidemiol.* 2016;69:225-234.

    doi: 10.1016/j.jclinepi.2015.06.005

17. Sterne JA, Hernan MA, Reeves BC, *et al*. ROBINS-I: A tool for assessing risk of bias in non-randomised studies of interventions. *BMJ.* 2016;355:i4919.

    doi: 10.1136/bmj.i4919

18. Wells GA, Shea B, O'Connell D, *et al*. *The Newcastle-Ottawa Scale (NOS) for Assessing the Quality of Nonrandomised Studies in Meta-Analyses*. Ottawa Hospital Research Institute; 2011. Available from: https://www.ohri.ca/programs/clinical_epidemiology/oxford.asp [Last accessed on 2024 Mar 20].

19. Downs SH, Black N. The feasibility of creating a checklist for the assessment of the methodological quality both of randomised and non-randomised studies of health care interventions. *J Epidemiol Community Health.* 1998;52(6):377-384.

    doi: 10.1136/jech.52.6.377

20. Viswanathan M, Berkman ND. Development of the RTI item bank on risk of bias and precision of observational studies. *J Clin Epidemiol.* 2012;65(2):163-178.

    doi: 10.1016/j.jclinepi.2011.05.008

21. Lo CK, Mertz D, Loeb M. Newcastle-Ottawa Scale: Comparing reviewers' to authors' assessments. *BMC Med Res Methodol.* 2014;14:45.

    doi: 10.1186/1471-2288-14-45

22. Hartling L, Milne A, Hamm MP, *et al*. Testing the newcastle ottawa scale showed low reliability between individual reviewers. *J Clin Epidemiol.* 2013;66(9):982-993.

doi: 10.1016/j.jclinepi.2013.03.003

23. Oremus M, Oremus C, Hall GB, McKinnon MC. Inter-rater and test-retest reliability of quality assessments by novice student raters using the Jadad and Newcastle-Ottawa Scales. *BMJ Open.* 2012;2(4):e001368.

doi: 10.1136/bmjopen-2012-001368

24. Margulis AV, Pladevall M, Riera-Guardia N, *et al*. Quality assessment of observational studies in a drug-safety systematic review, comparison of two tools: The Newcastle-Ottawa Scale and the RTI item bank. *Clin Epidemiol.* 2014;6:359-368.

doi: 10.2147/CLEP.S66677

25. Guyatt G, Drummond R, Meade M, Cook D. *The Evidence Based-Medicine Working Group Users' Guides to the Medical Literature.* 2nd ed. Chicago: McGraw Hill; 2008.

26. Oxman AD, Sackett DL, Guyatt GH. Users' guides to the medical literature. I. How to get started. The Evidence-Based Medicine Working Group. *JAMA.* 1993;270(17):2093-2095.

27. Von Niederhausern B, Schandelmaier S, Mi Bonde M, *et al*. Towards the development of a comprehensive framework: Qualitative systematic survey of definitions of clinical research quality. *PLoS One.* 2017;12(7):e0180635.

doi: 10.1371/journal.pone.0180635

28. Belcher BM, Rasmussen KE, Kemshaw MR, Zornes DA. Defining and assessing research quality in a transdisciplinary context. *Res Eval.* 2015;25(1):1-17.

doi: 10.1093/reseval/rvv025

29. Grobbee DE, Hoes AW. *Clinical Epidemiology: Principles, Methods, and Applications for Clinical Research.* United States: Jones and Bartlett Learning; 2014.

30. Haddaway NR, Page MJ, Pritchard CC, McGuinness LA. PRISMA2020: An R package and Shiny app for producing PRISMA 2020-compliant flow diagrams, with interactivity for optimised digital transparency and open synthesis. *Campbell Syst Rev*. 2022;18:e1230.

doi: 10.1002/cl2.1230

31. McGinn T, Wyer PC, Newman TB, Keitz S, Leipzig R, for GG. Tips for learners of evidence-based medicine: 3. Measures of observer variability (kappa statistic). *CMAJ.* 2004;171(11):1369-1373.

doi: 10.1503/cmaj.1031981

32. McHugh ML. Interrater reliability: The kappa statistic. *Biochem Med (Zagreb).* 2012;22(3):276-282.

33. Hallgren KA. Computing inter-rater reliability for observational data: An overview and tutorial. *Tutor Quant Methods Psychol.* 2012;8(1):23-34.

doi: 10.20982/tqmp.08.1.p023

34. Bujang MA, Baharum N. Guidelines of the minimum sample size requirements for Kappa agreement test. *Epidemiol Biostatist Public Health.* 2017;14(2):1-10.

doi: 10.2427/12267

35. Sim J, Wright CC. The kappa statistic in reliability studies: Use, interpretation, and sample size requirements. *Phys Ther.* 2005;85(3):257-268.

36. Groves T. What makes a high quality clinical research paper? *Oral Dis.* 2010;16(4):313-315.

doi: 10.1111/j.1601-0825.2010.01663.x

37. Post RE, Mainous AG 3rd, O'Hare KE, King DE, Maffei MS. Publication of research presented at STFM and NAPCRG conferences. *Ann Fam Med.* 2013;11(3):258-261.

doi: 10.1370/afm.1503

38. Widyahening IS, Wangge G, Saldi SR, *et al*. Quality and reporting of publications by Indonesian researchers: A literature survey. *J Evid Based Med.* 2014;7(3):163-171.

doi: 10.1111/jebm.12112

Appendix

Table A1. Data extraction form: Author and article characteristics

Article ID	Title	Institution of the CA	Specialty of the CA[a]	Professional qualification of the CA	Number of authors	Number of institutions	Number of overseas authors	Number of overseas institutions	Number of specialties/ disciplines of all authors	Journal name	Journal locality	Journal scope	Journal subscription
First name, year	Full title	Name, Country	(i) Family medicine (ii) Public health (iii) Medical (iv) Pediatric (v) Psychiatry (vi) Surgery (vii) O&G (viii) Orthopedic (ix) ENT (x) Eye (xi) Pharmacy (xii) Nursing (xiii) Dietetic (xiv) Biomedical	(i) PhD (clinician) (ii) PhD (non-clinician) (iii) MD (iv) Master (MMed) (v) Master (non-MMed) (vi) Bachelor (vii) Diploma (viii) Others (lower degrees) (ix) Not stated	1 to _	1 to _	0 to _	0 to _	1 to _	Full name	(i) Local-Malaysia (ii) Regional-within Asia (iii) International	General (multidisciplinary) Specific	OA Subscription

Note: [a]Up to two corresponding authors.
Abbreviations: CA: Corresponding author; ENT: Ear, nose, and throat; ID: Identity; MMed: Master's in Medicine; OA: Open-access; O&G: Obstetrics and gynecology.

Table A2. Example of a complete data extraction form: Author and article characteristics

Article ID	Title	Institution of the CA	Specialty of the CA[a]	Professional qualification of the CA	Number of authors	Number of institutions	Number of overseas authors	Number of overseas institutions	Number of specialties/ disciplines of all authors	Journal name	Journal locality	Journal scope	Journal subscription
Chan KE 1962 (2 variables)	String	String (2 variables)	Nominal	Ordinal Highest professional qualification	Scale	Scale	Scale	Scale Including local authors affiliated with overseas institutions	Scale	String	Ordinal Regional; i.e., Asian regions	Nominal General versus discipline-specific	Nominal OA versus traditional subscription-based

Note: [a]Up to two corresponding authors. Abbreviations: CA: Corresponding author; ID: Identity; OA: Open-access.

Table A3. Data extraction form: Research characteristics

Type of article	Field of study	Level of study	Class of study	Type of quantitative study	Data collection	Year when the study was conducted and completed	Number of study site	Setting[a]	Condition/ organ system studied[b]	Measures[c]	Intervention
(i) Research (original and reviews) (ii) Research protocol (iii) Audits (iv) Case report/ series (v) Commentary, quizzes, CME, etc. (vi) Letters	(i) Clinical (ii) Public health (iii) Health services (iv) Laboratory (v) Education	(i) Primary (ii) Secondary (database) (iii) Secondary (review) (iv) Opinion	(i) Quantitative (ii) Qualitative (iii) Mixed (iv) Others	(i) Prevalence (ii) Diagnostic (iii) Diagnostic test (iv) Prognostic (v) Etiologic (vi) Interventional (vii) Psychometric study	(i) Cross-sectional (ii) Cohort (iii) Case–control (iv) Nested case–control (v) RCT (vi) Quasi-RCT (voi) Cross-over (viii) Secondary data retrieval	Year started; year completed	1 to _	(i) Hospital (ii) Clinic (iii) Community (iv) Laboratory (v) University/ college	ICPC-2[d]	*Subjective*: (i) Self-report (ii) Other's report *Objective*: (i) Operator dependence (ii Non-operator-dependence (e.g., lab analyzer)	(i) No (ii) Drug (iii) Device, tool, or app (iv) Surgical procedure (v) Psychological or behavioral (vi) Socio-economic (vii) Health services

Notes: [a]Up to two corresponding authors; [b]consists of two variables, the primary and secondary settings; [c]consists of two variables, the subjective and objective outcome measures; [d]check Table A5.
Abbreviations: CME: Continuous medical education; RCT: Randomized controlled trial; ICPC-2: International classification of primary care (Second Edition).

Table A4. Example of a complete data extraction form: Research characteristics

Type of article	Field of study	Level of study	Class of study	Type of quantitative study	Data collection	Year when the study was conducted and completed	Number of study site	Setting[a]	Condition/ organ system studied[b]	Measures[c]	Intervention
Nominal (Only proceed with no. 1)	Nominal	Nominal	Nominal	Nominal	Nominal	Scale 2011, 2015 (2 variables)	Scale	Nominal	Nominal (2 variables- primary and secondary)	Nominal	Nominal

Notes: [a]Up to two corresponding authors; [b]consists of two variables, the primary and secondary settings; [c]consists of two variables, the subjective and objective outcome measures.

Table A5. International classification of primary care (ICPC) chapters and components

Chapter	Component
A	General and unspecified
B	Blood, blood-forming organs, lymphatics, spleen
D	Digestive
F	Eye
H	Ear
K	Circulatory
L	Musculoskeletal
N	Neurological
P	Psychological
R	Respiratory
S	Skin
T	Endocrine, metabolic, and nutritional
U	Urology
W	Pregnancy, childbirth, family planning
X	Female genital system and breast
Y	Male genital system
Z	Social problems

Journal of Clinical and Translational Research

Journal of Clinical and Translational Research (JCTR) welcomes submissions from various research topics that are centered on solving clinically-driven issues to ultimately benefit patients.

You will benefit from the following key features of JCTR as our author:

- Open access
- Author-friendly guidelines: 'your paper, your way'
- Reputable editorial board
- No word count or reference restrictions
- Double-blind review process to minimize bias
- Rapid production and publication
- Broad scope, interdisciplinary research exchange platform

The research areas that JCTR covers include, but are not limited to:

Internal medicine (all branches)	Gastroenterology and hepatology
Vascular medicine and phlebology	Surgery and transplantation
Oncology	Hematology
Cardiology	Nephrology
Intensive care medicine	Dermatology
Ophthalmology	Endocrinology and metabolism
Neurology and neurosciences	Anesthesiology
Anatomy, physiology, and embryology	Radiology and nuclear medicine
Pathology	Clinical chemistry
Clinical physics	Genetics and epigenetics
Epidemiology	Global health
Medical devices	Nutrition
Pharmacology	Immunology
Microbiology	Virology
Parasitology	Biomedical engineering

Biomedical spectroscopy and spectrometry

Thanks for considering the Journal of Clinical and Translational Research.

Editorial team JCTR

https://accscience.com/journal/JCTR

Contact
www.accscience.com
8 Burn Road, #15-03 Trivex, Singapore 369977
Email: editorial@accscience.com
Phone: +65 8182 1586